AUTOTAXIN IS NUTRITIONALLY REGULATED AND ALTERS MITOCHONDRIAL FUNCTION IN OBESITY-INDUCED INSULIN RESISTANCE

by

Kenneth D'Souza

Submitted in partial fulfilment of the requirements
for the degree of Doctor of Philosophy

at

Dalhousie University
Halifax, Nova Scotia
August 2019

Table of Contents

List of Tables

List of Figures

Abstract

The skeletal muscle is a major site of insulin stimulated glucose disposal. Skeletal muscle insulin sensitivity can be influenced by multiple circulating nutritional, hormonal, neuronal and bioactive factors, including adipose tissue secreted bioactive molecules known as adipokines. Autotaxin (ATX) is a novel adipokine that generates the bioactive lipid, lysophosphatidic acid (LPA). ATX-LPA signaling is increased in mouse models of diet-induced obesity and insulin resistance and clinically correlates with indices of insulin resistance. Prior studies have also suggested that the ATX-LPA pathway contributes to the development and/or exacerbation of systemic insulin resistance. However, it remained unclear how ATX is regulated in an obese-insulin resistant milieu and whether the ATX-LPA pathway influences insulin sensitivity in muscle under obese-insulin resistant conditions. ATX activity was demonstrated to be acutely and chronically nutritionally regulated by feeding/fasting and an obesogenic diet, respectively. We further identified glucose and insulin as novel regulators of ATX expression in adipocytes/adipose tissue. Glucose independently increased ATX expression in a time- and concentration-dependent manner. Insulin elicited a biphasic response; acute insulin stimulation increased ATX activity in a PI3Kinase-dependent and mTORC1-independent manner, whereas chronic insulin stimulation decreased ATX expression. Heterozygous whole body ATX knockout ($ATX^{+/-}$) mice were partially protected from high fat high sucrose (HFHS) diet-induced obesity, insulin resistance and glucose intolerance. HFHS-fed $ATX^{+/-}$ mice also showed improved insulin-stimulated AKT phosphorylation and glucose uptake in the soleus muscle. Mechanistically, ATX deficiency improved palmitate-linked mitochondrial respiration in the soleus, which was independent of broad changes in myofiber reprogramming, mitochondrial content and ADP sensitivity. Interestingly, mitochondrial H_2O_2 generation was increased, concomitant with generally decreased antioxidant gene expression. Similarly, LPA directly inhibited insulin signaling, mitochondrial respiration and H_2O_2 secretion in C2C12 myotubes. Taken together, my thesis work identified glucose and insulin as novel, critical regulators of ATX expression. Furthermore, chronic ATX deficiency improves skeletal muscle insulin sensitivity, which may be linked to amelioration of mitochondrial dysfunction induced by an obesogenic diet. This work also suggests that targeting the ATX-LPA signaling pathway may be a therapeutic strategy for treating obesity-induced insulin resistance.

List of Abbreviations and Symbols Used

4-HNE	4-hydroxynonenal
ACT	Actinomycin D
ADP	Adenosine Diphosphate
AMA	Antimycin A
AMPK	Adenosine Monophosphate-activated Protein Kinase
ANOVA	Analysis of Variance
ANT1	Adenine Nucleotide Translocase 1
ATF6	Activating Transcription Factor 6
ATX	Autotaxin
$ATX^{+/-}$	Heterozygous whole body ATX knockout
α	Alpha
B/M	Brefeldin A/Monensin
BAT	Brown Adipose Tissue
BMI	Body Mass Index
BMDM	Bone-Marrow Derived Macrophages
BSA	Bovine Serum Albumin
β	Beta
cAMP	cyclic Adenosine Monophosphate
CAT	Catalase
CCL2	C-C Motif Chemokine Ligand 2
chREBP	Carbohydrate Responsive Element Binding Protein
CHX	Cycloheximide
CREB	cAMP-Response Element Binding Protein
CRTC2	CREB-Regulated Transcriptional Coactivator-2
DG	Diacylglycerols

DMEM	Dulbecco's Modified Eagle Medium
DRP1	Dynamic Related Protein 1
δ	Delta
ECM	Extracellular Matrix
ENPP2	Ectonucleotide Pyrophosphatase/phosphodiesterase 2
ER	Endoplasmic Reticulum
ERK	Extracellular Signal Regulated Kinase
ERRγ	Estrogen Related Receptor γ
ε	Epsilon
η	Eta
FA	Fatty Acids
FAF	Fatty Acid Free
FAK	Focal Adhesion Kinase
$FATX^{-/-}$	Fat-specific ATX Knockout
FBS	Fetal Bovine Serum
FCCP	Carbonyl Cyanide-p-Trifluoromethoxyphenylhydrazone
FIS	Fission 1
FOXO1	Forkhead Box O1
GAS	Gastrocnemius
GCLC	Glutamate-Cysteine Ligase Catalytic Unit
GIR	Glucose Infusion Rate
GPX	Glutathione Peroxidase
GSK3	Glycogen Synthase Kinase 3
GSR	Glutathione Reductase
GTT	Glucose Tolerance Test
GWAS	Genome-Wide Association Studies

γ	Gamma
HFD	High Fat Diet
HFHS	High Fat High Sucrose
HG	High Glucose
HIF1α	Hypoxia Inducible Factor 1α
HOMA-IR	Homeostatic Model Assessment of Insulin Resistance
HSL	Hormone Sensitive Lipase
IKK	IκB Kinase
IL	Interleukin
ILK	Integrin-Linked Kinase
IR	Insulin Resistant
IRE1	Inositol-Requiring Enzyme 1
IRS	Insulin Receptor Substrate
IRX3	Iroquois Homeobox 3 Gene
IS	Insulin Sensitive
ITT	Insulin Tolerance Test
JAK	Janus Kinase
JNK	c-Jun N-terminal Kinase
KHB	Krebs-Henseleit Bicarbonate Buffer
LCAT	Lecithin-Cholesterol Acyltransferase
LDLR	Low Density Lipoprotein Receptor-Null
LPA	Lysophosphatidic Acid
LPA1-6	Lysophosphatidic Acid Receptors 1-6
LPC	Lysophosphatidylcholine
LPP	Lipid Phosphate Phosphatases
MG	Monoacylglycerol

MAPK	Mitogen Activated Protein Kinase
MCP1	Monocyte Chemoattractant Protein 1
MFN	Mitofusin
MiR05	Mitochondrial Respiration Medium
MORFO	Modulator of Oligodendrocyte Remodeling and Focal Adhesion Organization
mPA-PLA$_1$	Membrane-bound PA-selective PLA$_1$
mTORC	Mechanistic Target of Rapamycin Complex
MyHC	Myosin Heavy Chain
NEFA	Non-Esterified Fatty Acids
NF-κb	Nuclear Factor κ-Light-Chain-Enhancer of Activated B Cells
NLRP3	Nucleotide-binding Domain, Leucine-rich-containing Family, and Pyrin Domain-Containing-3
NOX	NAD(P)H Oxidase
NRF1	Nuclear Receptor Factor 1
NUC	Nuclease Domain
OPA1	Optic Atrophy 1
OXPHOS	Oxidative Phosphorylation
PA	Phosphatidic Acid
PC	Palmitoylcarnitine
PDE	Phosphodiesterase
PDK1	3-Phosphoinositide-Dependant Kinase 1
PERK	Protein Kinase RNA-like ER Kinase
PGAT	Perigonadal Adipose Tissue
PGC1α	Peroxisome Proliferator Activator Receptor γ Coactivator 1α
PH	Pleckstrin Homology
PI3K	Phosphoinositide-3-Kinase

PIP_3	Phosphoinositol-(3,4,5)-Triphosphate
PKA	Protein Kinase A
PP2A	Protein Phosphatase 2A
PPAR	Peroxisome Proliferator Activated Receptor
PRAS40	Proline-rich AKT Substrate of 40 kDa
PTB	Phosphotyrosine Binding
PTEN	Phosphatase and Tensin Homolog
Pyr	Pyruvate
R	Rapamycin
ROS	Reactive Oxygen Species
RPL	L Ribosomal Protein
SCAT	Subcutaneous Adipose Tissue
SFA	Saturated Fatty Acids
SGBS	Simpson-Golabi-Behmel Syndrome
SH2	Src Homology 2
SIK2	Salt Inducible Kinase 2
SMB	Somatomedin B
SOCS	Suppressor of Cytokine Signaling
SOL	Soleus
$sPLA_2$-IIA	Group IIA Secretory Phospholipase A_2
SREBP1	Sterol Regulatory Element Binding Protein 1
STAT	Signal Transduction and Activation of Transcription
T2D	Type 2 Diabetes
TFAM	Transcription Factor A, Mitochondrial
TIB	Tibialis
TG	Triacylglycerols

TGFβ	Transforming Growth Factor β
TLR	Toll-Like Receptors
TNFα	Tumor Necrosis Factor α
TRAF-2	Tumor Necrosis Factor Receptor-Associated Factor 2
TSC2	Tuberous Sclerosis Complex 2
TXN	Thioredoxin
TXNRD	Thioredoxin Reductase
θ	Theta
UCP	Uncoupling Protein
UPR	Unfolded Protein Response
W	Wortmannin
WHO	World Health Organization
XBP1	X-box Binding Protein 1
XO	Xanthine Oxidase
ζ	Zeta

Acknowledgments

First I would like to thank my supervisor Dr. Petra Kienesberger, who has shown me nothing but patience, guidance and unwavering support during my 4 years as a PhD candidate. Thank you for challenging me and allowing me to become an effective, independent and successful scientist.

Secondly, I would like to thank my supervisory committee, Dr. Roger McLeod, Dr. Neale Ridgway and Dr. Chris Sinal. Thank for you taking the time to attend my committee meetings and for your helpful comments and suggestions and probing questions. My thesis is undoubtable more complete as a result of your assistance. Thank you to the additional faculty members at DMNB, especially Dr. Thomas Pulinilkunnil and Dr. Keith Brunt, who I could always turn to for advice on both scientific and personal matters.

I would also like our collaborators, including Dr. Daniel Kane, Dr. Vassilis Aidinis, Dr. Thomas Eichmann, Dr. Mohamed Touaibia, Dr. Andrew Morris and Dr. Erin Kershaw. You're generosity in sharing reagents, protocols, services and helpful discussions allowed me to broaden my understanding and expand my technical expertise.

A big thanks to my lab members, past and present, including Purvi Trivedi, Logan Slade, Dipsikha Biswas, Carine Nzirorera and Geena Varghese. You made my experiences in the lab enjoyable, especially during the tough times when experiments were not working.

Finally, I would like to thank my family. Thank you to my parents, brothers and fiancée Alisha for their unending support, curiosity about my work and instilling in me a sense of pride and hard work. Finally, a big thanks to my daughter, Sophia. Having you arrive in the 3rd year of my PhD was by far the biggest challenge I faced in balancing my PhD project and personal life. However, I could not have asked for a more joyful presence in my life.

Chapter 1: Introduction

Figures 1.3-1.4, Table 1 and sections 1.6, 1.8-1.9 present in this chapter have been reproduced from *Nutrients*(1) from the following manuscript and edited as appropriate:

D'Souza, K., Paramel, G. V. and Kienesberger, P. C. (2018). Lysophosphatidic Acid Signaling in Obesity and Insulin Resistance. *Nutrients*. **10**(4): pii: E399.

Nutrients is an open-source journal and does not require copyright permission for use of text and figures.

1.1 Thesis Overview

An ever-increasing consumption of calorically dense foods coupled with an increasingly sedentary lifestyle leads to an energy imbalance in many populations across the globe. The product of this imbalance is obesity, a chronic metabolic disorder characterized by excessive adipose tissue that affects 650 million adults worldwide(2). Obesity is associated with many different co-morbidities, including insulin resistance, which can develop into type 2 diabetes (T2D)(3).

Apart from a remarkable capacity to act as a sink for excess nutrients, the adipose tissue also plays a key role in regulating systemic insulin sensitivity and glucose homeostasis(4). One major mechanism by which this occurs is through the secretion of bioactive molecules known as adipokines(5). Adipokines can act locally or systemically and can promote several signalling responses that directly influence insulin sensitivity(6). These adipokines can function as pro- and anti-inflammatory mediators, regulating tissue remodelling and influencing energy homeostasis(5),(7). Adipokine secretion is dynamic and is heavily influenced by adipose tissue mass and its metabolic state. Indeed, metabolic diseases such as obesity and insulin resistance result in drastic changes in the adipokine profile in pre-clinical models and humans; these changes can further exacerbate adipose tissue and systemic metabolic dysfunction.

Ectonucleotide pyrophosphatase/phosphodiesterase 2 (ENPP2), more commonly referred to as autotaxin (ATX), is a recently identified adipokine that generates the bioactive signaling lipid, lysophosphatidic acid (LPA)(8). Despite being best known for its role as a pro-oncogenic factor, by promoting proliferation, survival and metastasis, recent work has also implicated ATX-mediated signalling in metabolic diseases(9). The relationship between the ATX-LPA pathway and metabolic diseases, specifically obesity-induced insulin resistance, is the focus of this thesis.

The first chapter explores T2D, obesity-induced insulin resistance and mechanisms by which key insulin sensitive tissues contribute to this occurrence. This chapter will also introduce ATX-LPA signalling and summarize our knowledge of the mechanisms by which it promotes

obesity-induced insulin resistance. This chapter will establish the rationale for the second, third and fourth chapters which contain original research on questions pertaining to how ATX is regulated by an insulin resistant milieu and mechanisms by which ATX-LPA signaling alters tissue insulin sensitivity and mitochondrial function. The fifth and final chapter discusses implications of these results and future areas of research for exploring ATX-LPA signaling in obesity and insulin resistance.

1.2 Diabetes

1.2.1 Prevalence of Diabetes, Trends and Current Impact

The World Health Organization (WHO) estimates that in 2014, the number of adults living with diabetes was approximately 422 million; this represents an almost 4-fold increase in the incidence of diabetes since 1980(10). Current trends indicate that by 2045, this number will grow to a staggering 629 million(10). Diabetes is associated with several complications. Acute complications emanating from ketoacidosis due to hyperglycemia can be fatal. More prevalent are chronic complications that result in macrovascular diseases, including cardiovascular and cerebrovascular diseases and microvascular diseases, including retinopathy, nephropathy and neuropathy(3). As a result of these complications, an estimated $730 billion USD was spent on healthcare treating individuals with diabetes in 2013, which represents 12% of total worldwide healthcare costs(10). Despite these massive costs and efforts to treat this disease, diabetes was responsible for 4 million death in 2017(10). In line with worldwide trends, the number of Canadians living with diabetes has grown to nearly 3 million and accounts for 3.5% of public healthcare spending in direct costs(11).

Although no current statistics exist on the proportion of individuals with insulin resistance worldwide, the number likely far exceeds that of individuals with diabetes. Therefore, the high prevalence of diabetes and insulin resistance worldwide is a major economic burden for the health care system and an important concern for health care providers and policy makers.

1.2.2 Diagnosis

There are two major forms of diabetes, type 1 and type 2, both of which are characterized by an elevated blood glucose level (hyperglycemia). In type 1 diabetes, hyperglycemia results as a function of an autoimmune response that destroys insulin producing pancreatic β-cells within the islets of Langerhans(12). Type 2 diabetes (T2D) is far more common than type 1 diabetes, comprising approximately 85% of diabetes cases. In T2D, hyperglycemia results as a consequence of increased tissue insulin resistance coupled with a decline in β-cell islet secretory function(12). An earlier, clinically recognized state of T2D is prediabetes, which is characterized by peripheral insulin resistance, hyperglycemia and elevated insulin levels (hyperinsulinemia)(12).

As diabetes is a condition distinguished by chronic hyperglycemia, diagnosis can be made primarily by measuring blood glucose levels. Diabetes is diagnosed when fasting plasma glucose is ≥ 7.0 mM or when plasma glucose is ≥ 11.1 mM 2 hours after ingestion of a 75 g oral glucose load(13). Additionally, a diagnosis can also be made if glycated haemoglobin (HbA1c) levels are ≥ 6.5% of total hemoglobin levels. HbA1c levels reflect the average blood glucose concentrations over several weeks and thus provide a more stable readout of blood glucose levels compared to the other listed measurements(13).

Prediabetes can be diagnosed when fasting plasma glucose is between 6.1-6.9 mM or when plasma glucose is ≥ 7.8 mM, but less than 11.1 mM 2 hours after ingestion of a 75 g oral glucose load or when HbA1c levels are between 6.0-6.4%(13).

1.2.3 Current treatment and management options

An effective strategy for managing the complications from diabetes begins with lifestyle changes, either by decreasing calorie consumption and reducing obesity and/or via increasing energy expenditure through exercise(14). In addition to lifestyle changes, several oral antidiabetic medications were developed to control blood glucose levels. For individuals with type 2 diabetes,

the first-line drug prescribed for all age groups is the biguanide, metformin. Metformin primarily acts on the liver and activates adenosine monophosphate-activated protein kinase (AMPK) to promote glucose uptake and suppress hepatic glucose production(15,16). If HbA1c levels persist above 7.5% with metformin, typically a second medication is required, for example insulin secretion stimulators (e.g. incretin mimetics, sulfonylureas) and inhibitors of glucose reabsorption in the kidney (sodium-glucose cotransporter inhibitors)(13). If HbA1c levels are greater than 8.5%, insulin therapy can be used in combination with metformin and/or second-line drugs to achieve stable, acceptable blood glucose levels(13).

1.2.4 Etiology: The role of lifestyle, genetics and environmental factors

The risk of developing T2D is strongly influenced by three factors: lifestyle, environment and genetics.

A landmark study by Hu et al.(17) in 2001 suggested that the incidence of T2D could be lowered by the adoption of a healthier lifestyle. The most important predictor of T2D development was increased body mass index (BMI), with overweight or obese individuals having the highest risk. When compared to individuals with a BMI of <23, overweight (BMI between 25.1 and 29.9), obese class I (BMI between 30-34.9) and obese class II and III (BMI ≥ 35) individuals had a 7.6, 20.1 and 38.8 fold higher risk of developing diabetes(17). Subsequent studies have since demonstrated that increased visceral obesity and/or ectopic liver fat accumulation (steatosis), rather than BMI correlate best with risk of T2D development(18,19). Further risk factors for T2D include a lack of exercise, a poor diet high in carbohydrates, smoking and sleep deprivation(14,17).

In addition to lifestyle impacting T2D development, the environment also plays a crucial role. Epidemiological studies have shown an association between increased exposure to noise (>10 decibels over control)(20), airborne particular matter (≥10 $\mu g/m^3$)(21) or living on a busy residential road with T2D(22). The mechanisms underlying these associations are unclear, but

have been suggested to be related to stress and sleep disturbances(21, 22). Furthermore, stress due to work or 'burning out' were also reported to have a significant association with developing diabetes later in life(23,24).

Finally, the introduction of genome-wide association studies (GWAS) has allowed for the discovery of polymorphisms or loci that are tied to increased risk of developing T2D. To date, roughly 139 common variants and 4 rare variants have been associated with T2D(25). Variants code for genes that have broad functions, including those involved in β-cell function, adipocyte differentiation or glucose uptake(26). Moreover, T2D associated variants have also been shown to have effector roles on transcripts. For example, the *FTO* locus is the first and one of the best-known variants associated with obesity, with most focus placed on the *FTO* gene itself(27). However, it is now understood that the FTO locus can act as a long range enhancer of the Iroquois homeobox 3 gene (IRX3), with obesity-inducing variants reducing energy expenditure(28).

1.3. Peripheral Maintenance of Glucose Homeostasis and Deregulation in Obesity-Induced Insulin Resistance

The pancreas is exquisitely sensitive to changes in nutritional status and increases insulin secretion in response to a corresponding increase in blood glucose(4). Several peripheral tissues, including the liver, skeletal muscle and adipose tissue play a critical role in maintaining glucose homeostasis, primarily due to their responsiveness to insulin. The presence of obesity-induced insulin resistance can disrupt this delicate balance to maintain euglycemia and can ultimately lead to hyperglycemia and diabetes.

1.3.1 Liver

Insulin is secreted into the portal vein; therefore, the liver is exposed to higher insulin concentrations than other peripheral tissues(29). In response to an increase in insulin (i.e. during ingestion of a meal or post-prandially), glycogen storage (glycogenesis) and lipid synthesis (*de novo* lipogenesis) are increased, while endogenous glucose production (hepatic gluconeogenesis

and glycogenolysis) is suppressed(30,31). When insulin levels are lower (fasting), the liver maintains euglycemia by increasing glycogen breakdown (glycogenolysis) and synthesizing glucose from non-carbohydrate sources, including lactate, glycerol and alanine, in a process known as gluconeogenesis(31,32). Non-esterified fatty acid (NEFA) production from adipose tissue during fasting can also stimulate gluconeogenesis indirectly; acetyl-CoA generated from β-oxidation serves as potent activator of pyruvate carboxylase (32).

During obesity-induced insulin resistance, suppression of hepatic glucose production by insulin becomes blunted leading to increases in blood glucose during both fasting and fed states. Furthermore, glycogen metabolism is disrupted, with decreased glycogen synthesis and increased glycogenolysis seen during fed and fasting conditions, respectively(30,32,33). Taken together, increased glucose secretion from the liver can promote hyperglycemia and contribute to T2D.

1.3.2 Skeletal Muscle

The skeletal muscle is the primary site of insulin-stimulated glucose uptake, accounting for 75-80% of glucose disposal during hyperinsulinemic-euglycemic clamps and 25-30% of glucose disposal following a meal(34,35). Imported glucose is mainly shunted towards glycogenesis (~75%), although a significant portion is also oxidized due to increased flux(34,36,37). Fasting induces glycogenolysis of skeletal muscle stores to provide glucose to muscle for oxidation, along with glucose produced through hepatic gluconeogenesis(34,37).

Skeletal muscle insulin resistance results in reductions in insulin-stimulated glucose uptake and glycogen synthesis. Because skeletal muscle plays a major role in glucose disposal, muscle insulin resistance is believed to be the primary defect in T2D that promotes hyperglycemia(34,38).

1.3.3 White and Brown Adipose Tissue

Adipose tissue can be broadly classified in two types - white adipose tissue (WAT) and brown adipose tissue (BAT). WAT primarily serves as a nutrient sink post-prandially and

provides NEFA to other peripheral tissues during fasting. Consistent with its action as an anabolic hormone, insulin has a very powerful suppressive effect on triacylglycerol (TG) lipolysis in WAT. Raising insulin to post-prandial levels in rats can reduce NEFA levels by ~90% within 5 min(39). Insulin also promotes glucose uptake in adipose tissue. Although overall glucose disposal in adipose tissue is minor (~5%) compared to skeletal muscle, it is crucial for activating *de novo* lipogenesis in adipose tissue(40,41).

The function of BAT is to generate heat via non-shivering thermogenesis(42). BAT contains an abundance of mitochondria, with high expression of a protein known as uncoupling protein 1 (UCP1) in the inner mitochondrial membrane(42). UCP1 uncouples mitochondrial respiration from ATP production. Therefore, substantial levels of nutrients are oxidized, with heat rather than ATP generated as the major byproduct(43). BAT is activated by cold exposure, sympathetic innervation and nutrient excess and can utilize a high proportion of energy intake as fuel(43). Similar to WAT and skeletal muscle, BAT can also import glucose in response to stimuli, including insulin(44).

During WAT insulin resistance, insulin's ability to suppress lipolysis is impaired, resulting in increased lipolysis during both fed and fasted states. Additionally, NEFAs secreted from WAT are used by the liver to generate precursors for gluconeogenesis. BAT insulin resistance is characterized by increased lipid accumulation, reduced expression of UCP1 and decreased systemic energy expenditure (42,44).

1.3.3.2 Adipokines and lipokines as modulators of glucose uptake and insulin sensitivity

In addition to modulating glucose homeostasis through regulation of lipogenesis/lipolysis, WAT can also secrete bioactive proteins and lipids known as adipokines and lipokines, respectively. Adipokines are involved in regulating multiple processes governing glucose homeostasis, including insulin secretion(45), inflammation(7,46,47), and insulin sensitivity(48), and have autocrine effects on adipocyte differentiation and lipolysis(8,49).

Similarly, several classes of endogenous lipokines have been shown to play a role in regulating insulin sensitivity(50,51). Advances in lipidomics and proteomics have allowed for the rapid identification of an ever-expanding list of adipokines and lipokines. Indeed, current estimates place the number of unique adipokines at over 600(5).

1.4. Insulin Signaling Pathway and Metabolic Effects

Insulin induces a broad anabolic response in multiple target tissues. Insulin signaling begins by binding of insulin to the insulin receptor on the plasma membrane of targets cells, including hepatocytes, adipocytes and myotubes. The insulin receptor is a receptor tyrosine kinase; binding of insulin to the insulin receptor induces a conformation change within the receptor and causes *trans*-autophosphorylation of several tyrosine residues on the cytosolic side(52). These phosphotyrosine binding sites allow proteins with phosphotyrosine binding (PTB) or src homology 2 (SH2) domains to be recruited to the plasma membrane(52). The best-known insulin receptor binding proteins are the insulin receptor substrate (IRS) proteins, which become tyrosine phosphorylated and thereby can recruit further downstream signaling proteins. IRS proteins recruit the catalytic and regulatory subunit of phosphoinositide-3-kinase (PI3K)(53). Binding to IRS induces a conformational change within the catalytic subunit of PI3K, freeing it from its regulatory subunit and allowing it to form the signaling lipid, phosphoinositol-(3,4,5)-triphosphate (PIP_3)(54). Generation of PIP3 allows proteins with pleckstrin homology (PH) domains to be recruited to the plasma membrane, including the critical signaling node, AKT(55).

AKT is a serine/threonine kinase that mediates many of the metabolic effects of insulin (Fig. 1). AKT itself is phosphorylated at S^{473} by mechanistic target of rapamycin complex 2 (mTORC2) and at T^{308} by 3-phosphoinositide-dependant kinase 1 (PDK1) to achieve maximal activity(55). Once activated, it promotes glucose uptake by phosphorylating and inactivating TBC1D4, which promotes translocation of glucose transporter 4 containing vesicles to the plasma membrane(56). AKT also promotes glycogen storage via inactivation of glycogen synthase kinase 3 (GSK3), which relieves inhibition of glycogen synthase(57). AKT directly suppresses

gluconeogenesis in the liver by phosphorylating the transcription factor, forkhead box O1 (FOXO1), which causes its exclusion from the nucleus(4). The gluconeogenic program further relies on the cyclic adenosine monophosphate (cAMP)-response element binding protein (CREB)-CREB-regulated transcriptional coactivator-2 (CRTC2) program to enhance the expression of gluconeogenic genes during fasting; AKT regulates CRTC2 indirectly by activating salt-inducible kinase 2 (SIK2), which phosphorylates CRTC2 and excludes it from the nucleus(58).

Insulin-induced activation of protein synthesis involves activation of mTORC1, which occurs through AKT-mediated phosphorylation of tuberous sclerosis complex 2 (TSC2) and/or proline-rich AKT substrate of 40 kDa(59,60). AKT suppresses lipolysis in adipose tissue by phosphorylating phosphodiesterase 3B (PDE3B), which degrades cAMP to attenuate protein kinase A (PKA)-mediated pro-lipolytic signaling(61). PKA targets include hormone sensitive lipase (HSL) and the lipid droplet coat protein, perilipin 1(62). In coordination with suppression of lipolysis, insulin promotes lipogenesis directly via activation of lipogenic transcription factors, such as sterol regulatory element binding protein 1 (SREBP1) and carbohydrate responsive element binding protein (chREBP)(4,40).

1.5. Mechanisms of Insulin Resistance

Insulin resistance has a very complex etiology, with several tissue and/or cellular factors that can promote its development. These include hyperinsulinemia, lipotoxicity, endoplasmic reticulum (ER) stress, inflammation, fibrosis, and mitochondrial dysfunction (Fig. 1.2).

1.5.1 Hyperinsulinemia

Hyperinsulinemia is a primary hallmark of obesity and insulin resistance. It was originally thought to be a compensatory response to insulin resistance; however, it has been recently suggested that chronic hyperinsulinemia promotes insulin resistance (63). In support of this, mice that express 50% less insulin are protected from diet-induced obesity and hepatic

steatosis(64). These mice have increased energy expenditure with similar food intake, in part by increased adipose tissue innervation and expression of uncoupling protein 1 (UCP1)(64). Hyperinsulinemia can also increase adipose tissue inflammation in obese mice(65). A second potential mechanism by which hyperinsulinemia promotes insulin resistance is through increased ligand-induced internalization and reduction of the number of insulin receptors at the plasma membrane. Once internalized, the insulin receptor is degraded in the lysosome or recycled to the cell surface(52).

1.5.2 Inflammation

Since the original discovery that the pro-inflammatory cytokine, tumor necrosis factor α (TNFα), is increased in the adipose tissue of obese-insulin resistant humans and mice, numerous studies have strongly associated inflammation with insulin resistance(66,67). Inflammatory signaling is mediated by four major signaling pathways in insulin resistance: 1. IκB kinase-Nuclear factor kappa-light-chain-enhancer of activated B cells [IKK-NF-κB]; 2. c-Jun N-terminal kinase (JNK); 3. The inflammasome, including nucleotide-binding domain, leucine-rich-containing family, and pyrin domain-containing-3 (NLRP3); 4. Janus kinase-signal transduction and activation of transcription (JAK-STAT)(68).

Several factors can induce an inflammatory response *in vitro* and/or *in vivo*, including elevated levels of circulating cytokines and macronutrients such fatty acids (FA) and glucose. In addition to TNFα, several other pro-inflammatory cytokines are increased during insulin resistance, including but not limited to interleukin-6 (IL-6), IL-1β and C-C Motif Chemokine Ligand 2 (CCL2)(69). These cytokines can stimulate multiple inflammatory signaling pathways and inhibit insulin signaling. For example, chronic incubation of skeletal muscle with IL-6 activates both the JAK-STAT and JNK pathways(70). JAK-STAT can inhibit insulin signaling through upregulation of suppressor of cytokine signaling (SOCS), which blocks binding of IRS1 to the insulin receptor, whereas JNK increases inhibitory phosphorylation of IRS1 at S307(70).

Saturated fatty acids (SFA), such as palmitate, can bind to toll-like receptors (TLR2/4), activate the innate immune system and induce an inflammatory response(71). SFA activate both NF-κB and JNK signaling, resulting in increased secretion of pro-inflammatory cytokines such as TNFα and IL-6(71–73). Importantly, SFA-induced inflammation can be blocked by TLR deficiency in mice(71–73). Consistent with the role of inflammation, $TLR4^{-/-}$ mice are protected from diet-induced systemic and tissue insulin resistance(71). Additionally, SFA can directly activate the inflammasome, resulting in upregulation of IL-1β, a pro-inflammatory cytokine. Similar to $TLR4^{-/-}$ mice, $NLRP3^{-/-}$ mice are protected from SFA-induced insulin resistance and inflammation(74). Apart from having an effect on inflammatory signaling, palmitate is also required for the rate-limiting step of ceramide synthesis; a diet high in saturated fats (e.g. lard-based), can increase ceramide accumulation significantly, further linking increased SFA to lipotoxicity and insulin resistance(75).

Hyperglycemia, which is the defining characteristic of insulin resistance and T2D, can also induce an inflammatory response. Differentiation of 3T3-L1 adipocytes under hyperglycemic conditions (25 mM glucose) is associated with insulin resistance and increased secretion of pro-inflammatory IL-6 secretion when compared to low glucose concentrations(76,77). In this study, hyperglycemia was associated with an increase in phosphorylation of IRS1 at S307; although not examined explicitly, this is a well-known inhibitory phosphorylation site that is targeted by JNK(76,78).

1.5.3. ER Stress

Disturbances in ER function can lead to ER stress, accumulation of unfolded proteins and activation of the unfolded protein response (UPR). The UPR involves activation of three major branches: 1. Inositol-requiring enzyme 1 (IRE1), which activate the transcription factor X-box binding protein 1 (XBP1); 2. Activating transcription factor 6 (ATF6); 3. Protein kinase RNA-like ER kinase (PERK). Chronic ER stress was first observed in the liver of high fat diet (HFD)-fed and leptin deficient *ob/ob* mice, concomitant with increases in UPR signaling(79). Induction

of ER stress with tunicamycin *in vitro* impaired insulin signaling through JNK mediated inhibitory phosphorylation of $IRS1^{S307}$, while pre-treatment of cells with a JNK inhibitor preserved insulin signaling(79). ER-stress mediated activation of inflammatory signaling requires involvement of some aspects of the UPR. For example, IRE1α activation is known to recruit tumor necrosis factor receptor-associated factor 2 (TRAF-2) and activate JNK(80). Concurrent knockout of IRE1α in fibroblasts treated with tunicamycin prevented JNK activation and $IRS1^{S307}$ phosphorylation(79). However, broadly reducing the functionality of the UPR can also promote insulin resistance. For example, $XBP1^{+/-}$ mice show decreased expression of ER chaperones, strong upregulation of inflammatory signaling and impaired systemic glucose homeostasis when fed an obesogenic diet(79). Taken together, current data suggest that ER stress intersects with various inflammatory signaling pathways to promote insulin resistance(81).

1.5.4. Fibrosis

The extracellular matrix (ECM) undergoes dynamic remodeling in response to tissue repair or injury. However, during obesity and insulin resistance, production of excessive connective tissue can give rise to tissue fibrosis(82). Increased level of fibrosis is observed in multiple insulin sensitive tissues, including skeletal muscle, adipose tissue and liver(83).

Transforming growth factor β (TGFβ) is a primary driver of fibrosis by activating myofibroblasts, excess production of ECM and collagen deposition and inhibition of ECM degradation(83). For example, increased TGFβ and collagen deposition are observed in the skeletal muscle of obese-insulin resistant mice and humans(84–86). Concurrently, matrix metalloproteinase activity decreases, which prevents collagen degradation(86). Several putative mechanisms have been postulated by which increased fibrosis lead to obesity-induced insulin resistance. First, fibrosis can impair vascular development and can acts as a physical barrier for diffusion of glucose and insulin(87). Reduced capillary development, which can occur in matrix metalloproteinase knockout mice, lead to the development of insulin resistance(88). Secondly, communication between the ECM and cells occurs through cell surface receptors known as

integrins and activation of the intracellular signaling molecule, focal adhesion kinase (FAK) or integrin-linked kinase (ILK)(83). Integrins may coordinate with the insulin receptor and potentiate insulin signaling. For example, ILKs can act as scaffolds for the recruitment of multiple insulin signaling proteins, including PDK1, AKT and GSK3β(89). ILK expression is also lower in HF-fed mice(89). Finally, increased fibrosis is associated with increased expression of inflammatory markers(86). Pharmacological inhibition of fibrosis using sildenafil in mice resulted in a significant decrease of pro-inflammatory markers, F4/80 and TNFα(86).

Conflicting results are produced when knocking out integrin signaling in mice. For example, muscle specific deletion of integrin β1 reduces skeletal muscle glucose uptake and systemic insulin sensitivity(90). However, whole body deletion of integrin α2 ameliorates diet-induced skeletal muscle insulin resistance and improves insulin signaling(86). Hepatocyte specific ILK deficiency ameliorates insulin resistance in HF-fed mice, suggesting that the role of ILK as molecular scaffold in insulin signaling appears more complex and requires further examination(89). Similarly, knockdown of FAK using siRNA results in a marked induction of insulin resistance in chow-fed mice, with development of hyperglycemia and hyperinsulinemia(91).

1.5.5. Mitochondrial Dysfunction and ROS

Mitochondrial dysfunction is a broad term and can encompass a variety of factors, including changes in mitochondrial number, electron transport chain complexes, mitochondrial dynamics, oxidative phosphorylation (OXPHOS), reactive oxygen species (ROS) production and/or ADP sensitivity. Mitochondrial dysfunction during obesity-induced insulin resistance has been observed in all insulin sensitive tissues, including adipose, liver and skeletal muscle(76,92,93). However, most studies linking mitochondrial dysfunction and insulin resistance have focused on the skeletal muscle.

A fundamental series of papers in the 2000s first highlighted a relationship between mitochondrial function and insulin resistance/T2D. When compared to lean, insulin sensitive

controls, the skeletal muscle of T2Ds had significantly reduced complex I activity and OXPHOS(92). Similarly, gene expression microarrays suggested that there is a coordinated downregulation of peroxisome proliferation activator receptor γ coactivator 1α (PGC1α) and nuclear receptor factor 1 (NRF1)-sensitive genes in T2D and insulin resistant individuals; overall, this results in reduced oxidative phosphorylation(94,95). Subsequent proteomic analysis of human skeletal muscle revealed similar reductions in mitochondrial proteins in obese, diabetic patients(96). Changes in expression of mitochondrial proteins were functionally associated with reduced oxidative capacity. *In vivo* magnetic resonance spectroscopy imaging of insulin resistant individuals showed a 30-40% reduction in resting ATP synthesis rates(97,98). Importantly, decreases in ATP synthesis rates were additionally associated with an 80% increase in muscle TG, although levels of diacylglycerols (DG) and ceramides were not examined(98). Mitochondria in T2Ds or insulin resistant individuals may also appear smaller and less abundant when compared to control skeletal muscles, although this has not been observed in all studies(92,99,100). When decreases in mitochondrial OXPHOS were normalized to citrate synthase activity, the differences seen in T2D vs. controls were abolished, suggesting that mitochondrial dysfunction occurs because of reduced mitochondrial content rather than an intrinsic OXPHOS defect(101,102).

A fundamental question remains whether mitochondrial dysfunction is a driver or by-product of insulin resistance. Several studies have clearly dissociated mitochondrial dysfunction from insulin resistance in skeletal muscle. For example, muscle specific transcription factor A, mitochondria (TFAM) is a key transcription factor involved in the replication and maintenance of the mitochondrial genome. Surprisingly, muscle specific TFAM knockout mice show improved insulin sensitivity when subjected to an obesogenic diet, despite marked reductions in oxidative phosphorylation capacity (103). Similarly, skeletal muscle deletion of apoptosis initiating factor (AIF), a protein required for maintaining the electron transport chain, also improves insulin sensitivity despite markedly reducing oxidative phosphorylation (104).

It is unclear when mitochondrial dysfunction develops in an obese-insulin resistant milieu. Attempts to answer this question have focused on short-term obesogenic feeding studies in mice and rats. Interestingly, mitochondrial content tends to increase or remains unchanged in response to short term HF feeding, despite the presence of systemic insulin resistance(105–110). Several mechanisms have been proposed for these short-term increases, including FFA-induced activation of peroxisome proliferator activated receptor δ (PPARδ) and PGC-1α(107–109). However, despite increases in mitochondrial content, sensitivity of mitochondria from the muscle of HF-fed mice to ADP is reduced, leading to decreased mitochondrial respiration in skeletal muscle during physiologically relevant ADP concentrations(107). Furthermore, increasing β-oxidation by a HF diet can markedly increase ROS production, as discussed below(111). In agreement with clinical observations, the majority of rodent studies suggest that more prolonged high fat feeding (> 1 month) reduces mitochondrial content and/or OXPHOS(105,110). Increased nutrient influx coupled with decreased OXPHOS could promote steatosis and inflammation, leading to or exacerbating insulin resistance.

Apart from changes in mitochondrial content (mitochondrial number or protein levels), changes in mitochondrial dynamics can also influence mitochondrial function. Mitochondrial dynamics include fission and fusion, and both are critical to maintain the mitochondrial network(112). In healthy skeletal muscle, mitochondria form a highly reticular branched network(113). However, insulin resistance has been associated with increased network fragmentation in both mice and rats(114,115). Nutrient excess and reductions in fusion proteins, including mitofusin 2 (MFN2) and optic atrophy 1 (OPA1), are seen in an obese insulin resistant milieu and induce mitochondrial fragmentation(113,115). Concomitantly, key mitochondrial fission markers, including mitochondrial fission 1 (Fis1) and dynamin related protein 1 (Drp1), are increased(115). Despite the preponderance of studies that link increased mitochondrial fragmentation with insulin resistance, genetic manipulation of mitochondrial dynamics has yielded mixed results. For example, while HFD-fed MFN2-KO fed mice show impaired AKT

phosphorylation and systemic glucose homeostasis, HFD-fed OPA1-KO mice are protected from obesity and insulin resistance, despite marked mitochondrial dysfunction(116,117).

A final major hallmark of mitochondrial dysfunction is altered ROS production. The mitochondria are a major site for ROS generation(118). Under physiologically relevant conditions, 0.1-0.2% of O_2 is reduced by an electron escaping from the ETC, resulting in the generation of a superoxide radical ($O_2^{\cdot}$-)(118). Further conversion of $O_2^{\cdot}$- yields hydrogen peroxide (H_2O_2) and hydroxyl radicals ($OH^{\cdot}$-). ROS can have many detrimental effects on cells and can cause oxidative damage to lipids, proteins and DNA(119). To combat the potentially destructive production of ROS and limit oxidative damage, cells have evolved a complex antioxidant defense system(119).

Feeding mice a HFD for as short as 3 days or adult males a single HF meal can increase the ROS emitting potential of skeletal muscle significantly, in the absence of any changes in mitochondrial respiratory function(111). FA can induce higher levels of ROS production compared to non-FA substrates at similar concentrations, and can further lead to mitochondrial fragmentation(120). Prolonged, 6-week HF-feeding in rats can significantly shift the cellular redox state towards a more oxidized state, resulting in a significant decrease in the critical antioxidant, glutathione(111). Similarly, chronic HF-feeding studies also demonstrated a significant increase in protein carboxylation, a marker of oxidative stress(107,111). Use of various antioxidants ameliorates oxidative stress and ROS production, systemic glucose intolerance and tissue insulin resistance(110,111,121,122). Mechanistically, ROS can induce insulin resistance by activating several inflammatory pathways including IL-6, JNK phosphorylation and NFκB activation(76,123). However, acute elevation in ROS production is also needed for insulin signaling, as insulin-induced increases in H_2O_2 can reversibly oxidize and inhibit phosphatase and tensin homolog (PTEN), preventing it from terminating insulin signaling(124). Therefore, ROS signaling can be adaptive or maladaptive for insulin signaling, depending on the duration, amplitude and its source of production.

1.5.6. Lipotoxicity

Lipotoxicity occurs where excess lipids accumulate (steatosis) in non-adipose tissue, such as the liver and skeletal muscle. Some of the lipids that are implicated in lipotoxicity and may be increased in obesity-induced insulin resistance in mice and humans are TG, DG and ceramides.

Liver steatosis is extremely common and is present in nearly all obese people with T2D[57]. Accumulation of TG within the liver is a particularly strong predictor of insulin resistance in humans(126,127). Consequently, reducing levels of TG in mice, either through decreased *de novo* lipogenesis or increased oxidation, leads to improvements in insulin resistance(128,129). The association between skeletal muscle TG accumulation and insulin resistance is less clear; this is exemplified by the 'athlete's paradox', where highly trained athletes have increased skeletal muscle TG levels but are highly insulin sensitive(130,131). This broadly suggests that TG accumulation may itself not be insulin resistance promoting, but is rather a marker for increased accumulation of more lipotoxic species, as discussed below.

Increases in TG accumulation are also mirrored by increases in DG in the liver and skeletal muscle during obesity-induced insulin resistance(132). Clinically, levels of hepatic and skeletal muscle DG positively correlate with homeostatic model assessment of insulin resistance (HOMA-IR) measurements(133). DG are well known to recruit and activate classical (α, β, γ) and novel protein kinase C (PKC) (δ, ε, θ, η) isoforms to the plasma membrane, which can then activate several signaling pathways(134). In particular, several studies in mice and humans suggest that PKCε is the primary isoform recruited to the plasma membrane in response to insulin-resistance-inducing stimuli(135,136). PKCε can inhibit insulin signaling though inhibitory phosphorylation of the insulin receptor at Thr^{1160}, which maps to its activation loop(135,136). In skeletal muscle both PKCθ and PKCε are recruited to the plasma membrane and activated in response to increased DG(137,138). Interestingly, PKCθ is thought to inhibit insulin signaling in the muscle by phosphorylating IRS1 at Ser^{1101}, rather than by targeting the insulin receptor(139).

In addition, PKCθ has been reported to phosphorylate PDK1, which reduces AKT^{T308} phosphorylation and insulin signaling.

Ceramides are an additional class of lipids that are strongly associated with the development of insulin resistance. Overall ceramide levels are increased in many rodent models of diet-induced obesity(140–142). Similar associations have been shown clinically, with levels of skeletal muscle, adipose tissue and liver ceramides all positively correlating with HOMA-IR measurements(133,143,144). Interestingly, increases in the levels of 16:0 and 18:0 ceramides alone positively correlate with HOMA-IR in skeletal muscle of humans(145). In agreement with the insulin resistance promoting effect of ceramides, blocking ceramide biosynthesis *in vivo* using myriocin ameliorated the presence of obesity-induced insulin resistance in mice(140). Initial *in vitro* studies using short-chain ceramides in skeletal muscle cell lines demonstrated that these lipids induce insulin resistance primarily through inhibition of AKT via two mechanisms. First, ceramides increase protein phosphatase 2A (PP2A) activity, resulting in AKT dephosphorylation (146). Second, ceramides through the atypical PKCζ isoforms block translocation of AKT to the plasma membrane by interacting with AKT's PH domain(147). This interaction appears to be specific for AKT, as recruitment of PDK1 to the plasma membrane is unaffected(147). Taken together, these data suggest that ceramides can reduce activation of the insulin signaling pathway at the point of AKT. Ceramides are also strong inducers of inflammatory signaling, as discussed in section 1.5.6.

Most of the research on lipotoxicity and insulin resistance has focused on intracellular accumulation of TG, DG and ceramides and the signaling pathways they activate. However, extracellular lipids, such as SFA, can also be potent signaling molecules that induce insulin resistance(73). We will now focus on another potentially toxic extracellular lipid that has recently been implicated in obesity-induced insulin resistance.

1.6 Lysophosphatidic Acid (LPA) - a Potent Signaling Lipid/Lipokine

As illustrated above, the etiology of insulin resistance is very complex. Understanding and characterizing how insulin resistance develops is key to its treatment and prevention of T2D. In particular, one fascinating and ever-expanding area of interest is how adipokine/lipokine secretion changes during the development of insulin resistance and how this influences systemic and tissue insulin sensitivity. I will now focus my thesis on lysophosphatidic acid (LPA), a bioactive lipid that has been relatively newly implicated in obesity-induced insulin resistance, and the adipokine that produces the majority of LPA, ATX.

1.6.1 Synthesis and Degradation of LPA

Due to its potent bioactive nature, LPA levels are tightly regulated. Circulating, extracellular LPA can be generated through two distinct enzymatic mechanisms (Fig. 3). In the first, phosphatidic acid (PA) is converted to LPA through the actions of group IIA secretory phospholipase A_2 ($sPLA_2$-IIA) or membrane-bound PA-selective PLA_1 (mPA-PLA_1)(148,149). PA itself can be presented at the cell surface through phospholipid scrambling or generated extracellularly via phospholipase D-mediated cleavage of phosphatidylcholine (PC)(148,149). The second major mechanism of LPA synthesis involves the conversion of PC to lysophosphatidylcholine (LPC) through the actions of lecithin-cholesterol acyltransferase (LCAT) or $sPLA_2$-IIA(149). LPC can then be hydrolyzed to form LPA through the activity of the lysophospholipase D, ectonucleotide pyrophosphatase/phosphodiesterase 2 (ENPP2), an enzyme more commonly referred to as autotaxin (ATX)(150,151).

Several lines of evidence suggest that the ATX-mediated mechanism of LPA synthesis produces the majority of extracellular LPA in vivo. LPA formation is significantly restricted in plasma samples of LCAT-deficient patients(149). More strikingly, LPA levels closely correlate with ATX protein content and/or activity. Heterozygous whole body ATX knockout ($ATX^{+/-}$) and fat-specific ATX knockout ($FATX^{-/-}$) mice have approximately 50% and 40% less circulating

LPA than wild type mice, respectively(8,151–154). Inducible whole-body deletion of ATX in adult mice, resulting in ~80% reduction of ATX mRNA levels and plasma ATX activity, was similarly associated with a ~60% decrease in plasma LPA(155). Pharmacological inhibition of ATX, through the use of potent inhibitors such as PF-8380, led to a >95% decrease in plasma LPA(155,156). Conversely, overexpression of ATX in mice corresponded with increased circulating LPA levels(8,152,157).

The major route for LPA degradation involves its dephosphorylation to monoacylglycerol (MAG) through mammalian lipid phosphate phosphatases (LPP) (Fig. 3)(158,159). There are three enzymes characterized in this family: LPP1 [*PPAP2A*], LPP2 [*PPAP2C*] and LPP3 [*PPAP2B*](160). Knockdown of LPP1 in mice increased circulating LPA levels and extended the half-life of injected LPA 4-fold, with no obvious effect on phenotype(161). In contrast to LPP1 deficient animals, LPP3 knockout mice are not viable, due to their inability to form a chorio-allantoic placenta and vascular defects in the yolk sac(162). Culture of embryonic mouse fibroblasts lacking LPP3, however, resulted in a ~2.5-fold increase in extracellular LPA(162). LPP2 mice are viable with no overt phenotype, although levels of LPA were not reported(163). LPP2 may play a specific role in regulating the timing of cell cycle progression, as increasing LPP2 activity in fibroblasts led to the premature entry of cells into the S-phase of the cell cycle and decreased proliferation rate(164,165). LPP2 did not influence levels of LPA in these fibroblast models, suggesting that the effects of LPP2 modulation on cell cycle progression are not due to changes in LPA degradation(163). Taken together, these findings suggest that LPPs may play unique, isoform specific roles in regulating circulating LPA levels during development and post-natal life. Apart from degradation of LPA through LPPs, LPA is also cleared from circulation by nonparenchymal cells in the liver(166). Intravenously administered LPA rapidly accumulated in the mouse liver and ligation of the hepatic circulation blocked the clearance of LPA, suggesting that uptake of LPA by liver cells is an important mechanism for the regulation

of circulating LPA levels and contributes significantly to the short half-life [< 30s] of LPA in the blood stream(166).

1.6.2 Sources of Circulating LPA

LPA is primarily bound to serum albumin in the blood stream with reported concentrations of up to 1 μM in plasma and >10 μM in serum, demonstrating that LPA levels can vary greatly dependent on factors such as nutritional status and clotting (Fig. 4)(167). During clotting, platelets produce a significant amount of LPA. This is exemplified by a study showing that administration of an anti-platelet antibody in rats reduces serum LPA levels by almost 50%(149). Similarly, pharmacological inhibition of platelet aggregation using an integrin αIIbβ3 antagonist reduced circulating LPA levels by 70% in a mouse model of metastatic breast cancer(168). In addition to platelets, circulating lipoproteins serve as a source of LPA, particularly when subjected to oxidation. For example, it has been shown that the production of LPA from oxidatively modified low-density lipoproteins via ATX is critically required for monocyte recruitment and promotion of atherosclerosis(169). Moreover, ATX activity is associated with lipoprotein[a], which transports oxidized phospholipids and LPC generated by lipoprotein-associated PLA_2, suggesting that lipoprotein[a] also constitutes a source of LPA(170,171). Interestingly, a recent study demonstrated that exosomes may serve as a vehicle and/or delivery system for ATX-LPA (Fig. 4)(172). Packaging of LPA in exosomes may be a means by which LPA is delivered to target tissues and cells for signaling and could potentially increase the stability of circulating LPA. It remains to be determined whether LPA present in exosomes significantly contributes to circulating LPA levels in vivo and whether the concentration of LPA in exosomes changes during disease states. Moreover, future studies should investigate whether LPA derived from different sources varies in fatty acid composition and signaling properties.

1.6.3 Influence of Diet on LPA

Marked changes in ATX-LPA levels are associated with many physiological and pathophysiological processes including development, cell differentiation, cancer, atherosclerosis, myocardial infarction, and have also been linked to alterations in the nutritional status(154,173–175). Circulating LPA, along with ATX, are regulated by feeding-fasting, with higher levels of ATX-LPA detected in the fed vs. fasted state in animal models(176,177). In addition to acute nutritional regulation of ATX-LPA, several studies showed that chronic overfeeding of animal models with obesogenic diets results in altered circulating LPA levels. Feeding male FVB mice a HFHS, 45% kcal fat, 17% kcal sucrose diet for 13 weeks elevated plasma LPA levels by 62%(178). Increases in plasma LPA were also noted in male C57Bl6/J mice fed a HFHS diet or high fat diet [60% kcal fat, no added sucrose] for a shorter period of 9 and 8 weeks, respectively(179,180). Similarly, female low density lipoprotein receptor-null ($LDLR^{-/-}$) mice had increased unsaturated, but not saturated levels of LPA in the small intestine following consumption of a Western diet [42% kcal fat, 34% w/w sucrose, 0.2% w/w cholesterol] for only 3 weeks, which was also paralleled by an increase in 20:4 LPA in plasma(181). Since LPA content in the Western diet was lower than in the control chow diet and animals were fed the same amount [by weight] of diet, increased intestinal LPA in mice fed a Western diet is unlikely the result of higher consumption of preformed LPA(181). Taken together, these studies suggest that the consumption of a fat-rich diet leads to increased circulating levels of LPA in mice of different genetic backgrounds. While reports on LPA measurements in humans are limited, a very recent study showed that plasma LPA positively correlates with BMI, an indicator of nutritional imbalance(182). The same study also suggested that fasting has a marginal effect on circulating LPA concentrations in humans, although these data have not been adjusted for sex - LPA levels are higher in women compared to men - and the exact duration of fasting is unclear(182).

Although the precise mechanisms underlying the dietary regulation of LPA levels remain to be uncovered, it is possible that higher dietary content of preformed LPA contributes to

variations in circulating LPA levels. LPA has been detected in several plant and animal foods, including eggs(183), cabbage leaves, broccoli(184), soybeans, and sunflower seeds (Fig. 4)(185). Dietary LPAs, especially those containing mono- and poly-unsaturated fatty acids, appear to be well-absorbed in the mouse and rat intestine(181,186). Interestingly, however, a standard chow diet contains higher levels of preformed LPA than a Western diet, suggesting that increases in circulating and intestinal LPA in $LDLR^{-/-}$ mice following Western diet feeding were not due to increased absorption of preformed LPA(181). Therefore, it is plausible that obesogenic, lipid-rich diets increase LPA levels in vivo via a more indirect mechanism, e.g., by influencing levels of LPA precursor lipids [see above]. For example, PA can be converted to LPA by pancreatic phospholipase A_2 mediated hydrolysis. Since levels of preformed PA were much lower than levels of intestinal LPA in Western diet-fed $LDLR^{-/-}$ mice, this mechanism does not appear to significantly contribute to increased LPA content in this mouse model either(181).

However, compared to chow-fed mice, Western diet-fed $LDLR^{-/-}$ mice showed a 8- and 10-fold increase in intestinal and plasma LPC content, respectively(187), although preformed LPC or PC levels were similar or lower in the Western vs. chow diet(181,187). This suggests that increases in LPC content may underlie the Western diet-induced upregulation of LPA. Within the enterocyte, LPC can be converted to LPA via ATX-mediated hydrolysis(174). Interestingly, inhibition of ATX using PF-8380 only significantly decreased levels of unsaturated LPA in the jejunum, liver and plasma of male $LDLR^{-/-}$ mice fed chow diet supplemented with oleoyl-LPC [18:1 LPC], suggesting that saturated LPA is formed by an ATX-independent mechanism in the intestine(174).

The third, and perhaps most prominent mechanism by which diet can modulate LPA levels is through the upregulation of ATX. Prior studies using mice with high fat diet-induced obesity show increased ATX mRNA and protein expression in adipose tissue, a major source of circulating ATX(178,180); this is also reflected by increased circulating ATX and/or serum ATX activity in obese mice, which correlates well with increases in LPA(176,180). On the other hand,

a study by Nishimura *et al.*(8) showed that an obesogenic diet decreases ATX levels in adipose tissue and circulation. The reason for this discrepancy between studies is not immediately clear since only minor differences in experimental conditions are evident. Therefore, future studies need to clarify precisely how diet-induced obesity is linked to changes in ATX-LPA.

1.6.4 LPA Receptors and Downstream Signaling

LPA is a very potent signaling molecule, capable of activating a variety of signaling pathways via binding to six identified LPA receptors (LPA1-6) (Fig. 5)(167) LPA1-3 show sequence similarity to the endothelial differentiation gene family, while LPA4-6 are members of the purinergic family (167). All LPA receptors are class A rhodopsin-like GPCRs which transmit extracellular binding of LPA to intracellular signaling, via the activation of Gα proteins (167).

LPA is found in virtually all biological fluids and through LPA1-6 can influence cell proliferation and growth, cell survival, development, and calcium dynamics(167). The diversity of cellular responses to LPA is likely a result of the different expression patterns of LPA receptors. For example, while all six LPA receptors were expressed in the murine and human heart and cardiomyocytes, LPA3 mRNA was undetectable in murine cardiomyocytes and human subcutaneous adipose tissue(188).

However, a comprehensive understanding of LPA receptor expression at baseline and under pathophysiological conditions is still lacking in many tissues. This is exemplified by a study showing the presence of LPA1, 3 and 4 in mouse skeletal muscle, while it remains unclear whether LPA5 and 6 are present in this tissue(189). The importance of LPA receptors in disease has been underscored by studies linking aberrant LPA signaling to a broad range of pathophysiological conditions, including cancer, arthritis, pulmonary fibrosis, neurological disorders, and obesity-induced insulin resistance and impaired glucose homeostasis(167,173,190,191). LPA receptors have also emerged as promising drug targets. Indeed, modulators targeting LPA1-3 have passed clinical trials assessing their ability to treat

idiopathic pulmonary fibrosis and systemic sclerosis, suggesting that LPA receptor inhibitors could be used for the treatment of inflammatory diseases(192).

1.7 Structure and Activity of Autotaxin (ATX), an Adipokine that Produces LPA

As mentioned, ATX-mediated LPC hydrolysis is the major mechanism by which circulating LPA is produced(155,193). Increases in ATX expression markedly increase LPA levels and thus significantly influence LPA signaling in tissue.

ATX belongs to a family of ectonucleotide pyrophosphatase/phosphodiesterases (ENPP), of which there are seven members. ATX is the only member that shows lysophospholipase D activity; other ENPP members primarily act as nucleotide pyrophosphatases, ectophospholipase C and sphingomyelinases(194). ATX is structurally similar to ENPP1/3 and is defined by 2 N-terminal somatomedin B (SMB) domain, a central phosphodiesterase (PDE) domain and a C-terminal inactive nuclease (NUC) domain(195,196). ATX also has a large, lasso loop domain, which wraps around the PDE and NUC domains and maintains the structural integrity of the enzyme(195,196). What makes ATX a unique lysophospholipase D is the evolutionarily driven deletion of an 18 amino acid sequence within its central phosphodiesterase domain, which creates a deep lipid binding site(195,196).

Interestingly, crystal structures of ATX have revealed that the active site is organized in a tripartite, T-junction. One end of the T-junction contains the catalytic site, which is mediated by a single threonine residue and coordinated by 2 Zn^{2+} ions(195–198). The two other ends of the T-junction contain the hydrophobic pocket, which accommodates the acyl chain and an open tunnel, which is thought to release the product LPA(198).

1.7.1 Expression, Processing and Secretion of ATX

There are 3 major isoforms of ATX, named ATXα, ATXβ and ATXγ. ATXβ is the canonical ATX isoform, is ubiquitously expressed and is the most highly expressed isoform in the periphery and in circulation (199). ATXα is also ubiquitously expressed but is less abundant than

ATXβ. The α isoform has a 52 amino acid insertion in the PDE domain that confers specific binding to cell-surface heparin sulfate proteoglycans(200). ATXγ is only expressed in the brain and is characterized by a 21 amino acid insertion within the NUC domain. This insertion contains a modulator of oligodendrocyte remodeling and focal adhesion organization (MORFO) domains and is required for mediating anti-adhesive properties of oligodendrocytes(201).

ATX is synthesized as a pre-pro-enzyme and the vast majority (>95%) is secreted once proteolytically cleaved. The pre-pro-enzyme has a 27 amino acid N-terminal signal sequence that targets ATX to the classical secretion pathway and is cleaved via signal peptidases(202). The pro-enzyme is then processed by furin proteases, which is required for increased activation of ATX(202). ATX is also glycosylated at five aspartate residues; in particular, glycosylation at Asn-524 is structurally important and critical for ATX activity(203).

1.8. ATX-LPA Signaling in Obesity-Induced Insulin Resistance

In humans, the relationship between ATX-LPA and obesity remains somewhat unclear. In severely obese women [BMI 35.0-64.5], serum ATX did not correlate with markers of obesity, including weight, BMI or waist circumference(204). However, ATX mRNA was significantly increased in the visceral adipose tissue of massively obese female patients [BMI > 40.0] compared to non-obese controls [BMI < 25.0](153). Moreover, serum ATX correlated with both BMI and waist circumference in older, overweight or obese patients [BMI: 25.0-37 kg/m^2](205). Consistent with these data, 16:0 LPA was significantly increased in obese [BMI > 30.0] individuals compared to individuals with normal BMI [BMI 18.5-25.0](206). On the other hand, a different study showed that ATX levels in subcutaneous adipose tissue and serum negatively correlate with BMI, respectively(8). Notably, these data were not normalized to sex and the study population consisted almost exclusively of individuals with normal BMI or pre-obesity with less than < 1% individuals being obese based on BMI(8).

Overall, evidence to date suggests that tissue ATX expression and circulating ATX-LPA levels may not correlate well with parameters of obesity across different study populations. Our understanding of the relationship between the ATX-LPA pathway and obesity could be improved by examining circulating LPA levels in human cohorts, in addition to ATX expression and activity. A recent study by Brown et al. demonstrated that mRNA levels of distinct LPA receptors in insulin sensitive mouse and human tissues are associated with obesity(188). For example, LPA4, LPA5 and/or LPA6 were significantly increased in myocardial tissue and cells from HFHS-fed mice and humans with pre-obesity or obesity(188). These data suggest that changes in tissue LPA receptor expression may also contribute to alterations in ATX-LPA signaling during obesity.

1.8.1. ATX-LPA Signaling Promotes Preadipocyte Proliferation, while the Effect on Adipocyte Differentiation is Unclear

Adipocyte hyperplasia and hypertrophy are two mechanisms by which adipose tissue expands during development and obesity(207). Through autocrine and paracrine signaling, the ATX-LPA axis is believed to influence both processes and play a key role in altering adipose tissue biology and metabolism during obesity. The effect of ATX-LPA signaling on adipose tissue has been examined predominantly using preadipocyte models (Table 1). Preadipocytes secrete low levels of ATX into the extracellular medium, which, in the presence of LPC, results in the production of minimal levels of LPA(150). Nevertheless, even low concentrations of ATX-LPA stimulate preadipocyte proliferation, as was assessed in murine 3T3-L1 and 3T3-F442A preadipocytes, and primary Pref1+ CD34+ adipocyte progenitors, exposed to exogeneous ATX or LPA, consistent with the well-known mitogenic effect of LPA(8,208–210).

In agreement with these observations, mice with adipose-specific ATX deficiency had significantly less preadipocytes in the stromal vascular fraction of epididymal fat pads, suggesting that ATX-LPA signaling stimulates preadipocyte proliferation in vivo(8). ATX-LPA induced proliferation of white preadipocytes appears to be primarily mediated by LPA1, a major LPA receptor in Pref1^{+} CD34^{+} adipocyte progenitors, and possibly ras-mitogen activated protein

kinase (MAPK)(8,208,209,211). Interestingly, although knockdown of LPA1 diminished preadipocyte proliferation induced by LPA, it only resulted in partial reduction of ATX-induced proliferation, suggesting that ATX can promote preadipocyte proliferation independent from LPA-LPA1(8). Whether ATX influences preadipocyte signaling and metabolism in an LPA-independent manner is unclear, but may involve binding to heparin sulfate proteoglycans or integrins (190, 194). Contrary to the ATX-LPA-induced proliferation of white preadipocytes, neither LPA nor ATX inhibitors appeared to influence proliferation of primary murine brown preadipocytes(212), suggesting that the ATX-LPA pathway stimulates preadipocyte proliferation specifically in white preadipocytes.

While overwhelming evidence points towards a pro-proliferative effect of LPA in white preadipocytes, studies examining the role of LPA signaling in preadipocyte differentiation produced more ambiguous results (Table 1). Notably, levels of ATX mRNA and secreted ATX protein and activity increased markedly during differentiation in 3T3-L1, 3T3-F442A, and primary preadipocytes, indicating a prominent role of ATX-LPA signaling in preadipocyte differentiation(8,150,176). Indeed, some studies have suggested that LPA is a potent suppressor of preadipocyte differentiation. Murine 3T3-F442A and 3T3-L1 preadipocytes, porcine DFAT-P preadipocytes, human Simpson-Golabi-Behmel syndrome (SGBS) preadipocytes, and primary murine white and brown preadipocytes did not differentiate into mature adipocytes as efficiently when incubated with LPA, as determined by the expression of adipogenic and lipid metabolism markers and lipid droplet/triacylglycerol accumulation(212–214).

Conversely, inhibition of ATX activity promoted the differentiation of primary murine brown preadipocytes(212). The differentiation-inhibiting effects of ATX-LPA appear to be mediated through the LPA1-dependant downregulation of peroxisome proliferator-activated receptor γ2 [PPARγ2] in preadipocytes(213,214). ATX-LPA induced downregulation of PPARγ and PPARγ-sensitive proteins was also observed in mature 3T3-L1 adipocytes(176). In agreement

with this notion, the anti-adipogenic effect of LPA was not observed in preadipocytes isolated from LPA1-knockout mice, which may underlie the increased adiposity in these mice(214).

However, a recent study showed that $Pref1^{+}$ $CD34^{+}$ preadipocytes isolated from epididymal white adipose tissue from mice with global heterozygous ATX deficiency differentiated less efficiently than preadipocytes from wild type mice, suggesting that the ATX-LPA pathway promotes preadipocyte differentiation (Table 1)(8). It is possible that constitutive ATX deficiency and reduced LPA levels during and after development alter the adipogenic potential of preadipocytes in vivo. Indeed, the expression of adipogenic genes was reduced in preadipocytes from $ATX^{+/-}$ and $FATX^{-/-}$ mice(8), which may explain their impaired ability to differentiate.

1.8.2 ATX-LPA in Diet-Induced Obesity

The effect of ATX-LPA in diet-induced obesity is controversial with studies showing both a pro- and anti-obesogenic effect of the ATX-LPA axis. Despite the prominent role of ATX-LPA signaling in preadipocyte proliferation and differentiation demonstrated *in vitro*, modulation of the ATX-LPA pathway *in vivo* appears to have little effect on adiposity in mice at baseline(8,178,212,214). Having said that, the profound impact of ATX-LPA signaling on adiposity becomes evident when mice are fed an obesogenic diet (Table 1). For example, administration of the LPA1/3 antagonist, Ki16425, for six weeks increased fat mass and the size of white adipocytes in HFHS-fed C57Bl6 mice(179). The same group also showed that adipose-specific ATX deletion increases white and brown adipose tissue mass in HFHS-fed mice [on a mixed FVB/Bl6 background], which was associated with upregulated mRNA levels of PPARγ and PPARγ sensitive genes, including adiponectin and leptin, predominantly in subcutaneous adipose tissue from these mice(178). Conversely, a more recent study showed that global heterozygous and adipose-specific ATX deficiency protect mice on a C57Bl6 background from diet-induced obesity while adipose-specific ATX overexpression driven from the FABP4 promoter enhanced adiposity following high fat diet feeding(8). The resistance to diet-induced

obesity in FATX$^{-/-}$ mice was ascribed to improved brown adipose tissue (BAT) function, lipid oxidation capacity, and energy expenditure(8). Similarly, overexpression of ATX driven by the α1-antitrypsin promoter in FVB/N mice, resulting in a moderate increase in circulating ATX and LPA levels in adult mice, increased weight gain and adiposity following consumption of a HFHS diet(212). This effect was linked to reduced expression of BAT-related genes, indicative of lower brown adipocyte abundance, in peripheral white adipose tissue of HFHS-fed ATX transgenic mice(212). Differences in the background strain of mice and composition of obesogenic diets may have contributed to these, in part, divergent results among studies examining the role of ATX-LPA in diet-induced obesity(8,153,176,212). Clearly, more research is needed to address the precise role of ATX-LPA signaling in diet-induced obesity.

Future studies should employ ATX/LPA receptor inhibition/deletion in adult mice before and after the induction of obesity, to determine whether the ATX-LPA pathway impacts adiposity independent of its possible effect on preadipocyte development/programming and whether increased adiposity can be reversed or ameliorated by ATX-LPA modulation.

1.8.3 The ATX-LPA Axis Impairs Glucose Homeostasis and Promotes Insulin Resistance

Most studies to date suggest that ATX-LPA-LPA1/3 signaling promotes glucose intolerance and impairs systemic insulin sensitivity and tissue insulin signaling. Subjecting ATX$^{+/-}$ and FATX$^{-/-}$ mice to an obesogenic diet resulted in improvements in systemic glucose tolerance and insulin resistance compared to wild type(8,153). Interestingly, however, overexpression of ATX in mice did not significantly alter glucose tolerance(212). A single intraperitoneal injection of a supraphysiological dose [~1.4-1.5 mM] of LPA in male chow and HFHS-fed C57Bl6 mice impaired glucose tolerance(191). These acute systemic effects appear broadly mediated by LPA1 and LPA3, as pre-injection of a dual LPA1/3 antagonist, Ki16425, negated the LPA-mediated impairment in glucose tolerance(191). Importantly, chronic treatment

with Ki16425 also improved glucose and insulin tolerance in insulin resistant HFHS-fed mice(191).

Studies in humans showed that serum ATX levels correlate with several measures of glucose homeostasis and insulin sensitivity, including fasting glucose and insulin, glucose infusion rate (GIR), and HOMA-IR in overweight or obese non-diabetic individuals(204,205). Additionally, serum ATX was found to predict measures of glucose homeostasis and insulin sensitivity in older humans(205). In agreement with these studies examining ATX protein in serum, ATX mRNA levels were significantly higher in the intra-abdominal adipose tissue of massively obese women who exhibited impaired glucose tolerance or diabetes when compared to women with normal glucose tolerance(215). Taken together, clinical evidence suggests that the ATX-LPA axis is associated with impaired glucose homeostasis and insulin resistance and that ATX-LPA may serve as therapeutic target and/or marker for obesity-related insulin resistance in humans.

While a relationship between ATX-LPA and systemic glucose homeostasis has been well established (Table 1), the underlying mechanisms and effect of ATX-LPA signaling on tissue insulin function and metabolism are less well understood. Improved glucose tolerance in HFHS-fed mice subjected to chronic [3 weeks] administration of a LPA1/3 antagonist was associated with metabolic changes in multiple insulin sensitive tissues, including increased glycogen storage in the liver, glucose oxidation in skeletal muscle, and pancreatic islet mass(191). Increased hepatic glycogen synthesis was paralleled by reduced mRNA expression of enzymes involved in gluconeogenesis, including glucose-6-phosphatase and phosphoenolpyruvate carboxykinase, in HFHS-fed mice treated with LPA1/3 antagonist(191). In agreement with these findings, incubation of primary hepatocytes with LPA for 5-12 h led to inhibition of insulin-stimulated glucokinase expression and glycogen synthesis, effects that were mediated primarily by LPA3(206). In 3T3-L1 adipocytes, a more chronic [16 h] incubation with LPA impaired insulin signaling, as determined by reduced AKT phosphorylation(180). However, a 24-h inhibition of

ATX activity using PF-8380 did not alter insulin-stimulated AKT phosphorylation in insulin sensitive or insulin resistant 3T3-L1 adipocytes(176). Few studies have examined the effect of very acute stimulation with LPA on the cellular insulin signaling pathway with conflicting results; pre-incubation of primary rat hepatocytes with LPA for 15 min impaired insulin-stimulated AKT phosphorylation(206) while a 10-min incubation with LPA promoted increased AKT phosphorylation, GLUT4 translocation to the plasma membrane, and 2-deoxyglucose uptake in 3T3-L1 and L6-GLUT4myc myotubes at baseline, although the effect of LPA on insulin stimulated cells was not examined(216).

Future studies should clarify the precise molecular mechanisms by which the ATX-LPA pathway influences glucose homeostasis and insulin signaling in vivo and in vitro and examine the role of individual LPA receptors in this process.

1.9. Potential Mechanisms by Which The ATX-LPA Axis Promotes Insulin Resistance

The majority of studies examining ATX-LPA signaling in the development of insulin resistance have focused on the adipose tissue. However, as a circulating factor, ATX and LPA can influence insulin signaling in other key tissues, such as skeletal muscle and liver. In particular, the skeletal muscle is critical for insulin stimulated glucose uptake and can drive hyperglycemia, the defining characteristic of insulin resistance and diabetes. Identifying whether ATX-LPA acts as novel factors in promoting insulin resistance in this tissue is paramount to truly defining the role of this signaling axis in the etiology of this metabolic disorder.

1.9.1. ATX-LPA Signaling Upregulates Pro-Inflammatory Transcription Factors

Local and systemic inflammation constitute an important mechanism by which the ATX-LPA pathway promotes insulin resistance. As discussed above, inflammation is a major mechanism by which tissue and systemic insulin resistance can develop. Increased ATX-LPA signaling has been linked to inflammation and inflammatory disorders including rheumatoid

arthritis and hepatitis (Fig. 6)(190,217). Exposure of 3T3-L1 and 3T3-F442A adipocytes to the inflammatory cytokines, IL6 and TNFα, leads to the upregulation of ATX mRNA(180,215). Similarly, inhibiting the pro-inflammatory transcription factor NFκB in 3T3-L1 adipocytes downregulated ATX mRNA(180). ATX is not only stimulated by inflammation but appears to enhance inflammation in a feed-forward mechanism. FATX$^{-/-}$ mice show a significant decrease in adipose tissue and circulating levels of IL-6, TNFα, and MCP-1(8). Overexpression of ATX driven by the α1-antitrypsin promoter did not systemically alter IL-6 and TNFα(212). Although circulating ATX and LPA were elevated in this mouse model, adipose tissue levels of LPA were unchanged, suggesting that the ATX-LPA-induced stimulation of inflammatory cytokines is primarily due to enhanced ATX-LPA signaling in adipose tissue(212). Upregulation of pro-inflammatory cytokines in response to ATX-LPA pathway stimulation likely originates from immune cells. Co-culture of 3T3-L1 preadipocytes and bone-marrow derived macrophages (BMDM) increased levels of TNFα in BMDMs; these increases were abolished by ATX knockdown in preadipocytes(8).

Similarly, incubation of adipose tissue CD8+ T-cells with recombinant ATX increased expression of CD44 and interferon-γ, which play a predominantly pro-inflammatory role(8). Importantly, IL-6 mediated lipolysis and induction of systemic insulin resistance in HFD-fed mice required ATX and LPA1/3, since administration of Ki16425 for 1 week decreased plasma free fatty acids and improved glucose homeostasis(191). More recently, modulation of ATX has been shown to influence inflammatory signalling in tissues other than the adipose tissue. Global inducible post-natal inactivation of ATX was shown to protect mice from HF-feeding induced liver steatosis and inflammation(218). Similarly, administration of the ATX inhibitor, PF-8380, was shown to attenuate HF-diet induced cardiac inflammation in mice(219).

1.9.2 ATX-LPA Upregulate Transcription Factors Implicated in Fibrosis

Increases in ATX-LPA-LPA1 signaling have been linked to multiple fibrotic diseases, including idiopathic pulmonary fibrosis(220), chronic liver diseases(173) and renal fibrosis(221).

An unbiased, microarray-based approach in brown preadipocytes revealed that ATX-LPA signaling increases the expression of proteins involved in extracellular matrix remodeling(212). Treatment of obese-diabetic *db*/*db* mice with Ki16425 for 7 weeks improved systemic insulin sensitivity, which was associated with reduced adipose tissue fibrosis(222). Exposure of human adipose tissue explants to LPA increased collagen 3 and the pro-fibrotic cytokine, TBFβ, effects that were abolished upon co-incubation with Ki16425 and were dependant on activation of hypoxia inducible factor 1α (HIF1α)(222). Interestingly, adipose tissue of HFD-fed $ATX^{+/-}$ mice did not show any significant changes in collagen 1a or 6a mRNA levels, indicating the absence of overt fibrosis(8). Taken together, these studies suggest that the ATX-LPA pathway promotes fibrosis in severe cases of insulin resistance/diabetes [e.g., db/db mice], a mechanism by which ATX-LPA may further exacerbate impaired insulin function (Fig. 6).

1.9.3 ATX-LPA Suppresses PPARγ Signaling

The ATX-LPA pathway may contribute to obesity-induced insulin resistance by impairing PPARγ expression and activity (Fig. 6). Peroxisome proliferator-activated receptor gamma [PPARγ] is a ligand-activated transcription factor that regulates various metabolic processes, including glucose and lipid homeostasis(223). There are two major isoforms of PPARγ: PPARγ1, which is widely expressed, and PPARγ2, which is primarily expressed in adipose tissue(223). A role for PPARγ in insulin resistance is evident in that several dominant negative PPARγ mutations are present in some patients with severe insulin resistance; these individuals show lipodystrophy and accumulate lipids in non-adipose tissues, such as skeletal muscle and liver (224). Thiazolidinediones [TZD], a class of drugs that activate PPARγ, are used clinically for their ability to act as insulin sensitizers(223). The mechanisms by which PPARγ and TZDs promote insulin sensitivity are complex, multifactorial, and involve several tissues(225). Interestingly, treatment of 3T3-L1 and 3T3-F442A adipocytes with the TZD, rosiglitazone, decreased ATX mRNA, protein content, and secreted ATX activity, suggesting that PPARγ inhibits ATX-LPA signaling(176,215). The mechanism by which this occurs is unknown, but

could involve a negative regulation of pro-inflammatory cytokines and transcription factors by PPARγ agonists(226,227). Conversely, the ATX-LPA axis appears to reciprocally downregulate PPARγ signaling. FATX$^{-/-}$ mice fed an obesogenic diet show increased mRNA levels of PPARγ and PPARγ sensitive genes [adiponectin, glut-1, glut-4 and leptin] in subcutaneous adipose tissue, and elevated levels of circulating adiponectin(8,178). Notably, circulating adiponectin is inversely correlated with obesity and insulin resistance and has insulin sensitizing effects on skeletal muscle and liver(228–230). Inhibition of ATX activity in 3T3-L1 adipocytes resulted in increased protein levels of PPARγ, adiponectin, CD36, and Glut-4 at baseline, but was not able to restore levels of these proteins in insulin resistant adipocytes(176). The mechanism by which this occurs remains to be elucidated. It should also be clarified whether the reciprocal negative regulation of PPARγ and inflammatory cytokines and transcription factors involve the ATX-LPA axis.

1.9.4 ATX-LPA Signaling Impairs Energy Metabolism by Inhibiting Brown Adipose Tissue Development and Reducing Mitochondrial Function

Altered energy homeostasis, signified by greater intake than expenditure of calories, is a hallmark of obesity and obesity-induced insulin resistance. BAT thermogenesis through respiration uncoupling plays a key role in regulating energy expenditure in rodents and humans(231). Studies on humans demonstrated an inverse relationship between BAT activity and obesity/BMI(232). In line with this notion, increasing BAT activity through cold acclimatization increased glucose disposal and improved insulin sensitivity(233,234). Moreover, BAT transplants in the visceral cavity of mice improved glucose homeostasis, lowered fat mass, and reversed diet-induced insulin resistance(43). These studies demonstrate that BAT activity is a primary determinant of organismal energy expenditure in rodents. ATX-LPA signaling plays a key role in adipocyte proliferation and differentiation in both white and brown adipose tissue. Inhibition of ATX activity using HA155 or PF-8389 promoted the differentiation of primary BAT preadipocytes, concomitant with UCP1 upregulation(212). Conversely, adding recombinant ATX or LPA directly to BAT preadipocytes inhibited their differentiation and decreased UCP1 and

Prdm16, a master regulator of BAT differentiation(212). Similarly, a microarray-based approach in brown preadipocytes revealed that ATX-LPA signaling downregulates proteins involved in mitochondrial function and energy metabolism. Mice with ATX overexpression exhibited a reduction in inducible BAT, UCP1, and transcriptional regulators of mitochondrial biogenesis in white adipose tissue. Interestingly, while these mice showed increased diet-induced obesity, glucose homeostasis was unchanged(212). In HFD-fed FATX$^{-/-}$ mice, improved insulin sensitivity was associated with enhanced BAT activity and energy expenditure(8). Morphologically, 70% of adipocytes from HFD-fed FATX$^{-/-}$ mice showed multiple lipid droplets, compared to 30% of adipocytes from HFD-fed WT controls, which was mirrored by increased mRNA expression of UCP1 and PGC1α, along with increased mitochondrial membrane potential in FATX$^{-/-}$ mice(8).

Overall, these data suggest that ATX-LPA signaling inhibits BAT development and function, which may promote diet-induced insulin resistance (Fig. 6). Future studies should explore how altered ATX-LPA signaling in other metabolically active tissues, including skeletal muscle, influences energetics and mitochondrial mass and function.

1.10. Concluding Statements

Insulin resistance and T2D are increasingly prevalent pathophysiological conditions. Current treatments for T2D tend to lose effectiveness in the long term, require multiple drugs and cannot fully prevent micro- and macro-vascular complications. Identifying and characterizing novel targets that are implicated in obesity-induced insulin resistance and T2D is critical to develop new and effective therapies.

The ATX-LPA pathway is a relatively novel signaling axis that is upregulated in obesity-induced insulin resistance. Several mechanisms by which this occurs have been well defined in the adipose tissue, including inflammation, fibrosis, PPARγ suppression and mitochondrial dysfunction. However, it remains unclear how ATX-LPA can affect distal tissues, including heart, liver and skeletal muscle, which is the focus of my thesis. ATX-LPA being recently

implicated in adipose tissue and systemic insulin resistance and the importance of skeletal muscle in overall glucose homeostasis make this an attractive area of research.

Figures:

Figure 1.1. AKT mediates many of the metabolic actions of insulin.

AKT is a serine/threonine kinase that has a pleiotropic effect on glucose, protein and lipid metabolism. In response to insulin, AKT is phosphorylated at S^{473} by mechanistic target of rapamycin complex 2 (mTORC2) and at T^{308} by 3-phosphoinositide-dependant kinase 1 (PDK1). Once activated, AKT promotes glucose uptake and glycogen storage, while inhibiting gluconeogenesis. AKT promotes protein synthesis through activation of mTORC1 signaling. AKT also stimulates lipid synthesis through transcriptional activation of lipogenic programs and simultaneous suppression of lipolysis. chREBP, carbohydrate responsive element binding protein; CREB-CRTC2, cAMP-response element binding protein (CREB)-CREB-regulated transcriptional coactivator-2 (CRTC2); FOXO1, forkhead box O1; GSK3, glycogen synthase kinase 3; GSV, Glut4 secretory vesicles; PDE3B, phosphorylating phosphodiesterase 3B; PGC-1α, Peroxisome proliferator activated receptor gamma coactivator 1α; PKA, protein kinase A; PRAS40, proline-rich AKT substrate of 40 kDa; SREBP1c, sterol regulatory element binding protein 1c; TBC1D4, TBC1 domain family member 4; TSC2, tuberous sclerosis complex 2.

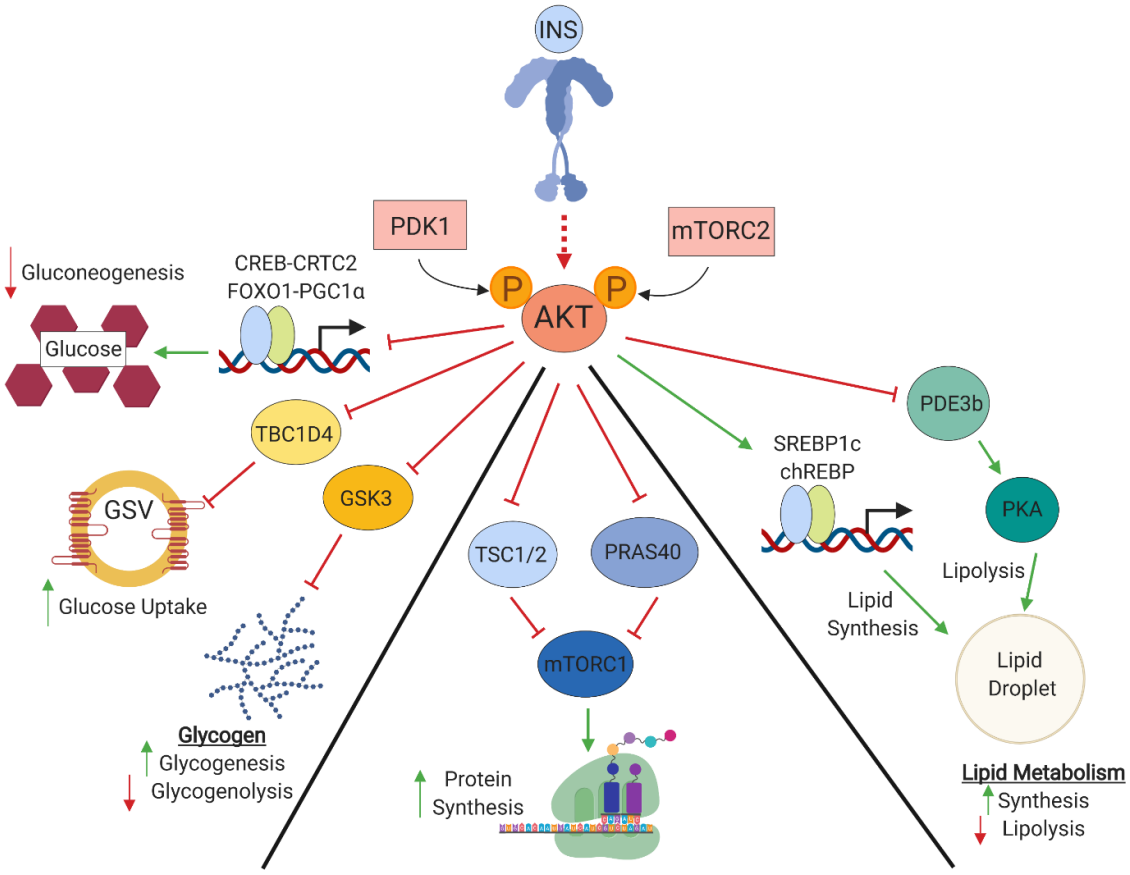
INS
PDK1
mTORC2
P
P
AKT
Gluconeogenesis
CREB-CRTC2
FOXO1-PGC1α
Glucose
TBC1D4
GSK3
GSV
Glucose Uptake
Glycogen
Glycogenesis
Glycogenolysis
TSC1/2
PRAS40
mTORC1
Protein
Synthesis
SREBP1c
chREBP
PDE3b
PKA
Lipolysis
Lipid
Synthesis
Lipid
Droplet
Lipid Metabolism
Synthesis
Lipolysis

Figure 1.2: Potential mechanisms by which insulin resistance develops.

Several potential mechanisms have been shown to promote tissue insulin resistance including hyperinsulinemia, lipotoxicity, endoplasmic reticulum (ER) stress, inflammation, fibrosis, and mitochondrial dysfunction.

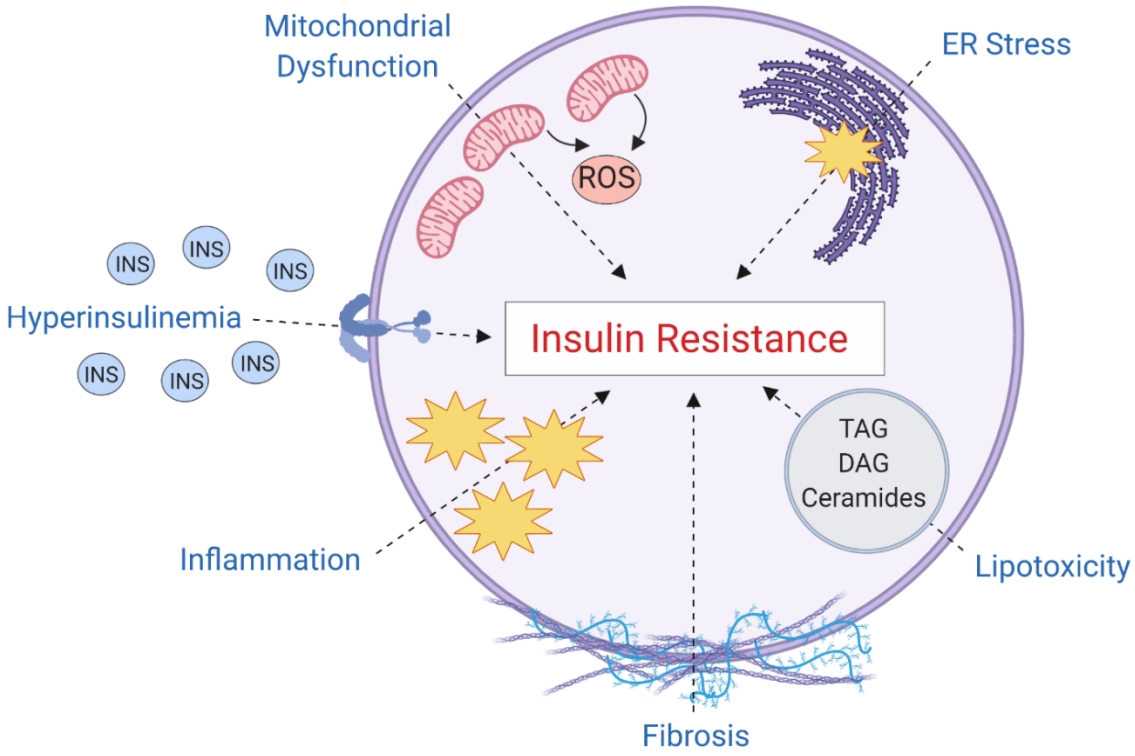
Mitochondrial Dysfunction
ROS
ER Stress
INS
INS
INS
Hyperinsulinemia
INS
INS
INS
Insulin Resistance
TAG
DAG
Ceramides
Inflammation
Lipotoxicity
Fibrosis

Figure 1.3: Circulating LPA can be metabolized via distinct mechanisms.

LPA is synthesized from PA through the actions of PLA_1/PLA_2 or via ATX mediated choline release of LPC. LPA is rapidly degraded to MAG through the actions of LPP1/3 or cleared from circulation via the liver. LPA, lysophosphatidic acid; LPC, lysophosphatidic choline; LPP, lipid protein phosphatase; MAG, monoacylglycerol; PLA, phospholipase A. Figure modified from D'Souza *et al*., *Nutrients*(1).

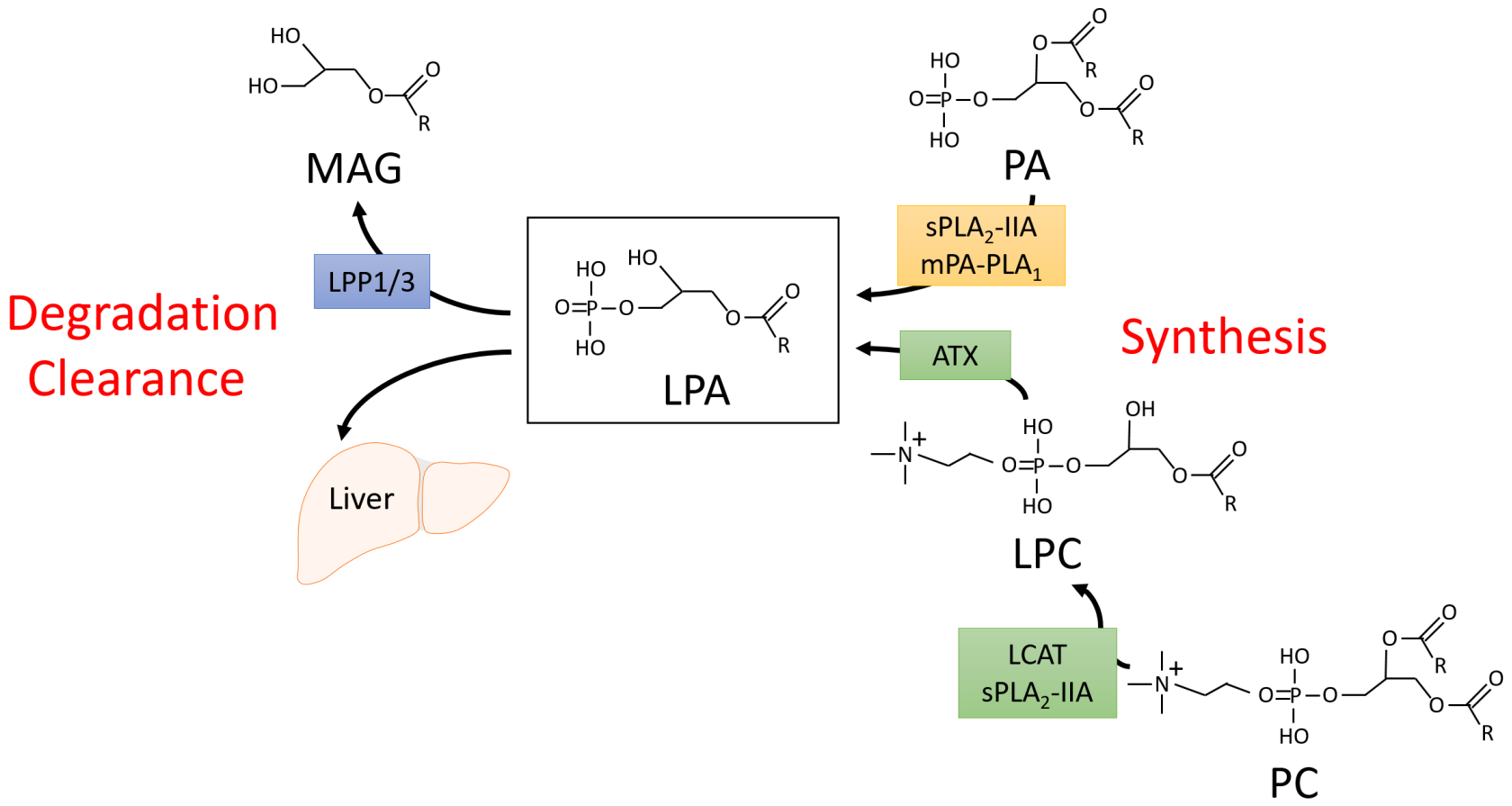
MAG
PA
sPLA2-IIA
mPA-PLA1
LPP1/3
Degradation
Clearance
LPA
ATX
Synthesis
Liver
LPC
LCAT
sPLA2-IIA
PC

Figure 1.4: Sources of circulating LPA.

Circulating LPA can be generated via multiple sources, including lipoproteins, exosomes, activated platelets and from the diet. Reproduced from D'Souza *et al*., *Nutrients*(1).

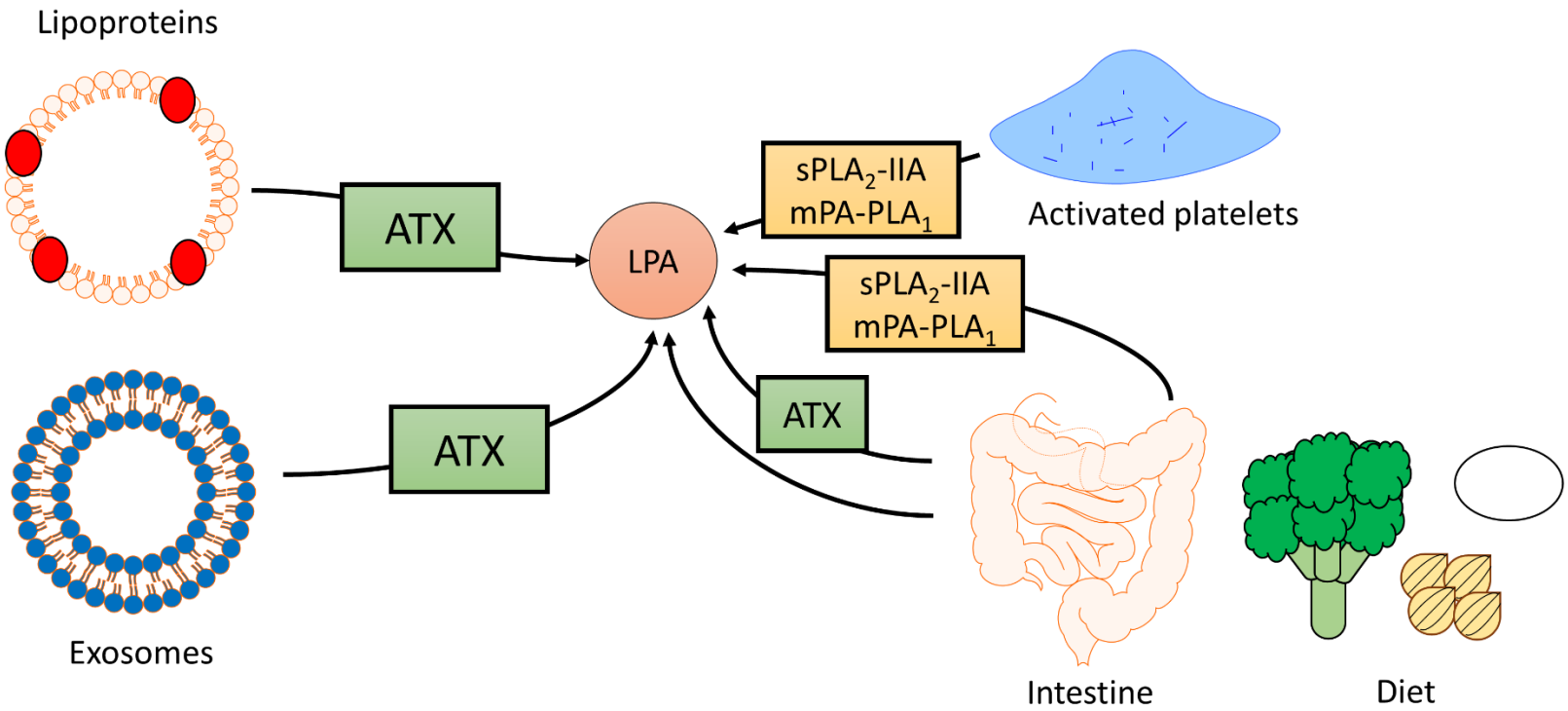
Lipoproteins
ATX
LPA
sPLA2-IIA
mPA-PLA1
Activated platelets
sPLA2-IIA
mPA-PLA1
ATX
ATX
Exosomes
Intestine
Diet

Figure 1.5: Summary of the major LPA signaling pathways

Six LPA receptors, LPA1-6, have been identified that mediate LPA signaling. LPA1-6 are G-protein coupled receptors (GPCR) that can couple via several Gα proteins to activate downstream signal transduction pathways.

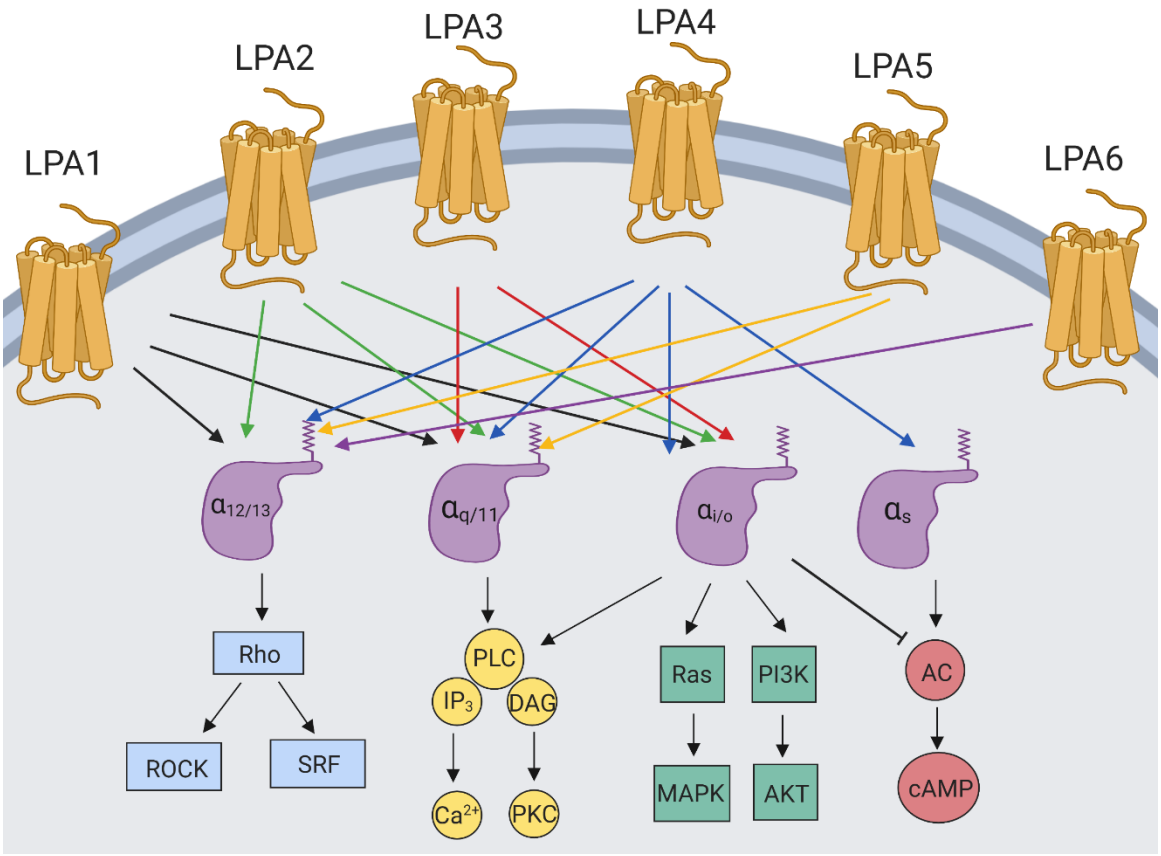
LPA1
LPA2
LPA3
LPA4
LPA5
LPA6
α12/13
αq/11
αi/o
αs
Rho
ROCK
SRF
PLC
IP3
DAG
Ca2+
PKC
Ras
PI3K
MAPK
AKT
AC
cAMP

Figure 1.6: Mechanisms by which ATX-LPA signaling can promote insulin resistance. ATX-LPA can promote insulin resistance via several potential mechanisms, including increased inflammation and fibrosis and suppression of BAT function and PPARγ signaling. BAT, brown adipose tissue; PPARγ, peroxisome proliferator activated receptor γ.

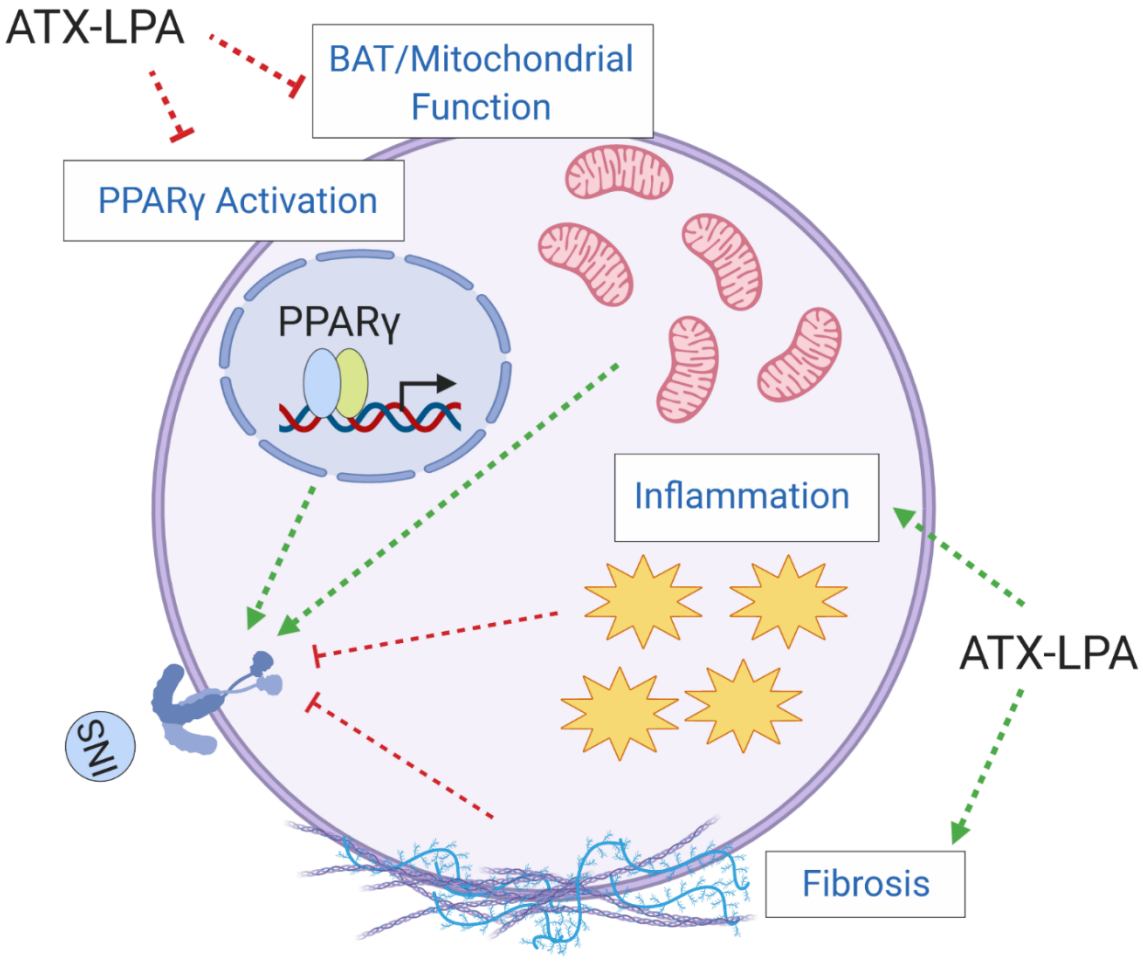
ATX-LPA
BAT/Mitochondrial Function
PPARγ Activation
PPARγ
Inflammation
ATX-LPA
INS
Fibrosis

Table 1.1. The influence of ATX-LPA signaling on adipocyte proliferation and differentiation, diet-induced obesity, insulin resistance (IR) and glucose intolerance (GI). Reproduced from D'Souza et al, *Nutrients*(1).

Effect of ATX and/or LPA on:				Models	Ref
Preadipocyte proliferation	**Preadipocyte differentiation**	**Diet-induced adiposity**	**Diet-induced IR/GI**		
↑	↓	↑	↑	3T3-L1 (pre-)adipocytes, primary murine pre-adipocytes, $ATX^{+/-}$ mice, $FATX^{-/-}$ mice, fat specific ATX-overexpressing mice	(8)
↑	n.d.	n.d.	n.d.	3T3-F442A preadipocytes, NIH-3T3 fibroblasts	(202, 204)
↑	↓	n.d.	n.d.	3T3-L1 pre-adipocytes, DFAT-P porcine preadipocytes	(213)
↔	↓	↑	↔	Primary murine brown pre-adipocytes, ATX-overexpressing mice	(212)
n.d.	↓	↓	n.d.	3T3-F442A pre-adipocytes, SGBS pre-adipocytes, LPA1-KO mice, primary murine pre-adipocytes	(214)
n.d.	n.d.	↓	↑	$FATX^{-/-}$ mice	(178)
n.d.	n.d.	↔	↑	Chow fed db/db mice treated with LPA1/3 antagonist (Ki16425)	(222)
n.d.	n.d.	n.d.	↑	Chow and HFHS-fed WT mice treated with Ki16425	(191)
n.d.	n.d.	↔	↑	3T3-L1 adipocytes, chow and high fat diet-fed WT mice treated with Ki16425	(180)

Thesis Hypothesis and Objectives

A growing number of preclinical and clinical studies support that the ATX-LPA pathway is enhanced during the development of obesity-induced insulin resistance. ATX has primarily been shown to be upregulated by pro-inflammatory mediators, suggesting that nutritional factors that are increased in a diabetic milieu may also regulate ATX expression. Furthermore, while several mechanisms have been postulated for how ATX-LPA may promote insulin resistance in adipose tissue, examination of whether this axis influences insulin function in skeletal muscle, the major site of insulin-stimulated glucose disposal, is unknown. I hypothesize that ATX expression and secretion in adipose tissue is regulated by a pro-diabetic milieu, specifically hyperglycemia and hyperinsulinemia. Furthermore, I hypothesize that increased ATX-LPA signaling promotes skeletal muscle insulin resistance by increasing inflammation, fibrosis and by altering mitochondrial function. Chapters 2-5 contain experiments that investigate these hypotheses through the following objectives:

1. Determine the effect of high levels of glucose and insulin on ATX expression in adipocytes.
2. Examine whether alterations in ATX-LPA signaling influence systemic insulin sensitivity and insulin function in metabolically relevant tissues.
3. Examine mechanisms by which the ATX-LPA axis influences skeletal muscle insulin signaling.

Chapter 2: Nutritional Regulation of ATX

2.1. Rationale and Objectives

As highlighted in the introduction, despite recent studies implicating adipose-derived ATX in metabolic disorders including obesity and insulin resistance, the nutritional and hormonal regulation of ATX in adipocytes remains unclear. Prior studies have shown that a pro-inflammatory milieu, marked by significant increases in inflammatory cytokines, such as TNFα and IL-6, strongly influence ATX expression(180,215). Direct addition of insulin to human adipose tissue significantly counteracted dexamethasone-induced repression of ATX mRNA expression(235). Conversely, use of the insulin sensitizing PPARγ agonist, rosiglitazone, reduced ATX expression(215). Taken together, these studies show that insulin can alter ATX expression. Interestingly, increases in adipose ATX expression also coincided with the development of hyperglycemia in leptin receptor deficient, *db*/*db* mice, suggesting that ATX expression could be additionally regulated by nutritional factors(215). Therefore, the first objective of this thesis was to examine the potential nutritional and hormonal regulation of ATX by glucose and insulin, respectively (Figure 2.1).

Figures 2.2A-C, 2.3, 2.5-2.7, 2.8A-B and 2.9 and portions of the text present in this chapter have been reproduced with copyright permission from *Endocrinology* (Appendix 1)(176) from the following manuscript and edited as appropriate:

D'Souza, K., Kane, D. A., Touaibia, M., Kershaw, E. E., Pulinikunnil, T. and Kienesberger, P. C. (2017). Autotaxin is regulated by glucose and insulin in adipocytes. *Endocrinology*. **158**(4): 791-803.

2.2. Materials and Methods

2.2.1 Chemicals and Reagents

Unless otherwise stated, chemicals and reagents were obtained from Sigma. The ATX inhibitor, PF-8380, was prepared in five steps from 2-benzoxazolone and 3-chloropropanoyl

chloride as detailed in(236) and provided by Dr. Mohamed Touaibia, Université de Moncton, Moncton, NB, Canada.

2.2.2 Animals

C57BL6/J mice were procured from The Jackson Laboratory. Mice were housed on a 12 h light: 12 h dark cycle at 23.5°C with ad libitum access to chow diet (LD5001 from Lab diet with 13.5 kcal% from fat, 3.02 kcal/g) or high fat-high sucrose (HFHS) diet (12451 from Research Diets with 45 kcal% from fat and 17 kcal% from sucrose, 4.70 kcal/g) and water. Nine to ten week-old male mice were randomly assigned to chow or HFHS cohorts and fed for 16 weeks. Mice were euthanized either in the fed state (1 h food withdrawal) or following a 16 h fast. Blood was spun at 2000 × g for 15 min at 4°C to collect serum, which was frozen and stored at -80°C until further use. All protocols involving mice were approved by the Dalhousie University Institutional Animal Care and Use Committee.

For explant studies, 25-40 week old female C57BL6/J mice from Jackson Laboratory was used.

2.2.3 Cell Culture

3T3-L1 cells (ATCC) were grown and differentiated to mature adipocytes, as previously described, with minor modifications(237). Briefly, 3×10^5 3T3-L1 cells were seeded in 35 mm dishes and maintained in Dulbecco's modified Eagle's medium (DMEM) containing high (25 mM) glucose concentration (DMEM-HG, SH3024301; Hyclone Laboratories) supplemented with 10% fetal bovine serum (FBS, 97068-085; Seradigm). Two days post-confluence (Day 0), cells were differentiated in DMEM-HG containing 10% FBS, 10 µg/ml insulin from bovine pancreas, 0.4 µg/ml dexamethasone and 0.5 mM 3-isobutyl-1-methylxanthine. After two days (Day 2), the media was changed to DMEM-HG supplemented with 10% FBS and 10 µg/ml insulin. At Day 4, the media was changed to DMEM-HG containing 10% FBS and 0.5 µg/ml insulin. After Day 6, cells were maintained in DMEM-HG containing 10% FBS. Experiments were performed with

adipocytes at Day 8-9. Treatment of adipocytes with different glucose, insulin or palmitate concentrations was performed either for 2-6 h (acute exposure) or up to 30 h (chronic exposure).

Insulin resistance was induced by 24-h exposure to high glucose and insulin, as previously described(238). Briefly, adipocytes were washed once in phosphate buffered saline (PBS) and incubated in 1 ml of DMEM (11966-025; Gibco, Thermo Fisher Scientific) supplemented with 4.5 g/L glucose (25.0 mM, Amresco), 0.5% (w/v) fatty acid-free (FAF) bovine serum albumin (BSA), 110 mg/ml sodium pyruvate (P2256, Sigma) and 100 nM insulin for 24 h. Insulin sensitive (IS) 3T3-L1 adipocyte controls were cultured in DMEM supplemented with 1.1 g/L glucose (6.1 mM), 0.5% (w/v) FAF-BSA and 110 mg/ml sodium pyruvate. Where indicated, 1 μM rosiglitazone was added to the media of insulin resistant (IR) or insulin sensitive (IS) adipocytes and cells were incubated for 24 h. Following incubation, media aliquots were collected and stored at -80ºC until further analysis. Adipocytes were washed once in PBS and acutely stimulated with 20 nM insulin in 1 ml DMEM + 1.1 g/L glucose for 15 min. Cells were washed and scraped in ice-cold PBS. Cells were subsequently pelleted through centrifugation at 10,000 × g for 10 min at 4°C, flash frozen in liquid nitrogen and stored at -80°C until further use. Cell pellets were lysed in 100 μL of lysis buffer (20 mM Tris-HCl pH 7.5, 5 mM EDTA, 10 mM Na4P2O7, 100 mM NaF, 1% NP-40) containing 2 mM sodium orthovanadate, 2 mM protease inhibitor cocktail (P8340, Sigma) and 100 μg/mL phosphatase inhibitor cocktail (524628, Calbiochem). Protein concentrations in cell lysates were quantified colorimetrically using a bicinchoninic acid (BCA) protein assay kit (Thermo Scientific) and BSA as standard.

To examine how glucose and insulin regulate ATX secretion acutely (6 h) and chronically (30 h), 3T3-L1 adipocytes were washed once in PBS and pre-incubated for 30 min with 1 ml of DMEM + 4.5 g/L glucose + 0.5% (w/v) FAF-BSA and 110 mg/ml sodium pyruvate with the following chemical inhibitors, as indicated: 5 mg/ml actinomycin D, 1 μM wortmannin, 100 nM rapamycin (Alfa Aesar), a combination of 5 μg/ml brefeldin A and 5 μM monensin (Enzo), or 10 μg/ml cycloheximide (Biovision). Following pre-incubation, 100 nM insulin or

PBS was added to adipocytes (t = 0). For acute stimulations, media aliquots of 100 µl were collected and stored at 2, 4 and 6 h following incubation with PBS or insulin. Due to the short half-lives of wortmannin, brefeldin A/monensin and cycloheximide, an equal volume of DMEM supplemented with 4.5 g/L glucose and 0.5% (w/v) FAF-BSA plus indicated inhibitors was added to cells after an aliquot of media was removed. For chronic stimulation, inhibitors were added every 6 h. ATX activity in the media was adjusted for dilution factor. Adipocytes were collected and homogenized as described above. All cell culture data reflect at least three independent experiments.

2.2.4 Subcutaneous Adipose Tissue Explants

Adipose tissue explants were prepared as previously described(239). Briefly, SCAT from the anterior of 25-40 week old female C57Bl6 mice from Jackson Laboratory was surgically removed, washed once in PBS and incubated in pre-warmed (37 °C) DMEM, no glucose media for 30 min. SCAT explants were cut into pieces (~20 mg) using scissors and incubated in 100 µl DMEM containing 2% FAF-BSA, 110 mg/ml sodium pyruvate and indicated glucose concentrations or insulin concentrations for 8 h. Thereafter, media aliquots were collected and stored at -80ºC until further analysis. SCAT explants were homogenized in ice-cold lysis buffer, incubated for 30 min on ice and spun at 14,000 x g for 30 minutes at 3°C. The resulting supernatants were spun again at 14,000 x g for 30 minutes at 3°C. Lysate protein concentrations were quantified using a BCA protein assay kit and BSA as standard.

2.2.5 ATX Activity Assay

2.2.5.1 FS-3

ATX activity in serum or conditioned media was determined using FS-3 (Echelon), a fluorogenic LPC analog (Fig. 2.2A) (240). 10 µl of serum or media were incubated with 10 µl of 100 µM FS-3 in 80 µl of freshly prepared assay buffer (50 mM Tris, 140 mM NaCl, 5 mM KCl, 1 mM $CaCl_2$, 1 mM $MgCl_2$, pH 8.0). Samples were incubated at 37°C for 2 h, during which

fluorescent measurements were taken every 5 min. ATX activity was quantitated by measuring the rate of linear increase in fluorescence at 528 nm with excitation at 485 nm and was expressed as relative fluorescence units/(min x mg cellular protein).

2.2.5.2 Choline Release Assay

ATX activity in plasma and serum was quantified as previously described(241). Briefly, 2 µl of plasma or serum was added to 18 µl buffer A containing 100 mM Tris-HCl, pH 9.0, 500 mM NaCl, 5 mM $MgCl_2$ and 0.05% v/v Triton X-100. For samples examined in the presence of the ATX inhibitor, PF-8380 or ONO-8430506(236), 5 µl of buffer A containing 10% DMSO or 5 mM PF-8380 was added. Samples were pre-incubated at 37°C for 30 min and 25 µl of 6 mM 1-myristoyl-2-hydroxy-sn-glycero-3-phosphocholine (14:0 LPC, Avanti Cat: 855575P) was added. The reaction mixture was incubated at 37°C for 6 h to allow for ATX-mediated choline release. Subsequently, 20 µl of sample was incubated with 90 µl of buffer C [9.65 ml buffer B (100 mM Tris-HCl, pH 8.5, and 5mM $CaCl_2$), 110 µl of 30 mM N-ethyl-N-(2-hydroxy-3-sulfopropyl)-3-methylaniline (TOOS, Cedarlane), 110 µl of 50 mM 4-aminotipyrine, 6.6 µl of 1000 U/ml horseradish peroxidase, and 110 µl of 300 U/ml choline oxidase] at 37°C for 20 min and choline oxidation was recorded at 550 nm for 30 min.

In the choline release assay, natural LPC is utilized as enzyme substrate, rather than the fluorescent LPC analog, FS-3. Recently, it has been demonstrated that lipids contained in serum may interfere with the fluorogenic ATX activity assay using FS-3 (241). Therefore, the choline release assay is more appropriate to assess ATX activity in plasma/serum.

2.2.6 Immunoblotting Analysis

Cells were homogenized in lysis buffer (20 mM Tris-HCl pH 7.5, 5 mM EDTA, 10 mM $Na_4P_2O_7$, 100 mM NaF, 1% NP-40) containing 2 mM sodium orthovanadate, 2 mM protease inhibitor cocktail (P8340, Sigma), and 100 µg/mL phosphatase inhibitor cocktail (524628,

Calbiochem) using a sonicator. Protein concentrations in tissue and cell lysates or plasma were quantified colorimetrically using a BCA protein assay kit and BSA as standard.

3T3-L1 cell lysates were subjected to SDS-PAGE and proteins were transferred onto a nitrocellulose membrane. Proteins were visualized using a reversible protein stain (Memcode, Pierce, Thermo Fisher Scientific), blocked for 1 hr in 1× TBST + 5% milk and incubated overnight in primary antibodies (1:1000 dilution). The list of primary antiobodies used to probe the membranes are summarized in Table 2.2. Immunoblots were developed using the Western Lightning Plus-ECL enhanced chemiluminescence substrate (Perkin Elmer). Densitometric analysis was performed using Image lab software (Bio-Rad). To normalize protein samples, densiometric analysis of protein loading was obtained through the Memcode protein stain and used to normalize the immunoblot signal to protein content. Phosphorylated protein levels were normalized to total protein levels and expressed as a ratio of phosphorylated protein/total protein. Representative immunoblots are shown.

2.2.7 RNA Extraction and Gene Expression Analysis

RNA was isolated from 3T3-L1 cells following indicated treatments using RIBOZOL (Amresco) and chloroform according to the manufacturer's directions. The RNA was re-suspended in 50 µL nuclease free water (Ambion). The quality and quantity of RNA was assessed using a QIAxcel Advanced System (Qiagen) and QIAxcel RNA QC Kit v2.0 (Qiagen) according to the manufacturer's instructions. cDNA was synthesized using qScript cDNA supermix (Quanta Biosciences) from 500 ng of RNA. qPCR reactions were carried out in 96-well plates on a ViiA7 Real-time PCR machine (Thermo Fisher Scientific) and contained 2 µl of cDNA template, 5µL of SYBR green Low ROX PCR supermix (Thermo Fisher Scientific), 0.25 µM for each forward and reverse primer, and nuclease free water in a total of 10 µL per reaction. Primer sequences are summarized in Table 1. ATX mRNA levels were determined using Biogazelle qbase + software and normalized to two reference genes, Rpl27 and Rpl41. ATX mRNA levels are presented as fold change.

2.2.8 Statistical Analysis

Results are expressed as mean ± SEM. Comparisons between two groups were performed using an unpaired, two-tailed Student's t-test. Comparisons between multiple groups were performed using a paired or unpaired one- or two- way analysis of variance (ANOVA) followed by a Tukey or Bonferroni post hoc test, as appropriate. All statistical analysis was performed using Prism (GraphPad Software). P-values of less than 0.05 were considered statistically significant. For animal studies, "n" refers to the number of mice used, unless otherwise specified. For cell culture studies, experiments were performed in triplicates and data are from at least two independent experiments.

2.3. Results

2.3.1 ATX is Regulated by Acute and Chronic Nutritional Stimuli *In Vivo*

It remains unclear how ATX is regulated by short-term (i.e. feeding/fasting) and long-term changes in nutritional status (i.e. obesity). Prior studies examining the regulation of ATX in murine adipose tissue during obesity provided conflicting results(8,178,215). To test whether serum ATX is regulated by acute nutritional changes in vivo, we isolated serum from fed and 16 h-fasted male C57Bl6 mice and measured ATX activity (Fig. 2.2A). The source of ATX in serum likely includes adipose tissue, platelets, liver, immune cells and endothelial cells, among other cell types(8,242). ATX activity was markedly decreased in serum from fasted mice compared to fed mice, suggesting acute nutritional regulation of ATX in vivo.

To examine whether this effect persists even after the induction of obesity, we subjected C57Bl6 mice to 16 weeks of HFHS or chow diet feeding. HFHS-fed mice displayed a 44% increase in body weight compared to chow-fed mice (Fig. 2.2B). As previously shown, this feeding regimen not only leads to obesity, but impaired glucose homeostasis (243). Serum ATX activity was upregulated in obese HFHS-fed mice compared to chow-fed mice (Fig. 2.2C). Fasting led to a decrease in serum ATX activity in both chow-fed and HFHS-fed mice (Fig.

2.2C). Since it has recently been suggested that lipids contained in serum may interfere with the fluorogenic ATX activity assay using FS-3(241), I also confirmed these nutritional changes in ATX activity by quantifying choline released from LPC (Fig. 2.2D). Taken together, these data suggest that acute fasting decreases serum ATX activity while the induction of obesity using a diet rich in fat and sucrose increases serum ATX in mice.

2.3.2 ATX is Increased in Insulin-Resistant 3T3-L1 Adipocytes Exposed to High Glucose and Insulin

Adipose tissue is a major source of circulating ATX, accounting for ~40% of serum ATX and LPA in mice(8,178). We used 3T3-L1 adipocytes, which display a marked increase in secreted ATX activity during differentiation (Fig. 2.3A), to examine the regulation of ATX in vitro. To determine whether the upregulation of ATX activity in serum from obese mice can be mimicked by exposing adipocytes to an obese-diabetic milieu, we incubated differentiated 3T3-L1 adipocytes in the presence of high levels of glucose (25 mM) and insulin (100 nM) for 24 h (Fig. 2.3B-E).

Subsequent insulin signaling analysis confirmed that adipocytes exposed to high glucose and insulin concentrations were insulin resistant since acute insulin stimulation failed to increase Akt phosphorylation at Ser473 (Fig. 2.3B and C), consistent with a previous study(238). Protein expression of ATX in the media and cell lysates was markedly increased in insulin resistant adipocytes compared to the insulin sensitive control cells (Fig. 2.3B and D). Upregulation of ATX protein expression was paralleled by a corresponding increase in ATX activity in the media from insulin resistant compared to insulin sensitive adipocytes (Fig. 2.3E). As expected, adiponectin levels in the media were reduced in insulin resistant adipocytes compared to control cells (Fig. 2.3B and D). Consistent with a prior study demonstrating that the insulin sensitizer and PPARγ agonist, rosiglitazone, diminishes ATX mRNA levels in 3T3F442A adipocytes(215), our data show that incubation with rosiglitazone decreases ATX mRNA and secreted ATX protein

levels and activity in both insulin sensitive and insulin resistant 3T3-L1 adipocytes (Fig. 2.3F-H). Our data also suggest that PPARγ is a potent inhibitor of ATX.

In contrast to the effect of high glucose and insulin on ATX levels and secretion, exposure of adipocytes to FFAs (0.3 and 1 mM palmitate) did not alter secreted ATX activity (Fig. 2.4 A and B). Taken together, these data suggest that chronic exposure of 3T3-L1 adipocytes to conditions that mimic an obese-diabetic environment, i.e. high glucose and insulin concentrations, lead to the upregulation of ATX expression and corresponding increase in secreted ATX activity, whereas PPARγ activation via rosiglitazone prevents these effects.

2.3.3 Glucose and Insulin Differentially Regulate ATX Acutely and Chronically in Adipocytes

To differentiate between the effect of glucose and insulin, per se, on the regulation of ATX expression and activity in adipocytes, we incubated 3T3-L1 adipocytes with either no glucose, low (6 mM) glucose or high (25 mM) glucose in the presence or absence of 100 nM insulin for 2 h, 6 h, or 30 h and determined ATX mRNA levels, cellular ATX protein levels, and secreted ATX activity (Fig. 2.5A-I). At 2 h, ATX mRNA, protein, and activity were similar across all groups (Fig. 2.5A-C). At 6 h, high (25 mM) glucose but not low (6 mM) glucose significantly upregulated ATX mRNA, which was paralleled by a mild increase in ATX protein and activity (Fig. 2.5D-F). Insulin increased ATX activity independent of glucose at 6 h (Fig. 2.5F). Interestingly, insulin-stimulated upregulation of secreted ATX was paralleled by a decrease in ATX mRNA levels in the high glucose group (Fig. 2.5D), whereas cytosolic ATX protein levels were not influenced by insulin at 6 h (Fig. 2.5E). At 30 h, both low (6 mM) and high (25 mM) glucose concentrations increased ATX mRNA, protein, and activity (Fig. 2.5G-I).

The glucose-induced upregulation of ATX mRNA, protein, and activity was inhibited by the mRNA synthesis inhibitor, actinomycin D (Fig. 2.6A-D), suggesting that stimulation of ATX mRNA synthesis is necessary for glucose-induced upregulation of ATX activity. Moreover, incubation of cells with cycloheximide, an inhibitor of protein synthesis, or a combination of

brefeldin A and monensin, inhibitors of protein secretion through the classical secretory pathway, diminished ATX activity in the high glucose group comparable to control (Fig. 2.6D), suggesting that the upregulation of ATX by glucose also involves the classical secretory pathway and synthesis of new ATX protein. As expected, cycloheximide decreased while brefeldin A/monensin increased cytosolic ATX protein levels (Fig. 2.6B and C). As no significant increases in secreted ATX are observed in brefeldin A and monensin treated adipocytes under hyperglycemic conditions, it is unlikely that secretion of ATX occurs via a non-classical pathway, such as through exosomes(172).

Interestingly, a 30 h-incubation with 100 nM insulin significantly reduced ATX mRNA levels, cytosolic ATX protein levels and ATX activity independent of glucose (Fig. 2.5G-I). To examine whether the effect of insulin on ATX is concentration-dependent, we incubated adipocytes with either 0, 0.01, 0.1, 1, 10, or 100 nM insulin for up to 30 h and determined secreted ATX activity. Insulin concentrations ranging from 0.1 to 100 nM gradually increased ATX activity for up to 16 or 24 h compared to controls incubated in the absence of insulin (Fig. 2.7A and B). However, the effect of insulin on ATX did not appear to be dose-dependent. At 30 h, 100 nM insulin reduced ATX activity although lower insulin concentrations had no effect on ATX activity (Fig. 2.7A and B).

To determine whether glucose and insulin modulate ATX also in whole adipose tissue, we incubated SCAT explants from female C57Bl6 mice with either glucose (6 and 25 mM) or 100 nM insulin for 8 h and determined secreted ATX activity compared to no glucose/no insulin controls (Fig. 2.8A and B). In contrast to the regulation of ATX by glucose in 3T3-L1 adipocytes, ATX activity was not upregulated by glucose in a concentration-dependent manner in SCAT explants, with only a ~3-fold increase observed in the high glucose group (Fig. 2.8A). Moreover, corresponding with upregulated ATX activity following acute (6 h) exposure of 3T3-L1 adipocytes to insulin, secreted ATX activity was increased ~2.3-fold in SCAT explants after incubation with 100 nM insulin for 8 h compared to control explants incubated without insulin

(Fig. 2.8B). The insulin-induced stimulation of ATX activity was paralleled by a trend towards increased Akt Ser473 phosphorylation (Fig. 2.8C and D). Taken together, these data suggest that glucose increases ATX mRNA expression, protein expression, and activity in a time-and concentration-dependent manner in murine adipocytes.

These data also suggest that exposure to high (100nM) insulin concentrations elicits a bi-phasic response in adipocytes – insulin initially increases secreted ATX activity, however, long-term incubation with 100 nM insulin decreases ATX activity due to downregulation of ATX mRNA and protein expression.

2.3.4 Acute Stimulation of ATX Secretion by Insulin is Dependent on PI3Kinase but not mTOR Activation

To examine potential mechanisms that underlie the transient stimulatory effect of insulin on ATX secretion, 3T3-L1 adipocytes were incubated with wortmannin, a PI3Kinase inhibitor, or rapamycin, an inhibitor of mTORC1, in the presence or absence of 100 nM insulin for 6 h. As expected, wortmannin diminished insulin-stimulated phosphorylation of Akt at Ser473 and p70S6K at Thr389 (Fig. 2.9A). Wortmannin also blunted the increase in ATX activity induced by insulin, suggesting that PI3Kinase activation was essential for insulin stimulation of ATX secretion (Fig. 2.9E). This was mirrored by decreased secreted and cellular ATX protein levels in the media of wortmannin-treated cells (Figure 2.9A-D). Incubation with rapamycin led to diminished phosphorylation of p70S6K at Thr389, a known mTOR target site, while Akt phosphorylation at Ser473 was unchanged (Fig. 2.9A). In contrast to PI3Kinase inhibition, inhibition of mTOR signaling using rapamycin had no significant effect on ATX activity or protein at baseline or in the presence of insulin (Fig. 2.9A-E). Incubation of adipocytes with brefeldin A/monensin blunted secreted ATX activity and protein levels in the absence and presence of insulin (Fig. 2.9C-E), which resulted in an increased accumulation of cellular ATX protein levels (Fig. 2.9A and B). Incubation of adipocytes with cycloheximide reduced cellular ATX protein levels, which was accompanied by a drastic reduction in secreted ATX activity and

protein in presence and absence of insulin (Fig. 2.9A-E). Taken together, these data suggest that acute insulin-stimulated ATX secretion is PI3Kinase-dependent but does not require mTOR activation. These data also suggest that ATX secretion at baseline and following acute insulin stimulation requires the classical secretory pathway and synthesis of new ATX protein.

2.4 Discussion

Adipose-derived ATX has been implicated in metabolic disorders including obesity and insulin resistance(8,178,180,215). However, the regulation of ATX in adipocytes remains incompletely understood. Specifically, it is unclear whether ATX secretion from adipocytes is influenced by modulators of energy metabolism. In this study we show that serum ATX activity is not only increased by chronic overfeeding in mice but responds acutely to nutritional stimuli as was evidenced by a downregulation of ATX activity upon fasting. In addition, ATX secretion from cultured adipocytes and explanted adipose tissue was acutely (6 h) stimulated by high levels of glucose and insulin in an additive manner. Moreover, we demonstrate that acute insulin stimulation of ATX secretion from adipocytes is mediated by PI3Kinase but not mTOR signaling. Our data also suggest that upregulation of ATX secretion by glucose and insulin requires the classical secretory pathway and synthesis of new ATX protein. In addition, glucose also increased ATX mRNA synthesis. Interestingly, while the stimulatory effect of glucose on ATX was also observed following prolonged incubation (30 h), chronic stimulation with high levels of insulin decreased ATX mRNA, protein, and activity, suggesting that insulin at concentrations mimicking an obese-insulin resistant milieu has a bi-phasic effect on ATX secretion in adipocytes. During acute changes in nutritional status (i.e. feeding), insulin may serve to increase ATX secretion; however, chronic increases in insulin may be associated with decreased ATX levels. To determine whether hyperinsulinemia downregulates ATX expression *in vivo* in insulin resistant/diabetic mice, it could be determined how circulating ATX activity changes in mice treated with streptozotocin(215). Taken together, this study suggests that ATX secretion from

adipose tissue is influenced acutely and chronically by changes in glucose homeostasis, which may underlie its regulation during feeding/fasting and obesity/insulin resistance.

Previous studies examining the regulation of ATX in adipocytes have shown that ATX is markedly upregulated during adipocyte differentiation(8,244). Ferry et al.(244) observed that ATX/Enpp2 mRNA expression increases during differentiation in cultured murine 3T3F442A adipocytes, peaking at 10 days following differentiation start. The increase in ATX mRNA expression coincided with elevated LPA levels in the media, consistent with an upregulation of ATX secretion(244). Differentiation-dependent upregulation of ATX mRNA was also observed in primary mouse preadipocytes with a peak at day 6-12 while it returned to lower levels as adipocytes matured and became hypertrophic(8,244). Consistent with these studies, we demonstrated a marked upregulation of secreted ATX activity during 3T3-L1 adipocyte differentiation starting from day 2 of differentiation.

The regulation of ATX during diet-induced obesity remains controversial as prior studies suggested that ATX is either upregulated(178), downregulated(8), or unchanged(215) in obese mice fed a high fat diet. This discrepancy was attributed to mouse strain differences, starting age of mice for high fat feeding, and possible environmental factors(8). It is plausible that diet composition and feeding duration also contributed to these differences. We showed that serum ATX activity is upregulated in obese mice with impaired glucose tolerance fed HFHS diet in both fed and 16-h fasted states, suggesting that ATX secretion from adipocytes is increased in our obesity model. Upregulation of ATX during diet-induced obesity in mice corresponds with prior studies from our group showing a positive correlation between serum ATX levels and measures of adiposity (BMI, waist circumference) as well as impaired glucose homeostasis/insulin resistance (fasting glucose, fasting insulin, 2 h glucose following an oral glucose tolerance test, glucose infusion rate during a hyperinsulinemic euglycemic clamp, HOMA-IR, QUICKI) in relatively large human cohorts of 60-101 non-diabetic individuals(204,205).

A study by Boucher et al.(215) suggested that two modulators of insulin sensitivity, TNFα and rosiglitazone, influence ATX expression in adipocytes. Specifically, while incubation of 3T3F442A adipocytes with the pro-inflammatory cytokine TNFα, which promotes insulin resistance, led to an increase in ATX mRNA expression, the insulin-sensitizing drug rosiglitazone decreased ATX mRNA levels(215). We demonstrated similar results in 3T3-L1 adipocytes where incubation with rosiglitazone decreased ATX mRNA, protein, and activity in both insulin sensitive and insulin resistant cells. These findings suggest that ATX expression is upregulated during insulin resistance-promoting conditions in adipocytes and can be decreased using insulin-sensitizing drugs. Consistent with this concept, ATX secretion is markedly increased following a 24-h incubation of 3T3-L1 adipocytes with high concentrations of insulin and glucose, which coincided with the development of insulin resistance in these cells. Interestingly, both insulin and glucose upregulated ATX secretion in adipocytes acutely and fasting decreased serum ATX activity in vivo. These data suggest that ATX secretion is modulated by short-term changes in energy metabolism. PI3Kinase activation appears to be critical for acute insulin-stimulated increases in ATX secretion, which is dependent, in part, on new protein synthesis and the classical secretory pathway. The latter observation is consistent with a previous study showing that secretion of human ATX expressed in HEK293T cells is blocked by the Golgi-disturbing agents, brefeldin A and monensin(245). Interestingly, prolonged stimulation with high levels of insulin led to the downregulation of ATX in adipocytes, which appeared to be driven by a reduction in ATX mRNA expression. Although the mechanisms for the insulin-mediated reduction in ATX mRNA expression have not been examined in this study, it is conceivable that ATX mRNA synthesis is under the control of transcription factors such as FoxO proteins, which are inhibited by insulin receptor-Akt signaling(246).

In contrast to insulin, high levels of glucose increased ATX mRNA synthesis in adipocytes both acutely and chronically, which coincided with increased ATX protein expression and secreted ATX activity involving new protein synthesis and the classical secretory pathway,

respectively. The mechanisms underlying the stimulatory effect of glucose on ATX secretion remain unclear, but may involve the induction of an inflammatory response and/or the generation of ROS, processes that are triggered by exposure of adipocytes to hyperglycemic conditions(76). It has previously been shown that high (25 mM) glucose concentrations in the media activate the pro-inflammatory transcription factor NFκB in vascular smooth muscle cells, which was paralleled by increased superoxide production. Hyperglycemia-induced upregulation of NFκB appeared to be dependent on protein kinase C activation, a mechanism that has been suggested to contribute to diabetes-related vascular smooth muscle cell injury(76). Han et al.(247) also reproduced these findings in 3T3-L1 adipocytes, where exposure to high glucose led to NFκB transactivation while transactivation of PPARγ, an anti-inflammatory transcription factor, was reduced. Interestingly, NFκB was required for TNFα-induced upregulation of ATX expression in hepatoma cells(248). A potent role of pro-inflammatory cytokines in the regulation of ATX has also been demonstrated by Benesch et al.(241) as both TNFα and interleukin β1 were able to negate the negative feedback inhibition of ATX expression by LPA and sphingosine 1-phosphate in thyroid cancer cells. Likewise, pro-inflammatory toll-like receptor 4/interferon signaling increased ATX expression via the JAK-STAT and PI3Kinase/Akt pathway in monocytic THP-1 cells(249). A role for the PI3Kinase/Akt signaling pathway in NFκB activation via IKK and FoxO1 has also been established in non-adipocyte cell types(250,251). Therefore, it is tempting to speculate that the regulation of ATX by glucose and insulin converges at the level of NFκB activation, which should be examined in future studies. In addition to the induction of adipocyte inflammation and ROS production, glucose could also regulate ATX secretion via modulation of protein glycosylation. It has previously been suggested that N-glycosylation is required for ATX secretion and activity in 3T3F442A adipocytes(252). Specifically, blockade of N-glycosylation using tunicamycin or deletion of glycosylation sites reduced ATX secretion.

Taken together, this study provides further insight into the regulation of ATX. Our data confirm that ATX is modulated by short-term and long-term changes in nutritional status. This

study also shows that cellular signaling triggered by glucose and insulin plays an important role in regulating ATX secretion from adipocytes, which may underlie changes in circulating ATX levels during feeding/fasting and obesity-related metabolic disease.

2.5 Figures

Figure 2.1: Schematic representation of chapter objectives. Using 3T3-L1 adipocytes, the regulation of ATX mRNA and protein expression and enzymatic activity by glucose and insulin will be examined.

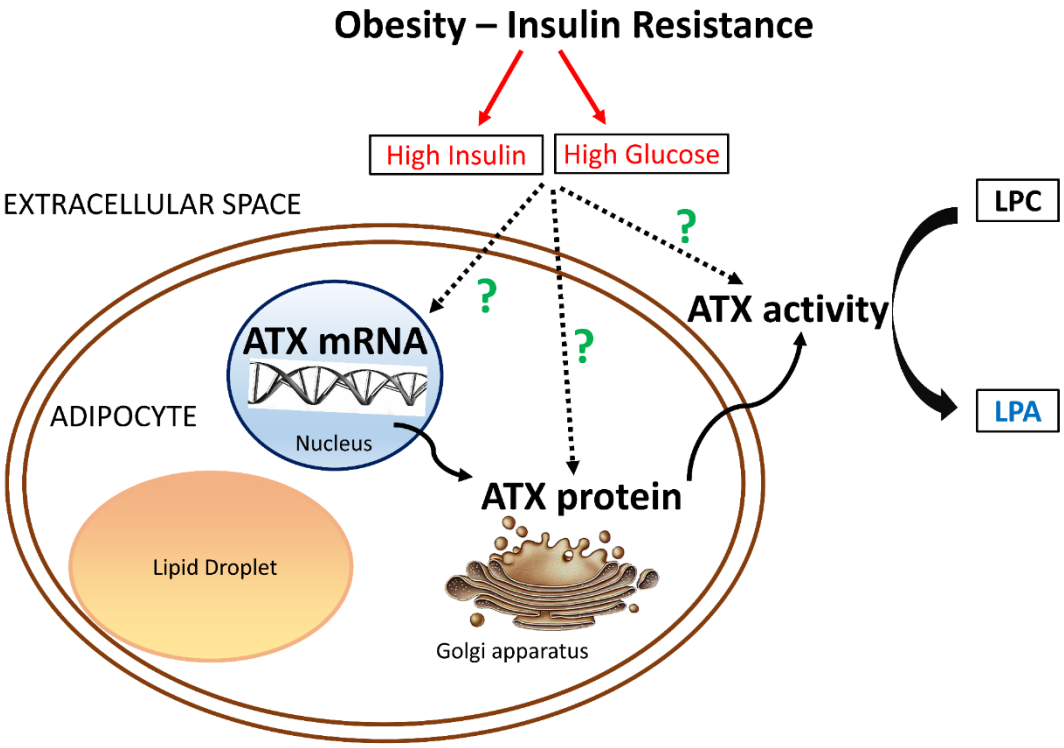
Obesity – Insulin Resistance
High Insulin
High Glucose
EXTRACELLULAR SPACE
?
?
?
ATX activity
LPC
LPA
ATX mRNA
Nucleus
ADIPOCYTE
ATX protein
Lipid Droplet
Golgi apparatus

Figure 2.2: ATX is regulated by acute and chronic nutritional stimuli in mice.

(A) Structure of FS-3 and examination of serum ATX activity using FS-3 in 8 week-old chow-fed male C57Bl6 mice following a 1-h food withdrawal (fed) or 16-h fasting (*n*=4). (B) Body weight and serum ATX activity (C) using FS-3 and (D) choline release assay in 25-26 week-old male C57Bl6 mice fed a chow or HFHS diet for 16 weeks (*n*=4-10). Statistical analysis was performed using an unpaired two-tailed Student's *t*-test (A and B) or a two-way ANOVA followed by a Tukey's multiple comparison test (C); ***$p<0.001$, ****$p<0.0001$, $^{\#\#\#\#}p<0.0001$ vs. Chow. (A-C) reproduced from D'Souza et. al, *Endocrinology*(176).

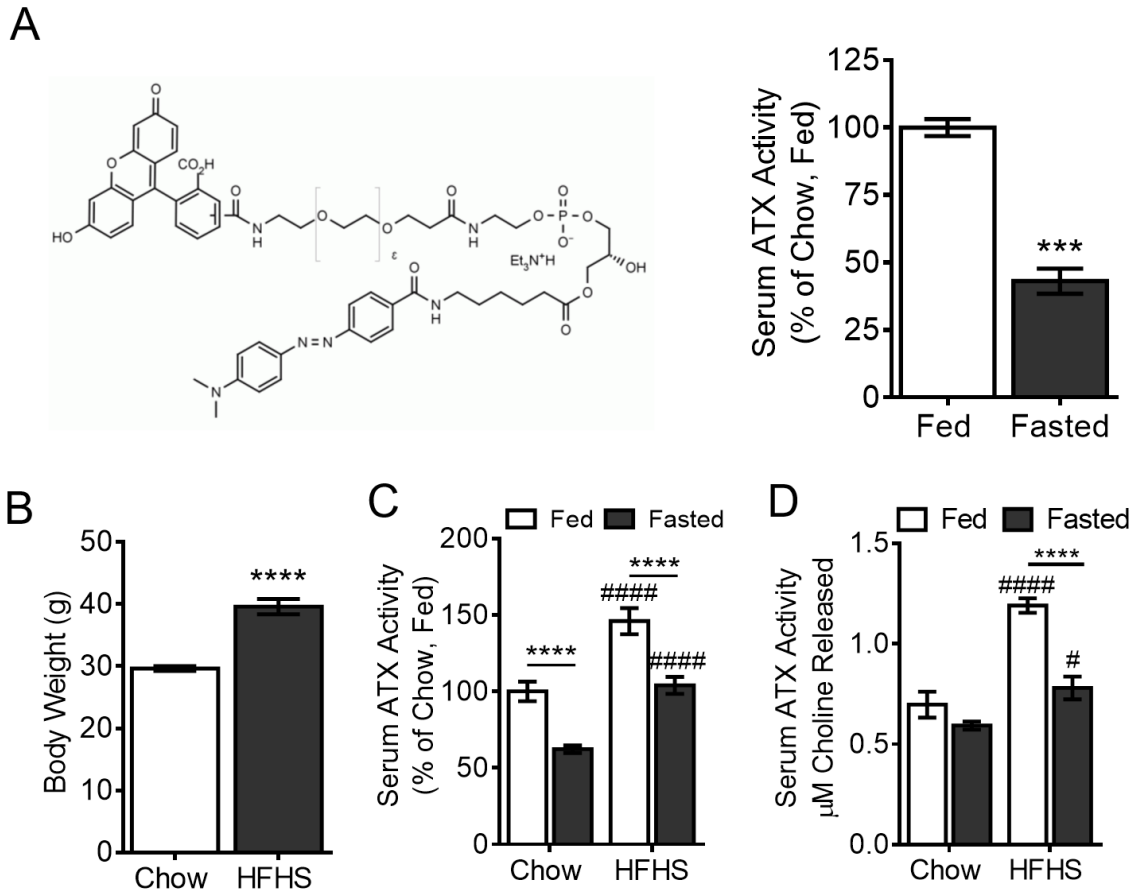
A
Serum ATX Activity
(% of Chow, Fed)
125
100
75
50
25
0
***
Fed
Fasted
B
Body Weight (g)
50
40
30
20
10
0
****
Chow
HFHS
C
Fed
Fasted
Serum ATX Activity
(% of Chow, Fed)
200
150
100
50
0
****
****
####
####
Chow
HFHS
D
Fed
Fasted
Serum ATX Activity
µM Choline Released
1.5
1.0
0.5
0.0
****
####
#
Chow
HFHS

Figure 2.3: ATX is upregulated in insulin resistant 3T3-L1 adipocytes.

(A) Secreted ATX activity during 3T3-L1 adipocyte differentiation from pre-adipocytes (Day 0) to mature, differentiated adipocytes (Day 8). (B, C) Differentiated 3T3-L1 adipocytes were incubated in presence of 25 mM glucose and 100 nM insulin for 24 h (IR) and induction of insulin resistance was determined through immunoblotting analysis of Akt phosphorylation at Ser^{473} following stimulation with 20 nM insulin for 10 min. Insulin sensitive (IS) 3T3-L1 adipocytes, incubated with 6 mM glucose and in the absence of insulin, were used as controls. (B, D) Protein levels of secreted and cellular ATX (ATX-S, ATX-C) and adiponectin (Adn-S, Adn-C). (E) Secreted ATX activity in the media of IS and IR 3T3-L1 adipocytes. (F) ATX/*Enpp2* mRNA, (G) secreted protein, and (H) activity following incubation of IS and IR adipocytes with 1 μM rosiglitazone (Rosi) or DMSO (control, Ctrl). Statistical analysis was performed using one-way ANOVA (A) or two-way ANOVA followed by a Tukey's multiple comparison test (C-D, F-H), or an unpaired two-tailed Student's *t*-test (E); $^{**}p<0.01$, $^{***}p<0.001$, $^{****}p<0.0001$; $^{\#\#\#}p<0.001$, $^{\#\#\#\#}p<0.0001$ vs. IS Ctrl; $n = 9$ from at least three independent experiments; S: secreted, C: cellular, PS: protein stain. (A-H) reproduced from D'Souza et. al, *Endocrinology*(176).

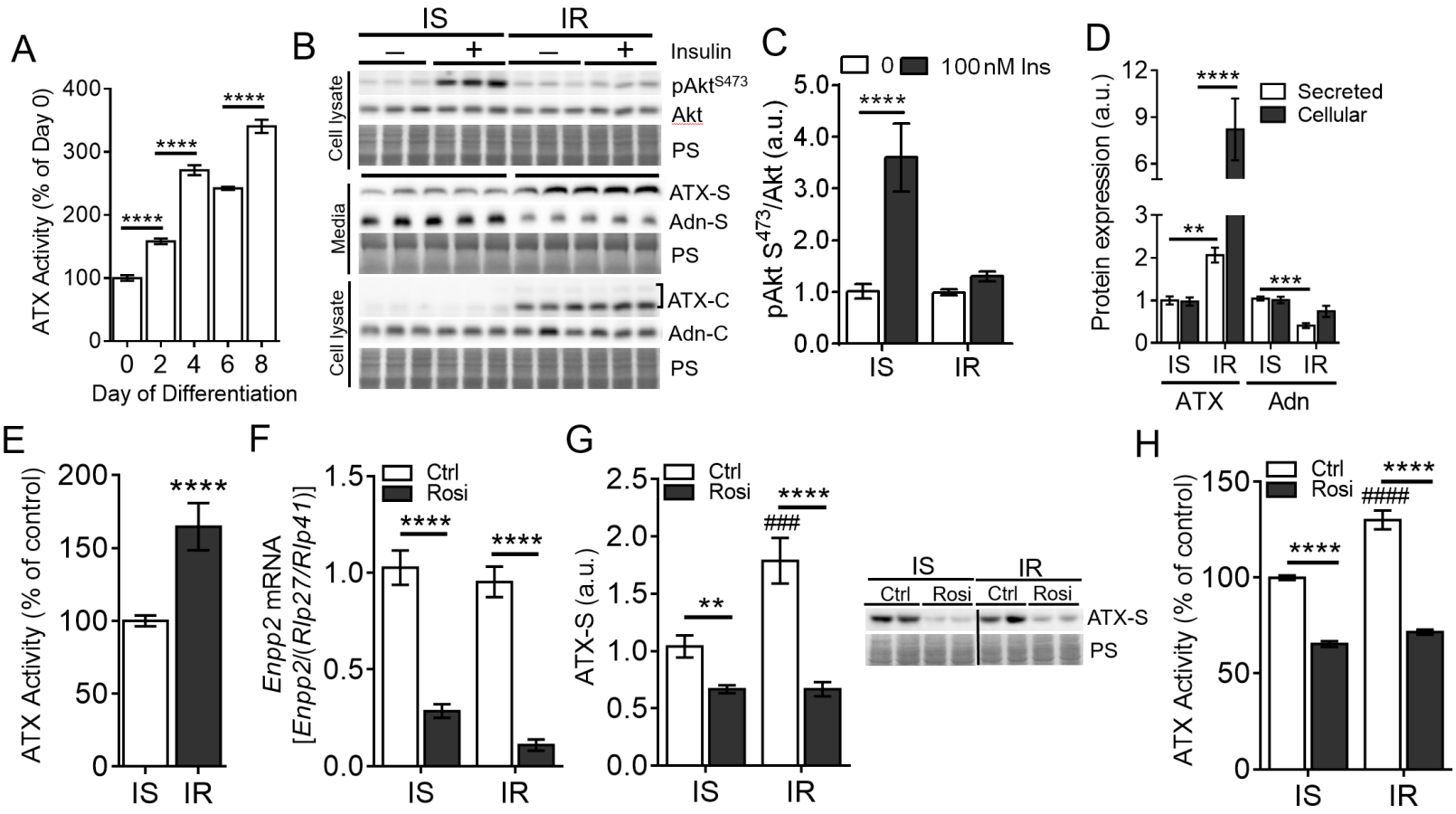
A
ATX Activity (% of Day 0)
400
300
200
100
0
****
****
****
0 2 4 6 8
Day of Differentiation
B
IS
IR
– + – +
Insulin
Cell lysate
pAkt^{S473}
Akt
PS
Media
ATX-S
Adn-S
PS
Cell lysate
ATX-C
Adn-C
PS
C
0
100 nM Ins
pAkt S^{473}/Akt (a.u.)
5.0
4.0
3.0
2.0
1.0
0.0
****
IS
IR
D
Protein expression (a.u.)
12
9
6
3
2
1
0
****
**
***
Secreted
Cellular
IS IR IS IR
ATX
Adn
E
ATX Activity (% of control)
200
150
100
50
0
****
IS IR
F
Enpp2 mRNA
[Enpp2/(Rlp27/Rlp41)]
1.5
1.0
0.5
0.0
Ctrl
Rosi
****
****
IS
IR
G
ATX-S (a.u.)
2.5
2.0
1.5
1.0
0.5
0.0
Ctrl
Rosi
**
****
###
IS
IR
IS
IR
Ctrl Rosi Ctrl Rosi
ATX-S
PS
H
ATX Activity (% of control)
150
100
50
0
Ctrl
Rosi
****
****
####
IS
IR

Figure 2.4: Palmitate does not alter ATX activity.

3T3-L1 adipocytes were incubated with media containing (A) 6 mM or (B) 25 mM glucose in the presence of 0, 0.3 mM or 1.0 mM palmitate for 30 h. Statistical analysis was performed using one-way ANOVA followed by a Tukey's multiple comparison test; $n = 9$ from at least three independent experiments.

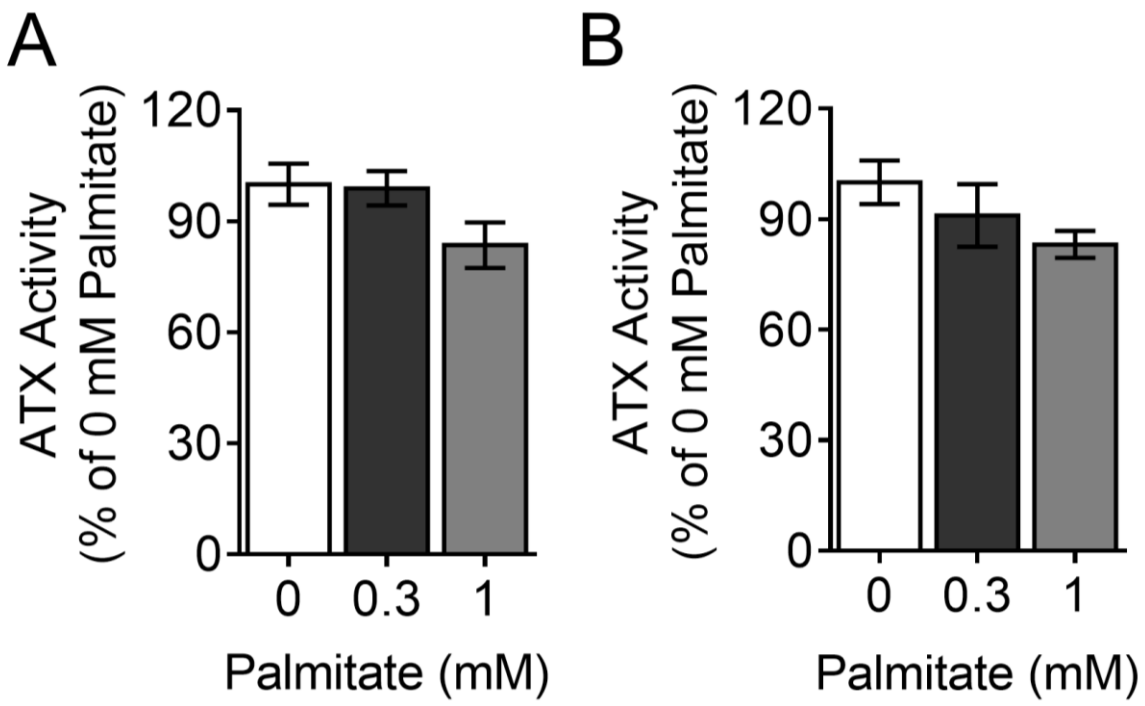
A
ATX Activity
(% of 0 mM Palmitate)
120
90
60
30
0
0
0.3
1
Palmitate (mM)
B
ATX Activity
(% of 0 mM Palmitate)
120
90
60
30
0
0
0.3
1
Palmitate (mM)

Figure 2.5: Glucose and insulin differentially regulate ATX in adipocytes.

3T3-L1 adipocytes were exposed to 0, 6 or 25 mM glucose in the presence or absence of 100 nM insulin for 2 h (A-C), 6 h (D-F) or 30 h (G-I) and (A, D, G) ATX/*Enpp2* mRNA, (B, E, H) cellular ATX protein levels and (C, F, I) secreted ATX activity were determined. Statistical analysis was performed using a two-way ANOVA followed by a Tukey's multiple comparison test; *$p<0.05$, **$p<0.01$, ****$p<0.0001$; $^{\#}p<0.05$, $^{\#\#\#}p<0.001$, $^{\#\#\#\#}p<0.0001$ vs. untreated controls; $n = 9$ from at least three independent experiments; C: cellular, PS: protein stain. (A-I) reproduced from D'Souza et. al, *Endocrinology*(176).

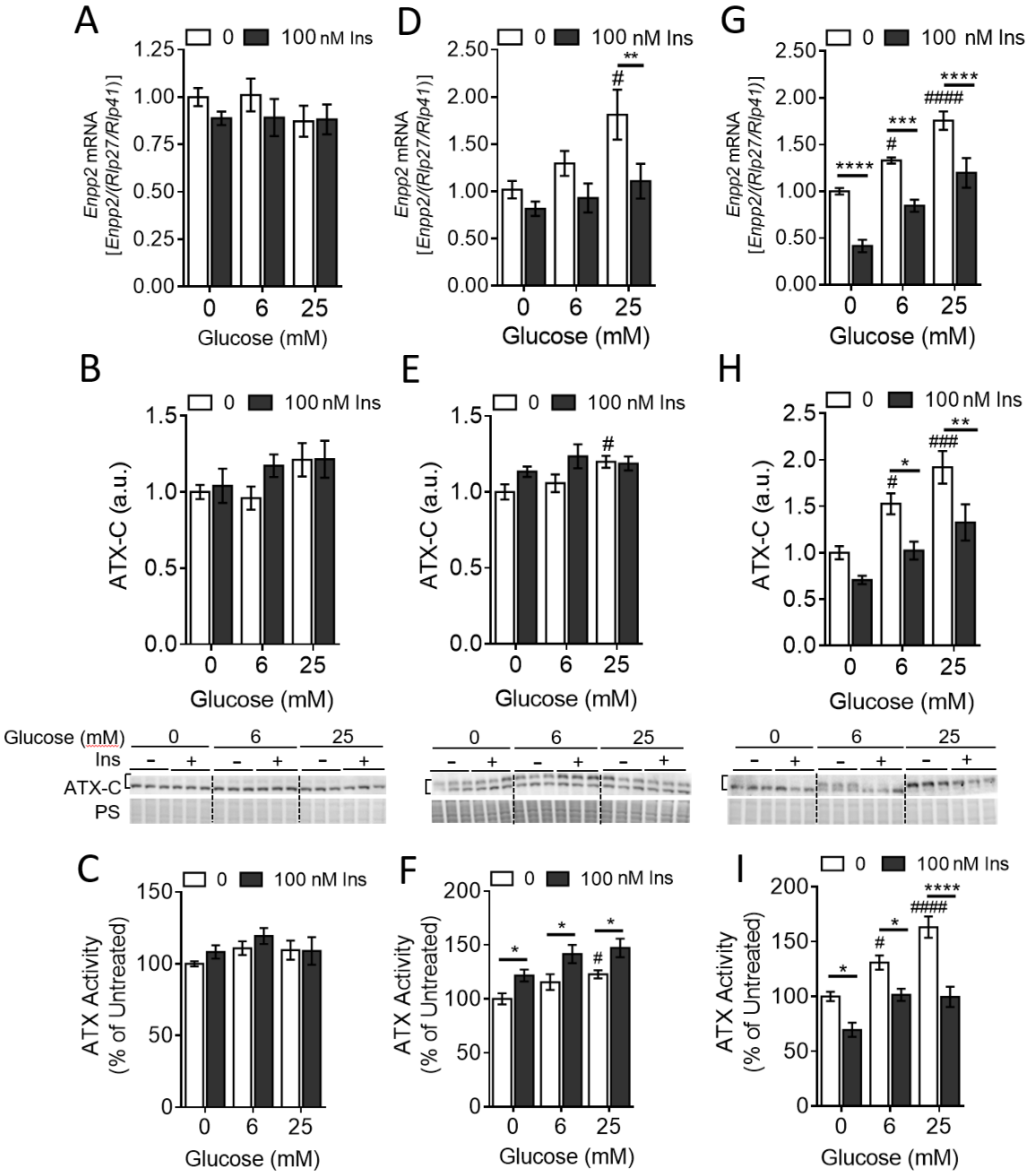
A
D
G
B
E
H
C
F
I
0
100 nM Ins
Enpp2 mRNA [Enpp2/(Rlp27/Rlp41)]
ATX-C (a.u.)
ATX Activity (% of Untreated)
Glucose (mM)
0
6
25
Ins
ATX-C
PS

Figure 2.6: The effect of glucose on ATX levels is transcriptionally mediated.

(A-D) 3T3-L1 adipocytes were incubated with media containing 0 or 25 mM glucose for 30 h. Where indicated, adipocytes were additionally incubated with either 5 µg/ml actinomycin D (ACT), 10 µg/ml cycloheximide (CHX), a combination of 5 µg/ml brefeldin A and 5 µM monensin (B/M) or DMSO/methanol (control, Ctrl). (A) ATX/*Enpp2* mRNA, (B, C) cytosolic ATX (ATX-C) protein expression, (D) secreted ATX activity. Statistical analysis was performed using a two-way ANOVA followed by a Tukey's multiple comparison test. In A, C, D, *p<0.05, **p<0.01, ***p<0.001, ****p<0.0001; $^{\#}p$<0.05, $^{\#\#\#\#}p$<0.0001 vs. no-glucose controls. n = 9 from at least three independent experiments; S: secreted, C: cellular, Ctrl: control. (A-D) reproduced from D'Souza et. al, *Endocrinology*(176).

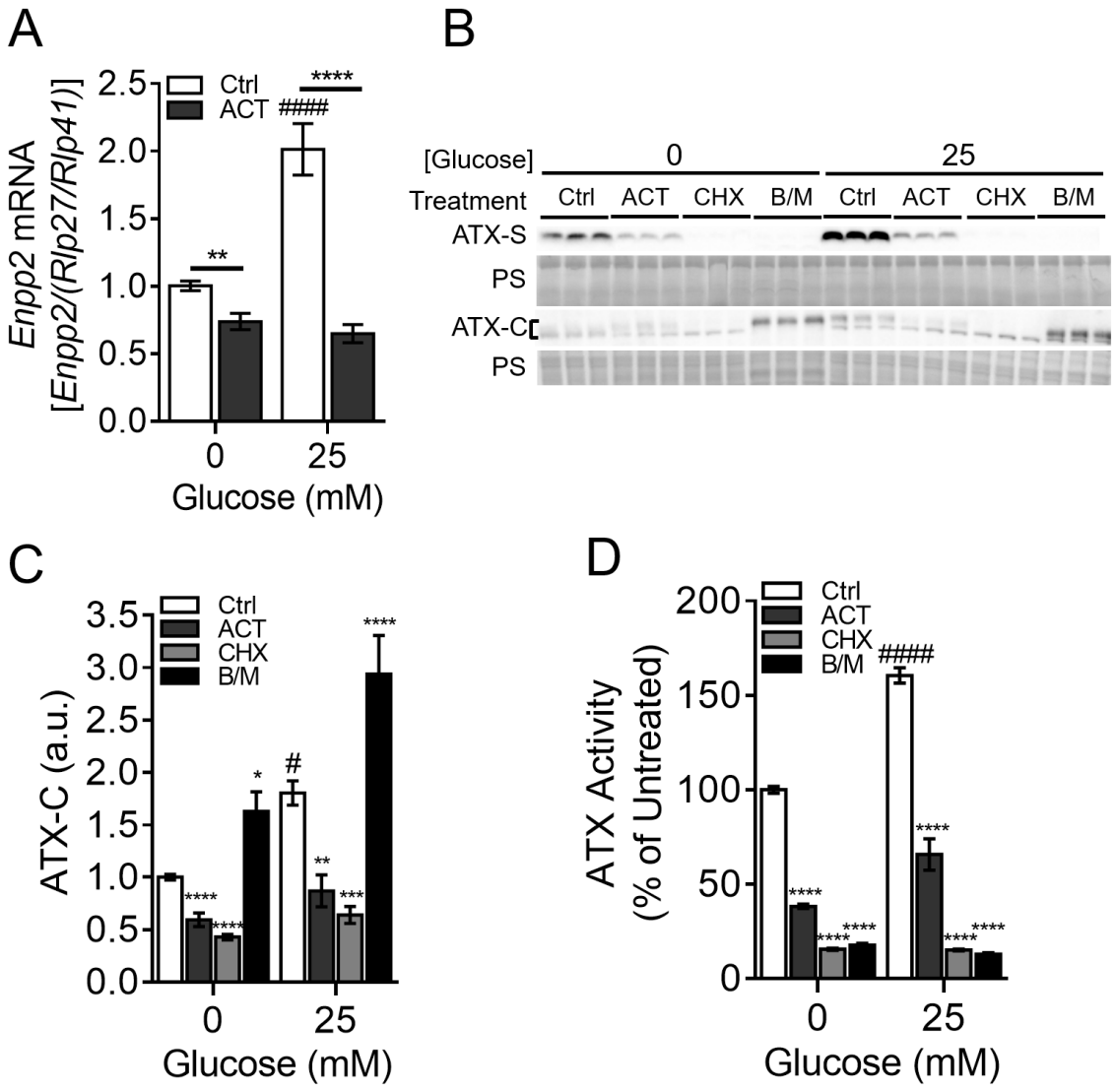
A
Enpp2 mRNA
[Enpp2/(Rlp27/Rlp41)]
Ctrl
ACT
2.5
2.0
1.5
1.0
0.5
0.0
**
****
####
0
25
Glucose (mM)
B
[Glucose]
0
25
Treatment
Ctrl
ACT
CHX
B/M
Ctrl
ACT
CHX
B/M
ATX-S
PS
ATX-C
PS
C
ATX-C (a.u.)
Ctrl
ACT
CHX
B/M
3.5
3.0
2.5
2.0
1.5
1.0
0.5
0.0
*
#
**
***
****
****
****
0
25
Glucose (mM)
D
ATX Activity
(% of Untreated)
Ctrl
ACT
CHX
B/M
200
150
100
50
0
####
****
****
****
****
****
****
0
25
Glucose (mM)

Figure 2.7: Insulin regulates ATX activity in a time- and concentration-dependent manner. (A, B) 3T3-L1 adipocytes were incubated in media containing 25 mM glucose and either 0, 0.01, 0.1, 1, 10 or 100 nM insulin for 0, 1, 4, 16, 24 or 30 h and secreted ATX activity was determined. Statistical analysis was performed using a two-way ANOVA followed by a Tukey's multiple comparison test; In A, $^{++++}p<0.0001$ for 0.01 nM vs. 0 nM insulin, $^{\#\#\#\#}p<0.0001$ for 0.1 nM vs. 0 nM insulin; in B, $^{\#\#}p<0.01$ and $^{\#\#\#\#}p<0.0001$ for 1 nM vs. 0 nM insulin, $^{++++}p<0.0001$ for 10 nM vs. 0 nM insulin, $^{***}p<0.001$ for 100 nM vs. 0 nM insulin; $n = 9$ from at least three independent experiments. (A-B) reproduced from D'Souza et. al, *Endocrinology*(176).

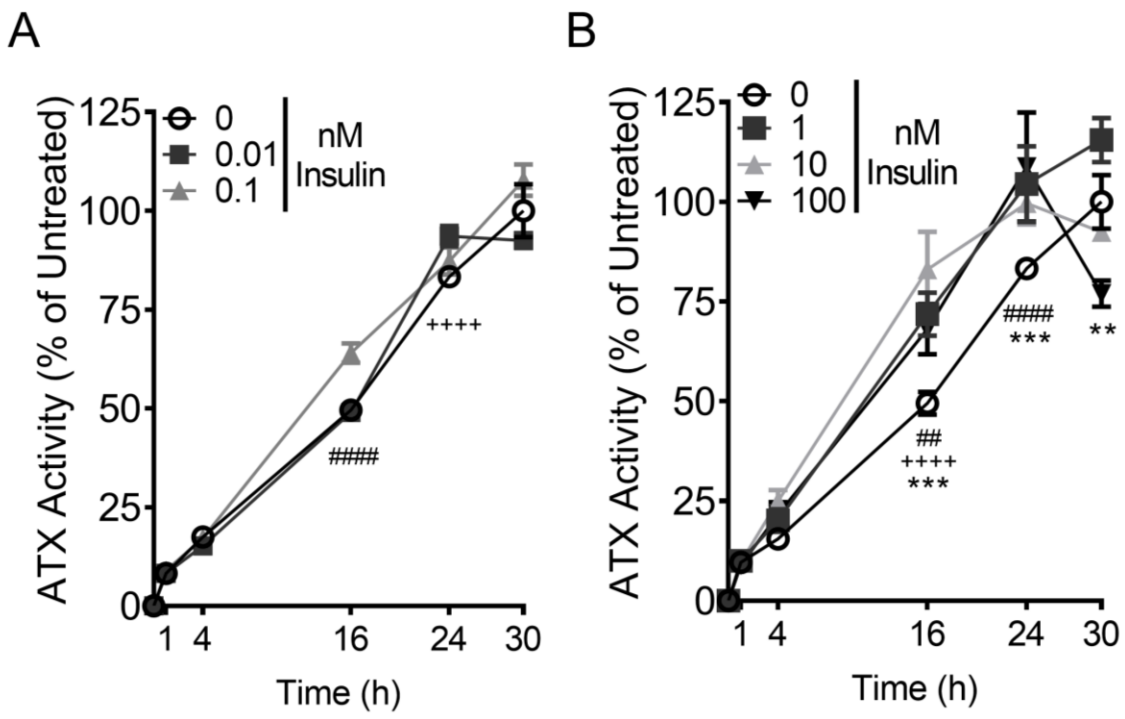
A
ATX Activity (% of Untreated)
125
100
75
50
25
0
0
0.01
0.1
nM
Insulin
++++
####
1
4
16
24
30
Time (h)
B
ATX Activity (% of Untreated)
125
100
75
50
25
0
0
1
10
100
nM
Insulin
####
***
**
##
++++
***
1
4
16
24
30
Time (h)

Figure 2.8: ATX is acutely upregulated by high glucose and high insulin in subcutaneous adipose tissue (SCAT) explants.

(A, B) SCAT explants from 25-40 week-old chow-fed female C57Bl6 mice were incubated in the presence of (A) 0, 6 or 25 mM glucose or (B) 0 or 100 nM insulin for 8 h and secreted ATX activity was determined. (C) Immunoblot analysis of secreted ATX (ATX-S) protein levels and (C, D) Akt phosphorylation at Ser^{473} in SCAT explants. Statistical analysis was performed using (A) one-way ANOVA followed by a Tukey's multiple comparison test or a (B-C) Student's *t*-test; *$p<0.05$, **$p<0.01$; n = 5-10 from 5-10 mice; S: secreted, PS: protein stain. (A-B) reproduced from D'Souza et. al, *Endocrinology*(176).

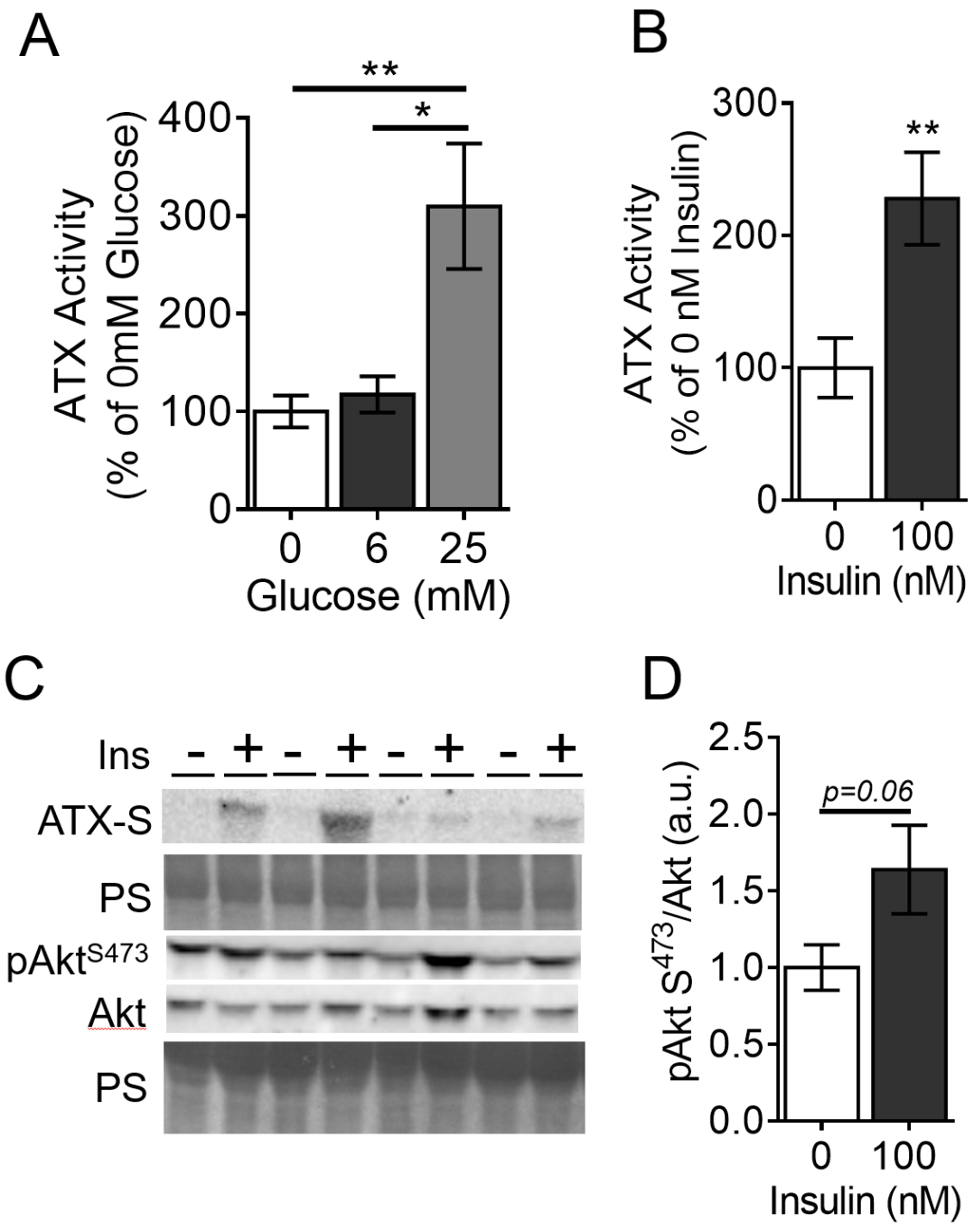
A
**
*
400
300
200
100
0
ATX Activity
(% of 0mM Glucose)
0
6
25
Glucose (mM)
B
300
200
100
0
**
ATX Activity
(% of 0 nM Insulin)
0
100
Insulin (nM)
C
Ins - + - + - + - +
ATX-S
PS
pAktS473
Akt
PS
D
2.5
2.0
1.5
1.0
0.5
0.0
p=0.06
pAkt S473/Akt (a.u.)
0
100
Insulin (nM)

Figure 2.9: Acute insulin stimulation of ATX secretion is PI3Kinase-dependent and mTOR-independent.

3T3-L1 adipocytes were incubated with media containing 25 mM glucose in the presence or absence of 0 or 100 nM insulin for 6 h. Where indicated, adipocytes were additionally treated with either 1 μM wortmannin (W), 100 nM rapamycin (R), 10 μg/ml cycloheximide (CHX) or a combination of 5 μg/ml brefeldin A and 5 μM monensin (B/M). (A, B) Cellular ATX protein expression, (C, D) secreted ATX protein expression, and (E) activity. Statistical analysis was performed using one-way ANOVA followed by a Tukey's multiple comparison test; **p*<0.05, **p<0.01, ****p*< 0.001, *****p*<0.0001 vs. untreated controls; $^{\#\#}p$<0.01, $^{\#\#\#}p$<0.001, $^{\#\#\#\#}p$<0.0001 for insulin plus chemical inhibitors vs. insulin minus chemical inhibitors; n = 9 from at least three independent experiments; C: cellular, S: secreted. (A-E) reproduced from D'Souza et. al, *Endocrinology*(176).

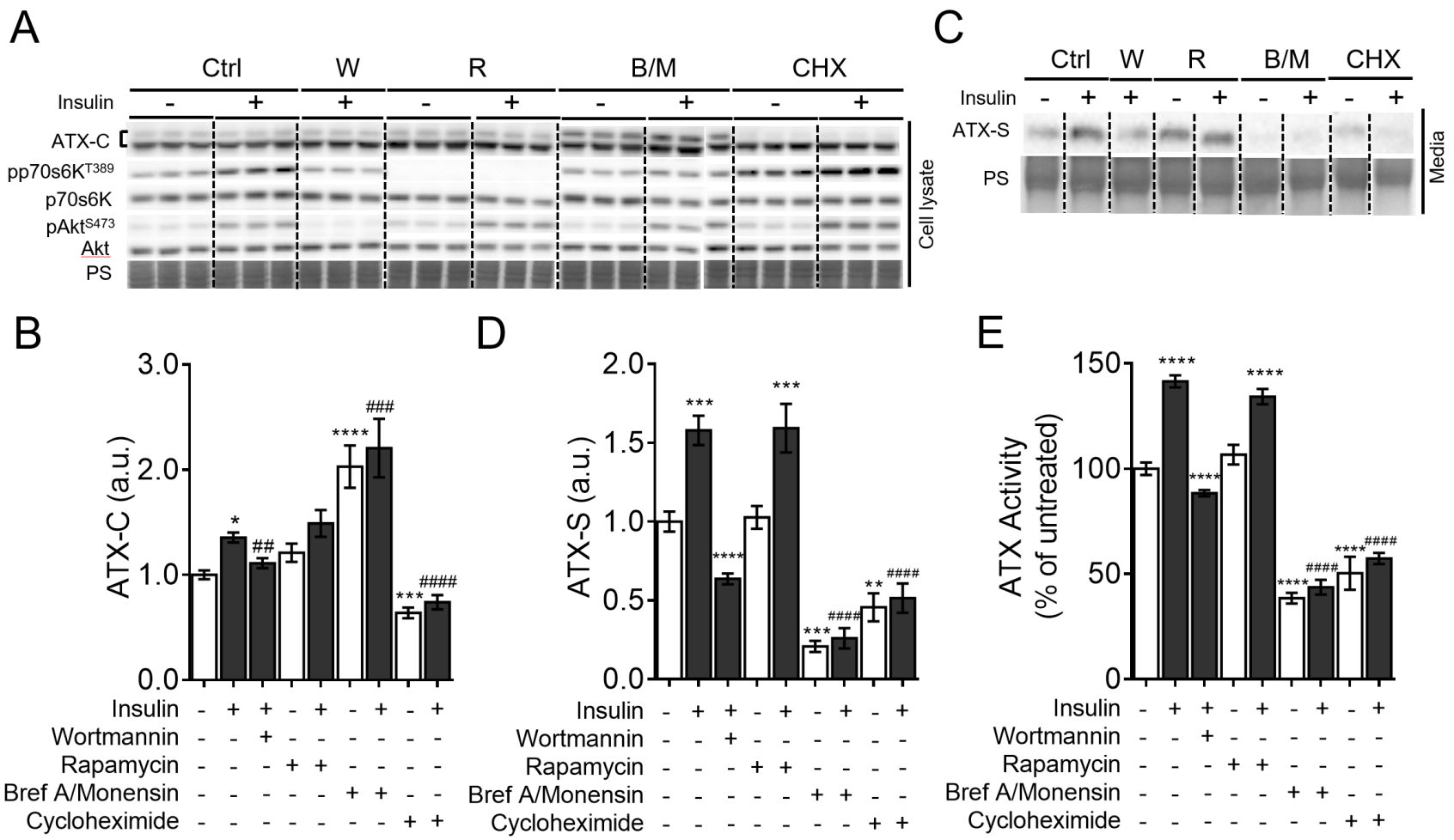
A
Ctrl
W
R
B/M
CHX
Insulin
ATX-C
pp70s6K^{T389}
p70s6K
pAkt^{S473}
Akt
PS
Cell lysate
C
ATX-S
PS
Media
B
ATX-C (a.u.)
D
ATX-S (a.u.)
E
ATX Activity (% of untreated)
Wortmannin
Rapamycin
Bref A/Monensin
Cycloheximide

Table 2.1: Primer sequences used to amplify murine mRNA.

Primer	**Sequence (5' to 3')**
ATX F	CTTGTGAAACGTTACGCTA
ATX R	CTTCATTATCTGATCGGTGT
RPL27 F	ACGGTGGAGCCTTATGTGAC
RPL27 R	TCCGTCAGAGGGACTGTCTT
RPL41 F	GCCATGAGAGCGAAGTGG
RPL41 R	CTCCTGCAGGCGTCGTAG

Table 2.2: List of primary antibodies used for immunoblots.

Target	**Company/Supplier, Catalog Number**
ATX	Cayman Chemicals, 10005375
Adiponectin	Novus, NBP2-22450
$pAKT^{S473}$	Cell Signaling, 9271
AKT	Millipore, 05-591
$pP70S6K^{T389}$	Cell Signaling,9234
P70S6K	Cell Signaling, 2708

Chapter 3: Investigating the Effect of ATX-LPA on Diet-Induced Insulin Resistance

3.1. Rationale and Objectives

Several studies from multiple groups have demonstrated a link between ATX-LPA signaling and obesity-induced insulin resistance(8,178,180,191). In Chapter 2, we demonstrated that ATX expression is regulated by certain factors that are increased in an insulin-resistant/diabetic milieu, such as glucose and insulin. However, it remains unclear whether the ATX-LPA pathway influences insulin function in target tissues, particularly skeletal muscle, the major site of insulin-stimulated glucose disposal. Therefore, the objective of this study was to test whether the ATX-LPA pathway impacts tissue and cellular insulin function using two mouse models with reduced ATX activity. The first model is a heterozygous whole body ATX knockout mouse with an approximately 50% reduction of circulating ATX and LPA. The second model is a mouse with pharmacological blunting of ATX activity.

Figures 3.2-3.6 and 3.11 and text present in this chapter have been reproduced from *The Journal of Lipid Research* article(253), below and edited as appropriate:

D'Souza, K., Nzirorera, C., Cowie, A., Varghese, G. P., Trivedi, P., Eichmann, T., Biswas, D., Touaibia, M., Morris, A. J., Aidinis, V., Kane, D. A., Pulinilkunnil, T. and Kienesberger, P.C. (2018). Autotaxin-Lysophosphatidic Acid Signaling Contributes to Obesity-Induced Insulin Resistance in Muscle and Impairs Mitochondrial Metabolism. *The Journal of Lipid Research.* **59**(10): 1805-1817.

The Journal of Lipid Research does not require copyright permission for use of text and figures.

3.2. Materials and Methods

3.2.1 Chemicals and Reagents

Unless otherwise stated, chemicals and reagents were obtained from Sigma. PF-8380 was provided by Dr. Mohamed Touaibia, Université de Moncton, NB, Canada.

3.2.2 Studies Involving Animals

All protocols involving mice were approved by the Dalhousie University Institutional Animal Care and Use Committee.

3.2.2.1 Whole Body Heterozygous ATX Knockout Mice

$ATX^{+/-}$ mice (C57Bl6/J-Enpp2<tm1.1Vart>/FLMG) were generated by Dr. Vassilis Aidinis, 'Alexander Fleming' Biomedical Sciences Research Center, Vari, Greece(154). Briefly, loxP-flanked neomycin selection cassettes were inserted upstream of exon 1 and downstream of exon 2(154). Transgenic expression of Cre recombinase in mice bearing this allele resulted in excision of both exons, thus abolishing protein expression. Experimental $ATX^{+/-}$ mice were on a C57Bl6/J background and bred with wild type (WT) mice. Upon arrival at the animal facility at Dalhousie Medicine New Brunswick, Saint John, NB, Canada, $ATX^{+/-}$ mice were bred with C57Bl6/J mice to expand the colony. Mice were genotyped as detailed previously(154). Mice were housed on a 12 h light: 12 h dark cycle with ad libitum access to chow diet (LD5001 from Lab diet with 13.5 kcal% from fat) or HFHS diet (12451 from Research Diets with 45 kcal% from fat and 17 kcal% from sucrose) and water. The HFHS diet was chosen to mimic a 'Western diet', which contains high levels of both fat and sugar. Seven to nine week-old male and female mice were randomly assigned to chow or HFHS cohorts and fed for 20 weeks. For food intake studies, male mice were individually housed and food consumption was monitored daily over a 5-day period 2 weeks post diet start. Mice were subjected to an insulin tolerance test (ITT) or glucose tolerance test (GTT) at 15 and 17 weeks post diet start, respectively. Peripheral fat accumulation in isoflurane-anesthetized mice was determined by X-ray imaging using a Bruker In-Vivo Xtreme imager 18 weeks post diet start. Planar X-ray images were analyzed using ImageJ software (NIH) and area of peripheral fat was expressed as percent of total body area.

Mice were euthanized by decapitation following a 3-h food withdrawal and tissues were collected. Perigonadal adipose tissue (PGAT) and BAT were weighed prior to being flash frozen.

EDTA-plasma was collected and spun at 15,600 × g for 10 min at 4°C. For serum collection, blood was spun at 2,000 × g for 15 min at 4°C. Plasma and serum were frozen and stored at -80°C until further use. A schematic of this experimental plan is shown in Figure 3.1A.

3.2.2.2 ITT and GTT

ITT and GTT were performed as previously described(254). For ITT, awake mice were injected intraperitoneally with 1 U human insulin (HumulinR, Eli Lilly)/kg body weight following a 3-h food withdrawal. For GTT, awake 16-h fasted mice were injected intraperitoneally with 20% (w/v) D-glucose at 2 g/kg body weight. Blood glucose was measured using an Aviva Nano glucometer (Accu-Chek).

3.2.2.3 Plasma and Serum Analysis

Serum insulin was determined using an ELISA kit assay (Crystal Chem). NEFA (WAKO Chemicals) and TG (Thermo Fisher Scientific) analysis were performed using colorimetric kit assays, as per the manufacturer's instructions. Plasma LPA levels were determined by HPLC/ESI/MS/MS analysis in collaboration with Dr. Andrew Morris at the University of Kentucky, Lexington, KY, USA as previously described(255).

3.2.2.4 *In vivo* and *Ex vivo* Insulin Signaling

For insulin signaling studies performed *in vivo*, mice were injected intraperitoneally with 10 U insulin/kg body weight or an equal volume of saline. After 10 min, mice were euthanized and tissues were collected. For *ex vivo* insulin signaling studies in muscle, isolated soleus muscles were pre-incubated for 30 min in pre-gassed (95% O2, 5% CO_2) Krebs-Henseleit bicarbonate buffer (KHB), pH 7.4 (118.5 mM NaCl, 4.7 mM KCl, 1.2 mM KH_2PO_4, 25 mM $NaCHO_3$, 2.5 mM $CaCl_2$, 1.2 mM $MgSO_4$ and 5 mM Hepes) at 37°C. Following subsequent incubation in buffer with or without 33 nM insulin for 10 min, muscles were removed, connective tissue, fat, and tendons were excised, and tissues were blotted dry and snap-frozen in liquid nitrogen.

3.2.2.5 Muscle Glucose Transport Assay

Glucose transport in soleus muscle was determined *ex vivo* as previously described(254), with slight modifications. Soleus muscles from mice were rapidly dissected, pre-incubated for 1 h in KHB containing 10 mM D-glucose at 37°C, and rinsed by incubation in KHB supplemented with 10 mM D-mannitol for 10 min. Glucose transport was assessed by incubation in KHB with 1 mM 2-deoxyglucose, 9 mM mannitol, 1.5 µCi/ml 2-deoxy-D-[1,2-^{3}H]glucose (Perkin Elmer), and 0.3 µCi/ml D-[1-^{14}C]mannitol (Perkin Elmer) for 20 min at 37°C. All buffers were pre-gassed with 95% O_2, 5% CO_2 and were supplemented with saline or 33 nM insulin. Basal and insulin-stimulated glucose transport were determined in contralateral muscles. Following the final incubation, muscles were cleaned by excising connective tissue, fat, and tendons, and tissues were blotted dry and snap-frozen in liquid nitrogen. Muscles were weighed and digested for 30 min in 300 µl of 1 N NaOH at 65°C and centrifuged at 13,000 x g for 10 min. Radioactivity in the supernatant was determined by liquid scintillation counting and glucose transport into tissues was calculated.

3.2.2.6 Pharmacological Inhibition of ATX in Mice *In Vivo*

The ATX inhibitor, ONO-8430506, was obtained from ONO Pharmaceutical Co., Osaka, Japan, and was dissolved in 7.5 mM NaOH as previously described(256). C57Bl/6J mice were obtained from The Jackson Laboratory and were placed on a chow or HFHS-diet for 20 weeks, starting at 8 weeks of age. At 17 weeks post-diet start, mice were orally gavaged with 30 mg/kg of vehicle (7.5 mM NaOH) or ONO-8430506 once daily for 3 consecutive weeks. GTT was performed at 15 weeks post-diet start to confirm the development of glucose intolerance and at 19 weeks post-diet start, after vehicle or ONO-8430506 were administered for 2 weeks. To determine food intake mice were individually housed and food consumption was monitored daily over a 5-day period 1 week before and after the start of vehicle or ONO-8430506 administration. A schematic of this experimental plan is shown in Figure 3.1B.

3.2.3 Cell Culture

Insulin resistance was induced in C2C12 cells as previously described(257). Following differentiation of myoblasts into myotubes, cells were serum starved for 24 h in DMEM-1x (Fisher Scientific, Cat: 11966025) supplemented with 5 mM glucose. Cells were then incubated in DMEM-1x supplemented with 5 mM glucose containing 2% (w/v) fatty acid-free (FAF) BSA and 0.8 mM sodium palmitate for 16-18 h, mimicking an insulin resistance state. Myotubes were cultured with 2% FAF-BSA in the absence of palmitate to mimic an insulin sensitive state. To examine insulin signaling, cells were incubated with 100 nM insulin or phosphate buffered saline (PBS) for 15 min. Cells were washed once and harvested in ice-cold PBS, followed by centrifugation at 20,000 × g for 10 min at 4°C.

Cell pellets were flash frozen in liquid nitrogen and stored at -80°C until further use. For experiments involving LPA, 1-oleoyl-2-hydroxy-sn-glycero-3-phosphate (18:1 LPA, Avanti, Cat: 857130) was dissolved in PBS + 0.1% FAF-BSA after evaporation of the chloroform solvent, gently shaken and mixed with DMEM-1x supplemented with 5 mM glucose prior to its addition to C2C12 myotubes. Cells were cultured in the absence of serum during LPA treatment to avoid potential additional sources of LPA, LPC, and ATX. For acute LPA experiments, C2C12 myotubes were pre-incubated in DMEM-1x supplemented with 5 mM glucose containing 2% FAF-BSA media for 10, 30 and 60min with 0, 1 and 10 μM. For chronic LPA experiments, C2C12 myotubes were co-incubated with 0, 1 and 10 μM for 16-18 h.

3.2.4 ATX Activity Assay – Choline Release Method

ATX activity in plasma and serum was quantified using the choline release assay described in Section 2.2.5.2.

3.2.5 Immunoblotting Analysis

Tissues and cells were homogenized in lysis buffer (20 mM Tris-HCl pH 7.5, 5 mM EDTA, 10 mM $Na_4P_2O_7$, 100 mM NaF, 1% NP-40) containing 2 mM sodium orthovanadate, 2

mM protease inhibitor cocktail (P8340, Sigma), and 100 µg/mL phosphatase inhibitor cocktail (524628, Calbiochem) using a tissue homogenizer (Omni TH, Omni International) or by sonication, respectively.

Immunoblotting was performed as described in Section 2.2.6. The primary antibodies used to probe the membranes are summarized in Table 3.1. Representative immunoblots are shown.

3.2.6 RNA Extraction and Gene Expression Analysis

RNA isolation, reverse transcription, and real-time quantitative PCR was performed as previously described(257) and as detailed in section 2.2.7. Primer sequences are provided in Table 3.2.

3.2.7 Statistical Analysis

Results are expressed as mean ± standard error of the mean (SEM). Comparisons between two groups were performed using an unpaired, two-tailed Student's t-test. Comparisons between multiple groups were performed using a paired or unpaired one- or two- way ANOVA followed by a Tukey or Sidak post hoc test, as appropriate. All statistical analysis was performed using Prism (GraphPad Software). P-values of less than 0.05 were considered statistically significant. For animal studies, "n" refers to the number of mice used, unless otherwise specified. For cell culture studies, experiments were performed in triplicates and data are from at least two independent experiments.

3.3. Results

3.3.1. Male Mice with Heterozygous ATX Deficiency ($ATX^{+/-}$) Have Reduced Obesity and Improved Glucose Homeostasis on an Obesogenic HFHS Diet

Although prior studies have suggested that ATX haploinsufficiency or adipocyte-specific ATX deficiency improves systemic glucose homeostasis in mice fed a high fat diet, the effect of ATX deficiency on adiposity and insulin signaling in different target tissues remains relatively unexplored (8,178). To clarify the role of ATX in diet-induced obesity, glucose metabolism, and

insulin signaling, we fed male WT and ATX$^{+/-}$ mice chow or HFHS diet for 20 weeks. In agreement with previous studies(8,154), plasma LPA levels, ATX activity, and ATX protein content were markedly reduced in ATX$^{+/-}$ mice compared to WT (Fig. 3.2A-E).

Body weights were similar between WT and ATX$^{+/-}$ mice immediately prior to HFHS feeding (WT: 22.45 ± 0.26 g, ATX$^{+/-}$ 22.30 ± 0.56 g, n = 15-18). However, HFHS-fed ATX$^{+/-}$ mice showed significantly reduced body weight gain compared to HFHS-fed WT mice while food intake was unchanged between genotypes (Fig. 3.3A, B). Total energy consumed, once accounting for different energy density between chow and HFHS diets, was unchanged between diets and genotypes. In agreement with lower body weight gain, HFHS-fed ATX$^{+/-}$ mice showed reduced peripheral fat accumulation and PGAT and BAT weights (Fig. 3.3C-E). Furthermore, HFHS-fed ATX$^{+/-}$ mice had improved glucose tolerance and insulin sensitivity, as assessed by a GTT and ITT, respectively (Fig. 3.3F, G). ATX$^{+/-}$ mice were also protected from HFHS diet-induced hyperglycemia (Fig. 3.3H), hyperinsulinemia (Fig. 3.3I), and hypertriglyceridemia (Fig. 3.3J), while serum NEFA levels were similar between groups (Fig. 3.3K). Taken together, these data suggest that partial ATX deficiency protects from diet-induced obesity and impaired glucose and lipid homeostasis in male mice.

3.3.2 Female Mice are Resistant to HFHS Diet-Induced Obesity and Changes in ATX Activity

HFHS-induced body weight gain was much less pronounced in female mice and was unchanged between genotypes (Fig. 3.4A). Modest body weight gain in female HFHS-fed WT mice was associated with unchanged serum ATX activity (Fig. 3.4B) and insulin-stimulated AKT phosphorylation in muscle when compared to chow-fed mice (Fig. 3.4C and D). Therefore, subsequent studies were performed in male mice.

3.3.3 HFHS-Fed ATX$^{+/-}$ Mice have Improved Insulin Signaling in Liver and Perigonadal Adipose Tissue

To examine whether enhanced tissue insulin function underlies the improvement in glucose homeostasis in HFHS-fed ATX$^{+/-}$ mice, we performed *in vivo* insulin signaling analysis in metabolically relevant tissues. HFHS-fed WT mice developed insulin resistance in the liver and PGAT as was evidenced by a two- to three-fold decrease in insulin-stimulated phosphorylation of AKT at S473 (Fig. 3.5A-C). Importantly, insulin-stimulated AKT phosphorylation in the liver was significantly improved in HFHS-fed ATX$^{+/-}$ mice compared to HFHS-fed WT mice, which was associated with reduced hepatic TG accumulation (Fig. 3.5D). Insulin-stimulated AKT phosphorylation was also unchanged in the PGAT of HFHS-fed ATX$^{+/-}$ mice compared to chow-fed ATX$^{+/-}$ mice (Fig. 3.5A, C). These results correspond with insulin-stimulated p70S6K phosphorylation at T389, where p70S6K phosphorylation was higher in liver and PGAT from insulin-injected HFHS-fed ATX$^{+/-}$ mice compared with WT mice (Fig. 3.5E, F). Taken together, our results suggest that ATX$^{+/-}$ mice are protected from HFHS diet-induced insulin resistance in liver and PGAT.

3.3.4 HFHS-Fed ATX$^{+/-}$ Mice have Improved Insulin Signaling in Muscle

We next examined insulin signaling in skeletal muscle. Similar to PGAT and liver, insulin-stimulated AKT phosphorylation in the gastrocnemius and soleus muscle, which consist of primarily glycolytic and oxidative fibers, respectively, was improved in HFHS-fed ATX$^{+/-}$ mice compared to WT (Fig. 3.6A-C). HFHS feeding resulted in significant reductions in insulin-stimulated p70S6K phosphorylation at T389 in the gastrocnemius and soleus of WT but not ATX$^{+/-}$ mice (Fig. 3.6A, D and E). Improved insulin signaling in skeletal muscle also corresponded with preserved insulin signaling in the heart of HFHS-fed ATX$^{+/-}$ mice(253).

To determine whether improvements in skeletal muscle insulin signaling in HFHS-fed ATX$^{+/-}$ mice are maintained in the absence of acute changes in circulating or neuronal factors, we performed insulin signaling analysis in soleus muscle *ex vivo* (Fig. 3.6A and F). Similar to

improved insulin signaling in gastrocnemius and soleus muscle from HFHS-fed ATX$^{+/-}$ mice *in vivo* (Fig. 3.6A-E), insulin-stimulated AKT phosphorylation *ex vivo* was higher in soleus muscle from HFHS-fed ATX$^{+/-}$ than HFHS-fed WT mice (Fig. 3.6A and F). Furthermore, sustained muscle insulin signaling in HFHS-fed ATX$^{+/-}$ mice was associated with preserved insulin-stimulation of glucose transport in soleus muscle of HFHS-fed ATX$^{+/-}$ mice *ex vivo* while the ability of insulin to stimulate glucose transport was reduced in soleus muscle from HFHS-fed WT compared to the chow control (Fig. 3.6G and H). In agreement with sustained insulin-stimulated glucose transport in HFHS-fed ATX$^{+/-}$ mice, soleus muscle from ATX$^{+/-}$ mice was protected from HFHS-induced decline of *Glut4* mRNA levels (Fig. 3.6I) while *Glut1* mRNA was unchanged between groups (Fig. 3.6J). Taken together, this suggests that insulin signaling is preserved in the muscle from HFHS-fed ATX$^{+/-}$ mice and that HFHS-induced reductions in glucose transport in the soleus are partially rescued by ATX deficiency.

3.3.5 The levels of distinct LPA receptors are altered in skeletal muscle from ATX$^{+/-}$ Mice

To determine whether levels of LPA receptors are altered in muscle from ATX$^{+/-}$ mice and by HFHS-feeding, we measured mRNA levels of LPA1-6 in the soleus muscle of 16-h fasted mice. *Lpa1-6* expression was not affected by diet (Fig. 3.7A-F). However, *Lpa2* and *Lpa4* were differentially expressed in HFHS-fed ATX$^{+/-}$ vs. WT mice, with reduced *Lpa2* levels and increased *Lpa4* levels in ATX$^{+/-}$ mice (Fig. 3.7B and D).

3.3.6 Pharmacological inhibition of ATX may moderately improve tissue insulin signaling *in vivo*

Heterozygous whole-body deletion of ATX resulted in improved systemic and tissue insulin sensitivity. To determine whether short-term pharmacological inhibition of ATX could also improve systemic glucose homeostasis and tissue insulin signaling, we administered vehicle or ONO-8403506 to male C57Bl6/J mice via oral gavage once a day for 3 consecutive weeks after 20 weeks of chow or HFHS feeding. Prior to gavage at 15 weeks post diet start, HFHS-fed

mice showed glucose intolerance as measured by a GTT (Fig. 3.8A and-B). Treatment with ONO-8403506 potently inhibited plasma ATX activity compared to vehicle control, with an 85% and 92% inhibition in chow and HFHS-fed mice, respectively (Fig. 3.8C). Glucose tolerance was similar between vehicle and ONO-8403506 groups after 2 weeks of treatment, although HFHS-induced changes in AUC did not reach statistical significance in the ONO-8403506 group (Fig. 3.8D and E). Food intake was similar between vehicle and ONO-8403506 groups prior to and following gavage, but gavage was associated with reduced food intake in HFHS-fed mice treated with ONO-8403506 (Fig. 3.8F). Body weight was similar between vehicle and ONO-8403506 groups, however, percentage of weight change over the 3-week gavage period was augmented in HFHS-fed mice treated with ONO-8403506 vs. vehicle (Fig. 3.8G and H). Interestingly, treatment with ONO-8403506 for 3 weeks ameliorated HFHS-induced hyperglycemia, suggesting that ONO-8403506 may improve systemic glucose homeostasis (Fig. 3.8I).

To determine whether ATX inhibition alters tissue insulin sensitivity, we performed an *in vivo* insulin signaling experiment. The livers of HFHS-fed mice treated with vehicle or ONO-8403506 showed insulin resistance when compared to the chow-fed controls, as measured by AKT phosphorylation at Ser473 (Fig. 3.9A and B). However, ONO-8403506 treatment appeared to lessen the degree of hepatic insulin resistance since Akt phosphorylation increased significantly following insulin stimulation in this group, which was not observed in HFHS-fed mice treated with vehicle (Fig. 3.9B). Interestingly, fold stimulation of AKT phosphorylation following insulin administration was greater in HFHS-fed mice receiving ONO-8403506 compared to vehicle (Fig. 3.9C). Taken together, these data suggest that pharmacological inhibition of ATX could potentially ameliorate systemic glucose homeostasis and liver insulin resistance in mice.

3.3.7. The effect of LPA on Insulin Signaling in C2C12 Myotubes is Time Dependent

So far, our *in vivo* studies suggested that partial ATX deficiency and reduced LPA production improve skeletal muscle insulin sensitivity. We next sought to investigate whether the

resistance of ATX$^{+/-}$ mice towards obesity-induced impairment of skeletal muscle insulin signaling is due to a direct effect of LPA on skeletal muscle cell insulin function. C2C12 myotubes were incubated with 1-oleoyl-LPA at concentrations of 1 and 10 μM to mimic physiological and pathophysiological LPA concentrations, respectively(8,9,178), for 10, 30, and 60 min followed by insulin signaling analysis. Pre-incubation of myotubes with LPA for 10 min had no effect on AKT Ser473 phosphorylation, despite LPA increasing extracellular signal regulated kinase (ERK) 1/2 phosphorylation, a known LPA signaling target (Fig. 3.10A-C). Interestingly, 30 min pre-incubation with either 1 or 10 μM LPA significantly increased insulin-stimulated AKT phosphorylation when compared to no-LPA controls (Fig. 3.10A, D), which corresponded with LPA-induced ERK phosphorylation (Fig. 3.10A, E). Surprisingly, when the LPA pre-incubation period was increased to 60 min, insulin-stimulated AKT phosphorylation was blunted with both 1 and 10 μM LPA (Fig. 3.10F). ERK phosphorylation was only increased by LPA under basal, but not insulin-stimulated conditions (Fig. 3.10G). Taken together, these data suggest that LPA influences insulin-stimulated AKT activation in C2C12 myotubes in a time-dependent manner with longer durations of LPA incubation resulting in insulin resistance. These data also suggest that physiological and pathophysiological levels of LPA can similarly impair insulin signaling in muscle cells.

3.3.8. Long-term LPA Treatment Impairs Insulin Signaling and Exacerbates Palmitate-Induced Insulin Resistance in C2C12 Myotubes

We next wanted to determine how a more chronic treatment with LPA in the absence or presence of high palmitate, thereby modelling an obese-insulin resistant milieu, influences myocyte insulin sensitivity. C2C12 cells do not secrete significant amounts of ATX, as measured by FS-3 activity assays (data not shown), therefore LPA was used to modulate ATX-LPA signaling. C2C12 myotubes were incubated for 18 h in the absence or presence of 1 or 10 μM LPA (Fig. 3.11A). Cells were also simultaneously incubated in the absence or presence of palmitate to induce insulin resistance, as determined by a 2-fold reduction in insulin-stimulated

AKT phosphorylation at S473 (Fig. 3.11A, B). At baseline, incubation with LPA impaired insulin-stimulated AKT phosphorylation in C2C12 myotubes, similar to palmitate (Fig. 3.11A, B). Moreover, LPA exacerbated the palmitate-induced reduction in insulin-stimulated AKT phosphorylation (Fig. 3.11A, B). Acute and prolonged treatment of C2C12 cells with LPA has been linked to the activation of ERK, which has been implicated with the development of insulin resistance (Fig. 3.10A, C, E, G)(189,258). LPA-induced impairment of insulin function and exacerbation of palmitate-induced insulin resistance in C2C12 cells was associated with an upregulation of ERK phosphorylation (Fig. 3.11A, C). Taken together, these data suggest that prolonged exposure of muscle cells to LPA directly promotes the development of insulin resistance and worsens impaired insulin signaling induced by a lipotoxic milieu.

3.3.9. Palmitate-Induced Lipotoxicity, but not Incubation with LPA is Associated with Marked Changes in LPA Receptor Levels in C2C12 Myotubes

Because distinct LPA receptors are altered with ATX deficiency in the soleus muscles of fasted mice (Fig. 3.7B, D), we next wanted to determine whether addition of LPA under insulin sensitive and resistance promoting conditions could alter *Lpa*1-6 mRNA expression in C2C12 myotubes. Palmitate-induced insulin resistance had a marked effect on all LPA receptors, with decreased mRNA levels of *Lpa1, 2*, and *3* (Fig. 3.12A-C) and increased levels of *Lpa4, 5*, and *6* following incubation with palmitate (Fig. 3.12D-F). The effect of palmitate on *Lpa3* was most pronounced, where incubation with palmitate diminished Lpa3 mRNA levels (Fig. 3.12C). Despite the marked impact of palmitate-induced lipotoxicity on LPA receptor expression, incubation of myotubes with 1 and 10 μM LPA did not significantly alter LPA mRNA levels (Fig. 3.12A-F). Taken together, this suggests that palmitate-induced lipotoxicity but not LPA change LPA receptor levels.

3.4 Discussion

Recent studies have implicated the ATX-LPA axis in obesity and impaired glucose homeostasis(8,178,180,204,205,212). Improvements in obesity-induced insulin resistance and

glucose intolerance in ATX mutant mice were primarily ascribed to changes in adipose tissue metabolism and function(8,178). It remained unclear whether changes in insulin signaling in other metabolically relevant tissues contribute to the protection of ATX deficient mice from diet-induced insulin resistance. . In this study, we show that amelioration of obesity and systemic insulin resistance in HFHS-fed mice with partial ATX deficiency is associated with increased insulin signaling in metabolically active tissues, including liver and adipose tissue.

Pharmacological inhibition of ATX activity *in vivo*, using ONO-8403506, appeared to ameliorate HFHS-induced hyperglycemia and tended to improve hepatic insulin signaling. In skeletal muscle, which accounts for the majority of insulin-stimulated glucose disposal(34), partial ATX deficiency led to improvements in insulin signaling and insulin-stimulated glucose transport following HFHS feeding.

Examination of LPA receptor gene expression suggested that alterations in *Lpa2* and *Lpa4* levels may also play a role in improved insulin sensitivity in muscle from HFHS-fed $ATX^{+/-}$ mice, although the contribution of distinct LPA receptors and downstream signaling to the regulation of tissue insulin function requires further investigation. In agreement with a potentially important role of these receptors, $Lpa4^{-/-}$ mice were protected from diet-induced insulin resistance, liver steatosis and systemic inflammation, but this effects was ascribed to increased PPARγ activity in adipose tissue (253). In C2C12 myotubes, LPA directly impaired insulin signaling and exacerbated palmitate-induced insulin resistance. While palmitate-induced lipotoxicity induced marked changes in LPA1-6 mRNA expression in C2C12 cells, the presence of LPA did not significantly alter LPA receptor levels.

The lack of coordinated changes in LPA receptors between our models may be related to the different presentation of disturbed metabolic homeostasis; our mouse model is characterized by hyperinsulinemia and hyperglycemia, whereas our C2C12 model is characterized by lipotoxicity-induced insulin resistance. Future work will utilize more complementary approaches of insulin resistance, such as feeding mice a high fat diet (60% calories from fat) to promote

lipotoxicity in vivo or incubating C2C12 myotubes under conditions mimicking hyperglycemia and hyperinsulinemia.

Our data suggest that the ATX-LPA pathway plays an important role in the development of obesity-induced insulin resistance in adipose tissue, liver, and skeletal muscle. Few prior studies have examined the effect of the ATX-LPA signaling pathway on tissue insulin function(180,191,206). Rancoule et al.(191) initially showed that administration of a LPA1/3 receptor antagonist in high fat diet-fed mice for three weeks improves insulin sensitivity and increases insulin-stimulated glucose oxidation in the soleus muscle *ex vivo*, suggesting that LPA signaling through LPA1/3 impairs muscle insulin function. However, systemic LPA1/3 administration had multiple effects on other tissues, including increased pancreatic islet mass and liver glycogen storage, which may have contributed to changes in glucose metabolism in muscle(191). Although our studies demonstrate that LPA receptor mRNA expression is unchanged by diet-induced obesity and insulin resistance (Fig. 3.7A and C), it is likely that the activity and downstream signaling of distinct LPA receptors are altered by HFHS-feeding. Indeed, a recent study showed that while adipose tissue Lpa4 levels are unchanged in HFD-fed mice, Lpa4 deficiency protects mice from diet-induced insulin resistance, hepatic steatosis and adipose tissue inflammation(259).

Notably, female mice showed a resistance to gaining weights and developing skeletal muscle insulin resistance on our HFHS feeding regimens. Intriguing, serum ATX activity was also not significantly increased during HFHS feeding. Future studies should address why female mice are resistant to increasing weight, including examining how food intake is altered.

Two very recent studies have provided more direct evidence for an inhibitory role of ATX-LPA signaling on tissue insulin function(180,206). Acute pre-treatment of primary rat hepatocytes with LPA decreased insulin-stimulated AKT phosphorylation, glucokinase and sterol regulatory element-binding protein (SREBP)-1c expression, PI3K activation, and glycogen synthesis, likely via LPA1 and/or LPA3(206). Moreover, inhibition of ATX protected against

interleukin 6-induced impairment of insulin-stimulated AKT phosphorylation in 3T3-L1 adipocytes(180).

In this study, we show that reduced ATX function ameliorates insulin resistance in skeletal muscle *in vivo*. Furthermore, chronic incubation with LPA directly impairs insulin signaling in C2C12 myotubes. Acute LPA treatment revealed a time-dependent effect of LPA on myotube insulin signaling. Pre-incubation of myotubes with LPA for 30 min increased insulin-stimulated AKT phosphorylation, which is likely due to a concurrent activation of PI3K signaling through $G\alpha_{i/o}$ proteins(167). In contrast, pre-incubation with LPA for 60 min significantly reduced insulin signaling in myotubes. Together, this suggests that longer LPA treatments induce insulin resistance in myotubes, possibly through activation of ERK or other stress kinases or via PI3K pathway de-sensitization(167,189). Future studies should identify the precise mechanisms that mediate LPA-induced muscle insulin resistance. Use of commercially available ERK or stress kinase inhibitors would allow to determine whether activation of these pathways are necessary for LPA-induced insulin resistance in muscle cells. It is also possible that $G\alpha_{13}$, a mediator downstream of most LPA receptors(167), plays a role in the inhibition of muscle insulin function by LPA since $G\alpha_{13}$ was shown to impair muscle glucose uptake and systemic insulin sensitivity in HFD-fed mice(260).

ATX inhibitors are currently in Phase 3 clinical trials for the treatment of idiopathic pulmonary fibrosis(261). Furthermore, use of the ATX inhibitor, PF-8380, in mice ameliorated HFD-diet induced cardiac hypertrophy, function and inflammation(219). Our work also suggests that pharmacological inhibition of ATX may hold potential as a potential treatment to improve systemic glucose homeostasis. Potent, 3-week inhibition of ATX is tolerated well in chow and HFHS-fed mice, with no obvious adverse effects. Importantly, ATX inhibition was associated with an amelioration of HFHS diet-induced systemic hyperglycemia and lessened the degree of hepatic insulin resistance, as measured by AKT phosphorylation at S473. However, much more work is required to determine whether pharmacological inhibition can treat diet-induced insulin

resistance. Future studies should address more comprehensively whether ATX inhibition alters skeletal muscle and adipose tissue insulin function.

Overall, this work suggests that, in addition to reduced adipose tissue accumulation, improved insulin signaling in adipose tissue, liver, and muscle contributes to preserved global insulin sensitivity in mice with partial ATX deficiency. Our data also suggest that the ATX-LPA pathway directly impairs insulin signaling and insulin-stimulated glucose transport in skeletal muscle (Fig. 3.13). Since impaired insulin signaling and metabolism in skeletal muscle are primary drivers of system insulin resistance and hyperglycemia(34), we propose that the obesity-induced upregulation of ATX and LPA receptor signaling in muscle are critical mechanisms of insulin resistance. Therefore, modulators of the ATX-LPA pathway may present novel strategies towards the prevention and treatment of obesity-associated insulin resistance and T2D.

3.5 Figures

Figure 3.1: Schematic of experimental plans using mouse models of reduced ATX activity

The experimental layout to examine glucose homeostasis and insulin function in **(A)** mice with global heterozygous ATX deficiency and **(B)** mice with pharmacological ATX inhibition.

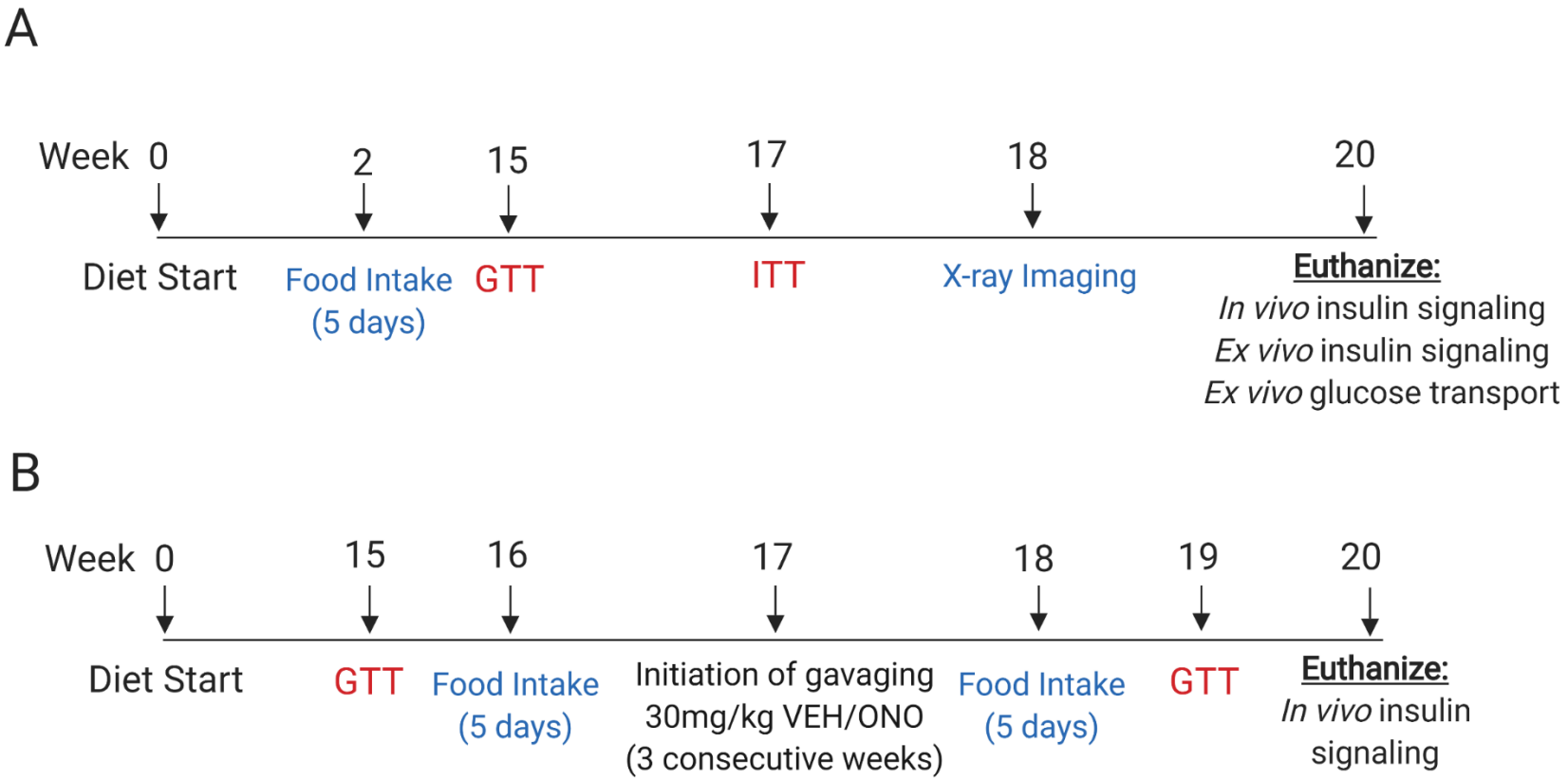
A
Week 0
2
15
17
18
20
Diet Start
Food Intake
(5 days)
GTT
ITT
X-ray Imaging
Euthanize:
In vivo insulin signaling
Ex vivo insulin signaling
Ex vivo glucose transport
B
Week 0
15
16
17
18
19
20
Diet Start
GTT
Food Intake
(5 days)
Initiation of gavaging
30mg/kg VEH/ONO
(3 consecutive weeks)
Food Intake
(5 days)
GTT
Euthanize:
In vivo insulin
signaling

Figure 3.2: Plasma ATX activity and protein levels are reduced in male chow and HFHS-fed ATX$^{+/-}$ mice.

(A) Plasma LPA levels (n = 7-8) in chow-fed WT and ATX$^{+/-}$ mice. **(B)** Plasma ATX activity (n = 9-11) and **(C, D)** ATX protein content (n = 5-6) in chow and HFHS-fed WT and ATX$^{+/-}$ mice. **(E)** Inhibition of ATX activity using PF-8380 blunts choline release, demonstrating that choline release is highly ATX dependant. **(A, E)** Statistical analysis was performed using a Student's t-test or **(B, C)** two-way ANOVA followed by a Tukey's multiple comparison test; (**A-C, E**) *$p < 0.05$, ****$p < 0.0001$ vs. chow/WT/ctrl; ##$p < 0.01$, ####$p < 0.0001$ as indicated. **(A-E)** reproduced from D'Souza et al, *Journal of Lipid Research*(253).

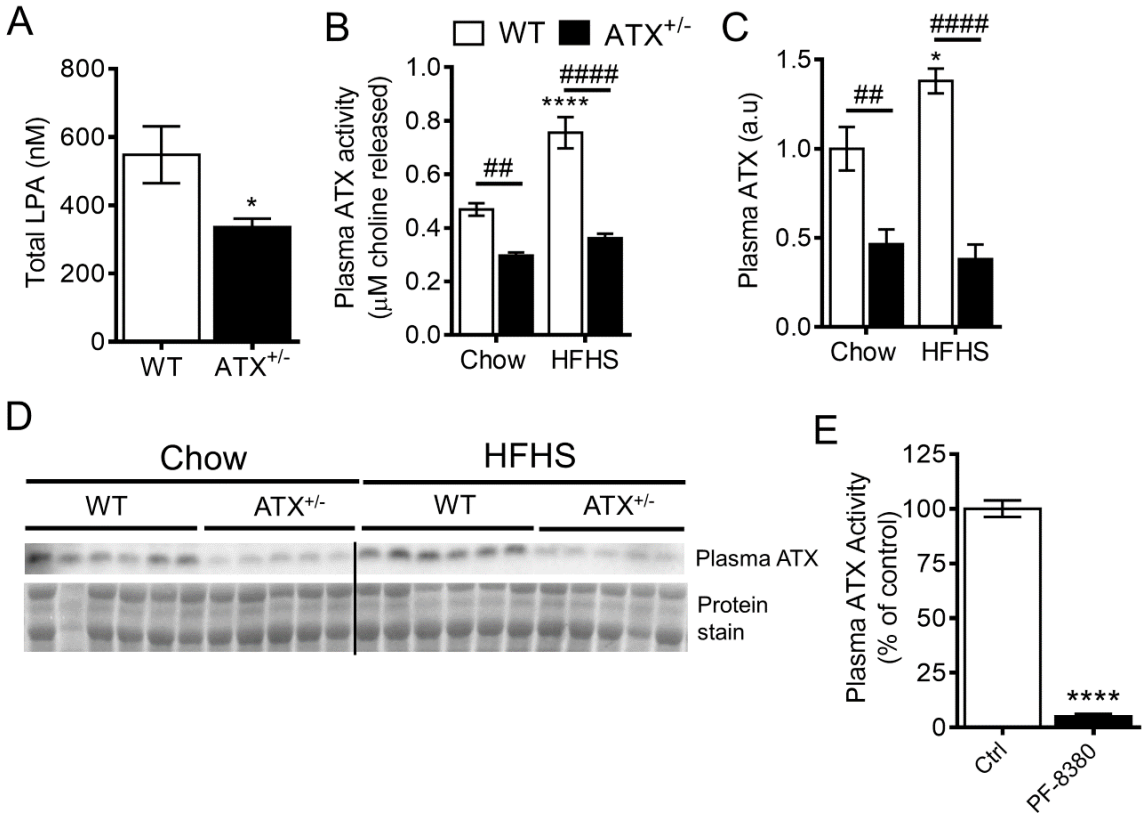
A
Total LPA (nM)
800
600
400
200
0
*
WT
ATX+/-
B
WT
ATX+/-
Plasma ATX activity
(μM choline released)
1.0
0.8
0.6
0.4
0.2
0.0
##
****
####
Chow
HFHS
C
Plasma ATX (a.u)
1.5
1.0
0.5
0.0
##
*
####
Chow
HFHS
D
Chow
HFHS
WT
ATX+/-
WT
ATX+/-
Plasma ATX
Protein
stain
E
Plasma ATX Activity
(% of control)
125
100
75
50
25
0
****
Ctrl
PF-8380

Figure 3.3: Partial ATX deficiency protects from HFHS diet-induced obesity and metabolic dysfunction in male mice.

(A) Body weight gain, (**B**) food intake, (**C**) peripheral fat accumulation, (**D**) PGAT weight, (**E**) BAT weight, **(F)** GTT following an intraperitoneal injection with D-glucose at 2 g/kg body weight, and **(G)** ITT following an intraperitoneal injection with human insulin at 1 U/kg body weight in male chow and HFHS-fed WT and $ATX^{+/-}$ mice (n = 14-26). **(H)** Blood glucose and serum **(I)** insulin, **(J)** TGs, and **(K)** NEFA in chow and HFHS-fed WT and $ATX^{+/-}$ mice following a 3-h food withdrawal (n = 5-13). **(A-K)** Statistical analysis was performed using a two-way ANOVA followed by a Tukey's multiple comparison test; **(A)** *$p < 0.05$, **$p < 0.01$ vs. $ATX^{+/-}$ HFHS; **(B-E, H-K)** $^{\#}p < 0.05$, $^{\#\#}p < 0.01$, $^{\#\#\#}p < 0.001$, $^{\#\#\#\#}p < 0.0001$ vs. chow; *$p < 0.05$ as indicated; **(F, G)** *$p < 0.05$, **$p < 0.01$, ***$p < 0.001$ for WT HFHS vs. chow; $^{\$\$}p < 0.01$ for $ATX^{+/-}$ HFHS vs. chow. **(A-K)** reproduced from D'Souza et al, *Journal of Lipid Research*(253).

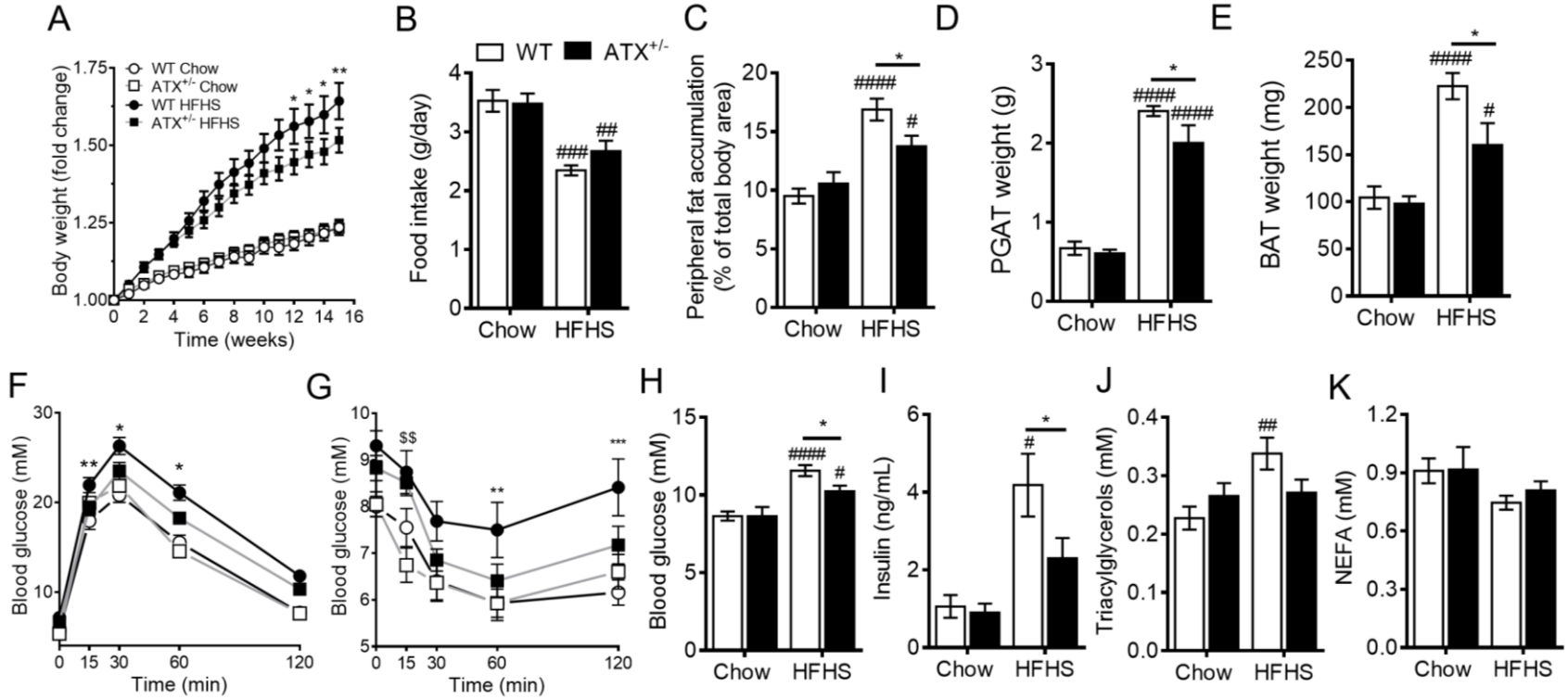
A
Body weight (fold change)
Time (weeks)
WT Chow
ATX+/- Chow
WT HFHS
ATX+/- HFHS
B
Food intake (g/day)
WT
ATX+/-
Chow
HFHS
C
Peripheral fat accumulation (% of total body area)
D
PGAT weight (g)
E
BAT weight (mg)
F
Blood glucose (mM)
Time (min)
G
Blood glucose (mM)
Time (min)
H
Blood glucose (mM)
I
Insulin (ng/mL)
J
Triacylglycerols (mM)
K
NEFA (mM)

Figure 3.4: Female mice are protected from HFHS diet-induced insulin resistance and upregulation of ATX.

(**A**) Body weight gain and (**B**) serum ATX activity in female chow and HFHS-fed WT and $ATX^{+/-}$ mice. (**C-D**) Immunoblot and densitometric analysis of AKT phosphorylation at S^{473} in gastrocnemius muscle from chow and HFHS-fed WT and $ATX^{+/-}$ mice subjected to a 3-h food withdrawal, followed by the intraperitoneal injection of saline or 10 U/kg insulin (n = 3-5). (**B-C**) Statistical analysis was performed using a two-way ANOVA followed by a Tukey's multiple comparison test; (**B**) $^{###}p < 0.001$ as indicated; (**C**) ****$p < 0.0001$ vs. saline. **(A-D)** reproduced from D'Souza et al, *Journal of Lipid Research*(253).

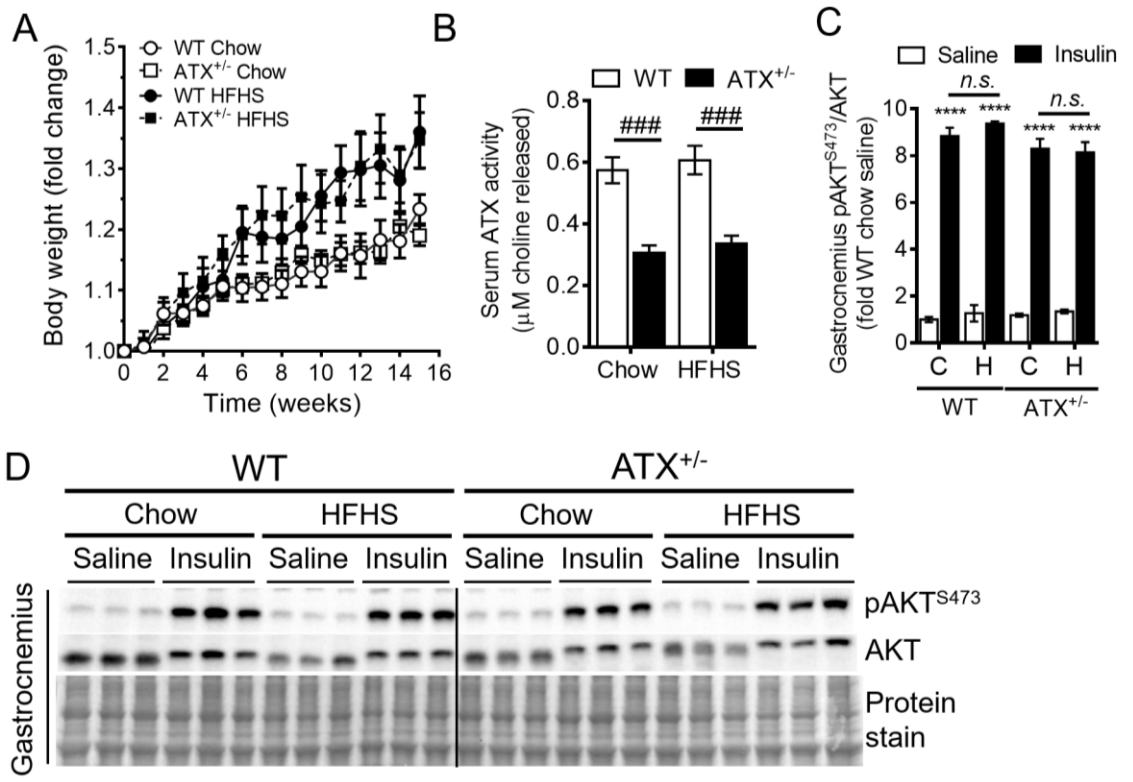
A
Body weight (fold change)
Time (weeks)
WT Chow
ATX+/- Chow
WT HFHS
ATX+/- HFHS
B
Serum ATX activity (μM choline released)
WT
ATX+/-
###
###
Chow
HFHS
C
Gastrocnemius pAKTS473/AKT (fold WT chow saline)
Saline
Insulin
n.s.
n.s.
****
C
H
C
H
WT
ATX+/-
D
WT
ATX+/-
Chow
HFHS
Chow
HFHS
Saline
Insulin
Saline
Insulin
Saline
Insulin
Saline
Insulin
Gastrocnemius
pAKTS473
AKT
Protein stain

Figure 3.5: HFHS-fed ATX$^{+/-}$ mice show improved insulin signaling in liver and PGAT. Immunoblot and densitometric analysis of AKT phosphorylation at S473 and p70S6K phosphorylation at T^{389} in **(A, B, E)** liver and **(A, C, F)** PGAT from chow and HFHS-fed male WT and ATX$^{+/-}$ mice subjected to a 3-h food withdrawal, followed by the intraperitoneal injection of saline or 10 U/kg insulin (n = 4-6). **(D)** Liver TGs from chow and HFHS-fed WT and ATX$^{+/-}$ mice subjected to a 3-h food withdrawal (n = 9) **(B-F)** Statistical analysis was performed using a two-way ANOVA followed by a Tukey's multiple comparison test; *p < 0.05, ***p < 0.001, ****p < 0.0001 vs. saline; #p < 0.05, ##p < 0.01, ####p < 0.0001 as indicated; C, chow; H, HFHS. **(A-F)** reproduced from D'Souza et al, *Journal of Lipid Research*(253).

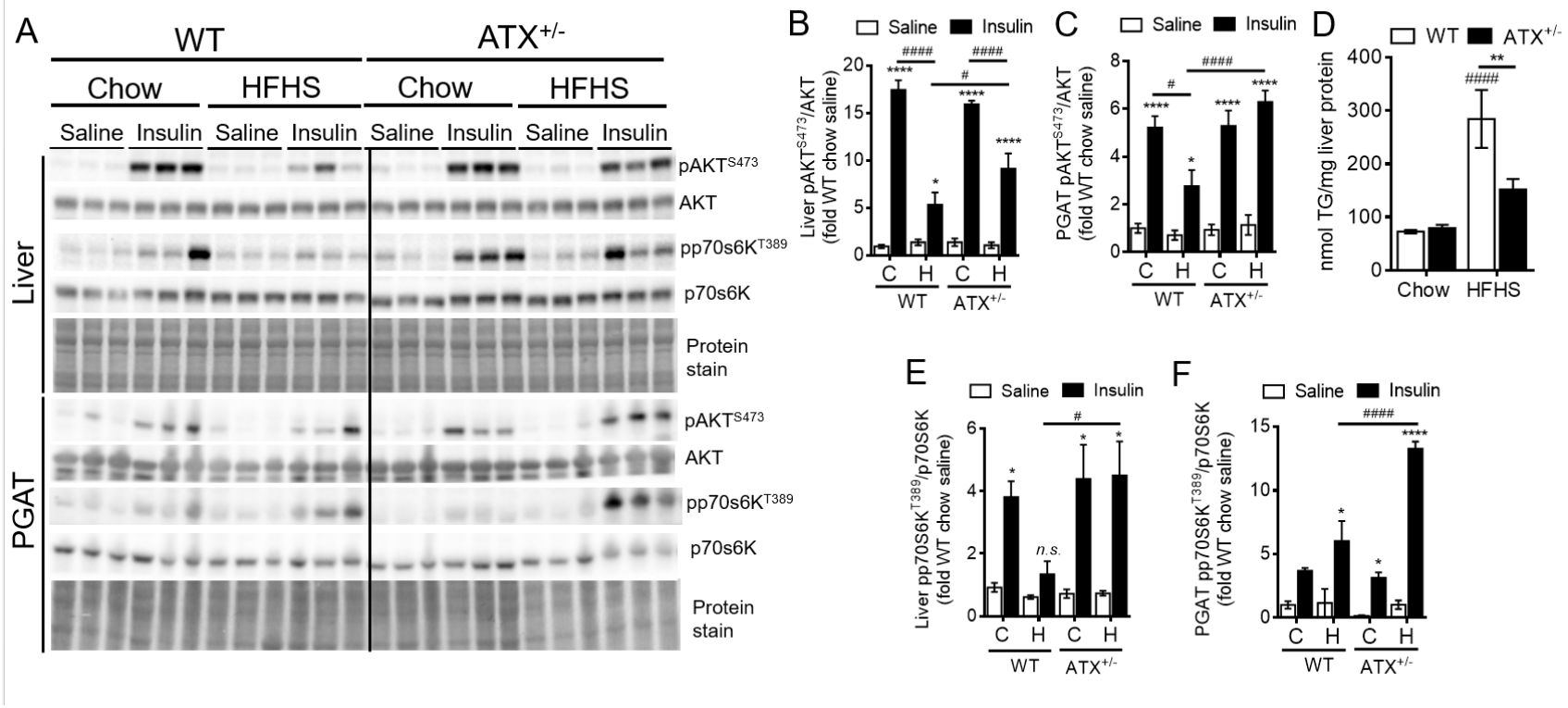
A
WT
ATX+/-
Chow
HFHS
Chow
HFHS
Saline
Insulin
Saline
Insulin
Saline
Insulin
Saline
Insulin
Liver
PGAT
pAKTS473
AKT
pp70s6KT389
p70s6K
Protein stain
pAKTS473
AKT
pp70s6KT389
p70s6K
Protein stain
B
Saline
Insulin
Liver pAKTS473/AKT (fold WT chow saline)
C H C H
WT
ATX+/-
C
Saline
Insulin
PGAT pAKTS473/AKT (fold WT chow saline)
C H C H
WT
ATX+/-
D
WT
ATX+/-
nmol TG/mg liver protein
Chow
HFHS
E
Saline
Insulin
Liver pp70S6KT389/p70S6K (fold WT chow saline)
n.s.
C H C H
WT
ATX+/-
F
Saline
Insulin
PGAT pp70S6KT389/p70S6K (fold WT chow saline)
C H C H
WT
ATX+/-

Figure 3.6: HFHS-fed ATX$^{+/-}$ mice show improved insulin signaling in skeletal muscle *in vivo* and *ex vivo*.

Immunoblot and densitometric analysis of AKT phosphorylation at S^{473} and p70S6K phosphorylation at T^{389} in **(A, B, D)** gastrocnemius muscle (Gastrocn.) and **(A, C, E)** soleus muscle from chow and HFHS-fed male WT and ATX$^{+/-}$ mice subjected to a 3-h food withdrawal, followed by the intraperitoneal injection of saline or 10 U/kg insulin (n = 4-6). **(A, F)** Immunoblot and densitometric analysis of AKT phosphorylation at S^{473} in soleus muscle isolated from chow and HFHS-fed male WT and ATX$^{+/-}$ mice following incubation with saline or 33 nM insulin *ex vivo* (n = 3-5). **(G)** Glucose transport rate and **(H)** fold stimulation of glucose transport in soleus muscle from chow and HFHS-fed male WT and ATX$^{+/-}$ mice incubated with saline or 33 nM insulin *ex vivo*. Gene expression analysis of **(I)** *Glut4* and **(J)** *Glut1* in soleus muscle from chow and HFHS-fed male WT and ATX$^{+/-}$ mice (n = 7-10). **(B-J)** Statistical analysis was performed using a two-way ANOVA followed by a Tukey's multiple comparison test; (**B-H**) *$p < 0.05$, ***$p < 0.001$, ****$p < 0.0001$ vs. saline; $^{\#}p < 0.05$, $^{\#\#\#\#}p < 0.0001$ as indicated; (**I, J**) *$p < 0.05$, **$p < 0.01$ vs. chow. C, chow; H, HFHS. **(A-J)** reproduced from D'Souza et al, *Journal of Lipid Research*(253).

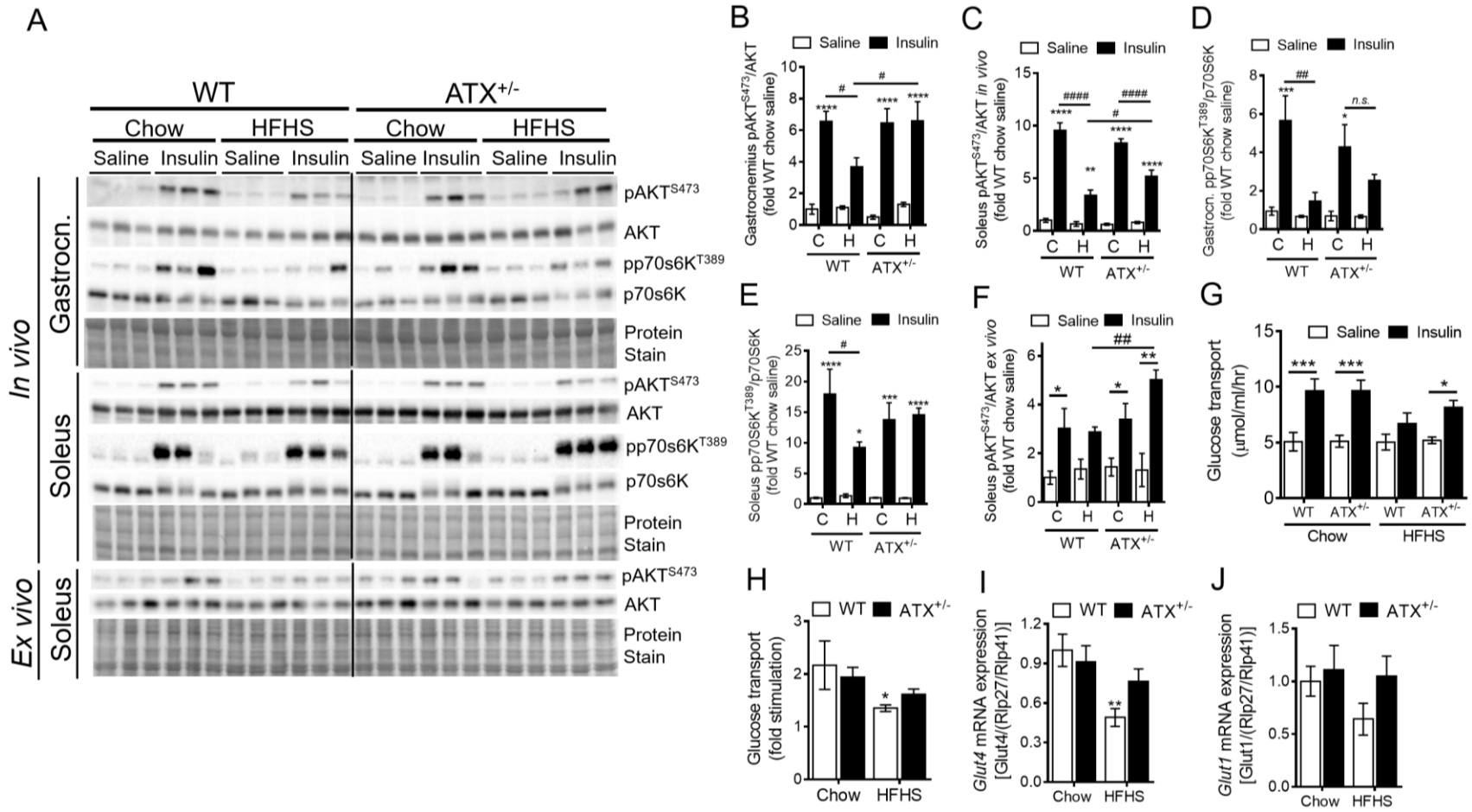
A
WT
ATX+/-
Chow
HFHS
Saline
Insulin
In vivo
Gastrocn.
Soleus
Ex vivo
Soleus
pAKTS473
AKT
pp70s6KT389
p70s6K
Protein Stain
B
Gastrocnemius pAKTS473/AKT (fold WT chow saline)
C
Soleus pAKTS473/AKT in vivo (fold WT chow saline)
D
Gastrocn. pp70S6KT389/p70S6K (fold WT chow saline)
E
Soleus pp70S6KT389/p70S6K (fold WT chow saline)
F
Soleus pAKTS473/AKT ex vivo (fold WT chow saline)
G
Glucose transport (µmol/ml/hr)
H
Glucose transport (fold stimulation)
I
Glut4 mRNA expression [Glut4/(Rlp27/Rlp41)]
J
Glut1 mRNA expression [Glut1/(Rlp27/Rlp41)]
C
H
n.s.

Figure 3.7: Levels of distinct LPA receptors are altered in the soleus muscle from ATX$^{+/-}$ mice.

Gene expression analysis of **(A-F)** *Lpa1-6* in soleus muscle from fasted chow and HFHS-fed male WT and ATX$^{+/-}$ mice (n = 9-11). Statistical analysis was performed using a two-way ANOVA followed by a Tukey's multiple comparison test; *$p < 0.05$.

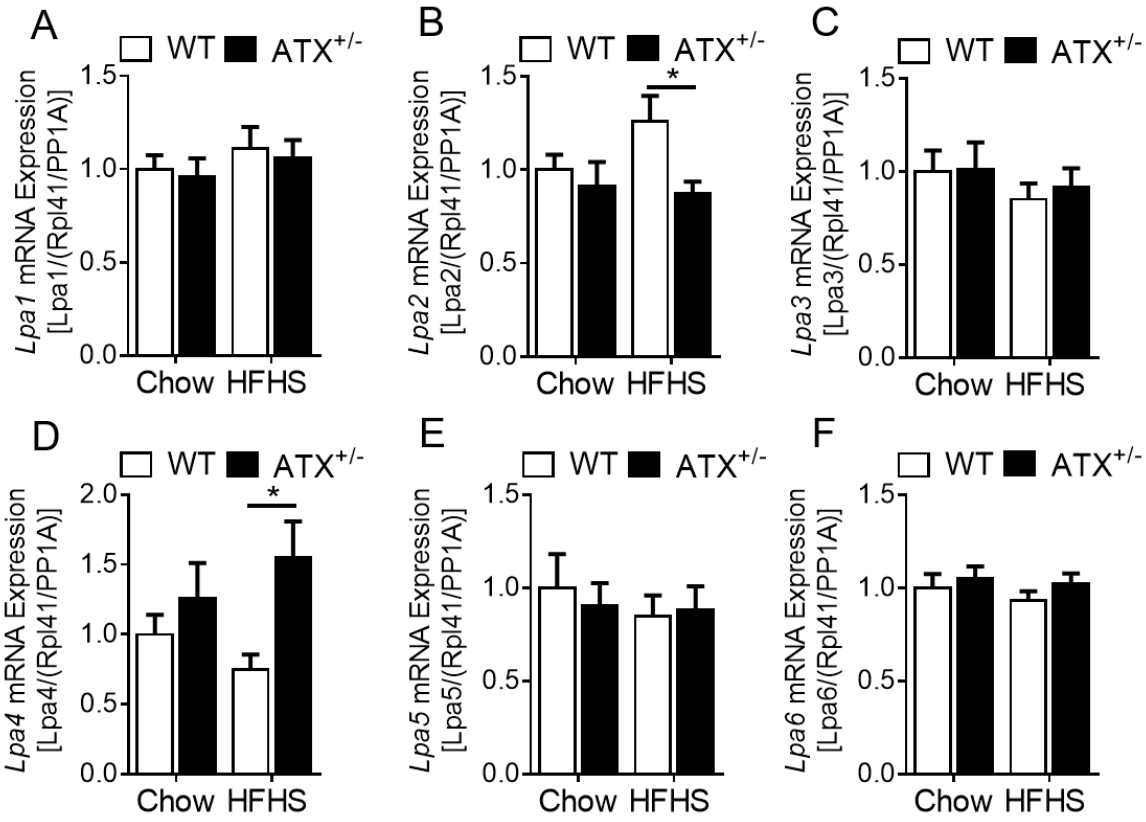
A
WT
ATX+/-
Lpa1 mRNA Expression [Lpa1/(Rpl41/PP1A)]
1.5
1.0
0.5
0.0
Chow
HFHS
B
WT
ATX+/-
*
Lpa2 mRNA Expression [Lpa2/(Rpl41/PP1A)]
1.5
1.0
0.5
0.0
Chow
HFHS
C
WT
ATX+/-
Lpa3 mRNA Expression [Lpa3/(Rpl41/PP1A)]
1.5
1.0
0.5
0.0
Chow
HFHS
D
WT
ATX+/-
*
Lpa4 mRNA Expression [Lpa4/(Rpl41/PP1A)]
2.0
1.5
1.0
0.5
0.0
Chow
HFHS
E
WT
ATX+/-
Lpa5 mRNA Expression [Lpa5/(Rpl41/PP1A)]
1.5
1.0
0.5
0.0
Chow
HFHS
F
WT
ATX+/-
Lpa6 mRNA Expression [Lpa6/(Rpl41/PP1A)]
1.5
1.0
0.5
0.0
Chow
HFHS

Figure 3.8: Pharmacological inhibition of ATX with ONO-8430506 for 3 weeks ameliorates HFHS diet-induced hyperglycemia.

(A) GTT following an intraperitoneal injection with D-glucose at 2 g/kg body weight in male C57Bl6/J mice after 15 weeks of chow or HFHS feeding, prior to vehicle or ONO-8430506 administration, and **(B)** AUC of GTT ($n = 20$). **(C)** Plasma ATX activity in mice fed chow or HFHS diet for 23 weeks 20 h following final administered with vehicle or ONO-8430506 ($n = 3$-4). **(D)** GTT in mice at 19 weeks post-diet start, following 2-week treatment with vehicle or ONO-8430506, and **(E)** AUC of GTT ($n = 10$). **(F)** Food intake 1 week before and after start of vehicle or ONO-8430506 administration ($n = 10$). **(G)** Body weight in chow and HFHS-fed mice following 3 weeks of vehicle and ONO-8430506 administration, and **(H)** percent change in body weight over the course of 3 weeks of vehicle and ONO-8430506 administration. **(I)** Blood glucose levels in 3 h-fasted chow and HFHS-fed mice following 3 weeks of vehicle and ONO-8430506 administration ($n = 10$). **(A-I)** Statistical analysis was performed using a two-way ANOVA followed by a Tukey's multiple comparison test; $^{*}p < 0.05$, $^{**}p < 0.01$, $^{***}p < 0.001$ and ****p < 0.0001, $^{\#\#\#}p < 0.001$, $^{\#\#\#\#}p < 0.0001$ vs. chow control. AUC, area under the curve.

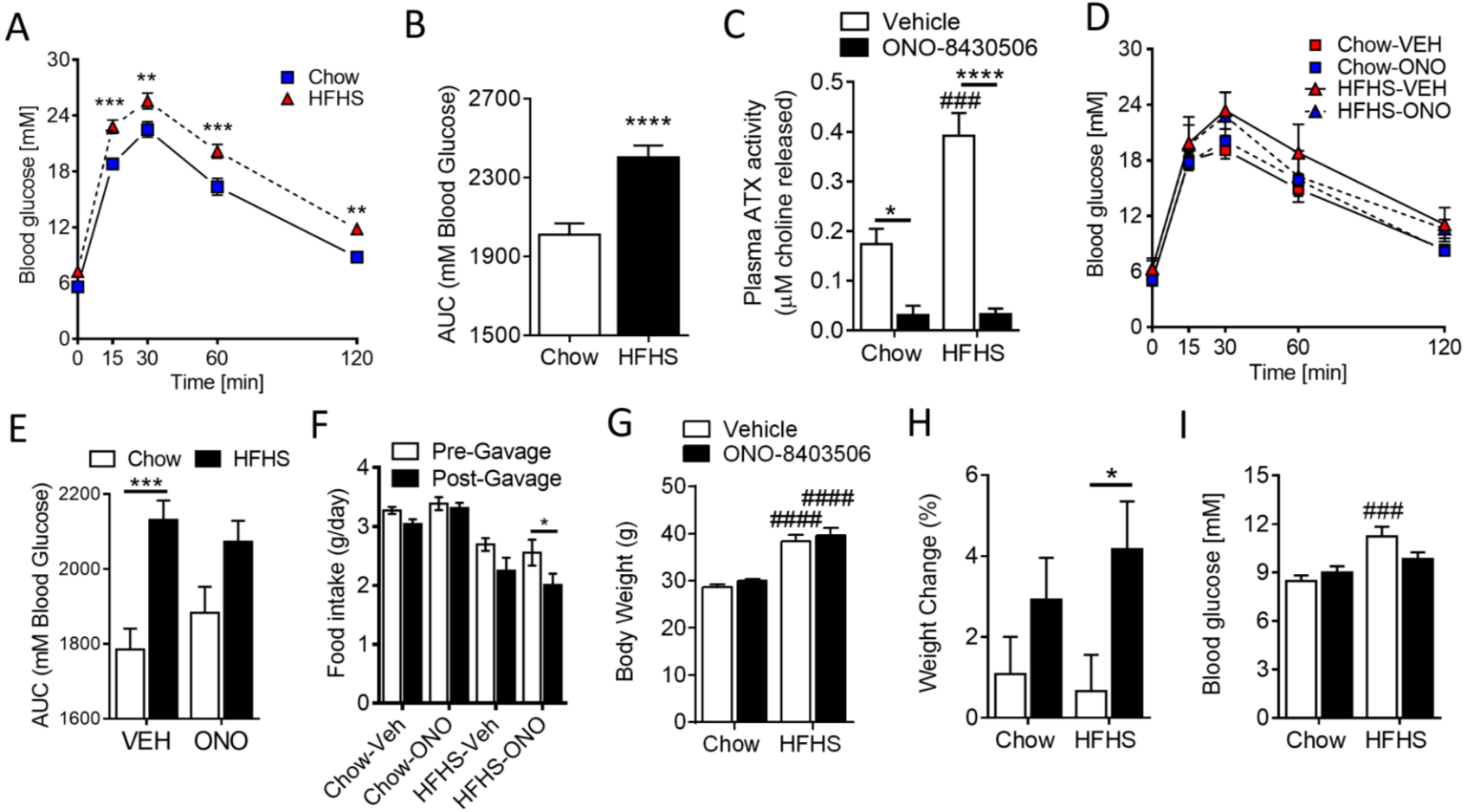
A
Blood glucose [mM]
Time [min]
Chow
HFHS
B
AUC (mM Blood Glucose)
Chow
HFHS
C
Vehicle
ONO-8430506
Plasma ATX activity (µM choline released)
Chow
HFHS
D
Blood glucose [mM]
Time [min]
Chow-VEH
Chow-ONO
HFHS-VEH
HFHS-ONO
E
Chow
HFHS
AUC (mM Blood Glucose)
VEH
ONO
F
Pre-Gavage
Post-Gavage
Food intake (g/day)
Chow-Veh
Chow-ONO
HFHS-Veh
HFHS-ONO
G
Vehicle
ONO-8403506
Body Weight (g)
Chow
HFHS
H
Weight Change (%)
Chow
HFHS
I
Blood glucose [mM]
Chow
HFHS

Figure 3.9: ONO-8430506 administration tends to ameliorate impaired insulin signalling in the liver from HFHS-fed mice.

(A) Representative immunoblot depicting levels of AKT phosphorylated at S473 and total AKT in liver from chow and HFHS-fed male C57Bl6/J mice following 3 weeks of vehicle (V) or ONO-8430506 (O) administration and after intraperitoneal injection of saline or 10 U/kg insulin, and **(B)** associated densitometric analysis (n = 3-4 for saline, n = 6-7 for insulin). Statistical analysis was performed using a two-way ANOVA followed by a Tukey's multiple comparison test; *$p < 0.05$, ***$p < 0.001$, ****$p < 0.0001$ vs. saline or as indicated; $^{\#}p < 0.05$, $^{\#\#}p < 0.01$ as indicated or vs. chow.

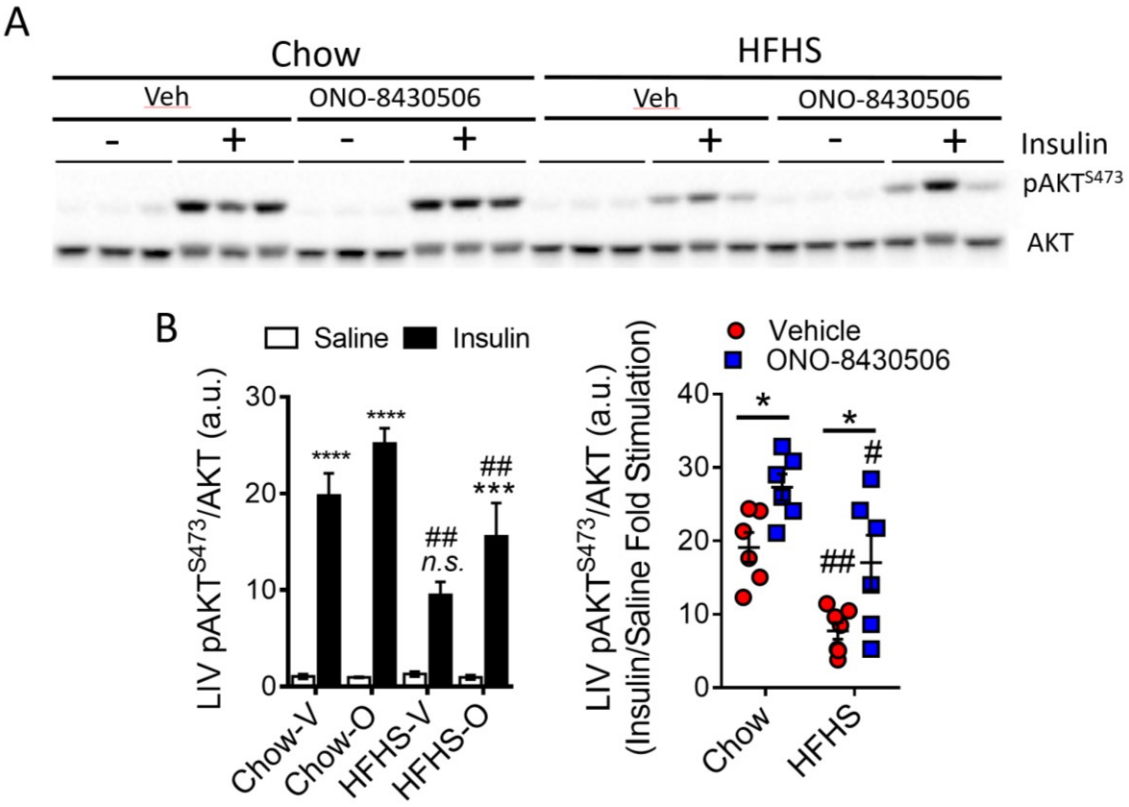
A
Chow
HFHS
Veh
ONO-8430506
Veh
ONO-8430506
-
+
-
+
+
-
+
Insulin
pAKTS473
AKT
B
Saline
Insulin
LIV pAKTS473/AKT (a.u.)
30
20
10
0
****
****
##
n.s.
##
***
Chow-V
Chow-O
HFHS-V
HFHS-O
Vehicle
ONO-8430506
LIV pAKTS473/AKT (a.u.)
(Insulin/Saline Fold Stimulation)
40
30
20
10
0
*
*
#
##
Chow
HFHS

Figure 3.10: LPA influences insulin signalling in C2C12 myotubes in a time-dependent manner

Immunoblot and densiometric analysis of **(A, B, D, F)** AKT phosphorylation at S^{473} and **(A, C, E, G)** ERK phosphorylation at $T^{202/}Y^{204}$ in C2C12 myotubes pre-incubated with 0, 1 or 10 μM LPA for **(A-C)** 10 min **(A, D-E)** 30 min, and **(A, F-G)** 60 min, followed by the stimulation with 20 nM insulin for 15 min (n = 6). **(B-G)** Statistical analysis was performed using a two-way ANOVA followed by a Tukey's multiple comparison test. *$p < 0.05$, **p < 0.01, ****$p < 0.0001$; $^{\#}p < 0.05$, $^{\#\#}p < 0.01$ as indicated or vs. no-LPA no-insulin controls; $^{\$}$p < 0.05, $^{\$\$}$p < 0.01 vs. no-LPA plus insulin controls. Ins, Insulin.

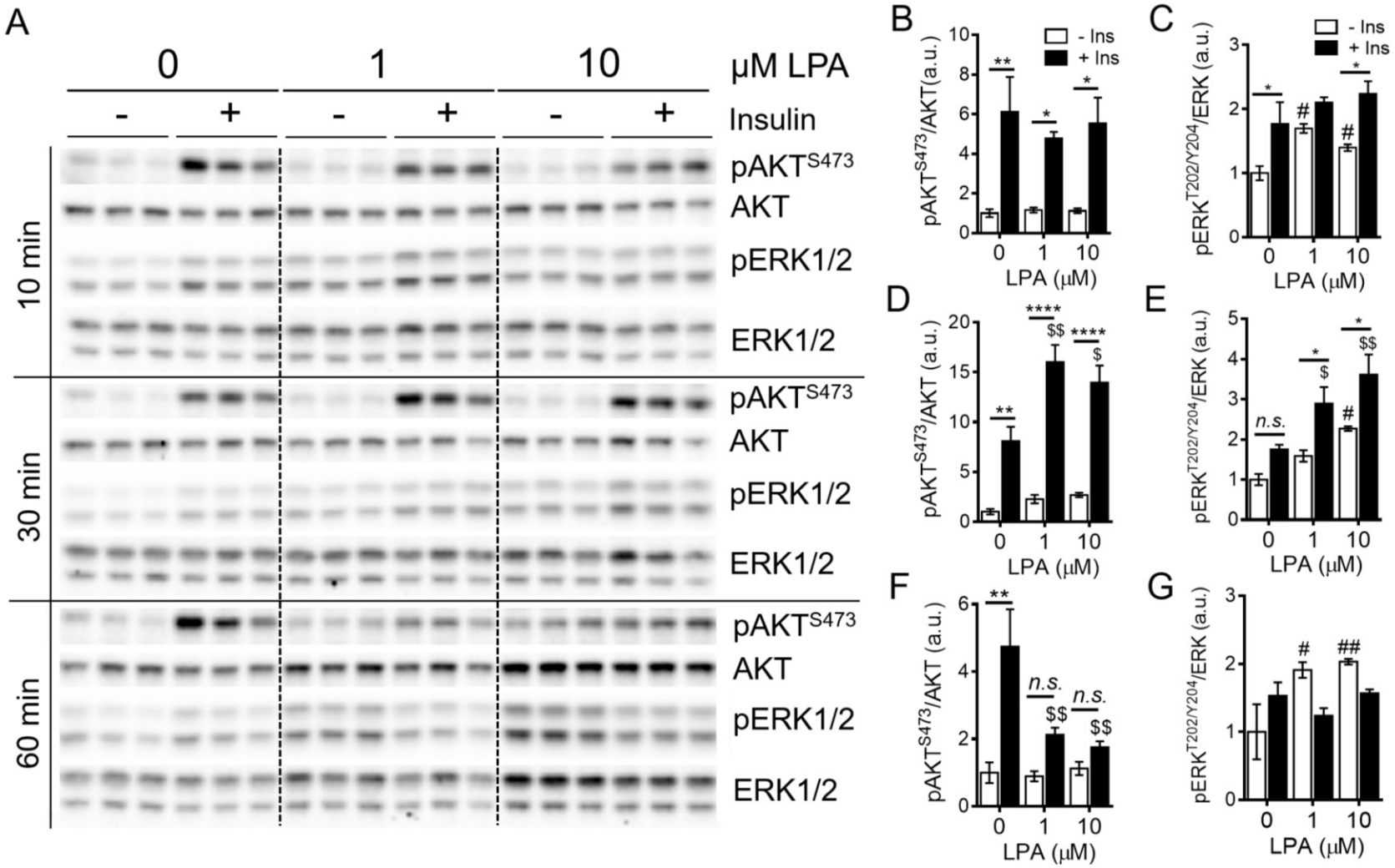
A
0
1
10
μM LPA
-
+
-
+
-
+
Insulin
10 min
30 min
60 min
pAKTS473
AKT
pERK1/2
ERK1/2
B
pAKTS473/AKT(a.u.)
- Ins
+ Ins
LPA (μM)
C
pERKT202/Y204/ERK (a.u.)
D
E
n.s.
F
G

Figure 3.11: LPA impairs insulin signaling and exacerbates palmitate-induced insulin resistance in C2C12 myotubes.

Immunoblot and densiometric analysis of **(A, B)** AKT phosphorylation at S^{473}, and **(A, C)** ERK phosphorylation at $T^{202/}Y^{204}$ in C2C12 myotubes incubated in the absence or presence of palmitate and 0, 1 or 10 μM LPA for 18 h, followed by the stimulation with 20 nM insulin for 15 min (n = 6). **(B-C)** Statistical analysis was performed using a two-way ANOVA followed by a Tukey's multiple comparison test. *$p < 0.05$, ****$p < 0.0001$ vs. no-Insulin; $^{\#}p < 0.05$, $^{\#\#}p < 0.01$, $^{\#\#\#}p < 0.001$, $^{\#\#\#\#}p < 0.0001$ vs. no-LPA controls. **(A-C)** reproduced from D'Souza et al, *Journal of Lipid Research*(253).

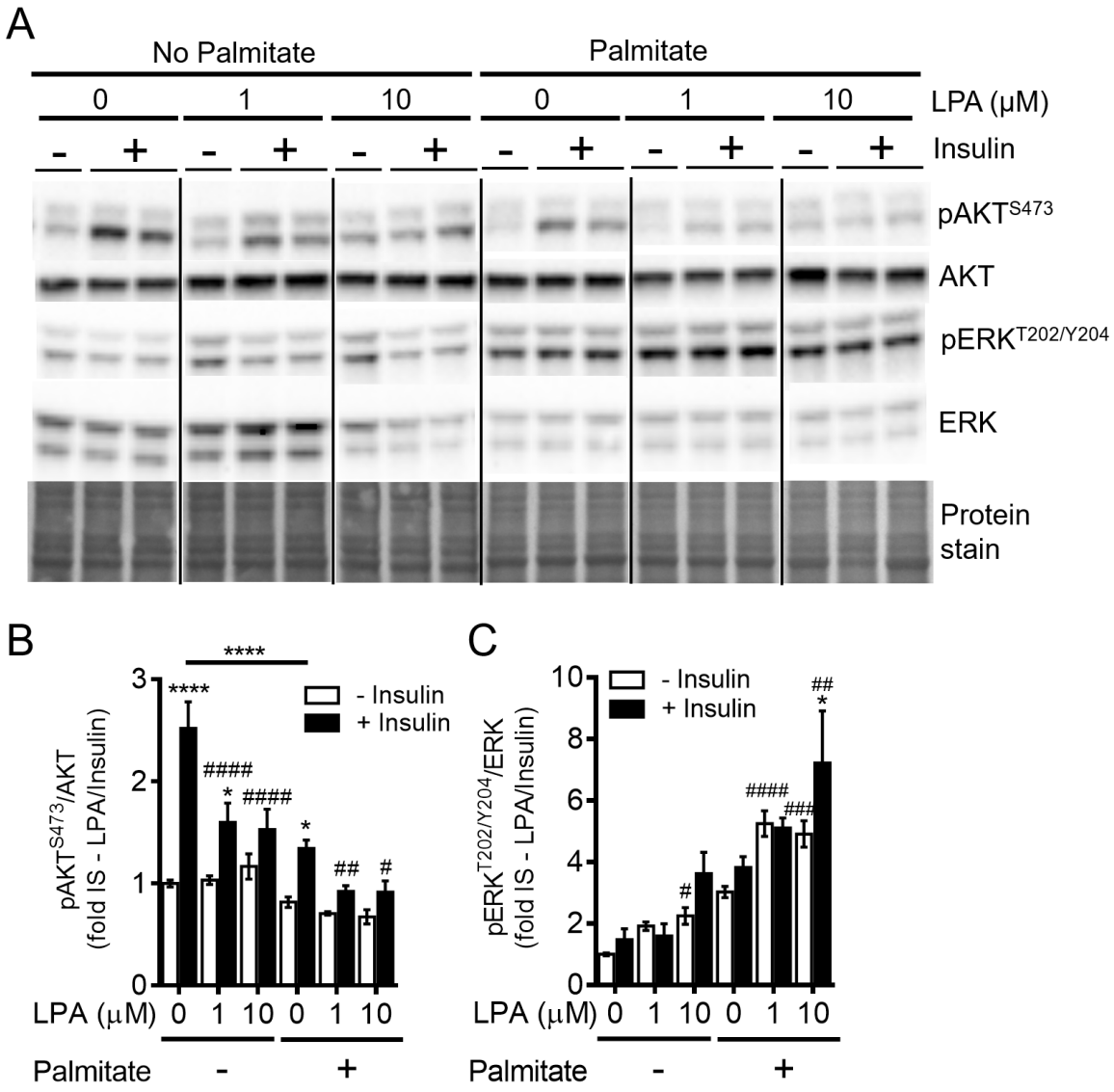
A
No Palmitate
Palmitate
0
1
10
0
1
10
LPA (μM)
- + - + - + - + - + - +
Insulin
pAKTS473
AKT
pERKT202/Y204
ERK
Protein stain
B
pAKTS473/AKT (fold IS - LPA/Insulin)
- Insulin
+ Insulin
****
LPA (μM) 0 1 10 0 1 10
Palmitate - +
C
pERKT202/Y204/ERK (fold IS - LPA/Insulin)
- Insulin
+ Insulin
LPA (μM) 0 1 10 0 1 10
Palmitate - +

Figure 3.12: LPA receptor levels are altered following induction of palmitate-induced insulin resistance, but not LPA treatment in C2C12 myotubes.

Gene expression analysis of **(A-F)** Lpa1-6 in C2C12 myotubes incubated in the absence or presence of 0.8 mM palmitate and 0, 1 or 10 μM LPA for 18 h (n = 12 from four different experiments). Statistical analysis was performed using a two-way ANOVA followed by a Tukey's multiple comparison test. *$p < 0.05$, **p<0.01, ***p<0.001, ****$p < 0.0001$. – Palm, no palmitate; + Palm, palmitate.

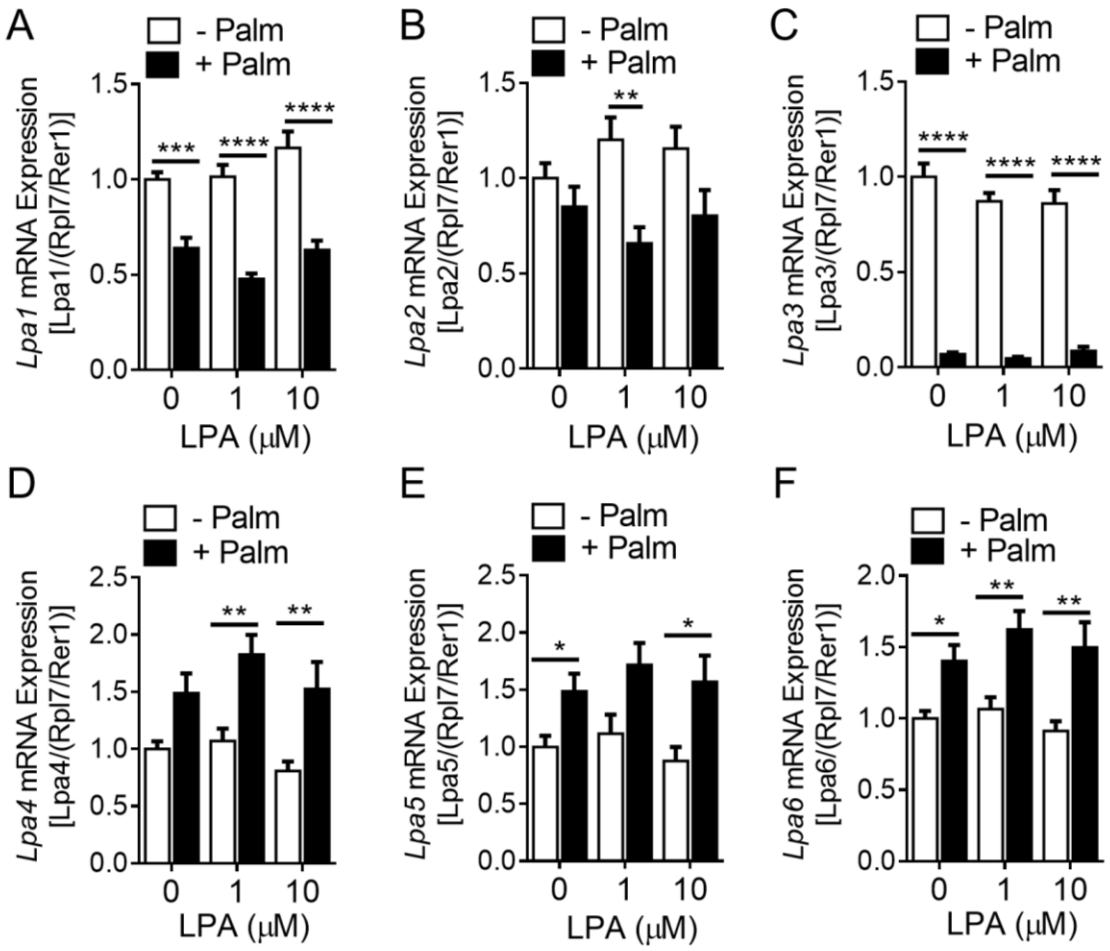
A
- Palm
+ Palm
Lpa1 mRNA Expression [Lpa1/(Rpl7/Rer1)]
1.5
1.0
0.5
0.0
***
****
****
0
1
10
LPA (μM)
B
- Palm
+ Palm
Lpa2 mRNA Expression [Lpa2/(Rpl7/Rer1)]
1.5
1.0
0.5
0.0
**
0
1
10
LPA (μM)
C
- Palm
+ Palm
Lpa3 mRNA Expression [Lpa3/(Rpl7/Rer1)]
1.5
1.0
0.5
0.0
****
****
****
0
1
10
LPA (μM)
D
- Palm
+ Palm
Lpa4 mRNA Expression [Lpa4/(Rpl7/Rer1)]
2.5
2.0
1.5
1.0
0.5
0.0
**
**
0
1
10
LPA (μM)
E
- Palm
+ Palm
Lpa5 mRNA Expression [Lpa5/(Rpl7/Rer1)]
2.5
2.0
1.5
1.0
0.5
0.0
*
*
0
1
10
LPA (μM)
F
- Palm
+ Palm
Lpa6 mRNA Expression [Lpa6/(Rpl7/Rer1)]
2.0
1.5
1.0
0.5
0.0
*
**
**
0
1
10
LPA (μM)

Figure 3.13: Proposed role of the ATX-LPA axis in skeletal muscle insulin function.

In diet-induced obesity, upregulation of the ATX-LPA pathway contributes to impaired skeletal muscle insulin signaling and glucose transport, a primary driver of systemic insulin resistance and T2D. Inhibition of the ATX-LPA pathway enhances skeletal muscle insulin signaling and glucose transport in an obesogenic milieu, thereby ameliorating diet-induced obesity and impaired glucose homeostasis. The specific role of distinct muscle LPA receptors in this process requires further investigation. GSV, Glut4 storage vesicles.

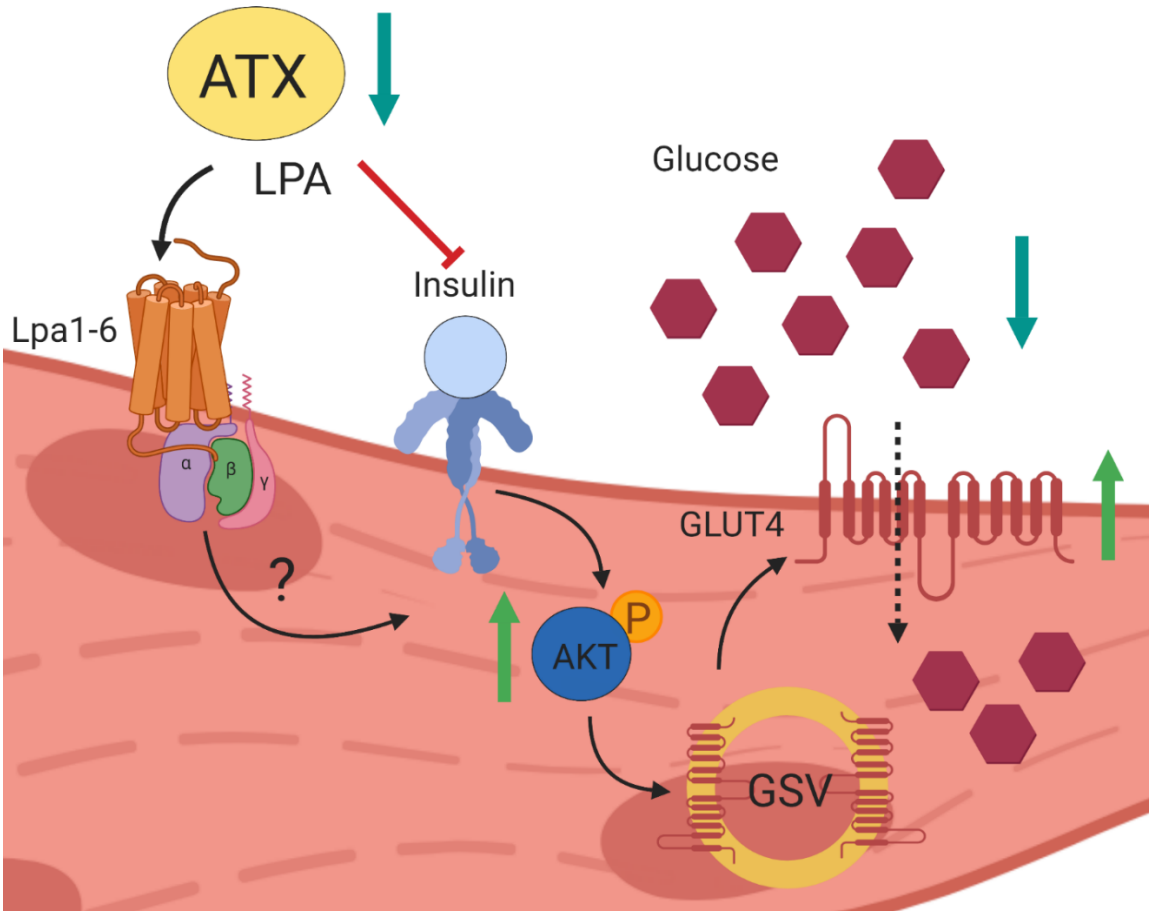
ATX
LPA
Insulin
Glucose
Lpa1-6
α
β
γ
?
GLUT4
AKT
P
GSV

3.6 Tables

Table 3.1: List of primary antibodies used for immunoblots.

Target	**Company, Catalog Number**
$pAKT^{S473}$	Cell Signaling, 9271
AKT	Millipore, 05-591
$pP70S6K^{T389}$	Cell Signaling,9234
P70S6K	Cell Signaling, 2708
$pERK^{T202/Y204}$	Cell Signaling, 9101
ERK	Cell Signaling, 9102

Table 3.2: List of mouse primers and sequences used in this study.

Primer	**Primer Sequence (5' to 3')**
Glut1 F	GGTGTGCAGCAGCCTGTGTACG
Glut1 R	TAGGACATCCAAGGCAGCCGTTC
Glut4 F	ACCGGCAGCCTCTGATCATCG
Glut4 R	GAGTGTCCGTCGTCCAGCTCGTT
LPA1 F	CTATGTTCGCCAGAGGACTAT
LPA1 R	GCAATAACAAGACCAATCCCG
LPA2 F	CACACTCAGCCTAGTCAAGA
LPA2 R	GTACTTCTCCACAGCCAGAA
LPA3 F	ACCAACGTCTTATCTCCACAC
LPA3 R	CAGTTCAGGCCGTCCAGC
LPA4 F	AGGATGGAGTCGCTGTTTAAG
LPA4 R	CACCACCATTATTTGTTGTTTGATC
LPA5 F	CCTCAGACTAATTTCTCTTCCC
LPA5 R	GTATCTCGATAGTCAGGGCAC
LPA6 F	CTCCAATGGCTCCCAGTG
LPA6 R	GGATATCAGCCCAAGCACG
RPL27 F	ACGGTGGAGCCTTATGTGAC
RPL27 R	TCCGTCAGAGGGACTGTCTT
RPL41 F	GCCATGAGAGCGAAGTGG
RPL41 R	CTCCTGCAGGCGTCGTAG

Chapter 4: Investigating the Mechanisms by which ATX-LPA Signaling Impairs Insulin Function

4.1. Rationale and Objectives

In chapter 3, we showed that reducing ATX-LPA levels *in vivo* through whole body heterozygous ATX deletion improves systemic glucose homeostasis and tissue insulin signaling in mice following HFHS diet feeding. Similar trends were also observed in HFHS-fed mice subjected to pharmacological inhibition of ATX. Conversely, adding LPA directly to C2C12 myotubes impaired insulin signaling, as measured by AKT phosphorylation. Despite these and other studies that have implicated altered ATX-LPA signaling in obesity-induced skeletal muscle insulin resistance, the mechanisms underlying these changes remain unclear[1]. Therefore, the objective of the study was to identify potential mechanisms by which the ATX-LPA pathway impairs insulin signaling in skeletal muscle (Fig 4.1). Because extensive work in adipose tissue has suggested that ATX-LPA signaling promotes inflammation(8,180,215), and fibrosis(222), and decreases PPARγ activity(8,176,178) and mitochondrial function(8,212), we aimed to examine whether amelioration of any/all of these mechanisms also played a role in improving insulin sensitivity in skeletal muscle.

Several figures and text present in this chapter have been reproduced with copyright permission from the *Journal of Lipid Research* article (Appendix 1)(253), below and edited as appropriate:

D'Souza, K., Nzirorera, C., Cowie, A., Varghese, G. P., Trivedi, P., Eichmann, T., Biswas, D., Touaibia, M., Morris, A. J., Aidinis, V., Kane, D. A., Pulinilkunnil, T. and Kienesberger, P.C. (2018). Autotaxin-Lysophosphatidic Acid Signaling Contributes to Obesity-Induced Insulin Resistance in Muscle and Impairs Mitochondrial Metabolism. *The Journal of Lipid Research.* **59**(10): 1805-1817.

The specific figures used from reference(253) are explicitly indicated in the figure legends.

4.2. Materials and Methods

4.2.1 Chemicals and Reagents

Unless otherwise stated, chemicals and reagents were obtained from Sigma.

4.2.2 Animals

Generation of $ATX^{+/-}$ mice and experimental procedures are described in Section 3.2.2.

4.2.3 Cell Culture

Induction of insulin resistance in C2C12 cells and co-treatment with LPA are described in Section 3.2.3.

4.2.4 Immunoblotting Analysis

Immunoblotting on tissues were performed as described in Section 3.2.5. The 4-HNE (Alpha Diagnostic International (Cat: HNE-11-S)) antibody was used at a 1:1000 dilution. The entire lane was quantified using densitometry.

4.2.5 Mitochondrial Analysis

Respiratory oxygen flux in permeabilized soleus muscle fibers and C2C12 myotubes was measured in high-resolution using the Oxygraph-2k (OROBOROS Instruments), which allows for the measurement of oxygen flux changes following the addition of different substrates of mitochondrial respiration. Permeabilized fibers were prepared as described(263). Briefly, soleus muscles were incubated in ice cold biopsy preservation solution (BIOPS, 10 mM Ca-EGTA buffer, 0.1 μM free Ca, 20 mM imidazole, 20 mM taurine, 50 mM K-MES, 0.5 mM DTT, 6.56 mM $MgCl_2$, 5.77 mM ATP, 15 mM phosphocreatine, pH 7.1). Excess connective tissue, fat, and tendons were removed and fiber bundles were mechanically separated using forceps. Fiber bundles were permeabilized in 2 ml of BIOPS containing 50 μg/ml saponin and gently agitated on ice for 30 min. Thereafter, fiber bundles were washed in mitochondrial respiration medium (MiR05) buffer (0.5 mM EGTA, 3 mM $MgCl_2$-$6H_20$, 60 mM lactobionic acid, 20 mM taurine, 10 mM KH_2PO_4, 20 mM

HEPES, 110 mM sucrose and 1 g/L FAF-BSA), fiber wet weights obtained, and samples were placed in the Oxygraph chambers.

Samples were assessed in 2 mL hyper-oxygenated MiR05 buffer at 37°C, and reoxygenated as necessary throughout the protocol. Instrumental background O_2 consumption was corrected using equations determined under the same parameters used for experimental data collection. Substrate linked respiration and reactive oxygen species (ROS) was examined by the sequential titration of malate, pyruvate/palmitoylcarnitine (PC) and ADP. LEAK respiration was examined by adding oligomycin prior to addition of substrates. Malate was added as it is a TCA cycle intermediate and anaplerotic substrate. Pyruvate and PC were added as indicators of glucose and fatty acid oxidation, respectively.

C2C12 myotubes (200,000 cells/mL) were incubated with saline or 10 µM LPA for 16 h prior to cell permeabilization with 3 µg/mL digitonin and mitochondrial respiration analysis. Thereafter, cells were collected and stored at -80°C until further analysis. Substrate linked respiration in C2C12 was examined similarly to soleus muscle fibers. Quantification of ROS was examined by adding oligomycin followed by addition of succinate.

The respirometric protocol for muscle fibers and C2C12 myotubes, involving the sequential addition of substrates, inhibitors and/or titration of substrates, as indicated in Table 4.1 and 4.2, respectively. Mitochondrial respiration was normalized to wet tissue weights in permeabilized fibers or cell number in C2C12 cells.

4.2.6 Citrate Synthase Activity Assay

Citrate synthase activity was determined as previously described, with minor modifications(264). Permeabilized skeletal muscle fibers or C2C12 cell pellets were homogenized in buffer containing 20 mM HEPES, 10 mM EDTA, and 10 µL/mL protease inhibitor, pH 7.4, and incubated on ice for 30 min. Samples were spun at 600 x g for 20 min at 4°C. An aliquot of the supernatant was used to determine protein concentration using a BCA assay. Homogenates were frozen for 1 h at -80 °C to liberate citrate synthase from the mitochondrial matrix. The reaction was

initiated by the addition of 227.5 µL reaction buffer containing 20 mM HEPES, 2 mM EGTA, 220 mM sucrose, 40 mM KCl, 0.1 mM 5,5′-Dithiobis(2-nitrobenzoic acid) (DTNB), 0.3 mM acetyl-CoA, pH 7.4 at 25°C. After 5 min, a baseline reading was obtained at 412 nm. The reaction was started by the addition of 0.5 mM oxaloacetate and monitored at 412 nm for 10 minutes.

4.2.7. Tissue lipid analysis

Lipidomic analysis was performed in collaboration with Dr. Thomas Eichmann, University of Graz, Graz, Austria. For targeted lipidomic analysis in muscle, total lipids of weighed muscle tissue explants (50-100 mg) were extracted twice according to Folch *et al.*(265) using 4 ml chloroform/methanol (2/1, v/v) containing 500 pmol butylated hydroxytoluene, 1% acetic acid, and 100 pmol of internal standards (ISTD, d18:1/17:0 CER, 14:0-14:0 DG, 15:0-15:0-15:0 TG Avanti Polar Lipids) per sample. Extraction was performed under constant shaking for 90 min at room temperature (RT). After addition of 800 µl dH_2O and further incubation for 30 min on RT, samples were spun at 1,000 x g for 15 min on RT to establish phase separation. The lower organic phase was collected, 2.5 ml chloroform were added to the remaining aqueous phase, and the second extraction was performed as described above (30 min on RT with subsequent centrifugation). Combined organic phases of the double-extraction were dried under a stream of nitrogen and lipids were resolved in 150 µl 2-propanol/methanol/water (6/3/1, v/v/v) for UPLC-MS analysis. For protein determination, the interphase was dried and lysed using 1.5 ml NaOH/SDS (0.3 N/0.1%). Chromatographic separation was modified after Knittelfelder *et al.*(266) using an AQUITY-UPLC system (Waters Corporation), equipped with a Kinetex EVO-C18 column (2.1x50 mm, 1.7 µm; Phenomenex) starting a 15 min linear gradient with 100% solvent A ($MeOH/H_2O$, 1/1, v/v; 10 mM ammonium acetate, 0,1% formic acid, 8 µM phosphoric acid).

A EVOQ Elite™ triple quadrupole mass spectrometer (Bruker) equipped with an ESI source was used for detection. Lipid species were analyzed by selected reaction monitoring (DG: [MNH4]+ to [RCOO+58]+ of the respective esterified fatty acid, 15 eV, 50 ms; TG: [MNH4]+ to [DG-H_2O]+ of the respective DG, 23eV, 30 ms; Ceramide: [MH]+ to m/z 264.3, 22 eV, 60 ms; the

resolution of Q1/Q3 were set to 0.7). Data were acquired with MS Workstation (Bruker). Data were normalized for recovery, extraction, and ionization efficacy by calculating analyte/ISTD ratios (AU) and expressed as AU/mg tissue protein. For species distribution analysis, data was expressed as % of total.

Analysis of triacylglycerol accumulation in the liver (20 mg) was performed using a colorimetric assay (Infinity Triglycerides reagent, Thermo Fisher Scientific) as previously described(243).

4.2.8 RNA Extraction and Gene Expression Analysis

RNA isolation, reverse transcription, and real-time quantitative PCR was performed as previously described(257) and as detailed in section 2.2.7. Primer sequences are listed in Table 4.3-4.5.

4.2.9 Statistical Analysis

Results are expressed as mean ± standard error of the mean (SEM). Comparisons between two groups were performed using an unpaired, two-tailed Student's t-test. Comparisons between multiple groups were performed using a paired or unpaired one- or two- way ANOVA followed by a Tukey or Sidak post hoc test, as appropriate. All statistical analysis was performed using Prism (GraphPad Software). P-values of less than 0.05 were considered statistically significant. For animal studies, "n" refers to the number of mice used, unless otherwise specified. For cell culture studies, experiments were performed in triplicates and data are from at least two independent experiments.

4.3. Results

4.3.1 ATX Deficiency is not associated with Marked Changes in Fibrotic and Inflammatory Gene Expression in the Soleus Muscle

We wanted to determine whether improvements in skeletal muscle insulin sensitivity of HFHS-fed $ATX^{+/-}$ mice are associated with changes in muscle fibrosis and/or inflammation. Therefore, we examined gene expression of fibrotic and inflammatory markers in the soleus of 16

h-fasted mice. Gene expression of *Tgfβ*, a master regulator of fibrosis, and *Col1a1*, a major collagen protein, was unchanged either by a HFHS diet or by ATX deficiency (Fig. 4.2A, B). Surprisingly, unlike the adipose tissue(8) and liver(218), no significant changes in inflammatory markers, such as *Tnfα*, *Il-6*, *Nlrp3*, *Il1β* and *Mcp1* were noted between groups (Fig 4.2C-G). Taken together, this suggests that neither changes in fibrotic nor inflammatory gene expression contribute to improved insulin signaling in the soleus skeletal muscle from HFHS-fed $ATX^{+/-}$ mice.

4.3.2. Partial ATX Deficiency does not Markedly Alter Lipid Accumulation in the Gastrocnemius Muscle

To explore possible mechanisms that underlie the blunted insulin resistance in skeletal muscle of HFHS-fed $ATX^{+/-}$ mice, we examined the accumulation of lipids that are typically associated with obesity-induced muscle insulin resistance via lipidomic analysis in gastrocnemius muscle. Total ceramide levels were unchanged regardless of diet or genotype (Fig. 4.3A). When examining the major ceramide species, we noted a slight but significant decrease in unsaturated species (24:1) and a shift toward saturated (22:0) species in HFHS-fed compared to chow-fed mice of both genotypes (Fig. 4.3B). Total DG levels increased 2.5-fold in HFHS-fed vs. chow-fed WT mice (Fig. 4.3C). Total DG levels were similar between genotypes in both chow and HFHS-fed states, although DG concentrations were not significantly increased in HFHS-fed vs. chow-fed $ATX^{+/-}$ mice (Fig. 4.3C). When examining the DG acyl chain composition, we noted a HFHS diet-induced increase in 36:2 DGs in WT and $ATX^{+/-}$ mice, and a decrease in 32:0 and 38:4 DG species in HFHS-fed compared to chow-fed $ATX^{+/-}$ mice (Fig. 4.3D). Total TG levels were increased in HFHS-fed WT and $ATX^{+/-}$ mice compared to the chow-fed controls and were similar between genotypes (Fig. 4.3E). TG species analysis revealed a HFHS diet-induced increase in TGs with longer acyl chains (54:2 and 54:3) and decrease in TGs with shorter acyl chains (48:2 and 48:3) (Fig. 4.3F). 48:3 TGs were also changed between genotypes with lower levels detected in chow and HFHS-fed $ATX^{+/-}$ mice compared to WT (Fig. 4.3F). Taken together, these data suggest that

partial ATX deficiency modestly protects from obesity-induced increases in DG accumulation and results in altered TG species composition in skeletal muscle. These data also suggest that improved muscle insulin sensitivity in $ATX^{+/-}$ mice is not accompanied by major changes in muscle lipid accumulation.

4.3.3. Improved Insulin Sensitivity in HFHS-fed $ATX^{+/-}$ mice is Associated with Enhanced Mitochondrial Respiration in the Soleus Muscle

We next wanted to determine whether mitochondrial respiration was altered by partial ATX deficiency. Permeabilized soleus fibers from 3- and 16-h fasted mice were examined for pyruvate (Pyr) and palmitoylcarnitine-linked (PC) respiration, respectively. Importantly, more physiological, non-saturating concentrations of ADP were used (0.5 mM), as saturating concentrations (5 mM) might mask differences in substrate-linked respiration(107). Pyr-linked respiration in the presence of ADP was unchanged by diet or ATX deficiency (Fig. 4.4A). Similarly, no significant changes were noted when leak respiration was examined (Fig. 4.4B). HFHS diet induced significant mitochondrial dysfunction when examining PC-linked respiration in WT mice (Fig. 4.4C). ATX deficiency ameliorated mitochondrial dysfunction, as assessed by PC-linked respiration, with an almost 50 percent increase in respiration seen in $ATX^{+/-}$ vs. WT fibers (Fig. 4.4C). PC-linked leak respiration was unchanged between groups (Fig. 4.4D). When respiration was uncoupled using FCCP, a significant increase in respiration was seen in $ATX^{+/-}$ mice under both chow and HFHS conditions (Fig. 4.4E). Taken together, this suggests that ATX deficiency ameliorates mitochondrial dysfunction during fat oxidation and increases substrate-linked respiration.

4.3.4. Partial ATX Deficiency is Not Associated with Major Changes in Fiber Type Composition in Skeletal Muscle

Changes in mitochondrial respiration, in the presence of acyl carnitines, may be due to reprogramming of skeletal muscle fibers to a more oxidative phenotype(260). Previous work has also demonstrated that modulation of Gα proteins, which couple ATX-LPA-LPA receptors to

intracellular signaling is linked to myofiber reprogramming(260). To examine whether reprogramming of muscle fibers occurs in $ATX^{+/-}$ mice, the mRNA levels of myosin heavy chain (MyHC) transcripts were quantified. Four MyHC isoforms were measured; MyHC1 and 4, which are associated with glycolytic (type IIX/IIB) fibers, and MyHC7 and 2, which are associated with oxidative (type I/IIA) fibers. In the soleus, *Myhc1* and *Myhc2* were significantly decreased in HFHS-fed $ATX^{+/-}$ mice when compared to WT controls (Fig. 4.5A and D). No significant changes in the levels of MyHC isoforms were observed in *Myhc4* and *Myhc7*, regardless of diet and genotype Fig. 4.5B and C). To determine whether fiber type composition could be altered in other skeletal muscle depots, we examined MyHC isoform levels in the tibialis (Fig. 4.5E-H) and gastrocnemius muscle (Fig. 4.5I-L). Interestingly, there was a significant decrease in *Myhc4* in both chow- and HFHS-fed conditions and a corresponding increase in *Myhc7* in HFHS-fed conditions in the tibialis muscle of $ATX^{+/-}$ vs. WT mice (Fig. 4.5F, G); this suggests that there may be a select reprogramming towards an oxidative phenotype in the tibialis muscle of $ATX^{+/-}$ mice. However, no significant changes in MyHC isoform levels were noted in the gastrocnemius muscle (Fig. 4.5I-L). Taken together, however, our data suggests that improvements in mitochondrial respiration in the soleus muscle from HFHS-fed $ATX^{+/-}$ mice are not broadly due to myofiber reprogramming in this muscle type.

4.3.5. Partial ATX Deficiency is not associated with Changes in Mitochondrial Content in the Soleus Muscle

We next wanted to determine whether mitochondrial content is altered with partial ATX deficiency, which may contribute to enhanced substrate oxidation in $ATX^{+/-}$ mice. First, citrate synthase activity, which strongly correlates with mitochondrial content(267), was measured in soleus muscle homogenates. Citrate synthase activity was not altered by HFHS feeding or ATX deficiency in 3- or 16-h fasted mice (Fig. 4.6A, B). Secondly, we measured gene expression of several key transcription factors involved in mitochondrial biogenesis and function(268).

Expression of *Pgc-1α*, estrogen related receptor γ (*Errγ*) and nuclear respiratory factor 1 (*Nrf1*) were unchanged by genotype and diet (Fig. 4.6C-E). Transcription factor A, mitochondria (*Tfam*) expression was significantly increased in chow-fed $ATX^{+/-}$ mice when compared to WT counterparts (Fig. 4.6F). However, HFHS feeding led to elevated *Tfam* mRNA levels only in WT mice and no difference was noted between HFHS-fed $ATX^{+/-}$ and WT mice (Fig. 4.6F). Taken together, this suggests that improvements in mitochondrial respiration in soleus muscle from $ATX^{+/-}$ mice are unlikely due to changes in mitochondrial content.

4.3.6. Muscle ADP Sensitivity is Unaffected by Partial ATX Deficiency

An additional mechanism by which a high fat/obesogenic diet can promote mitochondrial dysfunction is by decreasing ADP sensitivity(107). During obesity-induced insulin resistance, adenine nucleotide translocases lose sensitivity to ADP levels and decrease co-transport of ATP with ADP (104). To determine whether muscle ADP sensitivity is affected by ATX deficiency, we primed soleus fibers from chow and HFHS-fed $ATX^{+/-}$ and WT mice with saturating concentrations of malate/pyruvate and titrated ADP from 10-4000 μM during respirometric analysis (Fig. 4.7A). Calculation of kinetic parameters from the resulting curve showed that maximal respiration induced by ADP ($V_{max\ ADP}$) was significantly increased in both chow and HFHS-fed $ATX^{+/-}$ mice compared to WT (Fig. 4.7B). However, ADP sensitivity ($K_{m\ ADP}$) was unaffected by genotype or diet (Fig. 4.7C). Finally, to determine whether proteins involved in transport of ADP were altered, we measured gene expression of *Ant1* and *Ant2* (Fig. 4.7D, E). No significant changes in *Ant1* and *Ant2 levels* were noted. Taken together, although maximal respiration induced by ADP is increased in soleus muscle from $ATX^{+/-}$ mice, ADP sensitivity and gene expression of ADP transporters are not affected by ATX deficiency.

4.3.7. The Soleus Muscle from HFHS-fed $ATX^{+/-}$ Mice Shows Increased ROS Production and Reduced Antioxidant Gene Expression

Excess production of mitochondrial ROS is associated with obesity-induced insulin resistance(111). Interestingly, however, increased ATX-LPA signaling has been suggested to

promote an antioxidant response in cancer, glial cells and adipocytes(176,256,269). To determine how ATX deficiency influences mitochondrial ROS production in the soleus, we measured H_2O_2 production during substrate-linked respiration after the addition of the complex III inhibitor, AmA. Pyr-linked H_2O_2 production was unchanged by diet or ATX deficiency (Fig. 4.8A).

However, higher levels of H_2O_2 production were seen in HFHS-fed $ATX^{+/-}$ mice with PC, when compared to HFHS-fed WT mice (Fig. 4.8B). To determine whether changes in mitochondrial ROS production affect tissue oxidative stress, we measured protein levels of 4-hydroxynonenal (4-HNE), a major product of lipid peroxidation, in the soleus of 16 hr fasted mice(270). Interestingly, 4-HNE levels were significantly reduced in HFHS-fed WT mice compared to chow controls; however, in line with increased mitochondrial ROS secretion, levels of 4-HNE were slightly higher in HFHS-fed $ATX^{+/-}$ compared to WT mice (Fig. 4.8C, D). This suggests that increased H_2O_2 production and oxidative stress, as measured by 4-HNE, is not associated with insulin resistance in our HFHS-fed models.

In addition to increased ROS secretion, the antioxidant defense system could possibly be altered by ATX deficiency. Therefore, we examined gene expression of several enzymes involved in antioxidant defence in the soleus (Fig. 4.9). Expression of mitochondrial-specific superoxide dismutase 2 (*Sod2*) was significantly decreased when comparing HFHS-fed $ATX^{+/-}$ to WT mice, whereas expression of *Sod1* was unchanged between genotypes (Fig. 4.9A, B). Similarly, expression of catalase (*Cat*) was also unaffected (Fig. 4.9C). When examining glutathione-dependant enzymes, glutathione peroxidase 1 (*Gpx1*) expression was increased in HFHS-fed $ATX^{+/-}$compared to WT mice (Fig. 4.9D); however, *Gpx3* was significantly decreased by ATX deficiency in HFHS-fed mice (Fig. 4.9E). Glutathione reductase (*Gsr*), which is involved in generation of reduced glutathione, was unchanged by diet or genotype (Fig. 4.9F). Interestingly, glutamate-cysteine ligase catalytic unit (*Gclc*), which catalyzes the rate limiting step of glutathione synthesis, was also significantly decreased in HFHS-fed $ATX^{+/-}$ vs. WT mice (Fig. 4.9G). Levels of another antioxidant, thioredoxin (Txn), were unchanged between groups (Fig.

4.9H). However, when measuring levels of thioredoxin reductases (TXNRD), both *Txnrd1* and *Txnrd2* were significantly reduced in HFHS-fed ATX$^{+/-}$ vs. WT mice (Fig. 4.9I, J).

Finally, in response to increased fat oxidation, skeletal muscle mitochondria tend to uncouple respiration to reduce ROS production(271). To determine whether uncoupling is affected by HFHS diet or ATX deficiency, mRNA expression of *Ucp2* and *Ucp3* were examined. While *Ucp2* was unchanged, *Ucp3* expression was decreased to ~52.5% in HFHS-fed ATX$^{+/-}$ mice when compared to WT (Fig. 4.9K, L). Taken together, our data suggest that HFHS-fed ATX$^{+/-}$ mice have increased mitochondrial ROS production and overall decreased antioxidant gene expression in the soleus muscle compared to WT counterparts, indicating potentially increased oxidative stress in muscle from HFHS-fed ATX$^{+/-}$ mice.

4.3.8. LPA Directly Impairs Mitochondrial Respiration in C2C12 Myotubes

We demonstrated that LPA directly impairs insulin signaling in C2C12 myotubes in a time-dependent manner (see section 3.3.9). To determine whether the ATX-LPA pathway also influences mitochondrial function in C2C12 myotubes, similar to the soleus muscle in ATX$^{+/-}$ mice, we examined how mitochondrial metabolism is affected by LPA incubation in C2C12 cells. PC-linked respiration was significantly reduced in myotubes without palmitate following incubation with 1 μM LPA for 18 h (Fig. 4.10A). Palmitate significantly reduced PC-linked respiration; however, co-treatment with 1 μM LPA did not further exacerbate mitochondrial dysfunction as assessed by PC-linked respiration (Fig. 4.10A). Comparable trends were observed when assessing uncoupled respiration, where both LPA and palmitate incubation reduced respiration to a similar degree without further reduction upon co-incubation (Fig. 4.10B). Similar to observations in the soleus muscle from ATX$^{+/-}$ mice, changes in mitochondrial respiration were independent of changes in mitochondrial content in C2C12 cells incubated with or without LPA and/or palmitate, as measured by citrate synthase activity (Fig. 4.10C).

To determine whether ROS production is affected by addition of LPA and/or palmitate in C2C12 myotubes, we measured H_2O_2 production in myotubes in the presence of succinate as

substrate. In the absence of palmitate, LPA did not affect H_2O_2 production (Fig. 4.10D). As expected, incubation with palmitate led to augmented H_2O_2 production in C2C12 cells (Fig. 4.10D)(272). Interestingly, in support of an antioxidant role of LPA(256), co-incubation of myotubes with palmitate and LPA significantly decreased H_2O_2 production when compared to myotubes incubated with palmitate alone (Fig. 4.10D). Taken together, this suggests that LPA impairs mitochondrial respiration, while concurrently reducing H_2O_2 production in myotubes in presence of a lipotoxic milieu.

4.4 Discussion

Previous studies have implicated several mechanisms linking ATX-LPA signaling and obesity-induced insulin resistance in adipose tissue, including inflammation, fibrosis and mitochondrial dysfunction (Fig 4.1)(8,176,180,215,222). Although we (chapter 3) and others(191) have shown that reducing ATX-LPA signaling improves insulin signaling in skeletal muscle, it remains unclear whether similar mechanisms of actions occur as in adipose tissue. In this section, we show that changes in inflammatory or fibrotic gene expression are unlikely to contribute to ameliorated HFHS diet-induced insulin resistance in muscle from mice with partial ATX deficiency. However, ATX deficiency rescued HFHS induced decreases in PC-linked respiration in soleus muscle, independent of significant changes in fiber-type reprogramming, mitochondrial content and ADP sensitivity. Interestingly, ATX deficiency was also associated with increased mitochondrial H_2O_2 emission and generally decreased expression of antioxidant genes. In C2C12 myotubes, consistent with our studies in $ATX^{+/-}$ mice *in vivo*, LPA impaired PC-linked respiration without altering mitochondrial content. Furthermore, LPA decreased mitochondrial H_2O_2 emission in C2C12 cells. Taken together, these data suggest that the ATX-LPA pathway promotes the development of insulin resistance at least in part by inducing mitochondrial dysfunction.

Insulin resistance has been linked to altered mitochondrial function, although it remains uncertain whether changes in mitochondrial function are a cause or consequence of insulin

resistance(273). The ATX-LPA axis appears to impair mitochondrial function in brown adipose tissue(8,212). Microarray analysis of primary brown adipose tissue preadipocytes differentiated with LPA or ATX inhibitor revealed that the ATX-LPA pathway decreases the expression of many genes involved in mitochondrial function(212). Consistent with a role of ATX-LPA on the mitochondria, a study employing mice with adipose-specific ATX deficiency also suggested that the ATX-LPA pathway decreases mitochondrial content and membrane potential in BAT at baseline and following diet-induced obesity(212). Our study too suggests that the ATX-LPA pathway plays a role in modulating mitochondrial function during insulin resistance by reducing oxidative metabolism in muscle. Interestingly, improvements in respiration are independent of changes in mitochondrial content, which contrasts with what is seen in BAT(8). However, it is presently unclear whether the ATX-LPA-induced decrease in mitochondrial function in BAT is secondary to changes in preadipocyte differentiation(8).

Our data also indicate that enhanced PC-linked respiration in muscle from $ATX^{+/-}$ mice is not due to reprogramming of muscle fibers towards a more oxidative phenotype, although direct examination of ATX-LPA on myoblast differentiation has not been examined. While we did not see changes in pyruvate-linked respiration in $ATX^{+/-}$ mice, a study by Rancoule et al.(191) did note a significant increase in glucose oxidation in HFHS-fed mice treated with an LPA1/3 receptor antagonist for 3 weeks. Several potential explanations exist for this discrepancy.

Reduction in ATX-LPA signaling occurred over a longer term in our constitutive ATX knockout model, which could have led to compensatory changes in mitochondrial glucose metabolism. Furthermore, developmental effects due to constitutive ATX-LPA deficiency may influence mitochondrial metabolism, as has been shown in adipose tissue(8). Notably, in contrast to our study, unpermeabilized soleus muscle fibers were used in the study conducted by Rancoule et al(191). Therefore, it is possible that increased glucose import in mice treated with the LPA1/3 receptor antagonist may be primarily responsible for changes in glucose oxidation(191).

Despite significant increases in PC-linked respiration in the soleus muscle of HFHS-fed $ATX^{+/-}$ vs. WT mice, no marked changes in muscle lipid accumulation were noted in these mice. These data agree with a study by Nishimura *et al.*(8) showing that ectopic fat accumulation in skeletal muscle, liver, and heart is similar in WT and $ATX^{+/-}$ mice with diet-induced obesity. However, more recent work involving mice with post-natal onset of ATX deficiency suggests that HFHS-induced hepatic steatosis is ameliorated by ATX deficiency (218). While we did not observe changes in lipid accumulation in gastrocnemius muscle, a mixed oxidative/glycolytic muscle, from mice with ATX deficiency, it is conceivable that lipid accumulation is altered in the soleus muscle, which is predominantly oxidative and using which mitochondrial function was assessed. Therefore, examining how lipid accumulation is altered in the soleus is required to more conclusively determine if increased respiration reduces steatosis in soleus from HFHS-fed $ATX^{+/-}$ mice. Secondarily, we assessed muscle lipid accumulation in mice subjected to a 3-h food withdrawal. It remains to be determined whether levels of TGs, DGs and ceramides are significantly altered in HFHS-fed $ATX^{+/-}$ following prolonged, 16-h fasting, during which muscle lipid metabolism and turnover are highly upregulated.

Enhanced mitochondrial substrate, particularly PC-linked, respiration in soleus muscle from HFHS-fed $ATX^{+/-}$ mice was not associated with changes in mitochondrial content or ADP sensitivity, suggesting that other mechanisms underlie improved mitochondrial function in these mice. One possible mechanism that remains to be examined is altered mitochondrial dynamics, i.e., as fusion and fission. The connectivity of the mitochondrial network is critically influenced by nutrient status; nutrient excess, as seen in obesity-induced insulin resistance induces mitochondrial network fragmentation and decreases mitochondrial membrane potential and OXPHOS(112). Conversely, a more connected network is believed to be more efficient at ATP production and is associated with higher membrane potential and OXPHOS(112). Indeed, higher mitochondrial membrane potential is observed in the BAT of fat-specific ATX knockout mice on

a HFD(8). Future work should examine the mitochondrial dynamics and membrane potential in the soleus of HFHS-fed $ATX^{+/-}$ mice.

It is interesting that muscle from HFHS-fed $ATX^{+/-}$ mice exhibits increased ROS production and decreased expression of several antioxidant genes, despite enhanced insulin signaling. Some studies suggest that increased ROS production or oxidative stress can enhance mitochondrial fusion. Treatment of HeLa cells with sub-lethal doses of H_2O_2 (200μM) leads to hyperfused mitochondrial networks(274). Increases in oxidized glutathione can also promote dimerization of mitofusin molecules in *in vitro* mitochondrial fusion assays and in HeLa cells, which is required for the first step of mitochondrial fusion(275). However, whether a similar process takes place in skeletal muscle has not been fully explored. While one study showed that 250 μM H_2O_2 fragmented mitochondrial networks in C2C12 myotubes after 6 h, this effect was ameliorated after 24 hours following addition of H_2O_2(276).

The mechanism linking ATX-LPA signaling and oxidative stress is still unclear, but may involve NRF2, a transcription factor that increases expression of antioxidant genes. In cancer cells, LPA stabilizes *Nrf2 in vitro* and *in vivo*(256). In our study, several NRF2 regulated genes were downregulated, including *Gclc*, *Txnrd1* and *Txnrd2*, whereas others were unchanged, including *Txn* and *Gsr* (Fig. 4.9). Therefore, future studies should examine in greater detail whether NRF2 is activated in the soleus of $ATX^{+/-}$ mice or with LPA treatment in C2C12 myotubes. Physiological elevation in ROS production is also needed for insulin signaling, as insulin-induced increases in H_2O_2 can reversibly oxidize and inhibit phosphatase and tensin homolog (PTEN), preventing it from terminating insulin signaling(124). The main sources of this ROS appear to be NAD(P)H oxidases (NOX) and xanthine oxidase (XO), although mitochondrially produced ROS can also be involved(277). Therefore, future studies should also determine whether increases in ROS production from ATX-LPA deficiency are physiological and required as a mechanism to improve insulin signaling in HFHS-fed $ATX^{+/-}$ mice.

Overall, this works suggests that amelioration of fatty acid linked respiration is a major mechanism by which ATX-LPA deficiency improves soleus muscle insulin sensitivity. Improved fatty acid linked respiration is not likely due to myofiber reprogramming towards an oxidative phenotype or improved ADP sensitivity, but is paralleled by increased ROS secretion and decreased antioxidant gene expression (Fig. 4.11). Therefore, modulators of the ATX-LPA pathway may present novel strategies towards the prevention and treatment of skeletal muscle insulin resistance and mitochondrial dysfunction.

4.5 Figures

Figure 4.1: Mechanisms by which the ATX-LPA pathway can promote insulin resistance. Several potential mechanisms exist by which ATX-LPA can promote insulin resistance including increased inflammation and fibrosis and suppression of BAT function and PPARγ signaling. BAT, brown adipose tissue; PPARγ, peroxisome proliferator activated receptor γ.

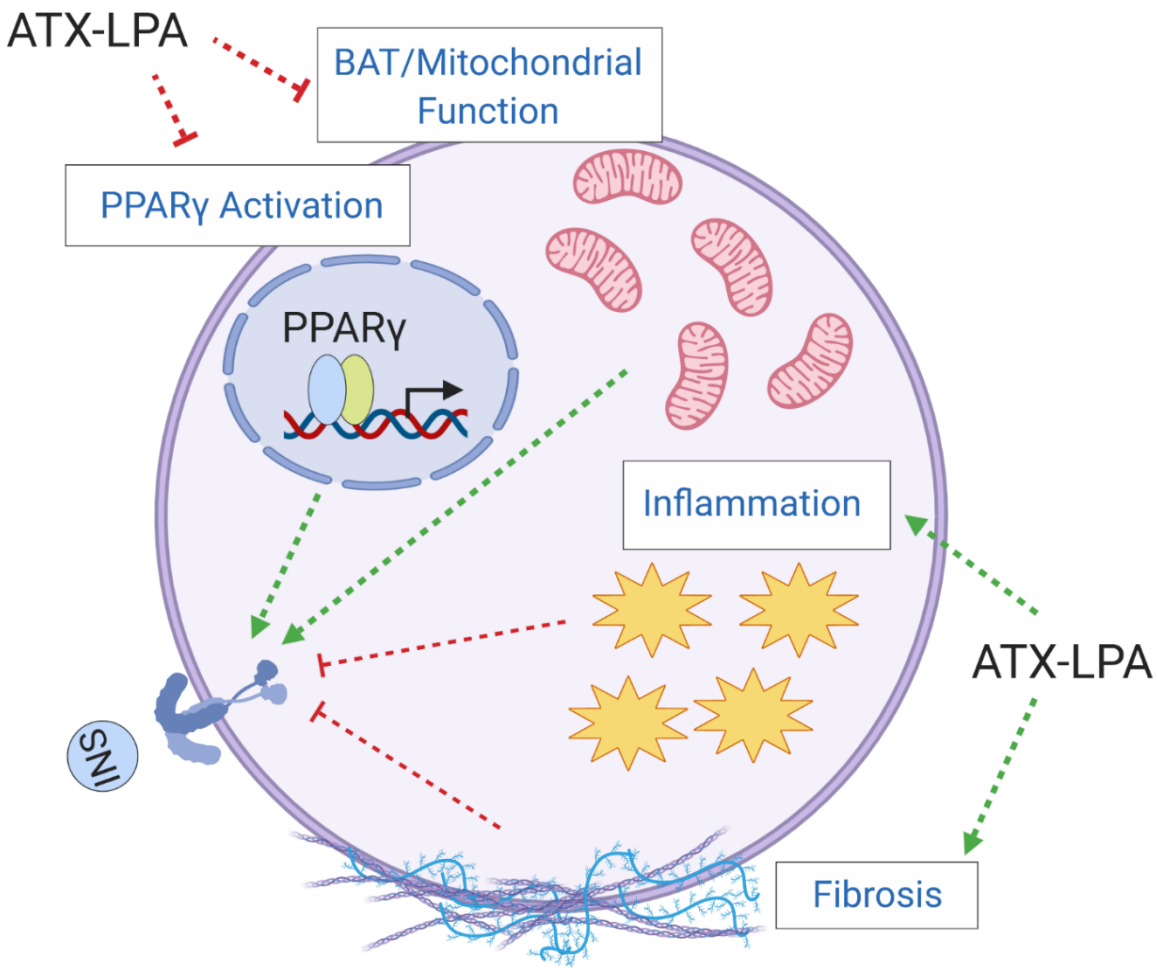
ATX-LPA
BAT/Mitochondrial Function
PPARγ Activation
PPARγ
Inflammation
ATX-LPA
INS
Fibrosis

Figure 4.2: Fibrotic and inflammatory gene expression is unchanged by partial ATX deficiency or HFHS feeding in soleus muscle.

Gene expression analysis of fibrotic markers, **(A)** *Tgfβ* and **(B)** *Col1a1*, and inflammatory markers, **(C)** *Tnfα*, **(D)** *Il-6*, **(E)** *Nlrp3*, **(F)** *Il1β*, and **(G)** *Mcp1* in the soleus muscle from 16-h fasted chow and HFHS-fed male WT and $ATX^{+/-}$ mice (n = 4-6). Statistical analysis was performed using a two-way ANOVA followed by a Tukey's multiple comparison test.

A
Tgfβ mRNA Expression
[Tgfβ/(Rpl41/Pp1a)]
B
Col1a1 mRNA Expression
[Col1a1/(Rpl41/Pp1a)]
C
Tnfα mRNA Expression
[Tnfα/(Rpl41/Pp1a)]
D
Il-6 mRNA Expression
[Il-6/(Rpl41/Pp1a)]
E
Nlrp3 mRNA Expression
[Nlrp3/(Rpl41/Pp1a)]
F
Il-1β mRNA Expression
[Il-1β/(Rpl41/Pp1a)]
G
Mcp1 mRNA Expression
[Mcp1/(Rpl41/Pp1a)]
WT
ATX+/-
Chow
HFHS

Figure 4.3: HFHS-fed ATX$^{+/-}$ mice do not show marked changes in skeletal muscle lipid accumulation.

Levels of **(A)** total ceramides, **(B)** ceramide species, **(C)** total diacylglycerols, **(D)** diacylglycerol species, **(E)** total triacylglycerols, and **(F)** triacylglycerol species in gastrocnemius muscle from chow and HFHS-fed male WT and ATX$^{+/-}$ mice subjected to a 3-h food withdrawal (n = 8). **(A-F)** Statistical analysis was performed using a two-way ANOVA followed by a Tukey's multiple comparison test; *$p < 0.05$, **$p < 0.01$, ****$p < 0.0001$ vs. chow; $^{\#\#}p < 0.01$, $^{\#\#\#\#}p < 0.0001$ as indicated. **(A-F)** reproduced from D'Souza et al, *Journal of Lipid Research*(253).

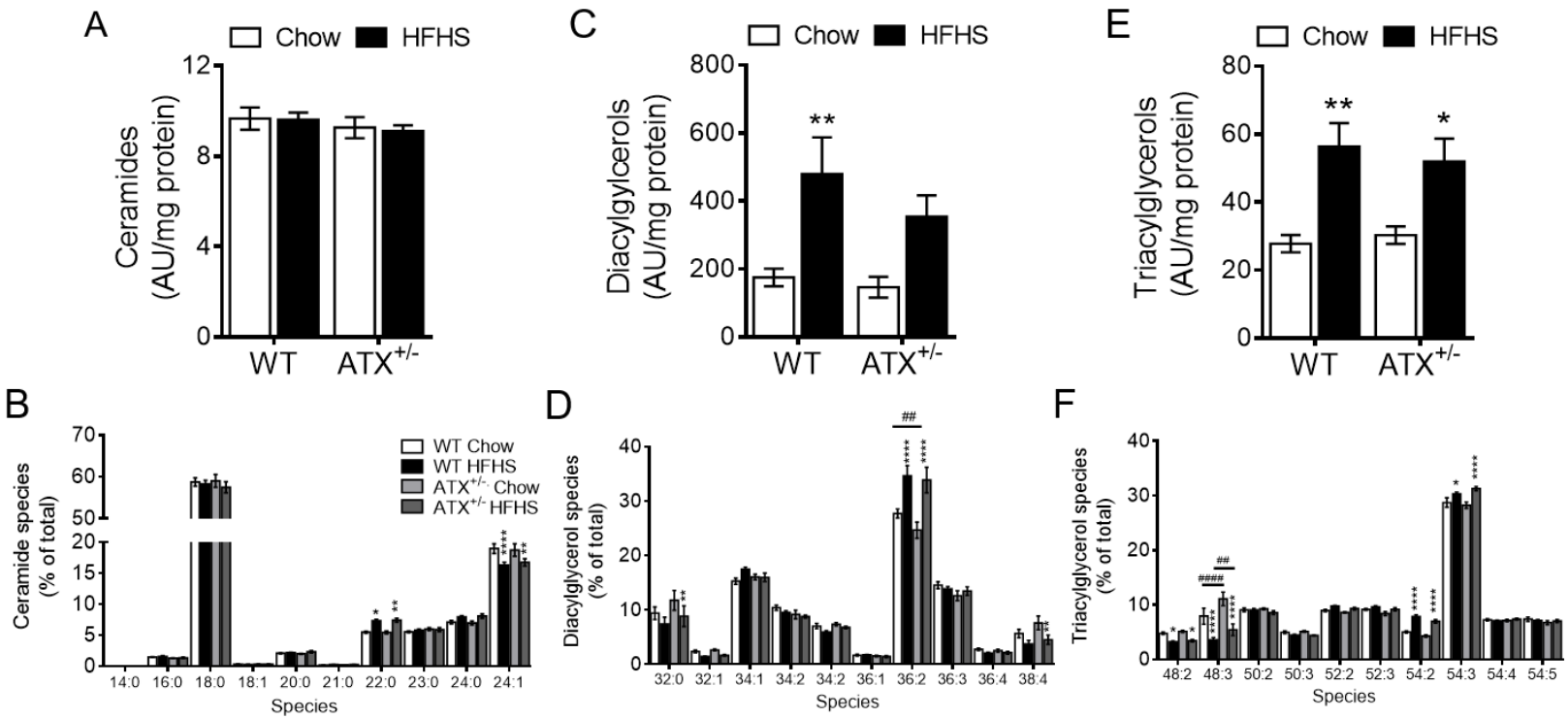
A
Chow
HFHS
Ceramides (AU/mg protein)
12
8
4
0
WT
ATX+/-
C
Chow
HFHS
Diacylglycerols (AU/mg protein)
800
600
400
200
0
**
WT
ATX+/-
E
Chow
HFHS
Triacylglycerols (AU/mg protein)
80
60
40
20
0
**
*
WT
ATX+/-
B
Ceramide species (% of total)
70
60
50
20
15
10
5
0
WT Chow
WT HFHS
ATX+/- Chow
ATX+/- HFHS
14:0
16:0
18:0
18:1
20:0
21:0
22:0
23:0
24:0
24:1
Species
D
Diacylglycerol species (% of total)
40
30
20
10
0
##
32:0
32:1
34:1
34:2
34:2
36:1
36:2
36:3
36:4
38:4
Species
F
Triacylglycerol species (% of total)
40
30
20
10
0
##
####
48:2
48:3
50:2
50:3
52:2
52:3
54:2
54:3
54:4
54:5
Species

Figure 4.4: Mitochondrial palmitoylcarnitine-linked respiration is increased in skeletal muscle from HFHS-fed ATX$^{+/-}$ mice.

Pyruvate-linked **(A)** respiration and **(B)** Leak respiration in 3-h fasted mice, and palmitoylcarnitine-linked **(C)** respiration and **(D)** Leak respiration in permeabilized soleus muscle fibers from chow and HFHS-fed male WT and ATX$^{+/-}$ mice. Pyruvate-linked respiration was examined in 3-h fasted mice, whereas palmitoylcarnitine-linked respiration was examined in 16-h fasted mice. **(E)** Uncoupled respiration in permeabilized soleus muscle fibers from 3-h fasted chow and HFHS-fed male WT and ATX$^{+/-}$ mice (n = 4-6). **(A-E)** Statistical analysis was performed using a two-way ANOVA followed by a Tukey's multiple comparison test; $^{\#\#}p < 0.01$ vs. chow; *p <0,05, **p < 0.01, *** p <0.001 as indicated. Pyr, pyruvate; PC, palmitoylcarnitine

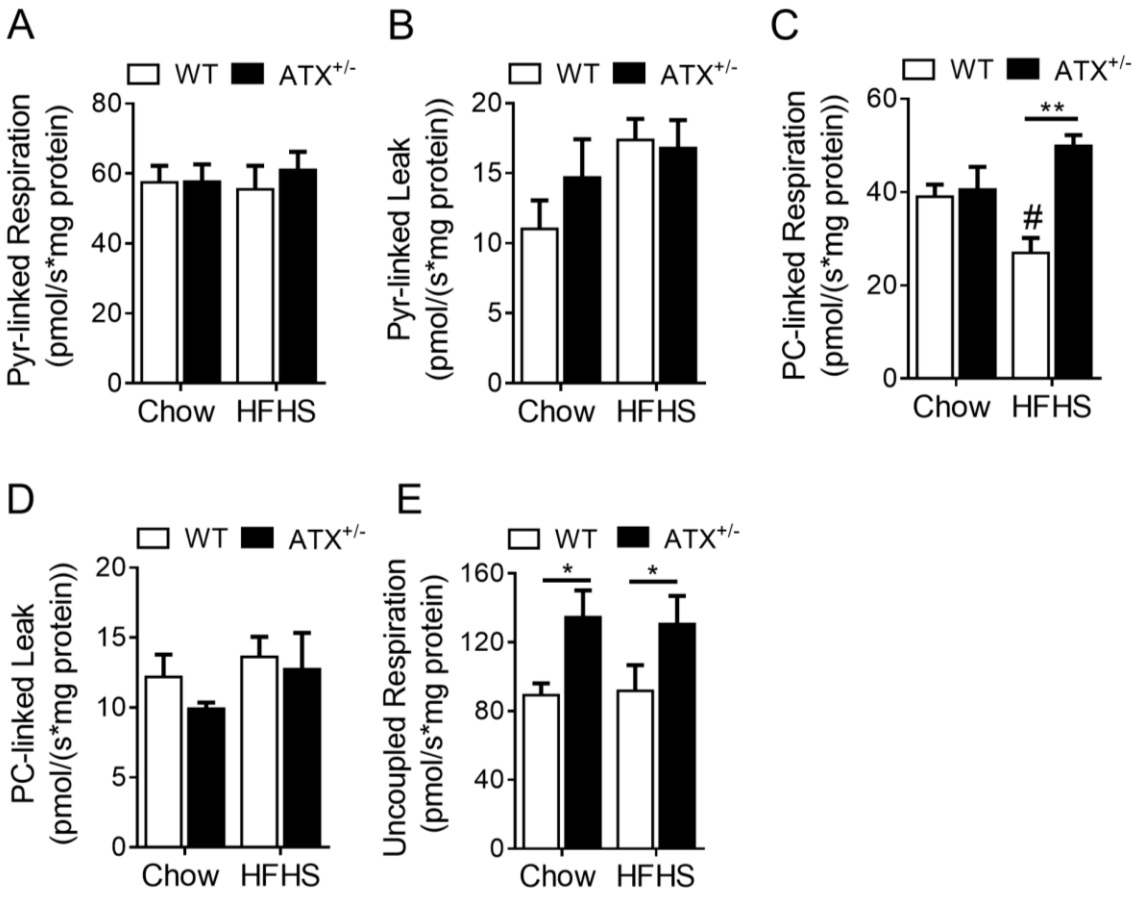
A
WT
ATX+/-
Pyr-linked Respiration (pmol/s*mg protein)
80
60
40
20
0
Chow
HFHS
B
WT
ATX+/-
Pyr-linked Leak (pmol/(s*mg protein))
20
15
10
5
0
Chow
HFHS
C
WT
ATX+/-
PC-linked Respiration (pmol/(s*mg protein))
60
40
20
0
**
#
Chow
HFHS
D
WT
ATX+/-
PC-linked Leak (pmol/(s*mg protein))
20
15
10
5
0
Chow
HFHS
E
WT
ATX+/-
Uncoupled Respiration (pmol/s*mg protein)
160
120
80
40
0
*
*
Chow
HFHS

Figure 4.5: Partial ATX deficiency is not associated with major changes in fiber type composition in skeletal muscle.

Gene expression analysis of **(A, E, I)** myosin heavy chain, *Myhc1* **(B, F, J)** *Myhc4* **(C, G, K)** *Myhc7* and **(D, H, L)** *Myhc2* in the soleus (SOL), tibialis (TIB) and gastrocnemius (GAS) from 16-h fasted chow and HFHS-fed male WT and $ATX^{+/-}$ mice, respectively (n = 10 for soleus, n = 5 for TIB and GAS). Statistical analysis was performed using a two-way ANOVA followed by a Tukey's multiple comparison test; $*p < 0.05$, $**p < 0.01$; $^{\#}p < 0.05$ vs. chow control as indicated. SOL, soleus; TIB, tibialis; GAS, gastrocnemius.

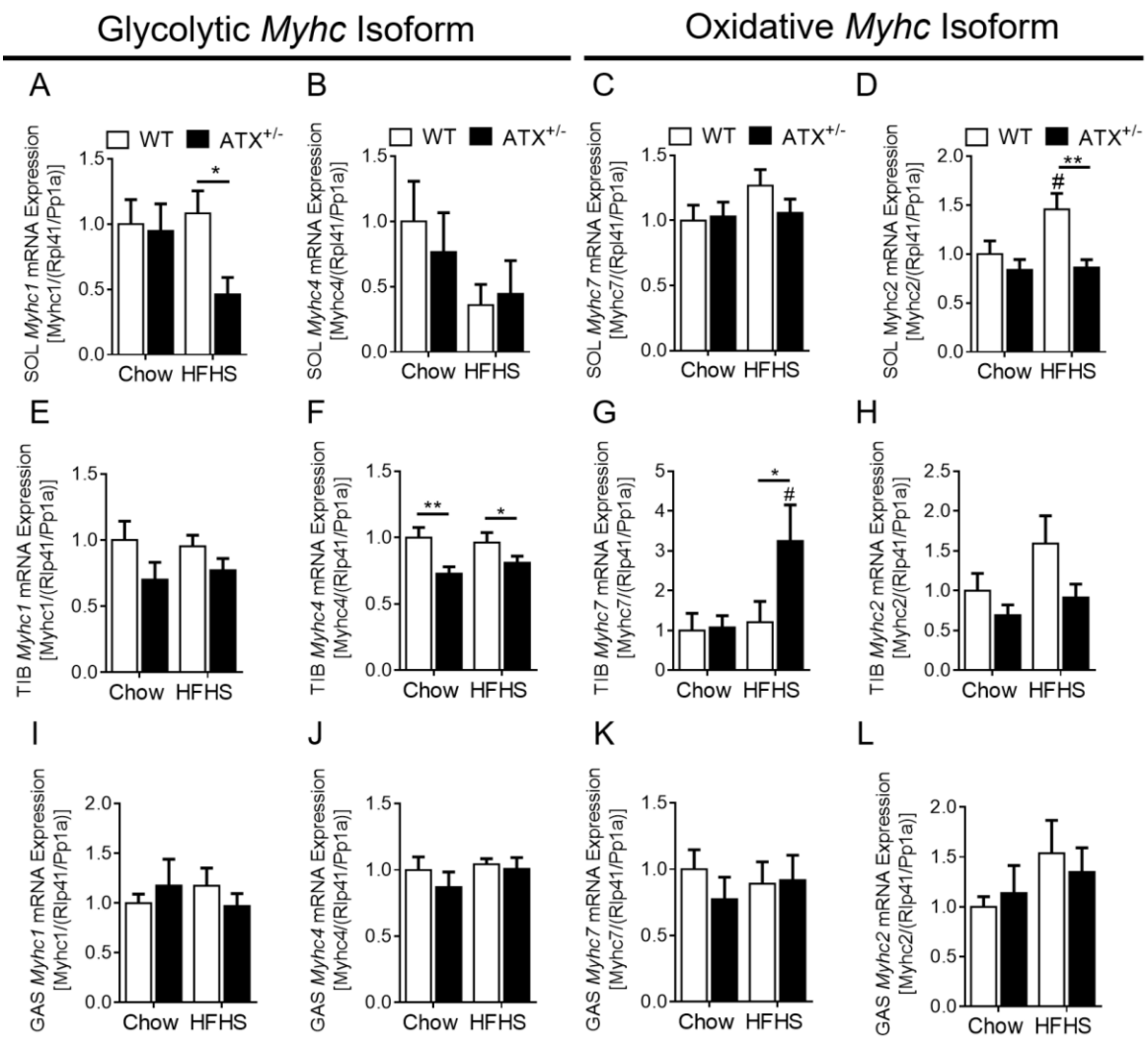
Glycolytic *Myhc* Isoform
Oxidative *Myhc* Isoform
A
B
C
D
E
F
G
H
I
J
K
L
WT
ATX+/-
SOL *Myhc1* mRNA Expression [Myhc1/(Rpl41/Pp1a)]
SOL *Myhc4* mRNA Expression [Myhc4/(Rpl41/Pp1a)]
SOL *Myhc7* mRNA Expression [Myhc7/(Rpl41/Pp1a)]
SOL Myhc2 mRNA Expression [Myhc2/(Rpl41/Pp1a)]
TIB *Myhc1* mRNA Expression [Myhc1/(Rlp41/Pp1a)]
TIB *Myhc4* mRNA Expression [Myhc4/(Rlp41/Pp1a)]
TIB *Myhc7* mRNA Expression [Myhc7/(Rlp41/Pp1a)]
TIB *Myhc2* mRNA Expression [Myhc2/(Rlp41/Pp1a)]
GAS *Myhc1* mRNA Expression [Myhc1/(Rlp41/Pp1a)]
GAS *Myhc4* mRNA Expression [Myhc4/(Rlp41/Pp1a)]
GAS *Myhc7* mRNA Expression [Myhc7/(Rlp41/Pp1a)]
GAS *Myhc2* mRNA Expression [Myhc2/(Rlp41/Pp1a)]
Chow HFHS

Figure 4.6: ATX deficiency is not associated with changes in mitochondrial content in the soleus.

Citrate synthase activity in the soleus muscle of **(A)** 3-h and **(B)** 16-h fasted chow and HFHS-fed male WT and $ATX^{+/-}$ mice (n = 4-6). Gene expression analysis of transcription factors implicated in mitochondrial biogenesis **(C)** *Pgc1α* **(D)** *Errγ* **(E)** *Nrf1* and **(F)** *Tfam* in 16-hr fasted chow and HFHS-fed male WT and $ATX^{+/-}$ mice (n=4-6). Statistical analysis was performed using a two-way ANOVA followed by a Tukey's multiple comparison test; $*p < 0.05$; $^{\#\#}p < 0.01$ vs. chow control as indicated. Pgc1α, Peroxisome proliferator activated receptor gamma coactivator 1 alpha; Errγ, estrogen related receptor γ; Nrf1, nuclear respiratory factor 1; Tfam, transcription factor A, mitochondria.

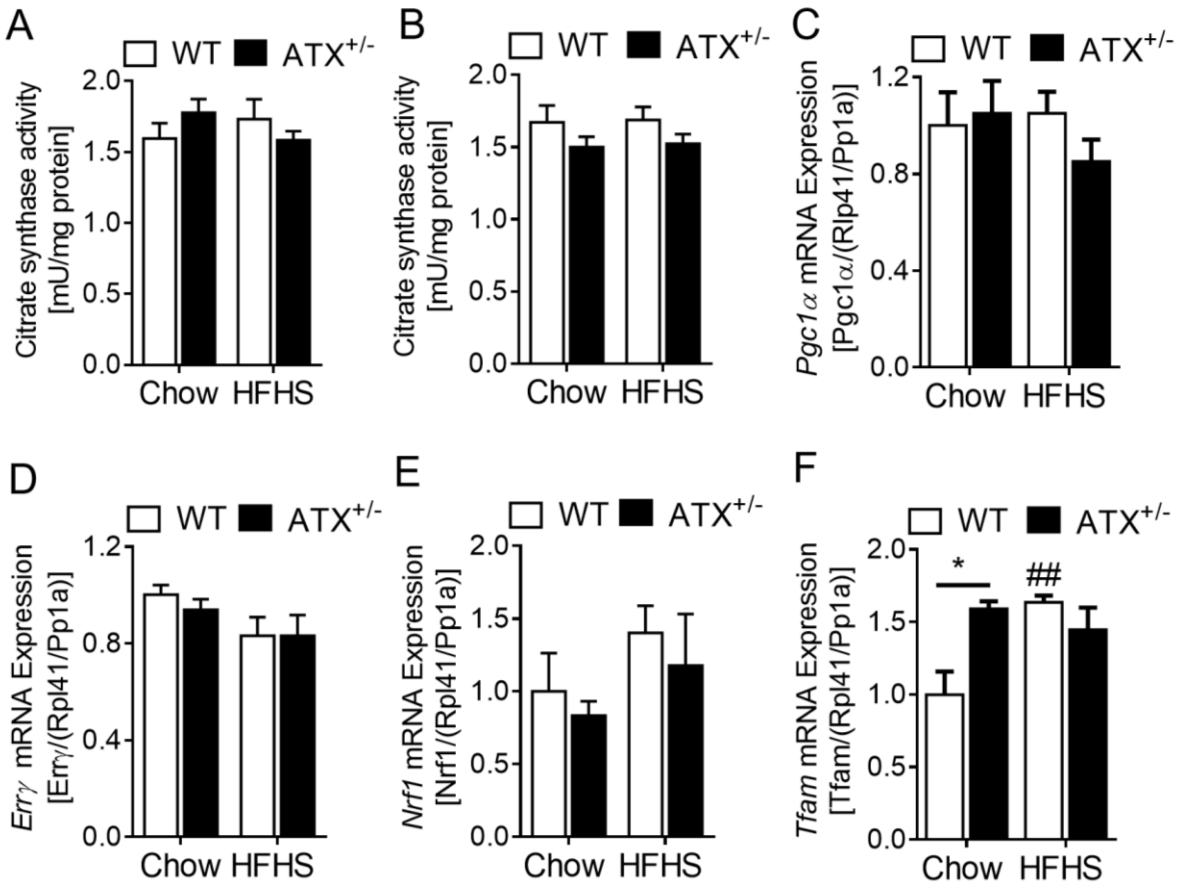
A
WT
ATX+/-
Citrate synthase activity [mU/mg protein]
2.0
1.5
1.0
0.5
0.0
Chow
HFHS
B
WT
ATX+/-
Citrate synthase activity [mU/mg protein]
2.0
1.5
1.0
0.5
0.0
Chow
HFHS
C
WT
ATX+/-
Pgc1α mRNA Expression [Pgc1α/(Rlp41/Pp1a)]
1.2
0.8
0.4
0.0
Chow
HFHS
D
WT
ATX+/-
Errγ mRNA Expression [Errγ/(Rpl41/Pp1a)]
1.2
0.8
0.4
0.0
Chow
HFHS
E
WT
ATX+/-
Nrf1 mRNA Expression [Nrf1/(Rpl41/Pp1a)]
2.0
1.5
1.0
0.5
0.0
Chow
HFHS
F
WT
ATX+/-
Tfam mRNA Expression [Tfam/(Rpl41/Pp1a)]
*
##
2.0
1.5
1.0
0.5
0.0
Chow
HFHS

Figure 4.7: ADP sensitivity is unaffected by ATX$^{+/-}$ deficiency in soleus.

(A) ADP kinetic curves **(B)** $V_{max\ ADP}$ and **(C)** $K_{m\ ADP}$ from permeabilized soleus muscle fibers from 3-h fasted chow and HFHS-fed male WT and ATX$^{+/-}$ mice (n = 4-6). Gene expression analysis of **(D)** *Ant1* and **(E)** *Ant2* in the soleus from chow and HFHS-fed male WT and ATX$^{+/-}$ mice (n = 4-6). Statistical analysis was performed using a two-way ANOVA followed by a Tukey's multiple comparison test; *$p < 0.05$, **p < 0.01. Ant1, adenine nucleotide translocase 1; Ant2, adenine nucleotide translocase 2.

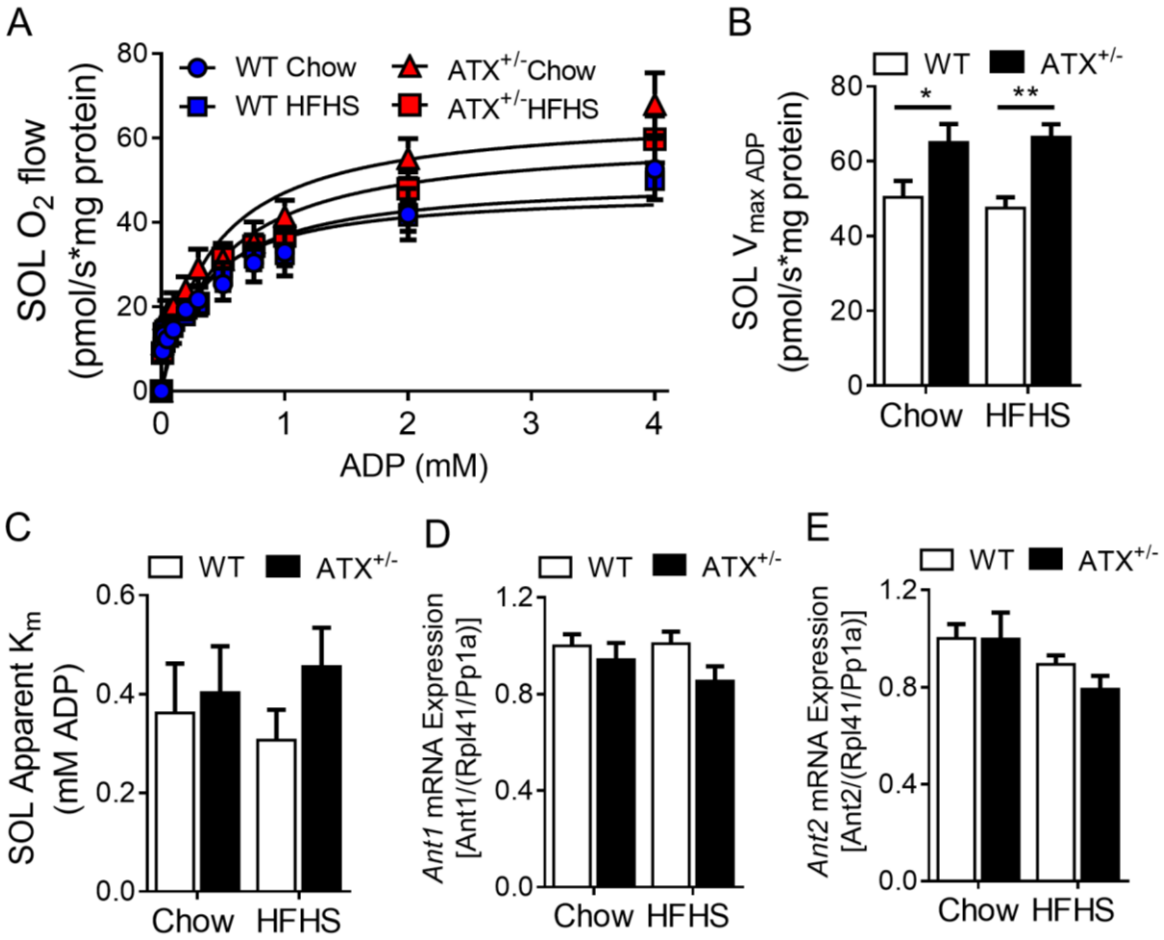
A
SOL O2 flow
(pmol/s*mg protein)
WT Chow
WT HFHS
ATX+/-Chow
ATX+/-HFHS
ADP (mM)
B
SOL Vmax ADP
(pmol/s*mg protein)
WT
ATX+/-
Chow
HFHS
C
SOL Apparent Km
(mM ADP)
D
Ant1 mRNA Expression
[Ant1/(Rpl41/Pp1a)]
E
Ant2 mRNA Expression
[Ant2/(Rpl41/Pp1a)]

Figure 4.8: The soleus from HFHS-fed ATX$^{+/-}$ mice shows increased levels of ROS production and 4-HNE staining

ROS secretion from mitochondria in the presence of **(A)** Pyr/AmA and **(B)** PC/AmA from permeabilized soleus muscle fibers from 3/16-h fasted chow and HFHS-fed male WT and ATX$^{+/-}$ mice (n = 4-6). **(C)** Immunoblot and **(D)** densitometric analysis of 4-HNE in the soleus muscle from 16-h fasted chow and HFHS-fed male WT and ATX$^{+/-}$ mice (n = 4-6). Statistical analysis was performed using a two-way ANOVA followed by a Tukey's multiple comparison test; $*p < 0.05$, $^{\#\#}p < 0.01$ vs. chow fed control. ROS, reactive oxygen species; Pyr, Pyruvate; PC, palmitoylcarnitine; AMA, antimycin A; 4HNE- 4-hydroxynoneal.

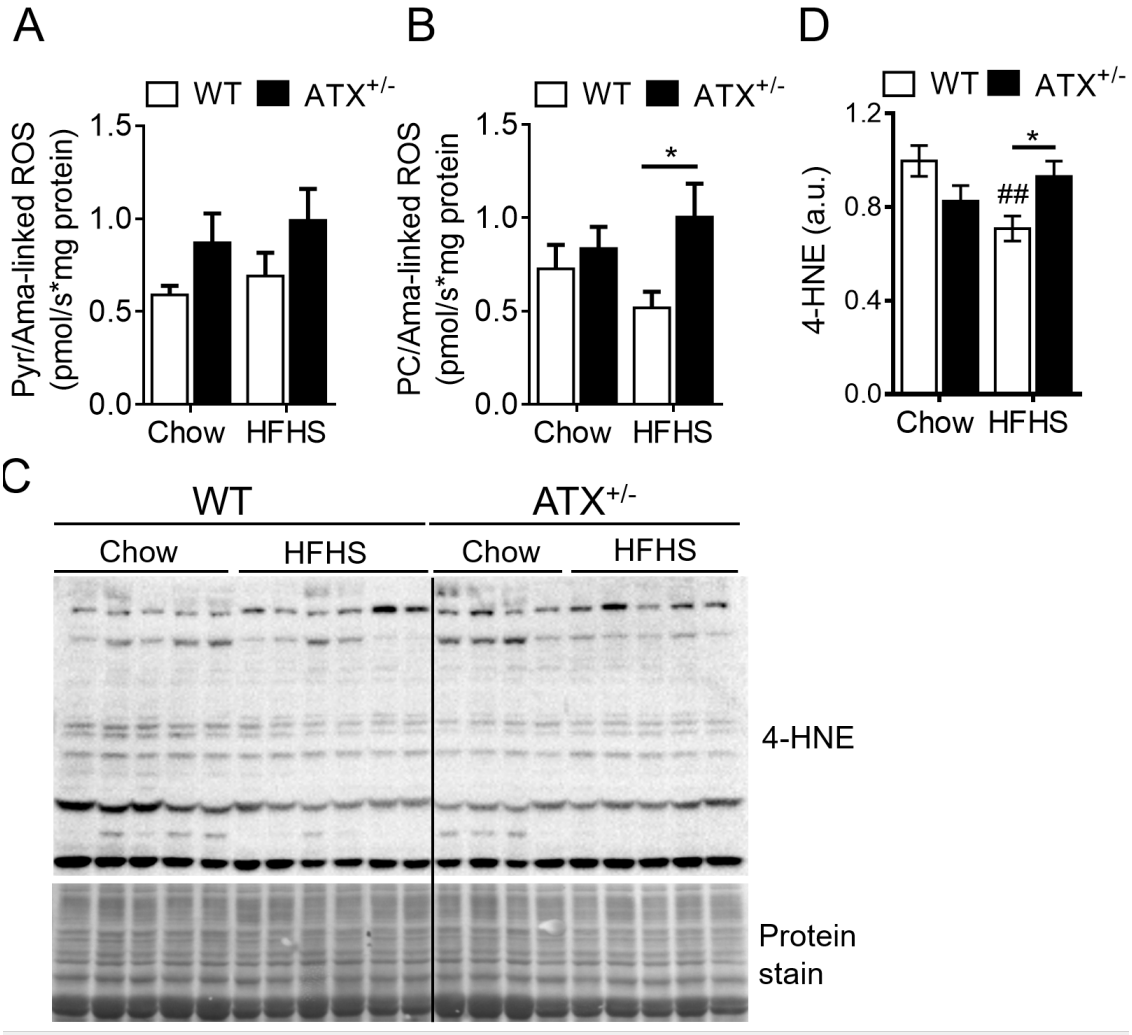
A
WT
ATX+/-
Pyr/Ama-linked ROS (pmol/s*mg protein)
1.5
1.0
0.5
0.0
Chow
HFHS
B
WT
ATX+/-
PC/Ama-linked ROS (pmol/s*mg protein
*
1.5
1.0
0.5
0.0
Chow
HFHS
D
WT
ATX+/-
4-HNE (a.u.)
1.2
0.8
0.4
0.0
##
*
Chow
HFHS
C
WT
ATX+/-
Chow
HFHS
Chow
HFHS
4-HNE
Protein stain

Figure 4.9. The antioxidant defense system tends to decrease in HFHS-fed ATX$^{+/-}$ mice. Gene expression analysis of **(A-C)** glutathione-independent, **(D-G)** glutathione-dependant dependant antioxidants Gene expression of **(H)** TXN, and (I-J) TXNRD1 and 2 and (K-L) uncoupling proteins from the soleus muscle of chow and HFHS-fed male WT and ATX$^{+/-}$ mice (n=4-6). Statistical analysis was performed using a two-way ANOVA followed by a Tukey's multiple comparison test; *$p < 0.05$, **$p < 0.01$; $^{\#\#}p<0.01$ vs. chow controls. SOD1/2, superoxide dismutase 1/2; CAT, catalase; GPX1/3, glutathione peroxidase 1/3; GSR, glutathione disulfide reductase; GCLC, Glutamate-Cysteine Ligase Catalytic Subunit; TXN, thioredoxin; TXNRD1/2, thioredoxin reductase 1/2; UCP2/3, uncoupling protein 2/3.

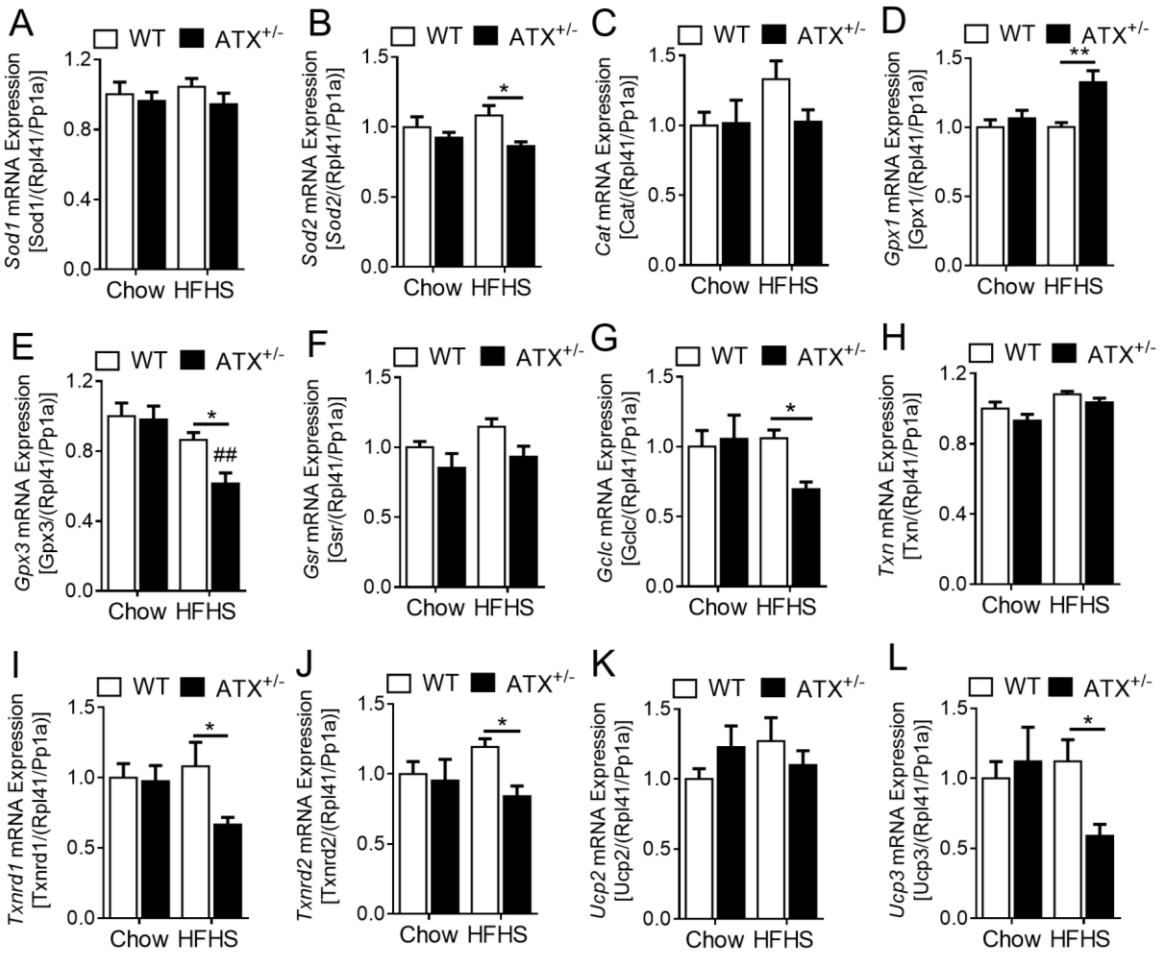
A
WT
ATX+/-
Sod1 mRNA Expression [Sod1/(Rpl41/Pp1a)]
Chow HFHS
B
Sod2 mRNA Expression [Sod2/(Rpl41/Pp1a)]
*
C
Cat mRNA Expression [Cat/(Rpl41/Pp1a)]
D
Gpx1 mRNA Expression [Gpx1/(Rpl41/Pp1a)]
**
E
Gpx3 mRNA Expression [Gpx3/(Rpl41/Pp1a)]
*
##
F
Gsr mRNA Expression [Gsr/(Rpl41/Pp1a)]
G
Gclc mRNA Expression [Gclc/(Rpl41/Pp1a)]
*
H
Txn mRNA Expression [Txn/(Rpl41/Pp1a)]
I
Txnrd1 mRNA Expression [Txnrd1/(Rpl41/Pp1a)]
*
J
Txnrd2 mRNA Expression [Txnrd2/(Rpl41/Pp1a)]
*
K
Ucp2 mRNA Expression [Ucp2/(Rpl41/Pp1a)]
L
Ucp3 mRNA Expression [Ucp3/(Rpl41/Pp1a)]
*

Figure 4.10: LPA directly impairs mitochondrial respiration in C2C12 myotubes

(A) PC-linked mitochondrial respiration, **(B)** uncoupled respiration, **(C)** citrate synthase activity, and **(D)** H_2O_2 production in permeabilized C2C12 myotubes incubated in the absence or presence of 0.4 mM palmitate and 1 μM LPA for 18 h (n = 5-6). **(A-D)** Statistical analysis was performed using a two-way ANOVA followed by a Tukey's multiple comparison test. *$p < 0.05$; $^{\#}p < 0.05$, $^{\#\#}p < 0.01$, $^{\#\#\#}p < 0.001$ vs. -Palm controls. PC, palmitoylcarnitine.

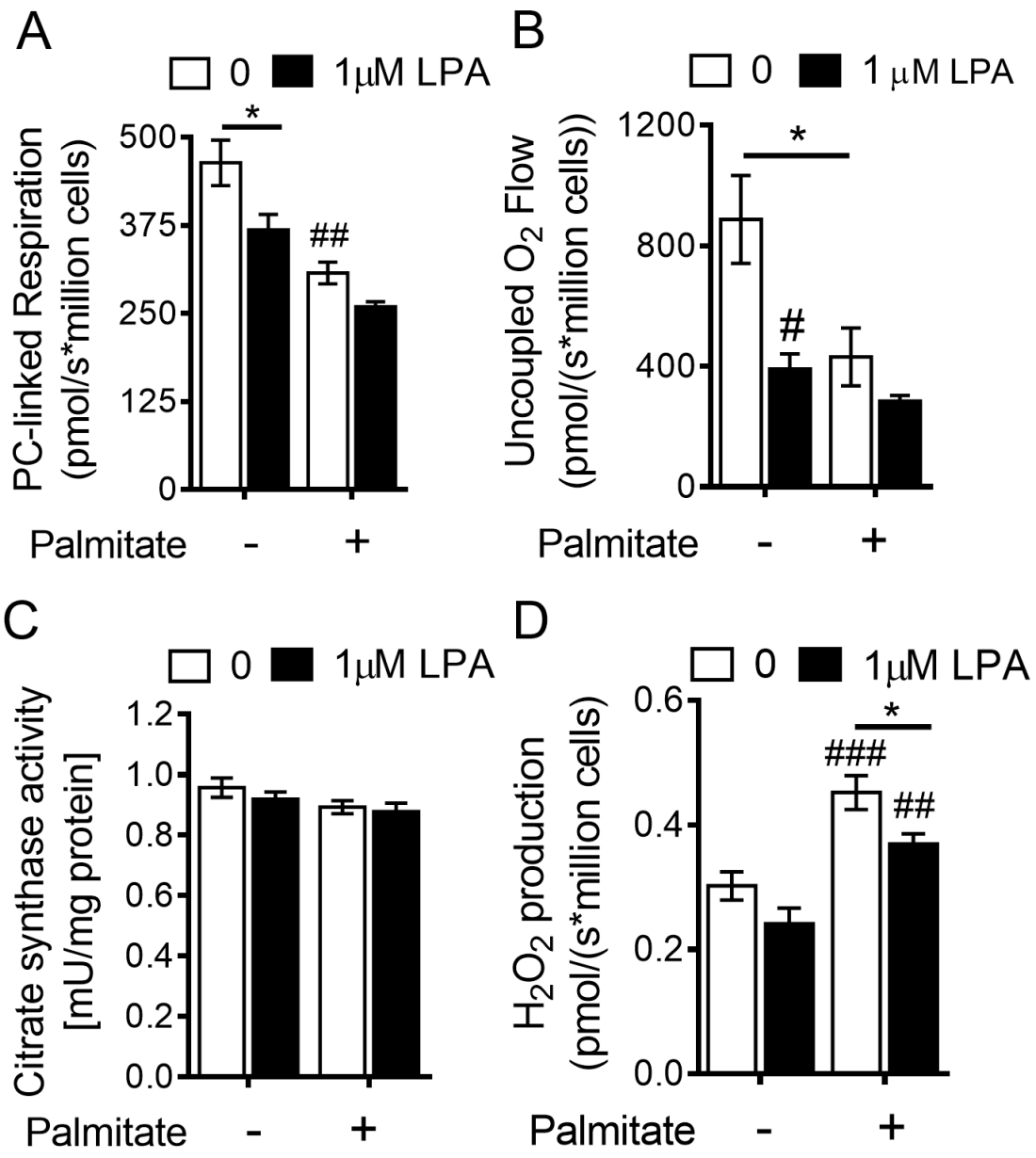
A
0
1μM LPA
PC-linked Respiration (pmol/s*million cells)
500
375
250
125
0
*
##
Palmitate
-
+
B
0
1 μM LPA
Uncoupled O2 Flow (pmol/(s*million cells))
1200
800
400
0
*
#
Palmitate
-
+
C
0
1μM LPA
Citrate synthase activity [mU/mg protein]
1.2
1.0
0.8
0.6
0.4
0.2
0.0
Palmitate
-
+
D
0
1μM LPA
H2O2 production (pmol/(s*million cells)
0.6
0.4
0.2
0.0
*
###
##
Palmitate
-
+

Figure 4.11. Proposed Mechanism by ATX-LPA promotes insulin resistance in skeletal muscle.

In diet-induced obesity, upregulation of the ATX-LPA pathway contributes to impaired skeletal muscle insulin signaling, glucose transport and fatty acid-linked mitochondrial respiration. Chronic ATX deficiency enhances skeletal muscle insulin signaling, glucose transport, mitochondrial respiration and reactive oxygen species (ROS) production in an obesogenic milieu, which ameliorates diet-induced obesity and impaired glucose homeostasis. The specific mechanism by which ATX-LPA improves mitochondrial respiration and increases ROS production requires further investigation. GSV, Glut4 storage vesicles; ROS, reactive oxygen species.

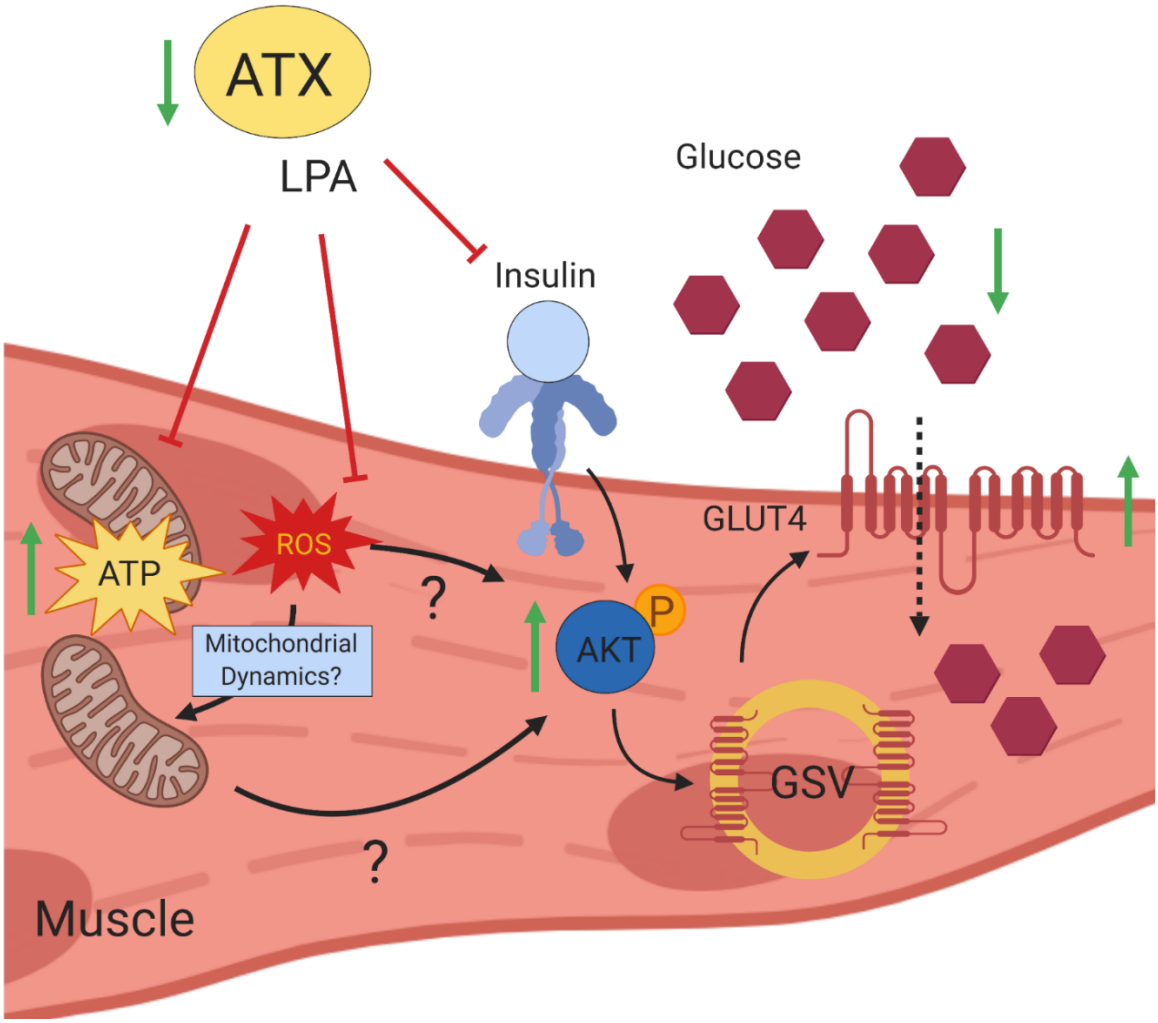
ATX
LPA
Insulin
Glucose
GLUT4
ATP
ROS
?
Mitochondrial
Dynamics?
AKT
P
GSV
?
Muscle

4.6 Tables

Table 4.1: Respirometric protocol in chronological order to examine substrate-linked, leak respiration and ROS production in permeabilized soleus muscle fibers from chow and HFHS-fed WT and $ATX^{+/-}$ mice.

Substrate-linked	**Concentration**	**Mark**
Amplex Red	10 µM	Amp
HRP	1 U/ml	HRP
H_2O_2 titration	0 - 0.2 µM	HP0-2
SOD	5 U/ml	SOD
Sample		
H_2O_2 titration	0 - 0.2 µM	HP0-2
Malate	0.5 mM	M
Palmitoylcarnitine Pyruvate	50 µM 2 mM	PC, Pyr
ADP	0.5 mM	D
FCCP	0.5 µM	FCCP
Antimycin A	2.5 µM	AmA
Leak	**Concentration**	**Mark**
Sample		
Oligomycin	2.5 µM	O
Malate	0.5 µM	M
Palmitoylcarnitine	50 µM	PC
ADP	0.5 mM	D

Table 4.2: Respirometric protocol in chronological order to examine substrate-linked and ROS production in permeabilized C2C12 myotubes incubated with/without 0.8 mM palmitate and co-incubated without or with1 µM LPA.

Substrate-linked	**Concentration**	**Mark**
Sample		
Malate	0.5 mM	M
Palmitoylcarnitine	50 µM	PC
ADP	5 mM	D
FCCP	0.5 µM	FCCP
ROS Production	**Concentration**	**Mark**
Sample		
Digitonin	8.1 µM	Dig
Amplex Red	10 µM	Amp
HRP	1 U/ml	HRP
H_2O_2 0	0	HP0
H_2O_2 1	0.1 µM	HP1.1
H_2O_2 2	0.2 µM	HP1.2
SOD	5 U/ml	SOD
Oligomycin	2.5 µM	O
Succinate	10 µM	S

Table 4.3: List of primers and sequences to examine fibrotic and inflammatory gene expression in mice.

Primer	**Primer Sequence (5' to 3')**
Fibrosis	
Tgfβ F	ACCGCAACAACGCCATCTATG
Tgfβ R	TGCTTCCCGAATGTCTGACGTA
Col1a1 F	CCTGGCAACAAAGGAGACACT
Col1a1 R	ACCACGGGCTCCTCGTTTT
Inflammation	
Tnfα F	CATCCATTCTCTACCCAGCCC
Tnfα R	CATGAGAGGCCCACAGTCCA
Il6 F	CACGGCCTTCCCTACTTCA
Il6 R	AACTCTTTTCTCATTTCCACGAT
Nlrp3 F	GCATCGGGAAAACCATCCTAG
Nlrp3 R	ACCTCTCGGCAGTGGATAAA
Il1b F	TGGGCAACCACTTACCTATTT
Il1b R	TCTAGAGAGTGCTGCCTAAT
Mcp1 F	TCGGAACCAAATGAGATCAGA
Mcp1 R	CAGATTTACGGGTCAACTTC
Reference Genes	
Rpl27 F	ACGGTGGAGCCTTATGTGAC
Rpl27 R	TCCGTCAGAGGGACTGTCTT
Rpl41 F	GCCATGAGAGCGAAGTGG
Rpl41 R	CTCCTGCAGGCGTCGTAG

Table 4.4: List of primers and sequences to examine fiber type and mitochondrial biogenesis genes in mice.

Fiber Type	
Myhc1 F	CTCTTCCCGCTTTGGTAAGTT
Myhc1 R	CAGGAGCATTTCGATTAGATCCG
Myhc2 F	TCACATCCAACAAGAAGCCAGAGC
Myhc2 R	CCCTGGCTGACAAATGGGTAATCA
Myhc4 F	AGTCCCAGGTCAACAAGCTG
Myhc4 R	TTTCTCCTGTCACCTCTCAACA
Myhc7 F	ACCAGGCCCTTTGACCTCAAGAAA
Myhc7 R	TCTTGTCGAACTTGGGTGGGTTCT
Mitochondrial Biogenesis	
Pgc1α F	TTTGCCCAGATCTTCCTGAAC
Pgc1α R	TCGCTACACCACTTCAATCCA
Errγ F	GACTTGGCCTTTTAAAACAAC
Errγ R	TGGCATTAACTAAACGGTCTT
Nrf1 F	GGAGCACTTACTGGAGTCC
Nrf1 R	CTGTCCGATATCCTGGTGGT
Tfam F	GCAAAGGATGATTCGGCTCAGGGAA
Tfam R	CCGGATCGTTTCACACTTCGACGG

Table 4.5: List of ADP transport, uncoupling and antioxidant mouse primers and sequences used in this study.

ADP Transport	
Ant1 F	ATTATGTACACGGGGACACTT
Ant1 R	TGGACCAAGCACCTTTGAAGA
Ant2 F	CGAGCTGCCTACTTTGGTATC
Ant2 R	ATATCAGTTCCTTTGCGTCC
Uncoupling Proteins	
Ucp2 F	ATTGAAGGTCCCCGTTTCTCC
Ucp2 R	ACATCTGTGGCCTTGAAACCAAC
Ucp3 F	GGACCCACGGCCTTCTACAAA
Ucp3 R	TTCCCGCAGTACCTGGACTTT
Antioxidant System	
Sod1 F	GAACCATCCACTTCGAGCAGA
Sod1 R	CGGGCCACCATGTTTCTTAG
Sod2 F	ATGTTACAACTCAGGTCGCTCTT
Sod2 R	AGACCCAAAGTCACGCTTGAT
Cat F	CTTTTCAATGCCATCGCCAAT
Cat R	TAGTCCTTGTGAGGCCAAACC
Gpx1 F	AGCAGTCTGGCAACTCCTAAG
Gpx1 R	AAATCAGGTGTTTCTCCGTG
Gpx3 F	TCCATCTGTGTTTACGGCTT
Gpx3 R	TTGTGTTTCCTTTGGGCTCAT
Gsr F	ACTGCCTTTACCCCGATGTAT
Gsr R	CATGTGAATGCCAACCACCTT

Antioxidant System Continued	
Gclc F	AAGGTTGTCATCAATGTGCCA
Gclc R	TCCGCATCTTCTGGAAATGTT
Txn F	TCAAGCCCTTCTTCCATTCCC
Txn R	TTTCCTTGTTAGCACCGGAGA
Txnrd1 F	CAAAATCGGTGAACACATGGAA
Txnrd1 R	TCTATGGTCTCCTCGCTGTTT
Txnrd2 F	AGAAGCCGTGCAAAACCATGT
Txnrd2 R	TACCTTGGCCGTCCTCCTGTA

Chapter 5: General Discussion and Conclusions

T2D is a major co-morbidity associated with obesity. The number of individuals with T2D is increasing rapidly, with projections suggesting that 629 million individuals will live with diabetes worldwide by 2045(10). Diabetes is associated with chronic complications that affect microvascular and macrovascular systems and costs hundreds of billions of dollars annually to manage. Although no current statistics exist on the proportion of individuals with insulin resistance, which precedes development of T2D, the number likely far exceeds that of individuals with T2D. Therefore, the high prevalence of diabetes and insulin resistance worldwide is a major economic burden for the health care system and an important concern for health care providers and policy makers.

Obesity-induced insulin resistance affects the ability of metabolically relevant peripheral tissues to maintain glucose homeostasis, including adipose tissue and skeletal muscle(4). In particular, the adipose tissue regulates systemic insulin sensitivity and glucose homeostasis in part through the secretion of bioactive molecules known as adipokines(5). Adipokines can act locally or systemically and can promote several signaling responses that directly influence insulin sensitivity(6). However, metabolic diseases such as obesity and insulin resistance result in drastic changes in the adipokine profile in pre-clinical models and in humans(46); these changes can further exacerbate adipose tissue and systemic metabolic dysfunction.

In 2004, mRNA expression of the adipokine, ATX, was first shown to be upregulated in obese, insulin resistant mice and human(215). Subsequent work demonstrated that adipose-specific ATX deficiency improves glucose intolerance in HFHS-fed mice(178). Similarly, LPA, the product of ATX activity, exacerbated systemic glucose intolerance in HFHS-fed mice, an effect that could be ameliorated with LPA receptor antagonism(191). Together, these studies implicated the ATX-LPA signaling axis in obesity-induced insulin resistance and laid the groundwork for modulation of this pathway as a potential therapeutic option. However, it remains to be determined which factors regulate ATX in an obese-insulin resistant milieu. Furthermore,

despite the wealth of evidence linking ATX-LPA signaling to adipose tissue insulin signaling and metabolism, it was unclear whether it similarly influences skeletal muscle, the primary site of insulin stimulated blood glucose disposal.

Thus, the overall goal of my thesis focused on two major questions regarding the role of ATX-LPA signaling in obesity-induced insulin resistance. First, we aimed to identify and characterize how nutritional and hormonal stimuli known to be deregulated by an obesogenic-insulin resistant milieu impact ATX expression. Secondly, we wanted to determine whether modulation of ATX-LPA signaling influences skeletal muscle insulin sensitivity and explore mechanistically how this could occur.

Herein, glucose transcriptionally upregulated ATX expression in a time- and concentration-dependant manner. Insulin elicited a biphasic response. Acute insulin stimulation increased ATX activity in a PI3Kinase-dependent and mTORC1-independent manner, whereas chronic insulin stimulation decreased ATX expression. HFHS-fed $ATX^{+/-}$ mice were partially protected from diet-induced obesity and exhibited improved systemic and skeletal muscle insulin sensitivity. ATX deficiency ameliorated HFHS-induced impairments in fatty acid-linked mitochondrial respiration, while gene expression of inflammatory and fibrotic markers were unchanged. Conversely, direct addition of LPA to myotubes impaired insulin signaling and fatty acidlinked mitochondrial respiration. Together, these experiments enhance our understanding of how ATX is regulated by an obese-insulin resistant milieu and the impact of ATX-LPA signaling on skeletal muscle insulin sensitivity and mitochondrial function. Furthermore, our work suggests that targeting the ATX-LPA axis could possibly be developed into a novel therapeutic option for the treatment and/or prevention of obesity-induced insulin resistance. The following sections will discuss how our work fits with our understanding of ATX-LPA signaling in pathophysiological conditions, remaining questions and future directions.

5.1. Regulation of ATX by acute and chronic stimuli

Obesity-induced insulin resistance, a chronic pathophysiological condition, induces broad changes in nutritional, hormonal and neuronal factors(4). Levels of these factors can also change acutely, as during feeding/fasting. Several independent studies have shown that ATX is upregulated by pathophysiological inflammatory conditions, such as obesity and arthritis, with cytokines such as TNFα and IL-6 increasing ATX expression(66,180). Furthermore, increases in adipose ATX mRNA also coincided with the development of hyperglycemia in db/db mice, suggesting that ATX expression could be additionally regulated by long term changes in nutritional factors(215). However, it was unclear whether ATX could be acutely regulated by nutritional stimuli. Recent evidence suggests that ATX expression can also be regulated post-transcriptionally by RNA binding proteins and miRNAs, suggesting that examination of ATX mRNA expression alone is insufficient to accurately identify potential modulators of ATX(278,279).

We showed that measurement of serum ATX activity in mice, which serves as a better indicator of ATX levels in circulation, was dynamically regulated both acutely, by feeding-fasting, and chronically, by diet-induced obesity(205). By examining nutritional and hormonal factors known to be regulated by acute and chronic alterations in nutritional status, we identified glucose and insulin as novel regulators of ATX expression in adipocytes/adipose tissue. Acutely, increases in both glucose and insulin stimulated ATX expression in 3T3-L1 adipocytes and adipose tissue explants. Physiologically, ATX-LPA is required for multiple aspects of adipose tissue function, including pre-adipocyte survival and proliferation, tissue remodelling, immune function and mitochondrial metabolism (8). However, whether dynamic changes in ATX expression play a role in acute adipose tissue responses, such as during feeding/fasting is unclear. For example, during fed conditions, when adipose tissue acts as a nutrient sink, it is unclear whether increases in ATX-LPA signaling promotes adipocyte hypertrophy through tissue remodeling and pre-adipocyte hyperplasia, and inhibit mitochondrial metabolism. Conversely, in

fasted adipocytes, do decreases in ATX-LPA signaling increase mitochondrial function or play a role in lipolysis(8,180)? Overall, our studies indicate that glucose and insulin appear to be fundamental physiological regulators of ATX expression in adipocytes. Circulating glucose levels can fluctuate between 4-10 mM in fed/fasting states, suggesting that glucose transcriptional promotes ATX secretion from adipocytes. In 3T3-L1 adipocytes and SCAT explants, we used 6 and 25 mM glucose to stimulate fasted and fed states, respectively, as previously used(280). Similarly, circulation insulin levels can vary broadly between fasting (<170 pM) and fed (up to 2nM) states(4), which are in the range of insulin concentrations that influence ATX expression in adipocytes in vitro.

The mechanisms that govern chronic ATX regulation by glucose and insulin are still unclear. While the effect of glucose on ATX expression was transcriptionally mediated, the effect of chronic insulin incubation on ATX expression is more complex. Insulin-mediated effects on ATX appear to be dose-dependent, with low insulin doses having a stimulatory effect and high doses of insulin having an inhibitory effect on ATX expression(235). It is possible that these divergent effects of insulin on ATX expression may be related to the degree of adipose insulin resistance induced by hyperinsulinemia. Low insulin (1 nM) can induce mild insulin resistance in adipocytes (data not shown) and upregulate ATX expression(235). Conversely, high doses of insulin (100 nM) cause severe insulin resistance and inhibit ATX expression in 3T3-L1 adipocytes. Therefore, it is unclear whether insulin acts as a transcriptional activator or inhibitor of ATX in an insulin resistant milieu. If insulin acts as a transcriptional inhibitor of ATX, it would be interesting to determine whether this inhibition is lost during longer term incubation under conditions mimicking hyperinsulinemia.

5.2. The role of ATX-LPA signaling in obesity-induced skeletal muscle insulin resistance

A major co-morbidity associated with obesity is insulin resistance, where tissues become resistant to the actions of insulin. ATX-LPA signaling has been shown by several independent

labs to be increased in preclinical models of obesity-induced insulin resistance, including in this study(8,178,180,191). Importantly, serum ATX protein levels were also shown to be an independent predictor of insulin resistance in older, obese humans that are not (yet) diabetic(205). Since ATX is an adipokine, the majority of studies on the mechanistic role of ATX-LPA signaling in insulin resistance have focused on the adipose tissue itself. However, whether ATX-LPA influence peripheral tissue insulin signaling, including in the skeletal muscle, as circulating factors, was unclear. It was for this reason that we characterized the effect that ATX-LPA signaling axis on diet-induced skeletal muscle insulin resistance. Consistent with observations in adipose tissue and liver, reducing ATX-LPA signaling was associated with improved insulin signaling in the skeletal muscle of HFHS-fed mice. Although skeletal muscle depots are known to be differentially susceptible to high fat feeding(281), improved insulin signaling was seen in both oxidative and oxidative/glycolytic mixed muscles from HFHS-fed $ATX^{+/-}$ mice. Examination of potential linkages between ATX-LPA and insulin signaling in the soleus determined that ATX deficiency improved mitochondrial dysfunction induced by a HFHS diet.

5.2.1 Mechanisms that link ATX-LPA signaling to insulin resistance are tissue specific

Several mechanisms, including fibrosis, inflammation, PPARγ modulation and mitochondrial dysfunction have been proposed to mediate ATX-LPA induced insulin resistance. While ATX-LPA deficiency improves insulin sensitivity in the adipose tissue(8,178,180,222), hepatocytes(206,218), cardiac tissue(219) and skeletal muscle, the mechanisms involved may be tissue and context specific. The adipose tissue of HFD-fed fat specific $ATX^{-/-}$ ($FATX^{-/-}$) mice shows reduced inflammation and increased PPARγ expression and activity(8). In line with a pro-inflammatory effect of ATX in adipose tissue, post-natal ATX deletion and inhibition of ATX activity pharmacologically with PF-8380 ameliorated hepatic and cardiac inflammation, respectively(218,219). Interestingly, we did not observe any significant change in mRNA expression of common inflammatory markers in the soleus muscle, which contrasts with what has

been reported for adipose tissue, liver and heart. However, it is unclear whether expression of inflammatory markers are similarly unchanged by ATX modulation in other skeletal muscle depots, such as the glycolytic EDL or the mixed glycolytic/oxidative tibialis and gastrocnemius muscles. The presence of inflammation in adipose tissue and liver also suggest that there are tissue specific responses to HFHS-feeding for 20 weeks(218). However, taken together this suggests that inflammation does not contribute to skeletal muscle insulin resistance in our HFHS-fed model.

mRNA expression of fibrotic markers was unchanged in the adipose tissue of HFD-fed mice(8). However, in the more severely diabetic *db/db* mouse model, fibrosis was reduced following 3 weeks of LPA receptor antagonist administration(222). siRNA mediated inhibition of ATX additionally ameliorated HFD-induced fibrosis in cardiac tissue through downregulation of TGFβ-SMAD3 signaling(282). Serum ATX levels correlate with liver fibrosis in humans, while increases in ATX expression were shown to directly promote hepatic fibrosis in mice through upregulation of TGFβ-Col3a1(173,283). Similar to inflammation, we did not notice any change in fibrotic gene expression markers in the soleus. Taken together, this suggests that fibrosis does not play a significant role in skeletal muscle insulin resistance in our HFHS-fed model or with $ATX^{+/-}$ mice. However, whether inhibition of ATX using ONO-8430506 or with Ki16425 ameliorates skeletal muscle insulin resistance remains to be examined.

The major mechanism that appears to link ATX-LPA signaling to insulin signaling in the muscle is mitochondrial function. ATX deficiency ameliorated HFHS-diet induced decreases in fatty-acid linked respiration in the soleus, which was independent from fiber-type reprogramming or changes in mitochondrial content and ADP sensitivity. A similar mechanism may operate in cardiac muscle, as siRNA mediated inhibition of ATX in HFD-fed mice improved ATP production, mitochondrial respiration and complex I activity(282). In brown adipose tissue, $FATX^{-/-}$ mice display increased mRNA expression of mitochondrial biogenesis markers, including PGC1α(8). Differences in mitochondrial phenotypes observed between muscle and

adipose tissue may depend on the tissue specific differences of ATX-LPA signaling in cell differentiation as well as the use of mouse models that completely(8) or partially abrogate ATX-LPA signaling.

5.2.2. Mechanisms that could link ATX-LPA signaling to mitochondrial dysfunction

Despite no observed changes in mitochondrial content, there are several mechanisms that could link ATX-LPA to insulin signaling and mitochondrial function in the setting of obesity-insulin resistance, although further studies are necessary to confirm these mechanisms. H_2O_2 secretion from mitochondria in permeabilized HFHS-fed $ATX^{+/-}$ soleus fibers was significantly increased, concomitant with a tendency towards decreased antioxidant gene expression. Interestingly, increased H_2O_2 secretion was also observed in insulin resistant 3T3-L1 adipocytes co-treated with the ATX inhibitor, PF-8380(176). Taken together, this suggests that ATX-LPA signaling may be involved in modulating ROS levels in multiple insulin sensitive tissues. Elevated ROS, including H_2O_2, has been implicated in adaptive (exercise) and maladaptive (obesity, insulin resistance) responses in the skeletal muscle(111,277). In addition to the magnitude of ROS secretion, the source of ROS (mitochondria, NAD(P)H oxidase, xanthine oxidase) and the duration of ROS production play important roles in determining whether ROS is adaptive or maladaptive. ROS levels are acutely increased following insulin stimulation and in turn potentiate insulin signaling by reversibly oxidizing protein phosphatases, such as PTEN and PTP1b(124,284). Acute incubation of EDL with H_2O_2 *ex vivo* increased insulin-stimulated glucose transport, an effect that was abolished with catalase treatment(285). Interestingly, in $GPX1^{-/-}$ mice, a model of chronic ROS elevation, improved insulin sensitivity was observed in the skeletal muscle of HFD-fed mice, but not adipose tissue or liver(124).

Critically, whether H_2O_2 secretion from skeletal muscle of $ATX^{+/-}$ mice is adaptive or maladaptive remains to be determined. Examination of GSSG:GSH ratios, which are indicative of the overall redox environment, will illuminate the potential impact of increased mitochondrial H_2O_2 secretion on the cell. Quantification of 4-HNE showed a significant decrease in WT HFHS-

fed soleus muscles and no difference between chow-fed WT mice and $ATX^{+/-}$ mice on either chow or HFHS diet. Therefore, overall, this suggests that our HFHS-feeding regimens did not cause oxidative stress, as measured by 4-HNE. However, whether examination of other markers of oxidative stress, including protein carbonylation and malondialdehyde, are similarly altered remained to be determined(286). Whether oxidation of protein phosphatases, such as PTEN or PTP1b, which potentiate insulin signaling, are increased in the soleus of HFHS-fed $ATX^{+/-}$ is unclear. Furthermore, whether ATX deficiency also changes ROS generation from NAD(P)H oxidase needs to be determined, as these enzymes predominantly generate H_2O_2 near the plasma membrane and can more directly influence insulin signaling(124).

The redox environment can also influence mitochondrial dynamics, including fusion and fission, to remodel in the mitochondrial network(112). A more fused network is characterized by increased OXPHOS and mitochondrial membrane potential, along with decreased ROS production(287). Promotion of mitochondrial fusion is also associated with improved skeletal muscle insulin signaling and insulin stimulated glucose uptake(287). The BAT of HFD-fed $FATX^{-/-}$ mice have increased mitochondrial membrane potential, whereas we showed that the soleus of HFHS-fed $ATX^{+/-}$ mice has increased OXPHOS and insulin sensitivity(8). ROS production is also increased, which argues against a more fused network. However, there is uncertainty of whether ROS that we see is within physiological ranges or whether it can promote fusion or fragmentation(274–276). Apart from ROS, lysophospholipids themselves can influence mitochondrial dynamics(288). Increases in LPA have been demonstrated to promote both mitochondrial fusion and fission due to its intrinsic high, negative curvature(288–290). It is unknown whether changes in extracellular ATX-LPA signaling induce changes in the intracellular LPA pool.

A final potential mechanism linking increased ATX-LPA signaling to mitochondrial dysfunction is via upregulation of glycolysis and coordinated impairment of oxidative phosphorylation. Treatment of cancer cells with LPA can impair FCCP-driven uncoupled

respiration, similar to our work in C2C12 myotubes, and is associated with increased extracellular acidification and lactate production(291). LPA upregulates many glycolytic genes through activation of transcription factors hypoxia-inducible factor 1α (HIF-1α) and/or E26 transformation-specific 1 (ets-1)(291–293). However, cancer cells utilize aerobic glycolysis to support increased ATP production, while skeletal muscle primarily relies on oxidative phosphorylation(291). Although increased glycolysis is observed in the skeletal muscle of diabetic patients, whether ATX-LPA plays any part in this is unknown(294).

5.3. LPA receptors as mediators of ATX-LPA signaling

It remains unclear which of the LPA receptors is involved in the modulation of insulin sensitivity by ATX-LPA(167). It also remains to be determined whether LPA receptor profiles in muscle change during obesity and insulin resistance in mice and humans. One study showed that LPA receptors are markedly altered in murine heart and PGAT during obesity-induced insulin resistance(188). Lpa3, 5 and 6 were significantly increased in the PGAT of fasted HFHS mice, whereas Lpa4-6 were similarly increased in the heart. Changes in LPA receptors are also seen in the atrial appendage and subcutaneous adipose tissue (SAT) of pre-obese and obese cardiac surgery patients(188). In human atrial appendage, increased LPA4 and LPA5 expression significantly correlated with BMI, but not HOMA-IR(188). Similarly, in human SAT, LPA4-6 were negatively correlated with BMI, but not associated with HOMA-IR(188). Our work suggests that neither obesity nor insulin resistance had an effect on LPA1-6 mRNA expression in the soleus muscle. However, ATX deficiency was associated with a decrease in LPA2 and increase in LPA4. Therefore, future studies should aim to target these receptors *in vivo* to determine whether they play a role in skeletal muscle insulin resistance. Work has already been undertaken on this front, with generation of a whole body LPA4$^{-/-}$ mouse, which showed improved adipose tissue insulin sensitive and reduced liver steatosis; however, the skeletal muscle was not examined(259).

While a HFHS-diet did not change LPA1-6 expression in muscle in vivo, incubation with palmitate, a lipid linked to obesity-related lipotoxicity, markedly affected all LPA receptors in

C2C12 myotubes. The discrepancy between our *in vivo* and *in vitro* experiments are unclear, but may be due to the fact that HFHS feeding did not significantly alter levels of albumin bound NEFA, despite inducing hyperglycemia and hyperinsulinemia. Although HFHS-feeding increased DG and TG levels in the gastrocnemius, ceramides were unchanged whereas treating C2C12 myotubes with palmitate increase TG, DG and ceramides(295). Future studies should attempt to induce insulin resistance in C2C12 myotubes using hyperglycemia and hyperinsulinemia or recapitulate our *in vitro* observations by feeding mice a diet with a higher fat content. For example, in addition to the HFHS (45% kcal) diet that we use, HF (60% kcal) diets exist.(8) The discrepancy in LPA receptor expression in muscle could also be due to the length of exposure to an obese-insulin resistant milieu. C2C12 cells were incubated with palmitate for a relatively short term (16-18 h), whereas WT and ATX+/- mice were fed a HFHS diet for 20 weeks. Furthermore, there are multiple skeletal muscle depots, with differences in their glycolytic and oxidative capacity(296). It would be interesting to see whether LPA receptors are similarly changed in different skeletal muscle tissues, such as the gastrocnemius, extensor digitorum longus (EDL) and the tibialis. Furthermore, as skeletal muscle is heterogenous in terms of its cell population, examination of LPA1-6 in isolated myotubes would be informative(296).

Activation of LPA1-6 can initiate different signaling pathways, which can converge on several aspects of insulin signalling (Fig. 1.5). In particular, LPA1-4 can signal through $G\alpha_{i/o}$ to activate PI3K-AKT signaling. Acute, 30 min LPA treatment in C2C12 myotubes augmented insulin-stimulated AKT phosphorylation. However, as LPA pre-treatment duration exceeded 60 min, we saw significant reductions in insulin-stimulated AKT phosphorylation, suggestive of insulin resistance. Long-term activation of the PI3K-AKT signaling axis, either through hyperinsulinemia or via LPA-Lpa1-4, may lead to pathway desensitization and insulin resistance(297). Alternatively, LPA induced activation of glycolysis in cancer cells was mediated through activation of $G\alpha_i$ and Lpa2-PI3K-AKT signaling(291,293). Apart from $G\alpha_{i/o}$, $G_{\alpha 12/13}$-Rho activation was demonstrated to reduce mitochondrial respiration and mass in adipose tissue; this

effect was mediated by Lpa4(259). $G_{\alpha 13}$-Rho signaling was also increased in the skeletal muscle of HFD-fed mice, with $G_{\alpha 13}$ ablation reprogramming fibers towards an oxidative phenotype(260). Teasing out which LPA receptors and downstream effectors mediate the impact of ATX-LPA on insulin resistance and mitochondrial dysfunction in skeletal muscle exposed to an obese-insulin resistant milieu will be a challenging task given that skeletal muscle expresses all 6 LPA receptors and these receptors can coupling to multiple Gα proteins.

It should be noted that changes in LPA receptor mRNA expression do not necessarily suggest that signaling through a particular LPA receptor is altered or contributes to diseaset. For example, HFHS-fed LPA4 KO mice show improved insulin sensitivity and reduced tissue inflammation, despite mRNA levels of this receptor being unchanged in WT chow and HFHS-fed mice. Similarly, LPA1/3 receptor antagonism improved LPA-induced glucose intolerance in HFHS-fed mice and lead to increased insulin stimulated glucose oxidation in the soleus(191); mRNA levels of these receptors were unchanged. Therefore, use of specific LPA receptor agonists/antagonists or generation of LPA receptor knockout/knockin cell lines/mice will better aid in determining key receptors and signaling mechanisms.

5.4. Therapeutic potential of the ATX-LPA-LPA1-6 signaling axis

Targeting the ATX-LPA-LPA1-6 pathway may be a therapeutic strategy for treating obesity-induced insulin resistance. Post-natal whole body deletion and long-term pharmacological inhibition of ATX in mice is well-tolerated, with no adverse effects noted(155). Thirty three different ATX inhibitors have been synthesized, with several reaching nanomolar IC_{50} values(298). ONO-8430506, for example, is a competitive ATX inhibitor that potently (IC_{50} 4.7–11.6 nM for plasma) reduces plasma LPA levels, even after 24 h following administration of a 3 or 30 mg/kg dose in rats(299). ONO-8430506 has a half-life of 3 h and a bioavailability of 52% following oral administration(299). Importantly, ONO-8430506 has been utilized in several syngeneic orthotopic mouse models of breast cancer to inhibit drug resistance, oxidative stress responses and delay tumor growth and metastasis(256,300). We also utilized ONO-8430506 to

inhibit ATX activity *in vivo* by 85 and 92% in chow and HFHS-fed mice, respectively. Three weeks of daily ONO-8430506 treatment, via oral gavage, moderately reduced HFHS-induced hyperglycemia and seemed to improve hepatic insulin signaling. However, we have yet to examine whether HFHS-fed mice treated with ONO-8430506 show systemic improvements in glucose tolerance, insulin sensitivity, along with improved skeletal muscle insulin signaling and mitochondrial function.

Another ATX inhibitor, PF-8380, has also been utilized to effectively inhibit ATX and LPA in pre-clinical models. Four weeks of daily, oral PF-8380 treatment ameliorated ileitis in SAMP1/Fc mice and improved nutrition absorption in the intestines(301). Similarly, an eight week daily intraperitoneal injection of PF-8380 reduced HFD-induced cardiac hypertrophy and inflammation, and improved cardiac function(219). Critically, the ATX inhibitor, GLPG1690, is currently in Phase III of clinical trials for the treatment of idiopathic pulmonary fibrosis (IPF)(261,302). IPF is a progressive, pathophysiological lung disease, characterized by fibrosis and inflammation. Currently, no medication has been proven to slow the progression for IPF, with patients only taking anti-inflammatory or immune suppressive drugs(261). Treatment of 17 patients with GLPG1690 in a Phase II clinical trial significantly improved lung capacity compared to placebo controls, suggesting that ATX inhibition may be a promising avenue for the treatment of IPF(303).

However, while mice with postnatal blunting of ATX-LPA signaling appeared normal, potential adverse effects of ATX-LPA inhibition may be possible. For example, fat specific ATX deficiency is associated with marked levels of pre-adipocyte death in the adipose tissue of both chow and HFD-fed mice (8). While these mice are protected from diet-induced obesity and insulin resistance, it should be noted that these studies were short term (10 weeks). It is unclear if a reduction in the pre-adipocyte population, which is necessary to maintain adipose tissue, adversely affects adipose tissue health in fat-specific ATX knockout mice in the long term.

Apart from inhibiting ATX activity, targeting LPA1-6 could be an alternative avenue to target the ATX-LPA signaling axis more specifically. LPA1/3 receptor antagonism has been demonstrated to have pleiotropic effects on insulin sensitive tissues and ameliorated HFHS-induced glucose intolerance(191). However, only several broad LPA receptor antagonists currently exist, with no LPA receptor specific antagonists being described so far(259). It is also unclear whether broad LPA receptor antagonism has any off-target effects. Therefore, more specific LPA receptor agonists and antagonists need to be developed to determine its viability in targeting the ATX-LPA axis.

Taken together, this suggests that inhibition of ATX or LPA receptor antagonism may be viable tools not only for the treatment of inflammatory and fibrotic diseases, but also metabolic diseases including obesity-induced insulin resistance and T2D. However, examination of potential adverse effects associated with long-term inhibition, especially on pre-adipocyte survival and adipose tissue health, is necessary to truly determine whether ATX-LPA signaling is a viable therapeutic target.

5.5 Perspectives and Concluding Remarks

Pre-clinical and clinical investigations have highlighted the importance of ATX-LPA signaling in physiological and pathophysiological conditions, including metabolic disorders such as obesity-induced insulin resistance. ATX-LPA levels are upregulated in obese-insulin resistant states and can contribute to the development and/or exacerbation of insulin resistance by promoting inflammation and fibrosis and inhibiting PPARγ activity and mitochondrial function. These mechanisms may be tissue-specific and modulated by differential expression of LPA receptors. Future studies will need to define more mechanistically how increases in ATX-LPA signaling occur in insulin resistance, as well as pinpoint specific signaling pathways that link ATX-LPA to adipose tissue, hepatic and skeletal muscle insulin resistance. These studies will also allow us to better assess whether targeting the ATX-LPA signaling axis could hold promise as a treatment of obesity-induced insulin resistance and T2D.

References

1. D'Souza, K., Paramel, G. V. and Kienesberger PC. (2018) Lysophosphatidic Acid Signaling in Obesity and Insulin Resistance. *Nutrients* **10** (4):pii: E399.

2. WHO (2015) Media Center: Obesity and Overweight Rates, World Health Organization. Available from: https://www.who.int/en/news-room/fact-sheets/detail/obesity-and-overweight

3. Guh, D. P., Zhang, W., Bansback, N., Amarsi, Z., Birmingham, L. and Anis, A. H. (2009) The incidence of co-morbidities related to obesity and overweight : A systematic review and meta-analysis. *BMC Public Health* **20** (88):1–20.

4. Petersen, M. and Shulman, G. (2018) Mechanisms of Insulin action and insulin resistance. *Physiol Rev* **98**(1):2133–223.

5. Lehr, S., Hartwig, S., Sell, H. (2012) Adipokines : A treasure trove for the discovery of biomarkers for metabolic disorders. *Proteomics Clin Appl.* **6** (1-2):91–101.

6. Cao, H. (2014) Adipocytokines in obesity and metabolic disease. *J Endocrinol*. **220** (2): T47-59

7. Sethi, J. K. and Hotamisligil, G.S. (1990) The role of TNF alpha in adipocyte metabolism. *Semin Cell Dev Biol* **10** (1):19–29

8. Nishimura, S., Nagasaki, M., Okudaira, S., Aoki, J., Ohmori, T., Ohkawa, R. et al. (2014) ENPP2 contributes to adipose tissue expansion and insulin resistance in diet-induced obesity. *Diabetes* **63** (12):4154–64.

9. Benesch, M. G. K., Ko, Y. M., McMullen, T. P. W and Brindley, D. N. (2014) Autotaxin in the crosshairs: Taking aim at cancer and other inflammatory conditions. *FEBS Lett*. **588** (16):2712–27.

10. WHO (2016) Global Report on Diabetes, World Health Organization. Available from: https://www.who.int/diabetes/global-report/en/

11. Doucet, G. (2010) An economic tsunami: The cost of diabetes in Canada. *Canadian Journal of Diabetes* 34 (1):27-29

12. Forbes, J. M. and Cooper, M. E. (2013) Mechanisms of diabetic complications. *Physiol Rev.* **93** (1):137–88.

13. Chaudhury, A., Duvoor, C., Reddy, V. S. D., Kraleti, S., Chada, A., Ravilla, R., et al. (2017) Clinical Review of Antidiabetic Drugs : Implications for Type 2 Diabetes Mellitus Management. *Front Endocrinol (Lausanne)*. **8** (1):1–12.

14. Kolb, H. and Martin, S. (2017) Environmental/lifestyle factors in the pathogenesis and prevention of type 2 diabetes. *BMC Med*. **15** (1):1–11.

15. Inzucchi, S. E., Lipska, K. J., Mayo, H., Bailey, C. J. and McGuire, D. K. (2014) Metformin in Patients With Type 2 Diabetes and Kidney Disease A Systematic Review. *JAMA* **312** (24):2668–75.

16. Rena, G., Hardie, D. G. and Pearson, E. R. (2017) The mechanisms of action of metformin. *Diabetologia* **60** (9);1577–85.

17. Hu, F. B., Manson, J. E., Stampfer, M. J., Colditz, G., Liu, S., Solomon, C. G., et al. (2001) Diet, Lifesytle and the Risk of Type 2 Diabetes Mellitus in Woman. *N Engl J Med*. **345** (11):790–8.

18. Neeland, I. J., Turor, A. T., Ayers, C. R., Powell-Wiley, T. M., Vega, G. L., Farzaneh-Far, R., et al. (2013) Dysfunctional Adiposity and the Risk of Prediabetes and Type 2 Diabetes in Obese Adults. *JAMA* **308** (11):1150–9.

19. Ballestri, S., Zona, S., Targher, G., Romagnoli, D., Baldelli, E., Roverato, A., et al. (2016) Nonalcoholic fatty liver disease is associated with an almost twofold increased risk of incident type 2 diabetes and metabolic syndrome: Evidence from a systematic review and meta-analysis. *J Gastroenterol Hepatol.* **31** (1):936–44.

20. Sorensen, M., Andersen, Z. J., Nordsborg, R. B., Becker, T., Tjonneland, A., Overvad, K. et al. (2013) Long-Term Exposure to Road Traffic Noise and Incident Diabetes: A Cohort Study. *Environ Health*. **121** (2):217–22.

21. Weinmayr, G., Hennig, F., Fuks, K., Nonnemacher, M., Jakobs, H., Möhlenkamp, S. et al. (2015) Long-term exposure to fine particulate matter and incidence of type 2 diabetes mellitus in a cohort study: effects of total and traffic-specific air pollution. *Environ Health* **14** (53):1–8.

22. Heidemann, C., Niemann, H., Paprott, R., Du, Y. and Rathmann, W. (2014) Residential traffic and incidence of Type 2 diabetes: the German Health Interview and Examination Surveys. *Diabet Med*. **31** (10):1269–76.

23. Giang, K. W., Novak, M. and Bjo, L. (2013) Perceived stress and incidence of Type 2 diabetes: a 35-year follow-up study of middle-aged Swedish men. *Diabetes Med*. **30** (1): e8–16.

24. Melamed, S., Shrimon, A., Toker, S. and Shapira, I. (2006) Burnout and Risk of Type 2 Diabetes : A Prospective Study of Apparently Healthy Employed Persons. *Psychosom Med*. **68** (6):863–9.

25. Xue, A., Wu, Y., Zhu, Z., Zhang, F., Kemper, K. E., Zheng, Z. et al. (2018) Genome-wide association analyses identify 143 risk variants and putative regulatory mechanisms for type 2 diabetes. *Nat Commun.* **9** (1):2941.

26. Barroso, I. and Mccarthy, M. I. (2019) The Genetic Basis of Metabolic Disease. *Cell* **177** (1):146–61.

27. Frayling, T. M., Timpson, N. J., Weedon, M. N., Freathy, R. M., Lindgren, C. M., Perry, J. R. B. et al. (2007) Childhood and Adult Obesity A Common Variant in the FTO Gene Is Associated with Body Mass Index and Predisposes to Childhood and Adult Obesity. **Science** *316* (5826):889–94.

28. Smemo, S., Tena, J. J., Kim, K. H., Gamazon, E. R., Sakabe, N. J., Gomez-Marin, C. et al. (2014) Obesity-associated variants within FTO form long-range functional connections with IRX3. *Nature* **507** (7492):371–5.

29. Sindelar, D. K., Balcom, J. H., Chu, C. A., Neal, D. W. and Cherrington, A. D. (1999) A comparison of the effects of selective increases in peripheral or portal insulin on hepatic glucose production in the conscious dog. *Diabetes* **45** (11):1594–604.

30. Samuel, V. T. and Shulman, G. I. (2012) Mechanisms for insulin resistance: Common threads and missing links. *Cell* **148** (5):852–71.

31. Cherrington, A. D., Edgerton, D. and Sindelar, D. K. (1998) The direct and indirect effects of insulin on hepatic glucose production *in vivo*. *Diabetologia*. **41** (9):987–96.

32. Perry, R. J., Camporez, J. G., Kursawe, R., Titchenell, P. M., Zhang, D., Perry, C. J., Jurczak, M. J., Abudukadier, A., Han, M. S., Zhang, X. M., Ruan, H. B., Yang, X., Caprio, S., Kaech, S. M., Sul, H. S., Birnbaum, M. J., Davis, R. J., Cline, G. W., Petersen, K. F., Shulman, G. I. (2015) Hepatic Acetyl CoA Links Adipose Tissue Inflammation to Hepatic Insulin Resistance and Type 2 Diabetes. *Cell* **160** (4):745–58.

33. Gastaldelli, A., Baldi, S., Pettiti, M., Toschi, E., Camastra, S., Natali, A. et al. (2009) Influence of obesity and Type 2 diabetes on gluconeogenesis and glucose output in humans. *Diabetes* **49** (8):1367–73.

34. DeFronzo, R. A. and Tripathy, D. (2009) Skeletal muscle insulin resistance is the primary defect in type 2 diabetes. *Diabetes Care* **32** (Suppl 2):S157-63.

35. Baron, A. D., Brechtel, G., Wallace, P., Edelman, S. V. and Wallace, P. (1988) Rates and tissue sites of non-insulin- and insulin-mediated glucose uptake in humans. *Am J Physiol.* **255** (6):E769-774.

36. Shulman, G. I., Rothman, D. L., Jue, T., Stein, P., DeFronzo, R. A., Shulman, R. G. (1990) Quantitation of muscle glycogen synthesis in normal subjects and subjects with non-insulin-dependent diabetes by 13C nuclear magnetic resonance spectroscopy. *N Engl J Med.* **322** (4):223–8.

37. Thiebaud, D., Jacot, E., DeFronzo, R. A., Maeder, E., Jequier, E. and Felber, J. P. (1982) The Effect of Graded Doses of Insulin on Total Glucose Uptake, Glucose Oxidation, and Glucose Storage in Man. *Diabetes* **31** (11):957–63.

38. Lillioja, S., Mott, D. M., Howard, B. V., Bennett, P. H., Yki-Järvinen, H., Freymond, D. et al. (1988) Impaired glucose tolerance as a disorder of insulin action. Longitudinal and cross-sectional studies in Pima Indians. *N Engl J Med.* **318** (19):1217–25.

39. Griffin, M. E., Marcucci, M. J., Cline, G. W., Bell, K., Barucci, N., Lee, D. et al. (1999) Free fatty acid-induced insulin resistance is associated with activation of protein kinase C theta and alterations in the insulin signaling cascade. *Diabetes.* **48** (6):1270–4.

40. Herman, M. A., Peroni, O. D., Villoria, J., Schon, M. R., Abumrad, N. A., Blu, M. et al. (2012) A novel ChREBP isoform in adipose tissue regulates systemic glucose metabolism. *Nature* **484** (7394):333–8.

41. Kowalski, G. M. and Bruce CR. (2014) The regulation of glucose metabolism : implications and considerations for the assessment of glucose homeostasis in rodents. *AJP-Endocrinology Metab*. **307** (10):E859-871.42.

42 Poher, A. L., Altirriba, J., Veyrat-Durebex, C. and Rohner-Jeanrenaud, F. (2015) Brown adipose tissue activity as a target for the treatment of obesity/insulin resistance. *Front Physiol*. **6** (1):1–9.

43. Stanford, K. I., Middelbeek, R. J., Townsend, K. L., An, D., Nygaard, E. B., Hitchcox, K. M., Markhan, K. R., Nakano, K., Hirshman, M. F., Tseng, Y. H. and Goodyear, L. J. (2013) Brown adipose tissue regulates glucose homeostasis and insulin sensitivity. *J Clin Invest.* **123** (1):215–23.

44. Kajimura, S. and Saito, M. (2014) A New Era in Brown Adipose Tissue Biology: Molecular Control of Brown Fat Development and Energy Homeostasis. *Annu Rev Physiol.* **76** (1):225–49.

45. Revollo, J. R., Korner, A., Mills, K. F., Satoh, A., Wang, T., Garten, A., et al. (2007) Nampt/PBEF/Visfatin Regulates Insulin Secretion in b Cells as a Systemic NAD Biosynthetic Enzyme. *Cell Metab.* **6** (5):363–75.

46. Maury, E. and Brichard, S. M. (2010) Adipokine dysregulation, adipose tissue inflammation and metabolic syndrome. *Mol Cell Endocrinol.* **314** (1):1–16.

47. Ouchi, N., Parker, J. L., Lugus, J. J. and Walsh, K. (2011) Adipokines in inflammation and metabolic disease. *Nat Rev Immunol* **11** (2):85–97.

48. Awazawa, M., Ueki, K., Inabe, K., Yamauchi, T., Kubota, N., Kaneko, K. et al. (2011) Adiponectin Enhances Insulin Sensitivity by Increasing Hepatic IRS-2 Expression via a Macrophage-Derived IL-6-Dependent Pathway. *Cell Metab* **13** (4):401–12.

49. Ertunc, M. E., Sikkeland, J., Fenaroli, F., Griffi, G., Daniels, M. P. and Cao, H. et al. (2015) Secretion of fatty acid binding protein aP2 from adipocytes through a nonclassical pathway in response to adipocyte lipase activity. *J Lipid Res.* **56** (2):423–34.

50. Yang, Z., Miyahara, H. and Hatanaka, A. (2011) Chronic administration of palmitoleic acid reduces insulin resistance and hepatic lipid accumulation in KK-A y Mice with genetic type 2 diabetes. *Lipids Health Dis.* **10** (1):120–7.

51. Yore, M. M., Syed, I., Moraes-vieira, P. M., Zhang, T., Herman, M. A., Homan, E.A. et al. (2014) Discovery of a Class of Endogenous Mammalian Lipids with Anti-Diabetic and Anti-inflammatory Effects. *Cell* **159** (2):318–32.

52. Haeusler, R. A., Mcgraw, T. E. and Accili, D. (2017) Biochemical and cellular properties of insulin receptor signalling. *Nat Rev Mol Cell Biol* **19** (1):31–44.

53. Taniguchi, C. M., Emanuelli, B. and Kahn, C. R. (2006) Critical nodes in signalling pathways : insights into insulin action. *Nat Rev Mol Cell Biol.* **7** (2):85–97.

54. Huang, X., Liu, G., Guo, J. and Su, Z. Q. (2018) The PI3K/AKT pathway in obesity and type 2 diabetes. *Int J Biol Sci.* **14** (11):1483–96.

55. Taniguchi, C. M., Emanuelli, B. and Kahn, C. R. (2006) Critical nodes in signalling pathways: insights into insulin action. *Nat Rev Mol Cell Biol* **7** (2):85–96.

56. Klip, A., Sun, Y., Chiu, T. T. and Foley, K. P. (2014) Signal transduction meets vesicle traffic: the software and hardware of GLUT4 translocation. *Am J Physiol Cell Physiol.* **306** (10):C879–86.

57. Cohen, P. (1998) The Croonian Lecture: Identification of a Protein Kinase Cascade of Major Importance in Insulin Signal Transduction. *Philos Trans Biol Sci.* **354** (1382):485–95.

58. Dentin, R., Liu, Y., Koo, S., Hedrick, S., Vargas, T., Heredia, J. et al. (2007) Insulin modulates gluconeogenesis by inhibition of the coactivator TORC2. *Nature* **449** (9):366–70.

59. Sancak, Y., Thoreen, C. C., Peterson, T. R., Lindquist, R. A., Kang, S. A., Spooner, E., et al. (2007) PRAS40 Is an Insulin-Regulated Inhibitor of the mTORC1 Protein Kinase. *Mol Cell.* **25** (6):903–15.

60. Huang, J., Dibble, C. C., Matsuzaki, M. and Manning BD. (2008) The TSC1-TSC2 Complex Is Required for Proper Activation of mTOR Complex 2. *Mol Cell Biol.* **28** (12):4104–15.

61. Dipilato, L. M., Ahmad, F., Harms, M., Seale, P., Manganiello, V. and Birnbaum, M. J. (2015) The Role of PDE3B Phosphorylation in the Inhibition of Lipolysis by Insulin. *Methods Enzymol*. **35** (16):2752–60.

62. Duncan, R. E., Ahmadian, M., Jaworski, K., Sarkadinagy, E. and Sul, H. S. (2007) Regulation of Lipolysis in Adipocytes. *Annu Rev Nutr.* **27**:79–101.

63. Buettner, C. (2012) Is Hyperinsulinemia Required to Develop Overeating-Induced Obesity. *Cell Metab* **16** (6):691–2.

64. Mehran, A. E., Templeman, N. M., Brigidi, G. S., Lim, G. E., Chu, K., Hu, X., et al. (2012) Hyperinsulinemia Drives Diet-Induced Obesity Independently of Brain Insulin Production. *Cell Metab* **16** (6):723–37.

65. Pedersen, D. J., Guilherme, A., Danai, L. V., Heyda, L., Matevossian, A., Cohen, J., et al. (2015) A major role of insulin in promoting obesity- associated adipose tissue inflammation. *Mol Metab* **4** (7):507–18.

66. Hotamisligil, G. S., Atkinson, R. L. and Spiegelman, B. M. (1995) Increased adipose tissue expression of tumor necrosis factor-alpha in human obesity and insulin resistance . *J Clin Invest.* **95** (5):2409–15.

67. Hotamisligil, G. S., Shargill, N. S. and Spiegelman, B. M. (1993) Adipose expression of tumor necrosis factor-alpha: Direct Role in Obesity-Linked Insulin Resistance. *Science* **259** (5091):87–91.

68. Chen, L., Chen, R., Wang, H. and Liang, F. (2015) Mechanisms Linking Inflammation to Insulin Resistance. *Int J Endocrinol.* **2015**:508409.

69. Shoelson, S. E., Herrero, L. and Naaz, A. (2007) Obesity, Inflammation, and Insulin Resistance. *Gastroenterology* **132** (6):2169–80.

70. Nieto-Vazquez, I., Fernandez-Veledo, S., De Alvaro, C. and Lorenzo M. (2008) Dual role of interleukin-6 in regulating insulin sensitivity in murine skeletal muscle. *Diabetes* **57** (12):3211–21.

71. Shi, H., Yin, H., Flier, J. S., Shi, H., Kokoeva, M. V., Inouye, K., et al. (2006) TLR4 links innate immunity and fatty acid–induced insulin resistance. **116** (11):3015–25.

72. Schaeffler, A., Gross, P., Buettner, R., Bollheimer, C., Buechler, C., Neumeier, M., et al. (2009) Fatty acid-induced induction of Toll-like receptor-4/nuclear factor-κB pathway in adipocytes links nutritional signalling with innate immunity. *Immunology* **126** (2):233–45.

73. Huang, S., Rutkowsky, J. M., Snodgrass, R. G., Ono-Moore, K. D., Schneider, D. A., Newman, J. W., et al. (2012) Saturated fatty acids activate TLR-mediated proinflammatory signaling pathways. *J Lipid Res* **53** (9):2002–13.

74. Vandanmagsar, B., Youm, Y. H., Ravussin, A., Galgani, J. E., Stadler, K., Mynatt, R. L., et al. (2011) The NLRP3 inflammasome instigates obesity-induced inflammation and insulin resistance. *Nat Med* **17** (2):179–89.

75. Ussher, J.R., Koves, T. R., Cadete, V. J. J., Zhang, L., Jaswal, J. S., Swyrd, S. J., et al. (2010) Inhibition of de novo ceramide synthesis reverses diet-induced insulin resistance and enhances whole-body oxygen consumption. *Diabetes* **59** (10):2453–64.

76. Lin, Y., Berg, A. H., Iyengar, P., Lam, T. K. T., Giacca, A., Combs, T. P, et al. (2005) The hyperglycemia-induced inflammatory response in adipocytes: The role of reactive oxygen species. *J Biol Chem*. **280** (6):4617–26.

77. Rønningen, T., Shah, A., Reiner, A. H, Collas, P. and Moskaug, J. (2015) Epigenetic priming of inflammatory response genes by high glucose in adipose progenitor cells. *Biochem Biophys Res Commun* **467** (4):979–86.

78. White, M. F., Davis, R., Uchida, T., Yenush, L., Aguirre, V. (2002) The c-Jun NH 2 - terminal Kinase Promotes Insulin Resistance during Association with Insulin Receptor Substrate-1 and Phosphorylation of Ser 307 . *J Biol Chem*. **275** (12):9047–54.

79. Ozcan, U., Cao, Q., Yilmaz, E., Lee, A. H., Iwakoshi, N. N., Ozdelen, E. et al. (2004) Endoplasmic Reticulum Stress Links Obesity, Insulin Action, and Type 2 Diabetes. *Science 306* (5695):457–61.

80. Urano, F., Wang, X., Bertolotti, A., Zhang, Y., Chung, P., Harding, H. P., et al. (2000) Coupling of stress in the ER to activation of JNK protein kinases by transmembrane protein kinase IRE1. *Science* **287** (5453):664–6.

81. Hotamisligil, G. S. (2010) Endoplasmic Reticulum Stress and the Inflammatory Basis of Metabolic Disease. *Cell* **140** (6):900–17.

82. Wick, G., Grundtman, C., Mayerl, C., Wimpissinger, T., Feichtinger, J., Zelger, B., et al. (2013) The Immunology of Fibrosis. *Annu Rev.* **31** (1):107–35.

83. Williams, A. S., Kang, L. and Wasserman, D. H. (2015) The extracellular matrix and insulin resistance. *Trends Endocrinol Metab* **26** (7):357–66.

84. Watts, R., Mcainch, A. J., Dixon, J. B., Brien, P. E. O. and Cameron-smith, D. (2013) Increased Smad Signaling and Reduced MRF Expression in Skeletal Muscle from Obese Subjects. *Obesity* **21** (3):525–9.

85. Richardson, D. K., Kashyap, S., Bajaj, M., Cusi, K., Mandarino, S. J., Finlayson, J., et al. (2005) Lipid Infusion Decreases the Expression of Nuclear Encoded Mitochondrial Genes and Increases the Expression of Extracellular. *J Biol Chem*. **280** (11):10290–7.

86. Kang, L., Ayala, J. E., Lee-Young, R. S., Zhang, Z., James, F. D., Neufer, P. D., et al. (2011) Diet-induced muscle insulin resistance is associated with extracellular matrix remodeling and interaction with integrin alpha2beta1 in mice. *Diabetes* **60** (2):416–26.

87. Jansson, P. (2007) Endothelial dysfunction in insulin resistance and type 2 diabetes. *J Intern Med.* **262** (2):173–83.

88. Kang, L., Mayes, W. H., James, F. D., Bracy, D. P. and Wasserman, D. H. (2014) Matrix metalloproteinase 9 opposes diet-induced muscle insulin resistance in mice. *Diabetologia* **57** (3):603–13.

89. Williams, A. S., Trefts, E., Lantier, L., Grueter, C. A., Bracy, D. P., James, F. D., et al. (2017) Integrin-Linked Kinase Is Necessary for the Development of Diet-Induced Hepatic Insulin Resistance. *Diabetes* **66** (2):325–34.

90. Zong, H., Bastie, C. C., Xu, J., Fassler, R., Campbell, K. P., Kurland, I. J., et al. (2009) Insulin Resistance in Striated Muscle-specific Integrin Receptor beta1-deficient Mice. *J Biol Chem.* **284** (7):4679–88.

91. Bisht, B., Srinivasan, K. and Dey, C. S. (2008) In vivo inhibition of focal adhesion kinase causes insulin resistance. *J Physiol.* **586** (16):3825–37.

92. Kelley, D. E., He, J., Menshikova, E. V. and Ritov VB. (2002) Dysfunction of mitochondria in human skeletal muscle in type 2 diabetes. *Diabetes* **51** (10):2944–50.

93. Nakamura, S., Takamura, T., Matsuzawa-Nagata, N., Takayama, H., Misu, H., Noda, H., et al. (2009) Palmitate induces insulin resistance in H4IIEC3 hepatocytes through reactive oxygen species produced by mitochondria. *J Biol Chem.* **284** (22):14809–18.

94. Patti, E. M., Butte, A. J., Crunkhorn, S., Cusi, K., Kashyap, S., Miyazaki, Y., et al. (2003) Coordinated reduction of genes of oxidative metabolism in humans with insulin resistance and diabetes : Potential role of PGC1 and NRF1. *Proc Natl Acad Sci U S A.* **100** (14):8466–71.

95. Mootha, V. K., Lindgren, C. M., Eriksson, K., Subramanian, A., Sihag, S., Lehar, J., et al. (2003) PGC-1 α -responsive genes involved in oxidative phosphorylation are coordinately downregulated in human diabetes. *Nat Genet.* **34** (3):267–74.

96. Hwang, H., Bowen, B. P., Lefort, N., Flynn, C. R., Filippis, E. A. De Roberts, C., et al. (2010) Proteomics Analysis of Human Skeletal Muscle Reveals Novel Abnormalities in Obesity and Type 2 Diabetes. *Diabetes* **59** (1):33–42.

97. Peterson, F. K., Befroy, D., Dufour, S., Dziura, J., Rothman, D. L., Dipietro, L., et al. (2003) Mitochondrial dysfunction in the elderly: possible role in insulin resistance. *Science* **300** (5622):1140–2.

98. Petersen, K. F., Dufour, S., Befroy, D., Garcia, R and Shulman, G. I. (2004) Impaired Mitochondrial Activity in the Insulin-Resistant Offspring of Patients with Type 2 Diabetes. *N Engl J Med.* **350** (7):664–72.

99. Morino, K., Petersen, K. F., Dufour, S., Befroy, D., Frattini, J., Pypaert, M., et al. (2005) Reduced mitochondrial density and increased IRS-1 serine phosphorylation in muscle of insulin-resistant offspring of type 2 diabetic parents *J Clin Invest*. **115** (12):3587–93.

100. Phielix, E., Schrauwen-hinderling, V. B., Mensink, M., Lenaers, E., Meex, R., Hoeks, J., et al. (2008) Lower Intrinsic ADP-Stimulated Mitochondrial Respiration Underlies In Vivo Mitochondrial Dysfunction in Muscle of Male Type 2 Diabetic Patients. *Diabetes* **57** (11):2943–9.

101. Boushel, R., Gnaiger, E., Schjerling, P., Skovbro, M., Kraunsoe, R. and Dela, F. (2007) Patients with type 2 diabetes have normal mitochondrial function in skeletal muscle. *Diabetologia* **50** (4):790–6.

102. Ara, I., Larsen, S., Stallknecht, B., Guerra, B., Morales-Alamo, D., Andersen, J. L., et al. (2011) Normal mitochondrial function and increased fat oxidation capacity in leg and arm muscles in obese humans. *Int J Obes.* **35** (1):99–108.

103. Wredenberg, A., Freyer, C., Sandström, M. E., Katz, A., Wibom, R., Westerblad, H., et al. (2006) Respiratory chain dysfunction in skeletal muscle does not cause insulin resistance. *Biochem Biophys Res Commun.* **350** (1):202–7.

104. Pospisilik, J. A., Knauf, C., Joza, N., Benit, P., Orthofer, M., Cani, P. D., et al. (2007) Targeted Deletion of AIF Decreases Mitochondrial Oxidative Phosphorylation and Protects from Obesity and Diabetes. *Cell*. **131** (3):476–91.

105. Chanseaume, E., Tardy, A. L., Salles, J., Giraudet, C., Rousset, P., Tissandier, A., et al. (2007) Chronological Approach of Diet-induced Alterations in Muscle Mitochondrial Functions in Rats. *Obesity* **15** (1):50–9.

106. Didier, L., Yerby, B., Deacon, R. and Gao, J. (2007) Diet-induced modulation of mitochondrial activity in rat muscle. *Am J Physiol Endocrinol Metab.* **293** (5):E1169-1177.

107. Miotto, P. M., LeBlanc, P. J. and Holloway, G. P. (2018) High fat diet causes mitochondrial dysfunction as a result of impaired ADP sensitivity. *Diabetes* **67** (11):2199–205.

108. Turner, N., Bruce, C. R., Beale, S. M., Hoehn, K. L., So, T., Rolph, M. S., et al. (2007) Excess lipid availability increases mitochondrial fatty acid oxidative capacity in muscle: evidence against a role for reduced fatty acid oxidation in lipid-induced insulin resistance in rodents. *Diabetes* **56** (8):2085–92.

109. Hancock, C. R., Han, D., Chen, M., Terada, S., Yasuda, T., Wright, C., et al. (2008) High-fat diets cause insulin resistance despite an increase in muscle mitochondria. *Proc Natl Acad Sci.* **105** (22):7815–20.

110. Bonnard, C., Durand, A., Peyrol, S., Chanseaume, E., Chauvin, M. A., Morio, B., et al. (2008) Mitochondrial dysfunction results from oxidative stress in the skeletal muscle of diet- induced insulin-resistant mice. *J Clin Invest.* **118** (2):789–800.

111. Anderson, E. J., Lustig, M. E., Boyle, K. E., Woodlief, T. L., Kane, D. A., Lin, C. T., et al. (2009) Mitochondrial H2O2 emission and cellular redox state link excess fat intake to insulin resistance in both rodents and humans. *J Clin Invest*.**119** (3):573–81.

112. Mishra, P. and Chan, D. C. (2016) Metabolic regulation of mitochondrial dynamics. *J Cell Biol.* **212** (4):379–87.

113. Fealy, C. E., Mulya, A., Axelrod, C. L. and Kirwan, J. P. (2018) Mitochondrial dynamics in skeletal muscle insulin resistance and type 2 diabetes. *Transl Res.* **202** (12):69–82.

114. Bach, D., Pich, S., Soriano, F. X., Vega, N., Baumgartner, B., Oiola, J., et al. (2003) Mitofusin-2 Determines Mitochondrial Network Architecture and Mitochondrial Metabolism. *J Biol Chem.* **278** (19):17190–7.

115. Liu, R., Jin, P., Wang, Y., Han, L., Shi, T. and Li, X. (2014) Impaired Mitochondrial Dynamics and Bioenergetics in Diabetic Skeletal Muscle. *PLoS One* **9** (3):e92810.

116. Sebastián, D., Hernández-alvarez, M. I., Segalés, J., Sorianello, E., Muñoz, J. P., Sala, D., et al. (2013) Mitofusin 2 link mitochondrial and endoplasmic reticulum function with insulin signaling and is essential for normal glucose homeostasis. *Proc Natl Acad Sci.* **109** (14):5523–8.

117. Pereira, R. O., Tadinada, S. M., Zasadny, F. M., Oliveira, K. J., Maria, K., Pires, P., et al. (2017) OPA 1 deficiency promotes secretion of FGF 21 from muscle that prevents obesity and insulin resistance. *EMBO J.* **36** (14):2126–45.

118. Tahara, E. B., Navarete, F. D. T., Kowaltowski, A. J. (2009) Tissue- , substrate- , and site-specific characteristics of mitochondrial reactive oxygen species generation. *Free Radic Biol Med* **46** (9):1283–97.

119. Tangvarasittichai, S. (2015) Oxidative stress , insulin resistance , dyslipidemia and type 2 diabetes mellitus. *World J Diabetes* **6** (3):456–80.

120. Seifert, E. L., Estey, C., Xuan, J. Y. and Harper, M. (2010) Electron Transport Chain-dependent and -independent Mechanisms of Mitochondrial H2O2 Emission during Long-chain Fatty Acid Oxidation. *J Biol Chem*. **285** (8):5748–58.

121. Houstis, N., Rosen, E. D. and Lander, E. S. (2006) Reactive oxygen species have a causal role in multiple forms of insulin resistance. *Nature* **440** (4):944–9.

122. Maddux, B. A., See, W., Lawrence Jr., J. C., Goldfine, A. L., Goldfine, I. D. and Evans, J. L. (2001) Protection against oxidative stress-induced insulin resistance in rat L6 muscle cells by micromolar concentrations of alpha-lipoic acid. *Diabetes* **50** (2):404–10.

123. Yeop, H. C., Kargi, A. Y., Omer, M., Chan, C. K., Wabitsch, M., O'Brien, K. D., et al. (2010) Differential effect of saturated and unsaturated free fatty acids on the generation of monocyte adhesion and chemotactic factors by adipocytes: dissociation of adipocyte hypertrophy from inflammation. *Diabetes* **59** (2):386–96.

124. Loh, K., Deng, H., Fukushima, A., Cai, X., Boivin, B., Galic, S., et al. (2009) Reactive Oxygen Species Enhance Insulin Sensitivity. *Cell Metab* **10** (4):260–72.

125. Bellentani, S., Scaglioni, F., Marino, M., Bedogni, G. (2010) Epidemiology of Non-Alcoholic Fatty Liver Disease. *Dig Dis.* **28** (1):155–61.

126. Korenblat, K. M., Fabbrini, E., Mohammed, B. S., Klein, S. (2008) Liver, Muscle, and Adipose Tissue Insulin Action Is Directly Related to Intrahepatic Triglyceride Content in Obese Subjects. *Gastroenterology* **134** (5):1369–75.

127. Marchesini, G., Brizi, M., Morselli-Labate, A. M., Bianchi, G., Bugianesi, E., McCullough, A. J., et al. (1999) Association of nonalcoholic fatty liver disease with insulin resistance. *Am J Med* **107** (5):450–5.

128. Muoio, D. M. and Neufer, P. D. (2012) Lipid-induced mitochondrial stress and insulin action in muscle. *Cell Metab* **15** (5):595–605.

129. Perry, R. J., Zhang, D., Zhang, X. M., Boyer, J. L. and Shulman GI. (2015) Controlled-release mitochondrial protonophore reverses diabetes and protonophore reverses diabetes and steatohepatitis in rats. *Science* **347** (6227):1253–6.

130. Lithell, H., Orlander, J., Schéle, R., Sjödin, B. and Karlsson J. (1979) Changes in lipoprotein-lipase activity and lipid stores in human skeletal muscle with prolonged heavy exercise. *Acta Physiol Scand.* **107** (3):257–61.

131. Goodpaster, B. H., He, J., Watkins, S. and Kelley, D. E. (2001) Skeletal muscle lipid content and insulin resistance: Evidence for a paradox in endurance-trained athletes. *J Clin Endocrinol Metab.* **86** (12):5755–61.

132. Camporez, J. P. G., Kanda, S., Petersen, M. C., Jornayvaz, F. R., Samuel, V. T., Bhanot, S., et al. (2015) ApoA5 knockdown improves whole-body insulin sensitivity in high-fat-fed mice by reducing ectopic lipid content. *J Lipid Res*. **56**(3):526–36.

133. Luukkonen, P. K., Zhou, Y., Sädevirta, S., Leivonen, M., Arola, J., Hyötyläinen, T., et al. (2016) Hepatic ceramides dissociate steatosis and insulin resistance in patients with non-alcoholic fatty liver disease. *J Hepatol.* **64** (5):1167–75.

134. Geraldes, P. and King, G. L. (2010) Activation of protein kinase C isoforms and its impact on diabetic complications. *Circ Res.* **106** (8):1319–31.

135. Samuel, V. T., Liu, Z. X., Wang, A., Beddow, S. A., Geisler, J. G., Kahn, M., et al. (2007) Inhibition of protein kinase Ce prevents hepatic insulin resistance in nonalcoholic fatty liver disease. *J Clin Invest*. **117** (3):739–45.

136. Petersen, M. C., Madiraju, A. K., Gassaway, B. M., Marcel, M., Nasiri, A. R., Butrico, G., et al. (2016) Insulin receptor Thr 1160 phosphorylation mediates lipid-induced hepatic insulin resistance *J Clin Invest.* **126** (11):4361–71.

137. Szendroedi, J., Yoshimura, T., Phielix, E., Koliaki, C., Marcucci, M., Zhang, D., et al. (2014) Role of diacylglycerol activation of PKCθ in lipid-induced muscle insulin resistance in humans. *Proc Natl Acad Sci.* **111** (26):9597–602.

138. Schmitz-Peiffer, C., Browne, C. L., Oakes, N. D., Watkinson, A., Chisholm, D. J., Kraegen, E. W., et al. (1997) Alterations in the expression and cellular localization of protein kinase C isozymes epsilon and theta are associated with insulin resistance in skeletal muscle of the high-fat-fed rat. *Diabetes* **46** (2):169–78.

139. Li, Y., Soos, T. J., Li, X., Wu, J., Degennaro, M., Sun, X., et al. (2004) Protein Kinase C theta Inhibits Insulin Signaling by Phosphorylating IRS1 at S1101. *J Biol Chem.* **1** (25):45304–7.

140. Kurek, K. M., Bart, B. A., Chabowski, A., Górski, J. and Ma, B. (2015) Inhibition of Ceramide De Novo Synthesis Ameliorates Diet Induced Skeletal Muscles Insulin Resistance. *J Diabetes Res.* **15** (2015):154762.

141. Holland, W. L., Bikman, B. T., Wang, L. P., Yuguang, G., Sargent, K. M., Bulchand, S., et al. (2011) Lipid-induced insulin resistance mediated by the proinflammatory receptor TLR4 requires saturated fatty acid – induced ceramide biosynthesis in mice. *J Clin Invest*. **121** (5):1858–70.

142. Holland, W. L., Brozinick, J. T., Wang, L., Hawkins, E. D., Sargent, K. M., Liu, Y., et al. (2007) Inhibition of ceramide synthesis ameliorates glucocorticoid-, saturated-fat-, and obesity-induced insulin resistance. *Cell Metab.* **5** (3):167–79.

143. Adams, J. M., Pratipanawatr, T., Berria, R., Wang, E., Defronzo, R. A., Sullards, M. C., et al. (2004) Ceramide Content Is Increased in Skeletal Muscle From Obese Insulin-Resistant Humans. *Diabetes* **53** (1):25–31.

144. Błachnio-Zabielska, A. U., Baranowski, M., Hirnle, T., Zabielski, P., Lewczuk, A., Dmitruk, I., et al. (2012) Increased Bioactive Lipids Content in Human Subcutaneous and Epicardial Fat Tissue Correlates with Insulin Resistance. *Lipids* **47** (12):1131–41.

145. Chung, J. O., Koutsari, C., Blachnio-zabielska, A. U., Hames, K. C. and Jensen MD. (2017) Intramyocellular Ceramides : Subcellular Concentrations and Fractional De Novo Synthesis in Postabsorptive Humans. *Diabetes* **66** (8):2082–91.

146. Powell, D. J., Hajduch, E., Kular, G. and Hundal, H. S. (2003) Ceramide Disables 3-Phosphoinositide Binding to the Pleckstrin Homology Domain of Protein Kinase B (PKB)/Akt by a PKCz -Dependent Mechanism. *Mol Cell Biol.* **23** (21):7794–808.

147. Stratford, S., Hoehn, K. L., Liu, F. and Summers, S. A. (2004) Regulation of Insulin Action by Ceramide. *J Biol Chem.* **279** (35):36608–15.

148. Le Balle, F., Simon, M-F., Meijer, S., Fourcade, O. and Chap, H. (1999) Membrane Sidedness of Biosynthetic Pathways Involved in the Production of Lysophosphatidic Acid. *Advan Enzym Regul.* **39** (98):275–84.

149. Aoki, J., Taira, A., Takanezawa, Y., Kishi, Y., Hama, K., Kishimoto, T., et al. (2002) Serum Lysophosphatidic Acid Is Produced through Diverse Phospholipase Pathways. *J Biol Chem.* **277** (50):48737–44.

150. Ferry, G., Tellier, E., Try, A., Grés, S., Naime, I., Simon, M. F., et al. (2003) Autotaxin is released from adipocytes, catalyzes lysophosphatidic acid synthesis, and activates preadipocyte proliferation. Up-regulated expression with adipocyte differentiation and obesity. *J Biol Chem*. **278** (20):18162–9.

151. Van Meeteren, L. A., Ruurs, P., Stortelers, C., Bouwman, P., Rooijen, M.A., Pradères, J. P., et al. (2006) Autotaxin , a Secreted Lysophospholipase D , Is Essential for Blood Vessel Formation during Development. *Mol Cell Biol.* **26** (13):5015–22.

152. Pamuklar, Z., Federico, L., Liu, S., Umezu-Goto, M., Dong, A., Panchatcharam, M., et al. (2009) Autotaxin/Lysopholipase D and lysophosphatidic acid regulate murine hemostasis and thrombosis. *J Biol Chem*. **284** (11):7385–94.

153. Rancoule, C., Dusaulcy, R., Tréguer, K., Grès, S., Guigné, C., Quilliot, D., et al. (2012) Depot-specific regulation of autotaxin with obesity in human adipose tissue. J *Physiol Biochem.* **68** (4):635–44.

154. Fotopoulou, S., Oikonomou, N., Grigorieva, E., Nikitopoulou, I., Paparountas, T., Thanassopoulou, A., et al. (2010) ATX expression and LPA signalling are vital for the development of the nervous system. *Dev Biol.***339** (2):451–64.

155. Katsifa, A., Kaffe, E., Nikolaidou-Katsaridou, N., Economides, A. N., Newbigging, S., McKerlie, C., et al. (2015) The bulk of autotaxin activity is dispensable for adult mouse life. *PLoS One.***10**(11):e0143083.

156. Gierse, J., Thorarensen, A., Beltey, K., Bradshaw-pierce, E., Cortes-burgos, L., Hall, T., et al. (2010) A novel autotaxin inhibitor reduces lysophosphatidic acid levels in plasma and the site of inflammation. *J Pharmacol Exp Ther.* **2** (1):310–7.

157. Yukiura, H., Kano, K., Kise, R., Inoue, A. and Aoki, J. (2015) Autotaxin Overexpression Causes Embryonic Lethality and Vascular Defects. *PLoS One* **10** (5):e0126734.

158. Tang, X., Benesch, M. G. K., Dewald, J., Zhao, Y. Y., Patwardhan, N., Santos, W. L., et al. (2015) Lipid phosphate phosphatase-1 expression in cancer cells attenuates tumor growth and metastasis in mice. *J Lipid Res.* **55** (11):2389–400.

159. Jasinska, R., Zhang, Q., Pilquil, C., Singh, I., Xu, J., Dewald, J., et al. (1999) Lipid phosphate phosphohydrolase-1 degrades exogenous glycerolipid and sphingolipid phosphate esters. *Biochem J.* **340** (3):677–86.

160. Sigal, Y. J., Dermott, M. I. M. C. and Morris, A. J. (2005) Integral membrane lipid phosphatases / phosphotransferases : common structure and diverse functions. *Biochem J.* **387** (2):281–93.

161. Tomsig, J. L., Snyder, A. H., Berdyshev, E. V., Skobeleva, A., Natarajan, V. and Brindley, D. N, (2010) Lipid phosphate phosphohydrolase type 1 (LPP1) degrades extracellular lysophosphatidic acid in vivo. *Biochem J.* **419** (3):611–8.

162. Escalante-alcalde, D., Hernandez, L., Stunff, H., Le, Maeda, R., Lee, H., Sciorra, V. A., et al. (2003) The lipid phosphatase LPP3 regulates extra-embryonic vasculogenesis and axis patterning. *Development.* **130** (19):4623–37.

163. Zhang, N., Sundberg, J. P. and Gridley, T. (2000) Mice Mutant for Ppap2c , a Homolog of the Germ Cell Migration Regulator Wunen Are Viable and Fertile. *Genesis* **27** (4):137–40.

164. Morris, K. E., Schang, L. M. and Brindley, D. N. (2006) Lipid Phosphate Phosphatase-2 Activity Regulates S-phase Entry of the Cell Cycle in Rat2 Fibroblasts. *J Biol Chem*. **281** (14):9297–306.

165. Brindley, D. N. and Pilquil, C. (2009) Lipid phosphate phosphatases and signaling. *J Lipid Res.* **50** (4):S225-230.

166. Salous, A. K., Panchatcharam, M., Sunkara, M., Mueller, P., Dong, A., Wang, Y., et al. (2013) Mechanism of rapid elimination of lysophosphatidic acid and related lipids from the circulation of mice. *J Lipid Res.***54** (10):2775–84.

167. Yung, Y. C., Stoddard, N. C. and Chun, J. (2014) LPA receptor signaling: pharmacology, physiology, and pathophysiology. *J Lipid Res* **55** (7):1192–214.

168. Boucharaba, A., Serre, C. M., Grès, S., Saulnier-Blache, J. S., Bordet, J. C., Guglielmi, J., et al. (2004) Platelet-derived lysophosphatidic acid supports the progression of osteolytic bone metastases in breast cancer. *J Clin Invest.* **114** (12):1714–25.

169. Zhou, Z., Subramanian, P., Sevilmis, G., Globke, B., Soehnlein, O., Karshovska, E., et al. (2011) Lipoprotein-derived lysophosphatidic acid promotes atherosclerosis by releasing CXCL1 from the endothelium. *Cell Metab*. **13** (5):592–600.

170. Bouchareb, R., Mahmut, A., Nsaibia, M. J., Boulanger, M. C., Dahou, A., Lépine, J. L., et al. (2015) Autotaxin derived from lipoprotein(a) and valve interstitial cells promotes inflammation and mineralization of the aortic valve. *Circulation* **132** (8):677–90.

171. Mahmut, A., Boulanger, M. C., El Husseini, D., Fournier, D., Bouchareb, R., Després, J. P., et al. (2014) Elevated Expression of Lipoprotein-Associated Phospholipase A2 in Calcific Aortic Valve Disease Implications for Valve Mineralization. *J Am Coll Cardiol.* **63** (5):460–9.

172. Jethwa, S. A., Leah, E. J., Zhang, Q., Bright, N. A., Oxley, D., Bootman, M. D., et al. (2016) Exosomes bind to autotaxin and act as a physiological delivery mechanism to stimulate LPA receptor signalling in cells. *J Cell Sci.* **129** (20):3948–57.

173. Kaffe, E., Katsifa, A., Xylourgidis, N., Ninou, I., Harokopos, V., Foka, P., et al. (2017) Hepatocyte Autotaxin expression promotes liver fibrosis and cancer. *Heptatology* **65** (4):1369–83.

174. Navab, M., Chattopadhyay, A., Hough, G., Meriwether, D., Fogelman, S. I., Wagner, A. C., et al. (2015) Source and role of intestinally derived lysophosphatidic acid in dyslipidemia and atherosclerosis. *J Lipid Res.* **56** (4):871–87.

175. Smyth, S. S., Mueller, P., Yang, F., Brandon, J. A. and Morris, A. J. (2014) Arguing the Case for the Autotaxin – Lysophosphatidic Acid – Lipid Phosphate Phosphatase 3-Signaling Nexus in the Development and Complications of Atherosclerosis. *Arterioscler Thromb Vasc Biol.* **34** (3):479–86.

176. D'Souza, K. D., Kane, D. A., Touaibia, M., Kershaw, E. E., Pulinilkunnil, T. and Kienesberger, P. C. (2017) Autotaxin Is Regulated by Glucose and Insulin in Adipocytes. *Endocrinology* **158** (1):791–803.

177. Ino, M., Shimizu, Y., Tanaka, T. and Tokumura, A. (2012) Alterations of Plasma Levels of Lysophosphatidic Acid in Response to Fasting of Rats. *Biol Pharm Bull.* **35** (11):2059–63.

178. Dusaulcy, R., Rancoule, C., Grès, S., Wanecq, E., Colom, A., Guigné, C., et al. (2011) Adipose-specific disruption of autotaxin enhances nutritional fattening and reduces plasma lysophosphatidic acid. *J Lipid Res.* **52** (6):1247–55.

179. Rancoule, C., Dusaulcy, R., Tréguer, K., Grès, S., Attané, C. and Saulnier-Blache, J. S. (2014) Involvement of autotaxin/lysophosphatidic acid signaling in obesity and impaired glucose homeostasis. *Biochimie* **96** (1):140–3.

180. Sun, S., Wang, R., Song, J., Guan, M., Li, N. and Zhang, X. (2017) Blocking gp130 signaling suppresses autotaxin expression in adipocytes and improves insulin sensitivity in diet-induced obesity. *J Lipid Res.* **58** (11):2102–13.

181. Navab, M., Hough, G., Buga, G. M., Su, F., Wagner, A. C., Meriwether, D., et al. (2013) Transgenic 6F tomatoes act on the small intestine to prevent systemic infl ammation and dyslipidemia caused by Western diet and intestinally derived lysophosphatidic acid. *J Lipid Res.* **54** (12):3403–18.

182. Michalczyk, A., Budkowska, M., Do, B., Chlubek, D. and Safranow, K. (2017) Lysophosphatidic acid plasma concentrations in healthy subjects : circadian rhythm and associations with demographic , anthropometric and biochemical parameters. *Lipids Health Dis.* **16** (1):140–9.

183. Nakane, S., Tokumura, A., Waku, K. and Sugiura, T. (2011) Hen Egg Yolk and White Contain High Amounts of Lysophosphatidic Acids , Growth Factor-Like Lipids: Distinct Molecular Species Compositions. *Lipids.* **36** (4):413–20.

184. Tanaka, T., Horiuchi, G., Matsuoka, M., Hirano, K., Koike, T. and Satouchi, K. (2009) Formation of Lysophosphatidic Acid , a Wound- Healing Lipid , during Digestion of Cabbage Leaves. *Biosci Biotechnol Biochem.* **73** (6):1293–300.

185. Lee, B., Choi, S., Kim, H., Jung, S., Kim, H. and Nah S. (2016) Plant Lysophosphatidic Acids: A Rich Source for Bioactive Lysophosphatidic Acids and Their Pharmacological Applications. *Biol Pharm Bull.* **39** (2):156–62.

186. Inoue, M., Adachi, M., Shimizu, Y., Tsutsumi, T. and Tokumura, A. (2011) Comparison of Lysophospholipid Levels in Rat Feces with Those in a Standard Chow. *J Agric Food Chem.* **59** (13):7062–7.

187. Chattopadhyay, A., Navab, M., Hough, G., Grijalva, V., Mukherjee, P., Fogelman, H. R., et al. (2016) Tg6F ameliorates the increase in oxidized phospholipids in the jejunum of mice fed unsaturated LysoPC or WD. *J Lipid Res*. **57** (5):832–47.

188. Brown, A., Hossain, I., Perez, L. J., Nzirorera, C., Tozer, K., D'Souza, K., et al. (2017) Lysophosphatidic acid receptor mRNA levels in heart and white adipose tissue are associated with obesity in mice and humans. *PLoS One* **12** (12):e0189402.

189. Jean-Baptiste, G., Yang, Z., Khoury, C. and Greenwood, M. T. (2005) Lysophosphatidic acid mediates pleiotropic responses in skeletal muscle cells. *Biochem Biophys Res Commun.* **335** (4):1155–62.

190. Nikitopoulou, I., Oikonomou, N., Karouzakis, E., Sevastou, I., Nikolaidou-Katsaridou, N., Zhao, Z., et al. (2012) Autotaxin expression from synovial fibroblasts is essential for the pathogenesis of modeled arthritis. *J Exp Med* **209** (5):925–33.

191. Rancoule, C., Attane, C., Gres, S., Fournel, A., Dusaulcy, R., Bertrand, C., et al. (2013) Lysophosphatidic acid impairs glucose homeostasis and inhibits insulin secretion in high-fat diet obese mice. *Diabetologia.* **56** (6):1394–402.

192. Stoddard, N. C. and Chun, J. (2015) Promising Pharmacological Directions in the World of Lysophosphatidic Acid Signaling. *Biomol Ther (Seoul)* **23** (1):1–11.

193. Tanaka, M., Okudaira, S., Kishi, Y., Ohkawa, R., Iseki, S., Ota, M., et al. (2006) Autotaxin stabilizes blood vessels and is required for embryonic vasculature by producing lysophosphatidic acid. *J Biol Chem.* **281** (35):25822–30.

194. Massé, K., Bhamra, S., Allsop, G., Dale, N. and Jones, E. A. (201) Ectophosphodiesterase/nucleotide phosphohydrolase (Enpp) nucleotidases: cloning, conservation and developmental restriction. *Int J Dev Biol.* **193** (7):181–93.

195. Nishimasu, H., Okudaira, S., Hama, K., Mihara, E., Dohmae, N., Inoue, A., et al. (2011) Crystal structure of autotaxin and insight into GPCR activation by lipid mediators. *Nat Struct Mol Biol.* **18** (2):205–12.

196. Hausmann, J., Kamtekar, S., Christodoulou, E., Day, J. E., Wu, T., Fulkerson, Z., et al. (2011) Structural basis of substrate discrimination and integrin binding by autotaxin. *Nat Struct Mol Biol* **18** (2):198–204.

197. Koh, E., Clair, T., Woodhouse, E. C., Schiffmann, E., Liotte, L. and Stracke, M. (2003) Site-directed mutations in the tumor-associated cytokine, autotaxin, eliminate nucleotide phosphodiesterase, lysophospholipase D, and motogenic activities. *Cancer Res.* **63** (9):2042–5.

198. Salgado-Polo, F., Fish, A., Matsoukas, M. T., Heidebrecht, T., Keune, W. J. and Perrakis, A. (2018) Lysophosphatidic acid produced by autotaxin acts as an allosteric modulator of its catalytic efficiency. *J Biol Chem.* **293** (37):14312–27.

199. Giganti, A., Rodriguez, M., Fould, B., Moulharat, N., Coge, F., Chomarat, P., et al. (2008) Murine and human autotaxin alpha, beta, and gamma isoforms: Gene organization, tissue distribution, and biochemical characterization. *J Biol Chem*. **283** (12):7776–89.

200. Houben, A. J. S., Van Wijk, X. M. R., Van Meeteren, L. A., Van Zeijl, L., Van De Westerlo, E. M. A., Hausmann, J., et al. (2013) The polybasic insertion in autotaxin alpha confers specific binding to heparin and cell surface heparan sulfate proteoglycans. *J Biol Chem.* **288** (1):510–9.

201. Fox, M. A., Colello, R. J., Macklin, W. B. and Fuss, B. (2003) Phosphodiesterase-Ialpha/ autotaxin: a counteradhesive protein expressed by oligodendrocytes during onset of myelination. *Mol Cell Neurosci.* **23** (3):507–19.

202. Jansen, S., Stefan, C., Creemers, J. W., Waelkens, E., Van Eynde, A., Stalmans, W., et al. (2005) Proteolytic maturation and activation of autotaxin (NPP2), a secreted metastasis-enhancing lysophospholipase D. *J Cell Sci* **118** (Pt 14):3081–9.

203. Jansen, S., Callewaert, N., Dewerte, I., Andries, M., Ceulemans, H. and Bollen, M. (2007) An essential oligomannosidic glycan chain in the catalytic domain of autotaxin, a secreted lysophospholipase-D. *J Biol Chem*. **282** (15):11084–91.

204. Rachakonda, V. P., Reeves, V. L., Aljammal, J., Wills, R. C., Trybula, J. S., Delany, J. P., et al. (2015) Serum autotaxin is independently associated with hepatic steatosis in women with severe obesity. *Obesity* **23** (5):965–72.

205. Reeves, V. L., Trybula, J. S., Wills, R. C., Goodpaster, B. H., Dubé, J. J., Kienesberger, P. C., et al. (2015) Serum Autotaxin/ENPP2 correlates with insulin resistance in older humans with obesity. *Obesity* **23** (12):2371–6.

206. Fayyaz, S., Japtok, L., Schumacher, F., Wigger, D., Schulz, T. J., Haubold, K., et al. (2017) Lysophosphatidic Acid Inhibits Insulin Signaling in Primary Rat Hepatocytes via the LPA 3 Receptor Subtype and is Increased in Obesity. *Cell Physiol Biochem.* **43** (2):445–56.

207. Jo, J., Gavrilova, O., Pack, S., Jou, W., Mullen, S., Sumner, A. E., et al. (2009) Hypertrophy and/or Hyperplasia: Dynamics of Adipose Tissue Growth. *PLoS One* **5** (3):e1000324.

208. Pages, C., Daviaud, D., An, S., Krief, S., Lafontan, M., Valet, P., et al. (2001) Endothelial Differentiation Gene-2 Receptor Is Involved in Lysophosphatidic Acid-dependent Control of 3T3F442A Preadipocyte Proliferation and Spreading. *J Biol Chem.* **276** (15):11599–605.

209. Fukushima, N., Ishii, S., Tsujiuchi, T., Kagawa, N. and Katoh, K. (2015) Comparative analyses of lysophosphatidic acid receptor-mediated signaling. *Cell Mol Life Sci* **72** (12):2377–94.

210. Radhika, V., Ha, J. H., Jayaraman, M., Tsim, S. and Dhanasekaran, N. Mitogenic signaling by lysophosphatidic acid (LPA) involves Ga12. *Onogene* **24** (28):4597–603.

211. Holmström, T. E., Mattsson, C. L., Wang, Y., Iakovleva, I., Petrovic, N. and Nedergaard, J. (2010) Non-transactivational , dual pathways for LPA-induced Erk1/2 activation in primary cultures of brown pre-adipocytes. *Exp Cell Res* **316** (16):2664–75.

212. Federico, L., Ren, H., Mueller, P. A., Wu, T., Liu, S., Popovic, J., et al. (2012) Autotaxin and its product lysophosphatidic acid suppress brown adipose differentiation and promote diet-induced obesity in mice. *Mol Endocrinol* **26** (5):786–97.

213. Nobusue, H., Kondo, D., Yamamoto, M., Kano, K. (2010) Effects of lysophosphatidic acid on the in vitro proliferation and differentiation of a novel porcine preadipocyte cell line. *Comp Biochem Physiol Part B* **157** (4):401–7.

214. Simon, M. F., Daviaud, D., Pradère, J. P., Grès, S., Guigné, C., Wabitsch, M., et al. (2005) Lysophosphatidic acid inhibits adipocyte differentiation via lysophosphatidic acid 1 receptor-dependent down-regulation of peroxisome proliferator-activated receptor gamma2. *J Biol Chem* **280** (15):14656–62.

215. Yea, K., Kim, J. and Lim, S. (2008) Lysophosphatidic acid regulates blood glucose by stimulating myotube and adipocyte glucose uptake. *J Mol Med.* **86** (2):211–20.

216. Boucher, J., Quilliot, D., Pradères, J. P., Simon, M. F., Grès, S., Guigné, C., et al. (2005) Potential involvement of adipocyte insulin resistance in obesity-associated up-regulation of adipocyte lysophospholipase D/autotaxin expression. *Diabetologia* **48** (3):569–77.

217. Farquhar, M. J., Humphreys, I. S., Rudge, S. A., Wilson, G. K., Bhattacharya, B., Ciaccia, M., et al. (2017) Autotaxin-lysophosphatidic acid receptor signalling regulates hepatitis C virus replication. *J Hepatol.* **66** (11):919–29.

218. Brandon, J. A., Kraemer, M., Vandra, J., Halder, S., Ubele, M., Morris, A. J., et al. (2019) Adipose-derived autotaxin regulates inflammation and steatosis associated with diet-induced obesity. *PLoS One* **14** (2):e0208099.

219. Weng, J., Jiang, S., Ding, L., Xu, Y., Zhu, X. and Jin, P. (2019) Autotaxin/lysophosphatidic acid signaling mediates obesity-related cardiomyopathy in mice and human subjects. *J Cell Mol Med.* **23** (2):1050–8.

220. Oikonomou, N., Mouratis, M., Tzouvelekis, A., Kaffe, E., Valavanis, C., Vilaras, G., et al. (2012) Pulmonary Autotaxin Expression Contributes to the Pathogenesis of Pulmonary Fibrosis. *Am J Respir Cell Mol Biol.* **47** (3):566–74.

221. Pradère, J. P., Klein, J., Grès, S., Guigné, C., Neau, E., Valet, P., et al. (2007) LPA 1 Receptor Activation Promotes Renal Interstitial Fibrosis. *J Am Soc Nephrol.* **18** (12):3110–8.

222. Rancoule, C., Viaud, M., Gres, S., Viguerie, N., Decaunes, P., Bouloumié, A., et al. (2014) Pro-fibrotic activity of lysophosphatidic acid in adipose tissue: In vivo and in vitro evidence. *Biochim Biophys Acta - Mol Cell Biol Lipids* **1841**(1):88–96.

223. Rosen, E. D. and Spiegelman, B. M. (2001) PPARgamma: a Nuclear Regulator of Metabolism, Differentiation, and Cell Growth. *J Biol Chem.* **276** (41):37731–5.

224. Barroso, I., Gurnell, M,. Crowley, V. E., Agostini, M., Schwabe, J. W., Soos, M. A., et al. (1999) Dominant negative mutations in human PPAR g associated with severe insulin resistance , diabetes mellitus and hypertension. *Nature* **402** (11):880–3.

225. Leonardini, A., Laviola, L., Perrini, S., Natalicchio, A. and Giorgino, F. (2009) Cross-Talk between PPARγ and Insulin Signaling and Modulation of Insulin Sensitivity. *PPAR Res.* ***2*009** (1):818945.

226. Miles, P. D., Romeo, O. M., Higo, K., Cohen, A., Rafaat, K. and Olefsky, J. M. (1997) TNF-alpha-induced insulin resistance in vivo and its prevention by troglitazone. *Diabetes* **46** (11):1678–83.

227. Souza, S. C., Yamamoto, M. T., Franciosa, M. D., Lien, P. and Greenberg, A. S. (1998) BRL 49653 blocks the lipolytic actions of tumor necrosis factor-alpha: a potential new insulin-sensitizing mechanism for thiazolidinediones. *Diabetes* **47** (4):691–5.

228. Hotta, K., Funahashi, T., Arita, Y., Takahashi, M., Matsuda, M., Okamoto, Y., et al. (2000) Plasma concentrations of a novel, adipose-specific protein, adiponectin, in type 2 diabetic patients. *Arterioscler Thromb Vasc Biol.* **20** (6):1595–9.

229. Fruebis, J., Tsao, T., Javorschi, S., Ebbets-reed, D., Erickson, R. S., Yen, F. T., et al. (2001) Proteolytic cleavage product of 30-kDa adipocyte complement-related protein increases fatty acid oxidation in muscle and causes weight loss in mice. *Proc Natl Acad Sci U S A.***98** (4):2005–10.

230. Berg, A. H., Combs, T. P., Du, X., Brownlee, M. and Scherer, P. E. (2001) The adipocyte-secreted protein Acrp30 enhances hepatic insulin action. *Nat Med.* **7** (8):947–54.

231. Yoneshiro, T., Aita, S., Matsushita, M., Kameya, T. and Nakada, K. (2009) Brown Adipose Tissue , Whole-Body Energy Expenditure, and Thermogenesis in Healthy Adult Men. *Obesity* **19** (1):13–6.

232. Saito, M., Okamatsu-Ogura, Y., Matsushita, M., Watanabe, K., Yoneshiro, T., Nio-Kobayashi, J., et al. (2009) High incidence of metabolically active brown adipose tissue in healthy adult humans: effects of cold exposure and adiposity. *Diabetes* **58** (7):1526–31.

233. Lee, P., Smith, S., Linderman, J., Courville, A. B. and Brychta, R. J. (2014) Temperature-Acclimated Brown Adipose Tissue Modulates Insulin Sensitivity in Humans. *Diabetes* **63** (11):3686–98.

234. Chondronikola, M., Volpi, E., Børsheim, E., Porter, C., Annamalai, P., Enerbäck, S., et al. (2014) Brown Adipose Tissue Improves Whole-Body Glucose Homeostasis and Insulin Sensitivity in Humans. *Diabetes* **63** (12):4089–99.

235. Meng, G., Tang, X., Yang, Z., Zhao, Y., Curtis, J. M., Mcmullen, T. P. W., et al. (2019) Dexamethasone decreases the autotaxin- lysophosphatidate-inflammatory axis in adipose tissue: implications for the metabolic syndrome and breast cancer. *Faseb J* **33** (2):1899–910.

236. Patrick-Denis, S-C., Ferguson, D., Morin, Jr. P, Touaibia, M. (2013) PF-8380 and Closely Related Analogs: Synthesis and Structure–Activity Relationship towards Autotaxin Inhibition and Glioma Cell Viability. *Arch Pharm Chem Life Sci.* **346** (2):91–7.

237. Kershaw, E. E., Hamm, J. K., Verhagen, L. A. W., Peroni, O. D., Katic, M. and Flier, J. S. (2006) Adipose Triglyceride Lipase : Function , Regulation by Insulin , and Comparison With Adiponutrin. *Diabetes* **55** (1):148–57.

238. Lo, K., Labadorf, A., Kennedy, N. J., Han, M., Yap, Y., Matthews, B., et al. (2013) Analysis of In Vitro Insulin-Resistance Models and Their Physiological Relevance to InVivo Diet-Induced Adipose Insulin Resistance. *Cell Rep* **5** (1):259–70.

239. Schweiger, M., Eichmann, T. O., Taschler, U., Zimmermann, R., Zechner, R. and Lass, A. (2014) Measurement of Lipolysis. *Methods Enzymol.* **538** (1):171–93.

240. Ferguson, C. G., Bigman, C. S., Richardson, R. D., Meeteren, L. A., Van Moolenaar, W. H. and Prestwich, G. D. (2008) A Fluorogenic Phospholipid Substrate to Detect Lysophospholipase D/Autotaxin Activity. *Org Lett.* **8** (10):2023–6.

241. Benesch, M. G. K., Zhao, Y. Y, Curtis, J. M., McMullen, T. P. W. and Brindley, D. N. (2015) Regulation of autotaxin expression and secretion by lysophosphatidate and sphingosine 1-phosphate. *J Lipid Res* **56** (6):1134–44.

242. Lin, M. E., Herr, D. R. and Chun, J. (2010) Lysophosphatidic acid (LPA) receptors: Signaling properties and disease relevance. *Prostaglandins Other Lipid Mediat* **91** (3–4):130–8.

243. Pulinilkunnil, T., Kienesberger, P. C., Nagendran, J., Sharma, N., Young, M. E. and Dyck, J. R. B. (2014) Cardiac-specific adipose triglyceride lipase overexpression protects from cardiac steatosis and dilated cardiomyopathy following diet-induced obesity. *Int J Obes (Lond)* **38** (2):205–15.

244. Ferry, G., Tellier, E., Try, A., Gre, S., Naime, I., Simon, M-F., et al. (2003) Autotaxin Is Released from Adipocytes , Catalyzes Lysophosphatidic Acid Synthesis , and Activates Preadipocyte Proliferation. *J Biol Chem.* **278** (20):18162–9.

245. Van Meeteren, L. A., Ruurs, P., Christodoulou, E., Goding, J. W., Takakusa, H., Kikuchi , K., et al. (2005) Inhibition of autotaxin by lysophosphatidic acid and sphingosine 1-phosphate. *J Biol Chem.* **280** (22):21155–61.

246. Nakae, J., Cao, Y., Oki, M., Orba, Y,. Sawa, H,. Kiyonari, H., et al. (2008) Forkhead Transcription Factor Fox01 in Adipose Tissue Regulates Energy Storage and Expenditure. *Diabetes* **57** (3):563–76.

247. Chang, Y. H., Subramanian, S., Chan, C. K., Omer, M., Chiba, T., Wight, T. N., et al. (2007) Adipocyte-derived serum amyloid A3 and hyaluronan play a role in monocyte recruitment and adhesion. *Diabetes* **56** (9):2260–73.

248. Wu, J-M,. Xu, Y., Skill, N. J., Sheng, H., Zhao, Z., Yu, M., et al. (2010) Autotaxin expression and its connection with the TNF-alpha-NF-kappaB axis in human hepatocellular carcinoma. *Mol Cancer* **9**:71.

249. Song, J., Guan, M., Zhao, Z,. and Zhang, J. (2015) Type i interferons function as autocrine and paracrine factors to induce autotaxin in response to TLR activation. *PLoS One* **10** (8):e0136629.

250. Bai, D., Ueno, L. and Vogt, P. K. (2009) Akt-mediated regulation of NFκB and the essentialness of NFκB for the oncogenicity of PI3K and Akt. *Int J Cancer.* **125** (12):2863–70.

251. Kim, D. H., Kim, J. Y., Yu, B. P. and Chung, H. Y. (2008) The activation of NFκB through Akt-induced FOXO1 phosphorylation during aging and its modulation by calorie restriction. *Biogerontology* **9**(1):33–47.

252. Pradère, J. P., Tarnus, E., Grès, S., Valet, P. and Saulnier-blache, J. S. (2007) Secretion and lysophospholipase D activity of autotaxin by adipocytes are controlled by N-glycosylation and signal peptidase. *Biochim Biophys Acta*. **771** (1):93–102.

253. D'Souza, K., Nzirorera, C., Cowie, A. M,. Varghese, G. P., Trivedi, P., Eichmann, T. O., et al. (2018) Autotaxin-LPA signaling contributes to obesity-induced insulin resistance in muscle and impairs mitochondrial metabolism. *J Lipid Res.* **59** (10):1805–17.

254. Kienesberger, P. C., Lee, D., Pulinilkunnil, T., Brenner, D. S., Cai, L., Magnes, C., et al. (2009) Adipose triglyceride lipase deficiency causes tissue-specific changes in insulin signaling. *J Biol Chem.* **284** (44):30218–29.

255. Kraemer, M. P., Halder, S., Smyth, S. S. and Morris, A. J. (2019) Measurement of lysophosphatidic acid and sphingosine 1 phosphate by liquid chromatography-coupled electrospray ionization tandem mass spectrometry. *Methods Mol Biol.* **1697 (**1):31–42.

256. Venkatraman, G., Benesch, M. G., Tang, X., Dewald, J., McMullen, T. P. and Brindley , D. N. (2015) Lysophosphatidate signaling stabilizes Nrf2 and increases the expression of genes involved in drug resistance and oxidative stress responses: implications for cancer treatment. *Faseb J* **29** (3):772–85.

257. Perez, L. J., Rios, L., Trivedi, P., D'Souza, K., Cowie, A., Webster, D., et al. (2017) Validation of optimal reference genes for quantitative real time PCR in muscle and adipose tissue for obesity and diabetes research. *Sci Rep*. **7** (1):1–13.

258. Fujishiro, M., Gotoh, Y., Katagiri, H., Sakoda, H., Ogihara, T., Anai, M., et al. (2003) Three Mitogen-Activated Protein Kinases Inhibit Insulin Signaling by Different Mechanisms in 3T3-L1 Adipocytes. *Mol Endocrinol.* **17** (3):487–97.

259. Yanagida, K., Igarashi, H., Yasuda, D., Kobayashi, D., Ohto-Nakanishi, T., Akahoshi, N., et al. (2018) The Ga12/13-coupled receptor LPA4 limits proper adipose tissue expansion and remodeling in diet-induced obesity. *JCI Insight.* **3** (24):e97293.

260. Koo, J. H., Kim, T. H., Park, S., Joo, M. S., Han, C.Y., Choi, C. S., et al. (2017) Ga13 ablation reprograms myofibers to oxidative phenotype and enhances whole-body metabolism. *J Clin Invest.* **127** (10):3845–60.

261. Maher, T. M., Kreuter, M., Lederer, D. J., Brown, K. K., Wuyts, W., Verbruggen, N., et al. (2019) Rationale, design and objectives of two phase III, randomised, placebo-controlled studies of GLPG1690, a novel autotaxin inhibitor, in idiopathic pulmonary fibrosis (ISABELA 1 and 2). *BMJ Open Respir Res.* **6** (1):e000422.

262. Aikawa, S., Hashimoto, T., Kano, K., and Aoki, J. (2015)Lysophosphatidic acid as a lipid mediator with multiple biological actions. *J Biochem.* **157** (2):81–9.

263. Kuznetsov, A. V., Veksler, V., Gellerich, F. N., Saks, V., Margreiter, R. and Kunz, W. S. (2008) Analysis of mitochondrial function in situ in permeabilized muscle fibers , tissues and cells. *Nat Protocols* **3** (6):965-76.

264. Boudina, S., Sena, S., Neill, B. T. O., Tathireddy, P., Young, M. E. and Abel, E. D.(2005) Reduced Mitochondrial Oxidative Capacity and Increased Mitochondrial Uncoupling Impair Myocardial Energetics in Obesity. *Circulation* **112**(17):2686–95.

265. Folch, J., Lees, M. and Sloane Stanley, G. H. (1953) A simple method for the isolation and purification of total lipides from animal tissues. *J Biol Chem*. **226** (1):497–509.

266. Knittelfelder, O. L., Weberhofer, B. P., Eichmann, T. O., Kohlwein, S. D. and Rechberger, G. N. (2014) A versatile ultra-high performance LC-MS method for lipid profiling. *J Chromatogr B* **951–952** (3):119–28.

267. Larsen, S., Nielsen, J., Hansen, C. N., Nielsen, L. B., Wibrand, F., Schroder, H. D., et al. (2012) Biomarkers of mitochondrial content in skeletal muscle of healthy young human subjects. *J Physiol.* **590** (14):3349–60.

268. Handschin, C., Chin, S., Li, P., Liu, F., Maratos-flier, E., Lebrasseur, N. K., et al. (2007) Skeletal Muscle Fiber-type Switching , Exercise Intolerance , and Myopathy in PGC-1a Muscle-specific Knock-out Animals. *J Biol Chem.* **282** (41):30014–21.

269. Awada, R., Rondeau, P., Grès, S., Saulnier-Blache, J. S., D'Hellencourt, C. and Bourdon, E. (2012) Autotaxin protects microglial cells against oxidative stress. *Free Radic Biol Med.* **52** (2):516–26.

270. Zhong, H. and Yin, H. (2015) Role of lipid peroxidation derived 4-hydroxynonenal (4-HNE) in cancer: Focusing on mitochondria. *Redox Biol.* **4** (1):193–9.

271. Anderson, E. J., Yamazaki, H. and Neufer, P. D. (2007) Induction of endogenous uncoupling protein 3 suppresses mitochondrial oxidant emission during fatty acid-supported respiration. *J Biol Chem.* **282** (43):31257–66.

272. Sadeghi, A., Sadat, S., Ebrahimi, S., Golestani, A. and Meshkani, R. (2017) Resveratrol Ameliorates Palmitate-Induced Inflammation in Skeletal Muscle Cells by Attenuating Oxidative Stress and JNK/NF-kB Pathway in a SIRT1-Independent Mechanism. *J Cell Biochem.* **2663** (10):2654–63.

273. Montgomery, M. K. and Turner, N. (2015) Mitochondrial dysfunction and insulin resistance: an update. *Endocr Connect* **4** (1):R1–15.

274. Yoon, Y., Yoon, D., Lim, I. N. K., Yoon, S., Chung, H., Rojo, M., et al. (2006) Formation of Elongated Giant Mitochondria in DFO-Induced Cellular Senescence : Involvement of Enhanced Fusion Process Through Modulation of Fis1. *J Cell Physiol.* **480** (6):468–80.

275. Shutt, T., Geoffrion, M., Milne, R. and McBride, H. M. (2012) The intracellular redox state is a core determinant of mitochondrial fusion. *EMBO Rep.* **13** (10):909–15.

276. Fan, X., Hussien, R. and Brooks, G. A. (2010) H2O2-induced mitochondrial fragmentation in C2C12 myocytes. *Free Radic Biol Med* **49** (11):1646–54.

277. Mason, S. and Wadley, G. D. (2014) Skeletal muscle reactive oxygen species: A target of good cop/bad cop for exercise and disease. *Free Radic Res.* ***1*9** (3):97–106.

278. Sun, S., Zhang, X., Lyu, L., Li, X., Yao, S. and Zhang, J. (2016) Autotaxin Expression Is Regulated at the Post-transcriptional Level by the RNA-binding Proteins HuR and AUF1. *J Biol Chem.* **291** (50):25823–36.

279. Wang, Y., Lyu, L., Zhang, X. and Zhang, J. (2019) Autotaxin is a novel target of microRNA-101-3p. *FEBS Open Bio.* **9** (4):707–16.

280. Lin, Y., Berg, A. H., Iyengar, P., Lam, T. K. T., Giacca, A., Combs, T. P., et al. (2005) The hyperglycemia-induced inflammatory response in adipocytes: The role of reactive oxygen species. *J Biol Chem.* **280** (6):4617–26.

281. Pinho, R. A., Sepa-Kishi, D. M., Bikopoulos, G., Wu, M. V., Uthayakumar, A., Mohasses, A, et al. (2017) High-fat diet induces skeletal muscle oxidative stress in a fiber type-dependent manner in rats. *Free Radic Biol Med* **110** (7):381–9.

282. Xu, Y., Wang, Y., Liu, J., Cao, W., Li, L., Du, H., et al. (2019) Adipose tissue-derived autotaxin causes cardiomyopathy in obese mice. *J Mol Endocrinol* pii: JME-18-0242.R2.

283. Yamazaki, T., Joshita, S., Umemura, T., Usami, Y., Sugiura, A., Fujimori, N., et al. (2017) Association of Serum Autotaxin Levels with Liver Fibrosis in Patients with Chronic Hepatitis C. *Sci Rep.***7** (46705): doi: 10.1038/srep46705.

284. Tiganis, T. (2011) Reactive oxygen species and insulin resistance: The good, the bad and the ugly. *Trends Pharmacol Sci* **32** (2):82–9.

285. Higaki, Y., Mikami, T., Fujii, N., Hirshman, M. F., Koyama, K., Seino, T. et al. (2008) Oxidative stress stimulates skeletal muscle glucose uptake through a phosphatidylinositol 3-kinase-dependent pathway. *Am J Physiol Endocrinol Metab.* **294** (5):E889–97.

286. Tiwari, B. K., Pandey, K. B., Abidi, A. B. and Rizvi, S. I. (2013) Markers of Oxidative Stress during Diabetes Mellitus. *J Biomarkers* **2013** (2013):13787908.

287. Jheng, H., Tsai, P., Guo, S., Kuo, L., Chang, C., Su, I., et al. (2012) Mitochondrial Fission Contributes to Mitochondrial Dysfunction and Insulin Resistance in Skeletal Muscle. *Mol Cell Biol.* **32** (2):309–19.

288. Frohman, M. A. (2016) Role of mitochondrial lipids in guiding fission and fusion. *J Mol Med.* **93** (3):263–9.

289. Ohba, Y., Sakuragi, T., Kage-nakadai, E., Tomioka, N. H., Kono, N., Imae, R., et al. (2013) Mitochondria-type GPAT is required for mitochondrial fusion. *EMBO J* **32** (9):1265–79.

290. Baba, T., Kashiwagi, Y., Arimitsu, N., Kogure, T., Edo, A., Maruyama, T., et al. (2014) Phosphatidic Acid (PA) -preferring Phospholipase A 1 Regulates Mitochondrial Dynamics. *J Biol Chem*. **289** (16):11497–511.

291. Ray, U., Chowdhury, S. R., Vasudevan, M., Bankar, K. and Roy, S. S. (2017) Gene regulatory networking reveals the molecular cue to lysophosphatidic acid-induced metabolic adaptations in ovarian cancer cells. *Mol Oncol.* **11** (5):491–516.

292. Mukherjee, A., Ma, Y., Yuan, F., Gong, Y., Fang, Z., Mohamed, E. M., et al. (2015) Lysophosphatidic Acid Up-Regulates Hexokinase II and Glycolysis to Promote Proliferation of Ovarian. *Neoplasia* **17** (9):723–34.

293. Ha, J. H., Radhakrishnan, R., Jayaraman, M., Yan, M., Mukherjee, P., Song, Y. S., et al. (2018) LPA Induces Metabolic Reprogramming in Ovarian Cancer via a Pseudohypoxic Response. *Cancer Res.* **78** (8):1923–34.

294. Simoneau, J. and Kelley, D. E. (1997) Altered glycolytic and oxidative capacities of skeletal muscle contribute to insulin resistance in NIDDM. *J Appl Physiol.* **83** (1):166–71.

295. Chavez, J. A. and Summers, S. A. (2003) Characterizing the effects of saturated fatty acids on insulin signaling and ceramide and diacylglycerol accumulation in 3T3-L1 adipocytes and C2C12 myotubes. *Arch Biochem Biophys* **419** (2):101–9.

296. Schiaffino, S. and Reggiani, C. (2011) Fiber Types in Mammalian Skeletal Muscles. *Physiol Rev.* **91** (4):1447–531.

297. Pirola, L., Bonnafous, S., Johnston, A. M., Chaussade, C., Portis, F. and Obberghen, E. (2003) Phosphoinositide 3-Kinase-mediated Reduction of Insulin Receptor Substrate-1/2 Protein Expression via Different Mechanisms Contributes to the Insulin-induced Desensitization of Its Signaling Pathways in L6 Muscle Cells. *J Biol Chem.* **278** (18):15641–51.

298. Nikolaou, A., Kokotou, M. G., Limnios, D., Psarra, A. and Kokotos, G. (2017) Autotaxin inhibitors : a patent review (2012-2016). *Expert Opin Ther Pat*. **27** (7):815–29.

299. Saga, H., Ohhata, A., Hayashi, A., Katoh, M., Maeda, T., Mizuno, H., et al. (2014) A Novel Highly Potent Autotaxin/ENPP2 Inhibitor Produces Prolonged Decreases in Plasma Lysophosphatidic Acid Formation In Vivo and Regulates Urethral Tension. *PLoS One* **9** (4):e93230.

300. Benesch, M. G. K., Tang, X., Maeda, T., Ohhata, A., Zhao, Y. Y., Kok, B. P. C., et al. (2014) Inhibition of autotaxin delays breast tumor growth and lung metastasis in mice. *Faseb J.* **28** (6):2655–66.

301. He, P., Haque, A., Lin, S., Cominelli, F. and Yun, C. C. (2018) Inhibition of autotaxin alleviates inflammation and increases the expression of sodium-dependent glucose cotransporter 1 and Na+/H+ exchanger 3 in SAMP1/Fc mice. *Am J Physiol Gastrointest Liver Physiol.* **315** (29):762–71.

302. Aar van der, E., Desrivot, J., Dupont, S., Heckmann, B., Fieuw, A., Stutvoet, S., et al. (2019) Pharmacodynamics of the Autotaxin Inhibitor GLPG1690 in Healthy Subjects : Phase 1 Randomized Trials. *J Clin Pharmacol.* doi: 10.1002/jcph.1424.

303. Maher, T. M., van der Aar, E. M., Van de Steen, O., Allamassey, L., Desrivot, J., Dupont, S., et al. (2018) Safety, tolerability, pharmacokinetics, and pharmacodynamics of GLPG1690, a novel autotaxin inhibitor, to treat idiopathic pulmonary fibrosis (FLORA): a phase 2a randomised placebo-controlled trial. *Lancet Respir Med* [**6** (8):627–35.

Appendix A. Copyright Permissions

Jul 04, 2019

This Agreement between Kenneth D'Souza ("You") and Oxford University Press ("Oxford University Press") consists of your license details and the terms and conditions provided by Oxford University Press and Copyright Clearance Center.

License Number	4602101441756
License date	Jun 04, 2019
Licensed content publisher	Oxford University Press
Licensed content publication	Endocrinology
Licensed content title	Autotaxin Is Regulated by Glucose and Insulin in Adipocytes
Licensed content author	D'Souza, Kenneth; Kane, Daniel A.
Licensed content date	Jan 16, 2017
Type of Use	Thesis/Dissertation
Institution name	
Title of your work	PhD Student
Publisher of your work	Dalhousie Medicine New Brunswick
Expected publication date	Aug 2019
Permissions cost	0.00 CAD
Value added tax	0.00 CAD
Total	0.00 CAD
Title	PhD Student
Institution name	Dalhousie Medicine New Brunswick
Expected presentation date	Aug 2019
Portions	Results, Figure 1-8, Conclusion
Requestor Location	Kenneth D'Souza 6401 Valiant Heights Mississauga, ON L5W1E2 Canada Attn: Kenneth D'Souza
Publisher Tax ID	GB125506730
Total	0.00 CAD
Terms and Conditions	